EXCITATION AND DE-EXCITATION OF SPUTTERED PARTICLES

Christopher Mark Loxton

A thesis submitted for the Degree of
Doctor of Philosophy of the Australian National University

May 1981

I hereby declare that the work reported in this thesis has not been submitted before for a higher degree or award at any other institution or university. All measurements associated with photon emission and the data analysis were the results of my own efforts unless otherwise acknowledged. Part of the Ta continuum emission study was undertaken with Dr P.J. Martin.

Chris Loxton

C.M. Loxton

ACKNOWLEDGEMENTS

Financial support for my studies has been provided by the Australian Government through a Commonwealth Post-graduate Research Award and the Australian National University for which I am most grateful.

This thesis is certainly not completely "a result of my own efforts" and I wish to express my sincere thanks to my supervisors, Professor R.J. MacDonald and Dr P.J. Martin for their suggestions, criticisms and encouragement for the duration of this study.

Many thanks must also go to my colleagues, Dr J. O'Connor, R.F. Garrett, Dr E. Taglauer (while visitor at A.N.U.) and those members of the Physics Department who have been of assistance. To my parents and family I express thanks for their support and encouragement. To my friends I must also extend my thanks for their help and patience. A special acknowledgement is made to Erica Persak for her help and understanding.

Technical support and help from A. Crawford and also W. O'Hare and his workshop staff was most appreciated. Photographic assistance was provided by K. Smith. For patiently cutting many targets for my use, I extend thanks to D. Price. Also appreciated was the assistance with the electronics from L. Batt and D. King.

The thesis has been admirably typed by Rosemary Drury.

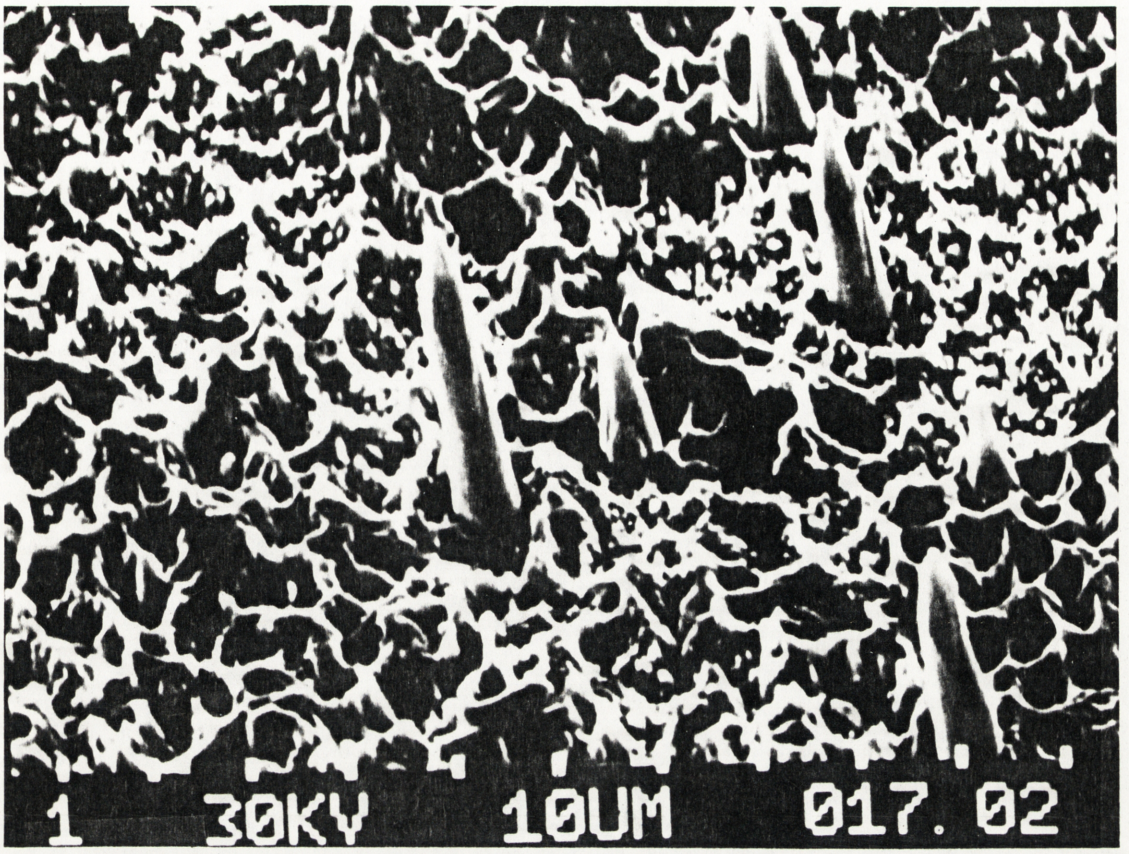

Surface features of a Ti N layer over a stainless steel substrate observed by a scanning electron microscope. The target has been bombarded by 55 keV Ar^+ under UHV conditions. Cone formation is evident and the length of some cones are > 30 microns. X-ray analysis † has shown that the cones are Ti, while the surrounding target is stainless steel, i.e. the ion beam has etched through the Ti N layer.

The cones will be sites for Ti^+ and Ti^* emission with ion bombardment. The photograph shows that surface morphology effects may be important in SIMS and photon depth profiling resolution done under UHV conditions.

† Scanning electron microscope facility, Australian National University (J. Preston).

CONTENTS

ABSTRACT

A study has been made of photon emission from sputtered excited particles in an attempt to gain some insight into the excitation processes. Particular care has been been taken to determine and discuss the influence of the experimental method on the results obtained because the method and experimental parameters are shown to have a strong influence on the observations.

A detailed study of the characteristics of neutral line emission from bombarded Ti and Ti compounds is discussed. Emphasis has been placed upon the measurement of the distributions of excited states, kinetic energy parameters characteristic of the excited atoms and the influence of surface and bulk contamination on the line emission. An attempt has been made to interpret the results using the band structure model and competing non-radiative de-excitation processes. Kinetic energy parameters have been determined from line profile measurements and from decay curve measurements using the model of Dzioba et al. This model predicts energy parameters similar to those obtained from line profile measurements for the Ti I system.

The measured characteristics of the Ti I photon emission have been compared with those obtained from other bombarded systems. These characteristics have been discussed with reference to the excitation process. The influence of surface oxygen contamination has been studied in detail for a series of elemental targets and Nb/V alloys.

The results show that the kinetic energy parameters of the excited particles and the behaviour with oxygen exposure is dependent upon the excitation energy of the level. The distribution of excited states of the sputtered Ti atoms is similar to a Boltzmann distribution and is shown to not change markedly with the chemical environment of the target. Oxygen exposure increases the intensity of the Ti I emission and is accompanied by a decrease in the kinetic energy parameter of the excited atoms. Other targets also display an increase in line intensity with oxygen exposure. However, this increase is not always accompanied by a change in the kinetic energy parameter. This parameter *increases* with oxygen exposure for the Aℓ I 309.2 nm line and remains constant for some Ni I and Si I emission lines. Ionised atom emission lines do not necessarily follow the trends of neutral emission lines.

The band structure model and in particular,the resonance ionisation process, do not appear to be applicable to the interpretation of the observed results. The excitation process for sputtered atoms is not known for UHV conditions. Quasimolecule formation cannot be ruled out as an excitation process under oxygen exposure conditions. Current theories of excitation and de-excitation do not readily explain the observed results.

The intensity changes with oxygen exposure for Nb I and V I lines from bombarded Nb/V alloys indicate that quantitative analysis of these alloys is not possible using photon emission when the surface is contaminated.

Quantitative analysis using this technique is possible under UHV conditions to an accuracy of about 5 atomic percent.

Continuum emission has also been studied. The excited species responsible for the emission is not known and hence any understanding of the excitation process is difficult. The dependence of this emission on the surface chemical state is consistent with the proposal by Rausch et al. that the source of this emission may be sputtered metal-oxides. Broad line emission has been observed from bombarded Nb and Ta. However, the nature of the emitting species has not been identified.

CHAPTER ONE

ION BOMBARDMENT PROCESSES AND SECONDARY PHOTON EMISSION

1.1 INTRODUCTION

Although ion bombardment of surfaces has been studied for a long period of time, this field has had renewed interest in the past two decades for several more practical reasons than merely the physics of particle interaction. Indeed, with many trends evident in the experimental data, a clear mathematical understanding of the processes involved in ion bombardment has still to emerge in many of the differing interactions. As will be discussed later, a major factor which has confused the observed trends has been the inability, until recently, to routinely produce an ultra high vacuum environment for experimentation.

Recent impetus for interest in ion bombardment processes and in particular, sputtering (the removal of surface particles by bombardment), has partly arisen through the requirements for nuclear fusion and fission reactor design, where information on the behaviour of surfaces under intense fluences of particles is needed. Ion and neutral bombardment of wall materials results in wall damage and erosion through sputtering. Additionally, such bombardment may induce desorption of gases from the wall which, in the case of plasma fusion devices, may seriously contaminate

the plasma and reduce its temperature. Consequently, the determination of sputtering coefficients, damage properties and desorption rates have been of considerable importance for combinations of bombarding particles and potential wall and limiter materials. Neutron bombardment damage is, of course, also of prime importance. Emphasis has been placed upon the measurement of radiation blistering and embrittlement, swelling, creep and ductility changes which may accompany the neutron bombardment. These processes have been discussed by Behrisch [1].

Ion bombardment has also been of great interest to the field of surface physics. Mass analysis of sputtered particles, analysis of emitted photons and Auger electrons and the measurement of the energies of scattered particles have made ion bombardment a qualitative and, to a limited extent, quantitative, surface analysis technique. It has also been used to moniter surface oxidation and cleanliness as well as surface structures and relaxations [reviewed in 2]. Ion implantation is a means of achieving above solubility doping of elements into matrices and this is of importance to the semi-conductor industry. The corrosion and wearing properties of surfaces are also modified by ion implantation. Ion implantation has been recently reviewed at length by Dearnaley et al. [3].

1.2 ION BOMBARDMENT PROCESSES

To put the field of Sputter Induced Photon Spectroscopy (SIPS) into perspective with other ion bombardment

related fields, it is worthwhile examining the processes which occur when an ion or neutral particle interacts with a solid. The major processes which accompany ion bombardment may be conveniently divided into elastic and inelastic processes, as shown in Figure 1.1. These processes will be discussed briefly with emphasis on those which are germane to this thesis.

1.2.1 *Ion Scattering*

At high incident ion energies (> 100 keV), scattering of a light mass incident particle in a backward direction is termed Rutherford Back-Scattering (RBS). This has become a useful tool for analysis and determining radiation damages and changes which occur in the bombardment target below the surface. Surface sensitivity is most easily achieved by using low energy incident ions (< 5 keV) and observing the scattered ions. Those particles which penetrate the surface are rapidly neutralised and the observation of scattered ions is then a surface sensitive technique. The technique using low energy ion scattering has been denoted Ion Scattering Spectroscopy (ISS) or Low Energy Ion Scattering (LEIS).

For an ion scattering event with a collision time much less than the lattice vibration period (the collision time $\approx 10^{-15}$ sec. for several keV incidence whereas the lattice vibration period is $\approx 10^{-13}$ sec.), the coupling between the target atom and neighbouring lattice atoms may be neglected and a binary collision event may be assumed. A binary collision event involving an energetic particle of

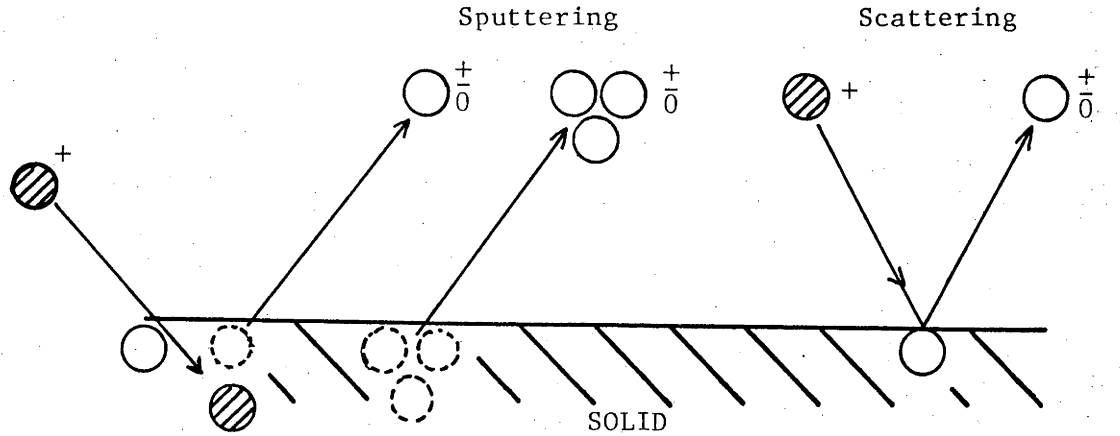

Figure 1.1(a) Elastic Processes resulting from ion bombardment.

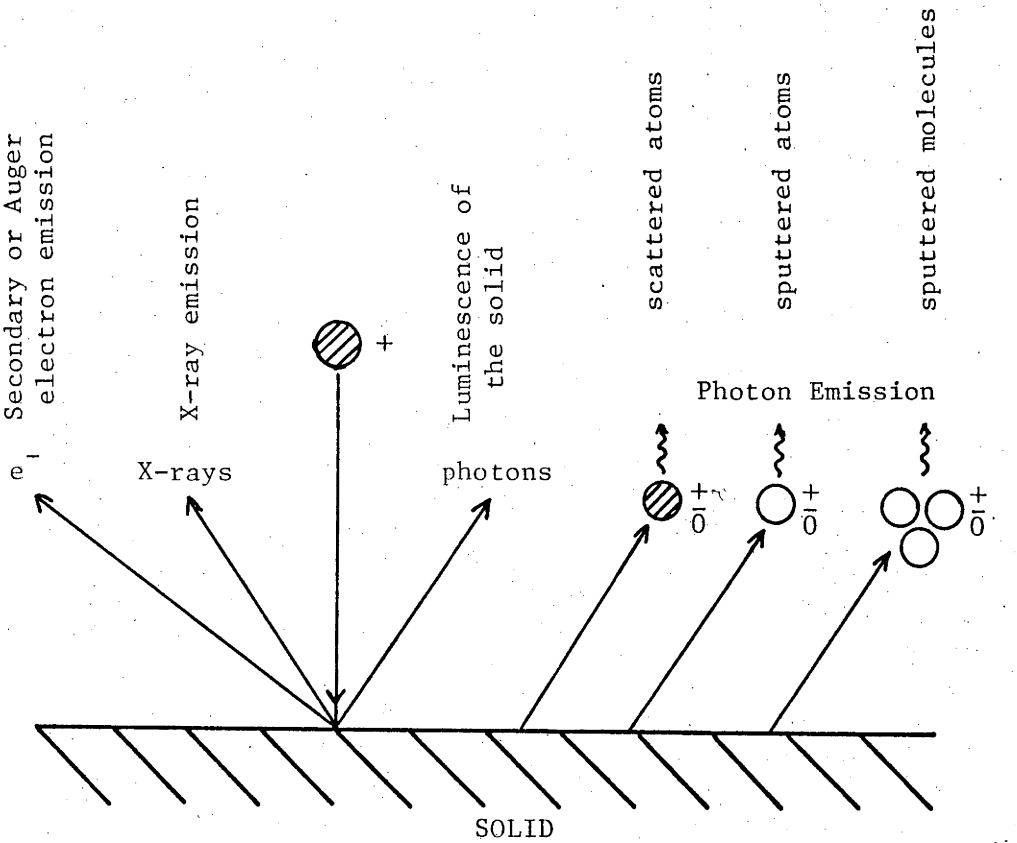

Figure 1.1(b) Inelastic processes resulting from ion bombardment.

mass M_1, energy E_0 and initial velocity v_0, scattered off a target atom of mass M_2 initially at rest, yields the following relations from consideration of the conservation of energy and momentum in the elastic collision:

$$\frac{E_1}{E_0} = \left[\frac{\cos\theta + \sqrt{\mu^2 - \sin^2\theta}}{1+\mu}\right]^2, \quad \mu = \frac{M_2}{M_1} > 1 \tag{1.1}$$

or

$$\frac{E_1}{E_0} = \left[\frac{\cos\theta \pm \sqrt{\mu^2 - \sin^2\theta}}{1+\mu}\right]^2, \quad \mu < 1 \tag{1.2}$$

where θ is the laboratory frame angle through which the incident particle is scattered and E_1 is the final energy of the scattered particle. By measuring the scattering angle and the incident and final energies of the incident particle, the mass of the target atom may be determined. This is the basis for surface compositional analysis. Equation (1.1) is the more important relation here, as ISS for compositional analysis requires a light mass bombarding ion to achieve reasonable mass resolution.

The role of inelastic collisional processes such as lattice electron excitation, which determines an energy loss, have been ignored in determining equations (1.1) and (1.2). Additional terms involving Q, the energy loss, may be included in these equations to take the inelastic energy losses into consideration. Also, for low incident ion energies where the collision time is similar to the lattice vibration time, the binary collision approximation may become invalid. Coupling between the target atom and lattice neighbours

increases the apparent mass of the target atom (then known as the apparent mass) and this results in E_1/E_0 values which depart from the predicted values. The lower limit of the binary collision model has been found to be usually of the order of 10's to 100's of eV [4], far lower than the energies used in obtaining data discussed here in Chapter 6.

Ion surface scattering may also occur through multiple scattering events at the target surface as well as the single scattering events discussed above. Multiple scattering occurs when the incident ion is scattered through a total angle θ by two or more "softer" collisions from two or more surface atoms, such that the sum of the scattering angles equals the total angle θ. A peak then appears in the scattered energy spectrum at the high energy side of the single scattering peak. The exception is when the total scattering angle is made up from two or more large angle ("hard") collisions resulting in a larger energy loss than in the case of single scattering.

There has been recent interest in the pronounced oscillatory scattered ion yield as a function of incidence energy for a particular class of target and incident ion combinations. This was first observed during ion scattering in 1975 by Erickson and Smith [5], although such behaviour had been found previously in atom-atom collisions [6]. The explanation for this oscillatory yield has been discussed in terms of the model of quasi-molecule formation [7], where the incident and target atoms are proposed to form a quasi-molecule. The oscillations are proposed to be a result of quantum mechanical phase interference between pairs of near resonant quasi-molecule levels [8].

ISS has also been recently used to determine desorption coefficients [9], surface structures [10] and inelastic energy loss [11]. Four different classes of energy dependent ion yields have been noted [12] and the behaviour of these classes for projectile target combinations is being further investigated.

1.2.2 *Sputtering*

Although sputtering has been known and studied for many years an understanding of the processes involves is still far from complete, particularly for single crystal targets. A theory of sputtering was proposed by Sigmund [13] in 1969, based upon collision cascade sequences initiated by a primary recoil of a lattice atom when struck by the incident ion. Sputtering was assumed to result when the collision cascade intersected the surface and transferred enough energy to the surface particle for it to overcome the surface potential barrier. This theory applied general transport theory and Boltzmann's equation to the random collision processes and has had some success in predicting the sputtering yields and their energy dependence. The random collision cascade model predicts a cosinal angular distribution of sputtered particles and an E^{-2} energy distribution of the sputtered particles as does a similarly based model by Thompson [14]. Elich et al. [15] have been able to extend these models to include single crystal bombardment by considering a random component, as well as a channeled component, to determine sputtering yields as a function of the angle of incidence.

Sputtered secondary ion emission and Secondary Ion Mass Spectrometry (SIMS) are less understood than sputtering and there have been a plethora of models advanced over the past decade in an attempt to explain some of the features of this emission. Secondary ion emission has received considerable attention due to the ease with which charged particles may be analysed and detected. The secondary ion emission models need not be discussed here and have been reviewed extensively in recent publications [16, 17]. Reference will be made to such models in later sections where relevant to photon emission studies. Some of these models include: the induced plasma in Local Thermodynamic Equilibrium (LTE) model [18], the kinetic model based upon electron promotion through quasi-molecule formation [19], quantum mechanical models [20, 21, 22] and the surface-polarization model [23]. These models have attempted to explain, at least in part, the observations of: positively, negatively and multiply charged species, the strong dependence upon the presence of electronegative or electropositive species and the strong, but non-monotonic variation with atomic number of the target.

The LTE model was proposed by Andersen et al. [18] after the observation that the ion yield followed a similar relationship to the Boltzmann equation for LTE plasmas. It was then concluded that the bombardment region may resemble a plasma in LTE. The model has been used with some success for analysis purposes although the physical basis for such a model has been extensively criticized [16, 17]. It will

be further examined with application to photon emission in the following chapter. Additional models have been proposed to account for the severe contamination induced changes in ion yield and these have included bond-breaking models [see, for example, 24].

Much of the current need in the field of sputtering remains with obtaining good experimental data under various experimental conditions to compare with theory. Further data is also required for applied purposes. It has been demonstrated that SIMS is particularly sensitive to surface contamination and consequently, much of the earlier work needs to be repeated. Such data has included the measurement of secondary ion energy spectra [25], energy and mass spectrometry of cluster emission [26] and the measurement of the energy spectra of sputtered neutrals by, for example, Doppler-shift laser spectrometry [27].

Applied sputtering measurements have been made for sputtering yields [28] and ionised fraction yields [29] where the data is useful in the planning of fusion devices and in controlling possible plasma contaminants. SIMS for depth profiling has also become important, particularly in relation to thin films in the semiconductor industry. Oxidation and the adsorption of impurities such as CO and O_2 have also been studied by SIMS [30].

1.2.3 *Electron and X-ray Emission*

The processes of electron and X-ray emission have been grouped together because the mechanism responsible for X-ray emission may also lead to electron emission. Secondary electron emission is conventionally divided into potential and kinetic emission, with the potential emission being associated with neutralisation of the incident ion before it reaches the solid while kinetic emission is associated with collision events inside the solid.

Potential secondary electron emission results from an Auger neutralisation process (discussed in section 2.1) where an electron tunnels from the solid to the incoming ion. This process is important for very low energy incident ions where the incident velocity is below or about 10^7cm/sec and has been reviewed in detail by Hagstrum [31, 32]. For incident ion velocities lower than the atomic electron velocity, potential emission is expected to be independent of the incident ion energy [2].

Kinetic emission contrasts to this by being more important at higher energies and usually has a well defined threshold at lower incidence energies and a gradual decrease towards high energies. The initial model by Parilis et al. [33] for lower energies was based upon an internal Auger process initiated by the collision of the incident particle with the lattice atom. This raises an electron from the valence to the conduction band forming an electron-hole pair. Subsequent recombination of the electron-hole pair results in the ejection of a second electron from the

conduction band. The yield of emitted electrons is then related to the deposition of electron excitation energy near the surface, determined by the electronic stopping power of the bombarding ion [34]. Kinetic emission may be divided into two contributions, firstly from direct collisions between the bombarding ion and the target atoms and secondly, the indirect contribution from collisions between recoil atoms and other target atoms. The latter contribution was ignored in the earlier theories [33, 34] and has only recently been taken into account by Holmen et al. [35]. The electron yield has been determined from general stopping theory including both direct and recoil processes.

Electron ejection may also occur by direct binary collisions of the incident ion with free valence-band electrons. This process has been found to be particularly important for low energy light ion bombardment [36].

The secondary electron energy distribution usually peaks at about several eV and has a continuous high energy tail. In addition to this high energy tail, some structure is evident which has been attributed to the Auger de-excitation of an excited sputtered atom with an internal vacancy [37]. The production of such an internal vacancy is usually explained in terms of the Fano-Lichten model of molecular orbital promotion [7]. During the formation of the quasi-molecule, the energy levels are perturbed and some levels become degenerate allowing an electron to transfer to a vacant level. As the atoms separate, the energy levels return to those appropriate for the isolated atoms, with one atom having a vacancy in an inner shell. When

this vacancy is filled by an Auger de-excitation, an Auger electron is emitted. The vacancies which are formed may be predicted using "correlation" diagrams for the energy levels of the emitting atom and the quasi-molecule and by considering the level crossing curves in the manner of Barat et al. [7].

Current research on electron emission from ion bombarded surfaces has concentrated on obtaining good data for various angles of incidence and emission angle and energy to compare with theory. In the case of Auger electron production, interest is in the measurement of the Auger electron spectra and in determining the cause of excitation, through either symmetrical collisions (i.e. colliding nuclei are the same) or asymmetrical collisions (i.e. the colliding nuclei are different). As an example using Argon Auger emission, Ar^+ bombardment of K,Ca and first series transition metals produce high Ar Auger yields as the asymmetrical collisions are numerous and effective. However, with light metal targets, only rare symmetrical Ar collisions against pre-implanted Ar can lead to Ar Auger emission [38] and the Ar Auger yield is much lower.

With reference to the use of the LTE model in secondary ion emission and the concept of thermal spikes, Hofer et al. [39] have studied the secondary electron emission (SEE) induced by cluster bombardment to investigate thermal spike influences on the electron emission. Although very high energy density cascades were produced (up to 9 atoms/cluster),

non-linearities in the SEE were not observed and it was concluded that contributions to the SEE due to elastic collision spikes could be neglected. In another parallel with SIMS studies, Hasselkamp et al. [40] have studied the electron yields with adsorbed oxygen. It was found that the decreased electron yield was related to the amount of adsorbed oxygen and the decreased yield was thought to be at least partially caused by an increase in the work function.

Production of the inner shell vacancy by quasi-molecule formation, as proposed above, may also result in X-ray emission in addition to Auger electron emission. The two emission processes are competing de-excitations for the excited atom. The probability for X-ray emission is termed the fluorescence yield ω where

$$\omega = \frac{\delta_X}{\delta_X + \delta_A} ,$$

and δ_X and δ_A are the X-ray emission and Auger emission cross-sections respectively. The probability for X-ray emission increases with mass number of the target atom as shown in Figure 1.2 and is equal to Auger emission when the target mass number is about that of Arsenic.

The molecular orbital model [7] is most appropriate for vacancy production due to heavy ion bombardment. X-ray emission by light ion bombardment is thought to proceed by vacancy production induced by direct Coulomb interaction of the bound electron and the incident particle [2].

Auger electron and X-ray emission have practical application for qualitative analysis and also depth profiling.

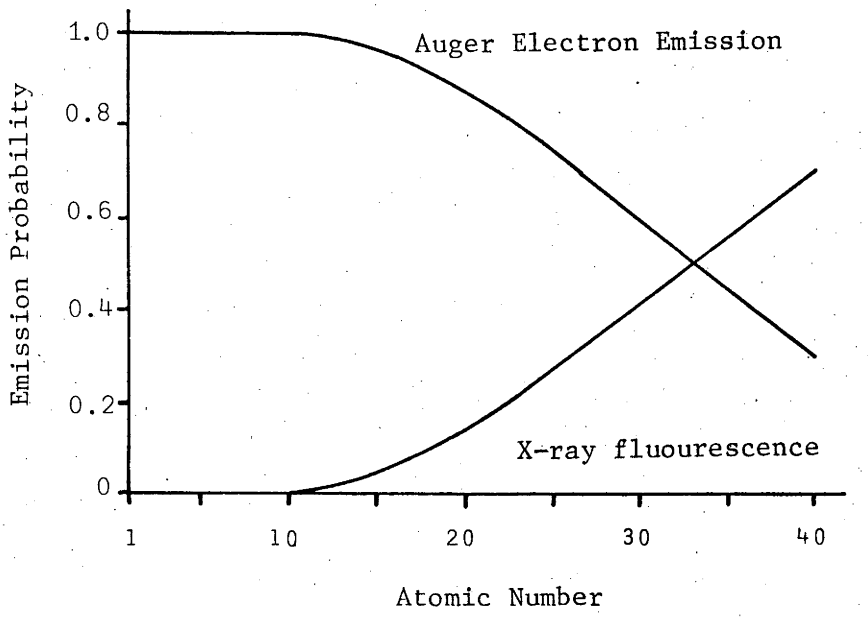

Figure 1.2 Probability of Auger electron emission and X-ray fluorescence as a function of atomic number [41].

1.2.4 *Photon Emission*

There are several sources of photon emission from ion bombarded surfaces and it is important to distinguish between these. Firstly, the incident ion may be excited during the scattering event at the surface and may then de-excite by photon emission. Secondly, the sputtered particles (atoms/ions/clusters) may be in an excited state and these may decay radiatively. These emissions result from particles decaying radiatively in front of the target

surface. Thirdly, photon emission may result from within the solid itself due to, for example, excitation of electrons within the solid or by radiative recombination of electron-hole pairs. This results in a broad band continuum and is particularly evident in the bombardment of insulators. Luminescence has also been observed due to H^+ and He^+ bombardment of certain metals. Finally, the photon emission may originate from the surface where surface molecules may be excited and subsequently decay radiatively resulting in molecular band emission.

The excitation and de-excitation processes for scattered and sputtered particles may be similar and these will be discussed in detail in the next chapter. Suffice it to say that photon emission from scattered and sputtered monatomic particles results in line emission in the visible and UV regions. Broad band emission and in some cases, discrete molecular bands, have also been observed from sputtered particles and have been attributed to de-exciting sputtered molecules. For the purposes of this chapter, only photon emissions from the solid or surface layers will be briefly discussed.

Broadband continuum radiation arising from the bombardment of insulators was the first of the photon emission observed from the solid and has been investigated by several groups [42, 43], usually for the bombardment of Alkali halides by H^o,H^+,He^o or He^+. Tolk et al. [42] observed that the continuum radiation spectrum for 5 keV He, H and H_2 bombardment of calcium fluoride

decreased by at least three orders of magnitude and was dominated entirely by the line spectrum of sputtered particles when heavier projectiles (Ne^o,Ar^o,$N_2{}^o$) of the same energy were used. It was further noted that the same continuum radiation could be produced by low energy (200eV - 3keV) electron bombardment of the CaF_2. Tolk et al. concluded that the continuum radiation for low Z bombardment was produced by radiative recombination of electrons with a self trapped ν_k centre of the F_2^- molecule from the CaF_2 crystal. The ν_k centre was thought to arise from inelastic energy loss (to the bound electrons). For higher Z neutral particle bombardment,where elastic energy loss dominates (from nuclear collisions), the continuum would be expected to decrease and this is experimentally observed. High Z *ion* bombardment did produce this continuum,however this could be quenched by neutralizing the surface by electron bombardment. In this case, the continuum was concluded to arise as a result of charge build up in the insulator which was sufficient to induce potentials to create excitation by bombardment of the accelerated secondary electrons.

The broadband luminescence spectra for several alkali halides are shown in Figure 1.3 and are similar for either H^+ or He^+ bombardment. Bazhin et al. [43] have measured the induced luminescence for KCl and KBr as a function of target temperature, ion dose and also with oxygen contamination. The luminescence was found to peak at about 0°C and then decrease as the temperature increased. With oxygen exposure, the luminescence continuum for KBr was found to be dominated by a peak at 530 nm which was

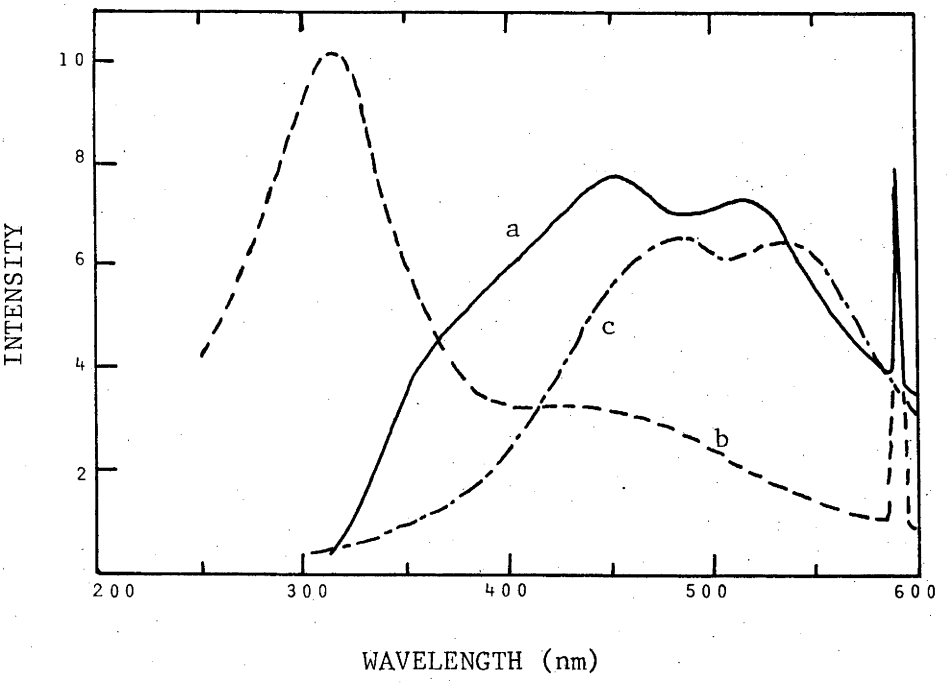

Figure 1.3 Luminescence spectra produced by 25 keV projectile bombardment of alkali halides at room temperature. (a) $H^+ \rightarrow NaC\ell$ (b) $He^+ \rightarrow NaF$ (c) $H^+ \rightarrow KBr$ (after [43]).

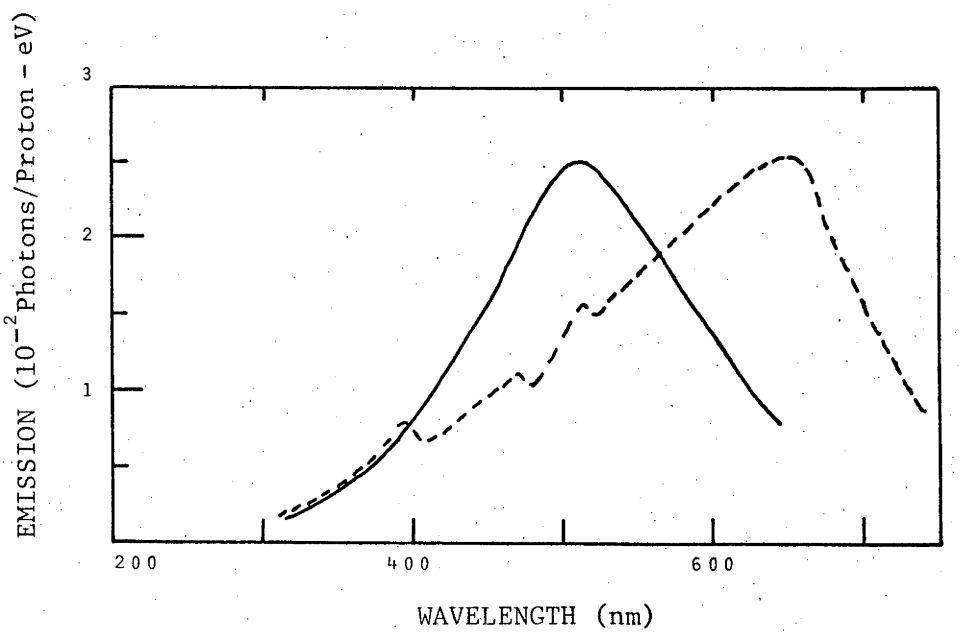

Figure 1.4 Luminescence spectra produced by 25 keV H^+ bombarded $A\ell$ at 45° incidence. The solid line shows the experimental spectrum and the dashed curve is the spectrum predicted by electron-hole recombination (after [44]).

attributed to oxygen impurities on the surface. Consideration of the temperature dependence of the intensity, that the ion-induced luminescence was unchanged by white light bleaching and estimates of the energy levels, led Bazhin et al. to conclude that the KBr peaks at 500 and 350 nm, as shown in Fig. 1.3, were due to V_3 and V_4 centres respectively.

A similar broadband luminescence has been observed by Zivitz et al. [44] for medium energy (10-30 keV) H^+ and He^+ bombardment of Al. Again H^+ and He^+ bombardment were found to produce a similar luminescence continuum which extended from 300 to 600 nm. The integrated photon intensity represented about 0.02 photons per 25 keV H^+ incident ion. By consideration of the range of the incident particles in Al, the emitting sites were estimated to be at or within 10 nm of the surface. It was assumed that the mechanism responsible for the luminescence was the radiative recombination of electrons with holes generated in the conduction band. The number of emitted photons per unit energy interval was then calculated assuming a uniform distribution of electron-hole pairs and the recombination of the holes with electrons from band 1 of the Al band structure. The observed and predicted emissions are shown in Figure 1.4 and the agreement was considered adequate for such a simple model to be consistent with the assumption of electron-hole recombination. Luminescence spectra for Cu and Mo have been similarly observed [45].

Broadband emissions which may originate from below the surface have also been observed recently which are

attributable to the decay of bound-excited rare gas molecules [46-49]. These broad emissions occur in the vacuum ultraviolet region and have been observed and shown by Bhattacharya et al. [48] to extend from 68-99 nm for He^+, 70-95 nm for Ne^+ and 109.5 - 142.5 nm for Ar^+ bombardment of Al. It was noted that these broad emissions were not present upon initial irradiation and increased in intensity with ion dose. Furthermore, the continua were relatively independent of the target material, as shown in Figure 1.5(a). To confirm the assumption that rare gas molecules were responsible for these continua, Hill et al. [47] were able to excite the second ultra-violet continuum of Ar_2 by He^+ bombardment of a Si sample which had previously been bombarded by Ar^+ (shown in Figure 1.5(b)).

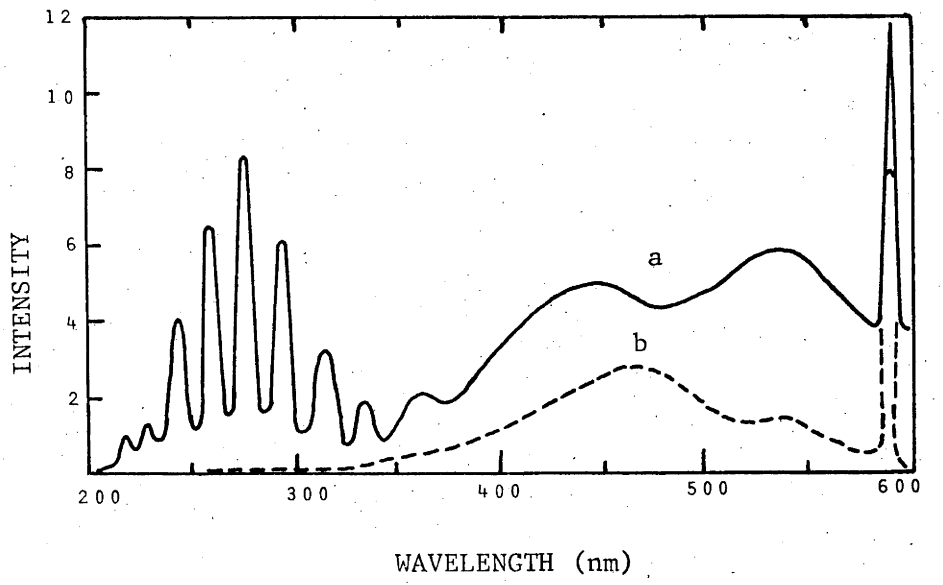

Fig. 1.6 Luminescence spectra induced by 20 keV He^+ bombardment of NaCl at 26°C. Line (a) is for a crystal after exposure to H_20 vapour and line (b) is for the same sample after annealing to 450°C [50].

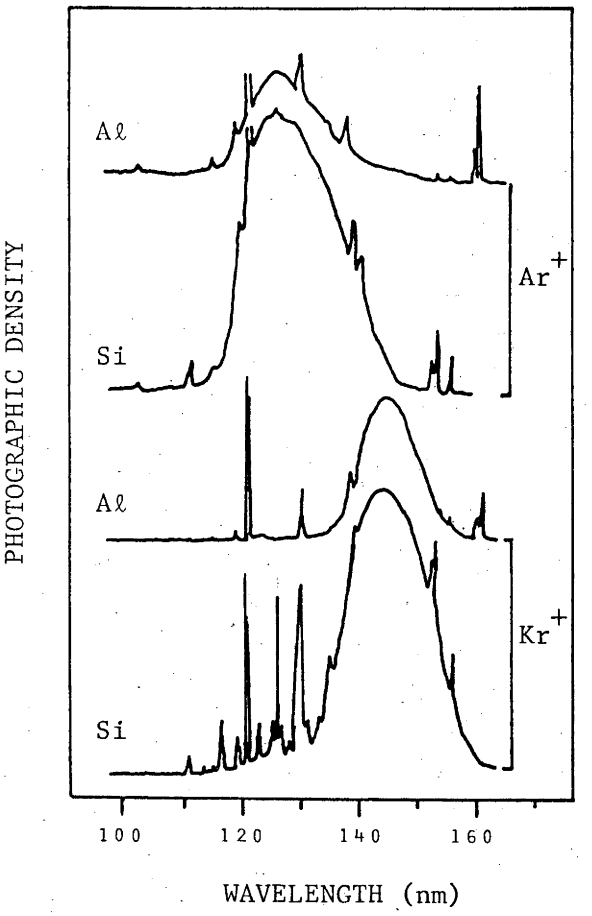

Figure 1.5(a) Spectra obtained during 100 keV Ar^+ and Kr^+ bombardment of Aℓ and Si (after [47]).

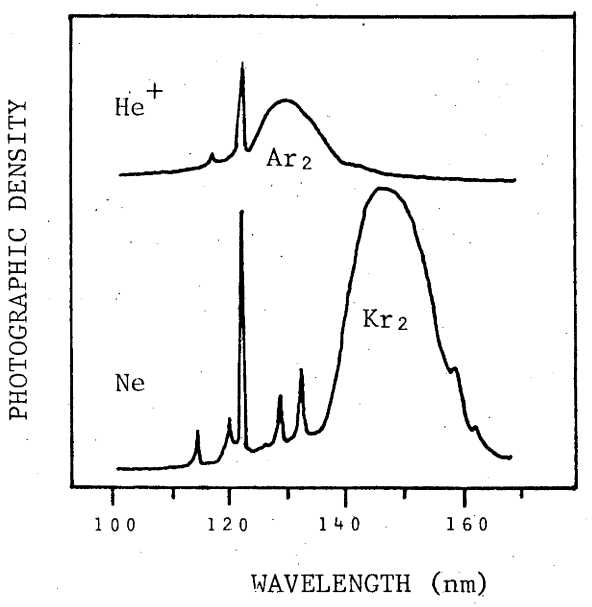

Figure 1.5(b) Spectra obtained by He^+ and Ne^+ bombardment of a Si target which has previously been irradiated with Ar^+ and Kr^+ respectively. Continua associated with the previously incident ion are observed (after [47]).

Band emission emanating from the surface of the bombarded target has been reported by Bazhin et al. [50]. This emission has been attributed to excitation of the CN radical on the surface of the bombarded alkali halide. Previously unbombarded NaCl was found to produce a series of regularly spaced broadbands as shown in Figure 1.6. The bands were found to disappear with annealing. By doping the crystal with CN or by bombarding the crystal in a cyanogen gas environment, the spectra shown in Figure 1.6 could be reproduced and it was concluded that the bands were that of CN. The bands were further identified as from the $D^2\pi \rightarrow X^2\Sigma^+$ transition of CN.

Some research in photon emission induced by ion bombardment has concentrated on the measurement of data to test different excitation models. Unfortunately, little attention has been concentrated on determining the influence of parameters such as the angle and energy of the incident particle on the characteristics of the photon emission. Most of the earlier work was performed with little regard for surface cleanliness. Consequently, many of the observed trends have varied between different researchers. This criticism also applies to some SIMS studies.

There has been interest in comparing photon and ion emissions. Relationships between the two secondary emissions have been noted in several studies (discussed in Chapter 2). An interesting result by Braun et al. [51] for 40 keV He^+ bombardment of Al showed a pronounced enhancement of the Al I intensity associated with a sudden increase in the erosion rate of Al and in surface exfoliation due to

radiation blistering. Application of photon emission to qualitative and, to some extent, quantitative analysis and depth profiling has been made, similar to those studies using SIMS.

1.3 CONCLUSIONS

It can be seen from the discussions outlined previously that there are unfortunate gaps in the current knowledge of ion bombardment processes. Much of the current research has been restricted to data gathering and the observation of qualitative phenomena. Relatively little understanding of the basic excitation/ionisation mechanisms has been gained in the fields of photon emission, secondary ion emission and secondary electron emission, where theoretical models are often very difficult to apply to the data. Nevertheless, some basic similarities emerge from the previous outlines, one of which is the regularity of use of the quasi-molecule molecular orbital model [7]. This may show the strength of the model for data explanation, due to the usually large number of possible curve crossing excitations, although its use in ISS, X-ray and Auger electron emission appears more justified. Predictive power using this model for secondary ion and photon emission appears difficult.

It is disappointing that, to date, these different fields have developed in some isolation. Relatively few studies have been devoted to more than one of the ion bombardment induced emissions and far less of these have been in an ultra high vacuum environment. Such an approach

would seem immediately obvious, an example being the complimentary nature of ISS and Auger emission for surface characterization in photon emission and SIMS studies. It may be useful to investigate the energy spectra of sputtered neutrals and ions in relation to that of the excited neutrals and ions as well as their dependence upon incidence energy and angle and surface conditions. Some attempts have been made to observe another of the emissions together with photon emission, notably; SIPS and SIMS [52, 53], SIPS and SEE [54], SIPS and ISS [55] and, more recently, SIPS, SIMS and ISS [56, 57]. There have also been attempts to compare SIPS with gas scattering [58] and SIPS, ISS and gas scattering [59]. MacDonald (Newcastle University) now has the facility to study SIPS, SIMS, ISS and SEE in the one system at UHV. It would appear that such investigations are needed in the future to tell us more about the excitation and ionisation processes. This thesis attempts to use ISS and SIMS as adjuncts to the study of photon emission from sputtered particles. These experiments will be discussed in Chapters 4, 5 and 6.

REFERENCES

[1] R. Behrisch, Nucl. Instr. Methods 132 (1976) 293.

[2] G.M. McCracken, Rep. Prog. Phys. 38 (1975) 241.

[3] G. Dearnaley, J.H. Freeman, R.S. Nelson and J. Stephens, Ion Implantation (Nth. Holland, Amsterdam, 1973).

[4] W. Heiland and E. Taglauer, Nucl. Instr. Methods 132 (1976) 535.

[5] R.L. Erickson and D.P. Smith, Phys. Rev. Letts. 34 (1975) 297.

[6] See, for example: N.H. Tolk, C.W. White, S.H. Dworetsky and L.A. Farrow, Phys. Rev. Letters 25 (1970) 1251.

[7] U. Fano and W. Lichten, Phys. Rev. Letters 14 (1965) 627
W. Lichten, Phys. Rev. 164 (1967) 131
M. Barat and W. Lichten, Phys. Rev. A 6 (1972) 211.

[8] N.H. Tolk, J.C. Tully, J. Kraus, C.W. White and S.H. Neff, Phys. Rev. Letters 36 (1976) 747.

[9] E. Taglauer, G. Marin and W. Heiland, Appl. Phys. 13 (1977) 47.

[10] D.J. O'Connor and R.J. MacDonald, Nucl. Instr. Methods 170 (1980) 494.

[11] D.J. O'Connor and R.J. MacDonald, Radiation Effects 45 (1980) 205.

[12] T.W. Rusch and R.L. Erickson, Inelastic Ion-Surface Collisions, eds. N.H. Tolk, J.C. Tully, W. Heiland and C.W. White (Academic Press, 1977).

[13] P. Sigmund, Phys. Rev. 184 (1969) 383.

[14] M.W. Thompson, Phil. Mag. 18 (1968) 377.

[15] J.J. Elich, H.E. Roosendaal and D. Onderdelinden, Radiation Effects 14 (1972) 93.

[16] P. Williams, Surface Sci. 90 (1979) 588.

[17] K. Wittmaack, Inelastic Ion Surface Collisions, eds. N.H. Tolk, J.C. Tully, W. Heiland and C.W. White (Academic Press, 1977).

[18] C.A. Andersen and J.R. Hinthorne, Anal. Chem. 45 (1973) 1421.

[19] P. Joyes, Radiation Effects 19 (1973) 235.

[20] J.M. Schroeer, T.N. Rhodin and R.C. Bradley, Surface Sci. 34 (1973) 571.

[21] Z. Sroubek, Surface Sci. 44 (1974) 47.

[22] M. Cini, Surface Sci. 54 (1976) 71.

[23] P. Williams and C.A. Evans Jr., Surface Sci. 78 (1978) 324.

[24] G. Slodzian, Surface Sci. 48 (1975) 161.

[25] M.A. Rudat and G.H. Morrison, Int. J. Mass Spectrom. Ion Phys. 30 (1979) 233.

[26] A. Benninghoven, Surface Sci. 53 (1975) 596.

[27] W. Husinsky, R. Bruckmüller, P. Blum, F. Viehböck, D. Hammer and E. Benes, J. Appl. Phys. 48 (1977) 4734.

[28] P.J. Martin and W.O. Hofer, Appl. Phys. 16 (1978) 271.

[29] A.R. Krauss and D.M. Gruen, J. Nucl. Mat. 85, 86 (1979) 1179, to be published 1981.

[30] P. Dawson, J. Vac. Sci. Techn. 16 (1979) 1.

[31] H.D. Hagstrum, Phys. Rev. 96 (1954) 325, 336.

[32] H.D. Hagstrum, Inelastic Ion-Surface Collisions, eds. N.H. Tolk, J.C. Tully, W. Heiland and C.W. White, (Academic Press, 1977).

[33] E.S. Parilis and L.M. Kishinevski, Sov. Phys. Sol. State 3 (1957) 885.

[34] E.J. Sternglass, Phys. Rev. 108 (1957) 11.

[35] G. Holmen, B. Svensson, J. Schou and P. Sigmund, Phys. Rev. B 20 (1979) 2247.

[36] R.A. Baragiola, E.V. Alonso and A.O. Florio, Phys. Rev. B 19 (1979) 121.

[37] F. Louchet, L. Viel, C. Benazeth, B. Fagot and N. Colombie, Radiation Effects 14 (1972) 123.

[38] P. Viaris de Lesegno and J.F. Hennequin, Surface Sci. 80 (1979) 656

[39] F. Thum and W.O. Hofer, Surface Sci. 90 (1979) 331 W.O. Hofer, Nucl. Instr. Methods 170 (1980) 275.

[40] D. Hasselkamp, A. Scharmann and N. Stiller, Nucl. Instr. Methods 168 (1980) 579.

[41] D.M. Hercules, Anal. Chem. 44 (1972) 106R.

[42] N.H. Tolk, D.L. Simms, E.B. Foley and C.W. White, Radiation Effects 18 (1973) 221.

[43] A.I. Bazhin, E.O. Rausch and E.W. Thomas, Phys. Rev. B 14 (1976) 2583.

[44] M. Zivitz and E.W. Thomas, Nucl. Instr. Methods 132 (1976) 411.

[45] M. Zivitz and E.W. Thomas, Phys. Rev. B 13 (1976) 2747.

[46] D.J. Nagel, J. Comas, K.W. Hill and A.R. Knudsen, Bull. Am. Phys. Soc. 21 (1976) 671.

[47] K.W. Hill, J. Comas, D.J. Nagel and A.R. Knudsen, Phys. Scripta 20 (1979) 652.

[48] R.S. Bhattacharya, K.G. Lang, A. Scharmann and K.H. Schartner, J. Phys. D: Appl. Phys. 11 (1978) 1935.

[49] M. Braun and B. Emmoth, Nucl. Instr. Methods 170 (1980) 585.

[50] A.I. Bazhin, E.O. Rausch and E.W. Thomas, J. Chem. Phys. 65 (1976) 3897.

[51] M. Braun and B. Emmoth, App. Phys. Lett 29 (1976) 545.

[52] R. Shimizu, T. Okutani, T. Ishitani and H. Tamura, Surface Sci. 69 (1977) 349.

[53] R.B. Wright, M.V. Liu and D.M. Gruen, J. Nucl. Mat. 76, 77 (1978) 205.

[54] J.G. Martel and N.T. Olsen, Nucl. Instr. Methods 105 (1972) 269.

[55] E.O. Rausch, A.I. Bazhin and E.W. Thomas, J. Chem. Phys. 65 (1976) 4447.

[56] R.J. MacDonald, E. Taglauer and W. Heiland, Appl. Surface Sci. 5 (1980) 197.

[57] E. Tagla er, W. Heiland and R.J. MacDonald, Surface Sci. 90 (1979) 661.

[58] K.J. Snowdon, G. Carter, D.G. Armour, B. Andersen and E. Veje, Radiation Effects 43 (1979) 201.

[59] E. Taglauer, W. Heiland, R.J. MacDonald and N.H. Tolk, J. Phys. B: Molec. Phys. 12 (1979) L533.

CHAPTER TWO

PHOTON EMISSION FROM SPUTTERED AND SCATTERED PARTICLES

In this chapter, experimental studies of photon emission from scattered particles, sputtered atomic particles and sputtered molecules will be reviewed with emphasis on those measurements which have yielded information on the excitation and de-excitation processes. The excitation processes leading to photon emission from these particles may be similar and should not be examined in isolation. Where relevant to the bombarded surface processes, photon emission from bombarded foils and from atom-atom collisions will also be discussed. Emphasis will be placed upon the experimental conditions and methods used, as these will be shown to be of particular importance and have often been poorly defined in the past.

2.1 INTRODUCTION

The field of photon emission from ion bombarded surfaces has been reviewed previously in some detail [1,2,3] and again recently in more specific terms by Tsong [4] and MacDonald et al. [5]. The review by G. Thomas [3] gives a good account of the history of photon emission from bombarded surfaces since it was first observed in 1897. Consequently, there is little need for a general literature survey here.

Each of these reviews primarily deals with the characteristics of photon emission from sputtered neutral

target atoms, although emission from sputtered ions has also been mentioned. Broad band and molecular emissions have also been noted and these will also be discussed here in a later section.

For targets with low mass and low ionisation coefficients such as Aℓ, Si and Ge, photon emission from ionised species may also be detected. Emission lines from $Aℓ^{++}$, Si^{++} and Ge^{+++} have been identified from 55 keV Ar^{+} bombardment of the elements [6]. These observations have usually been in the visible and near UV spectral regions. There has also been some interest in observing emission in the vacuum UV region as spectral lines from elements such as O,C are expected in this region. Knudsen et al. [7] have observed CℓI and CI emission lines in the vacuum UV region, elements which have not previously been observed by photon emission in the visible region. OI,II and III spectra have also been observed in the vacuum UV regions [8,9], although Braun et al. [8] used O^{+} as the incident ion and the emission lines are probably from backscattered oxygen. Reports of OII emission in the visible region have been claimed by Kerkdijk and Kelly [10] and Kelly et al. [11]. Examination of wavelength tables [12] would suggest that improved resolution is needed to identify these emissions to obtain more convincing data, although Kelly et al. [11] observe some internal consistency for cascading features of OII emission. These observations demonstrate the possibility of monitoring surface contamination during ion bombardment by observing photon emission.

Surface contamination or reactive gas environments have been shown to strongly influence the photon emission, particularly for neutral atom emission [1-5]. It is then vitally important that the surface of the bombarded target be clean to negate the observation of any artifacts caused by surface contamination. Equally important is the elimination of any artifacts produced at the edge of the bombarded spot where the surface may not be sufficiently cleaned by the incident beam - these are the so called "edge effects". Ideally, photon emission studies should be done using a rastered beam with the photon signal electronically gated to discriminate against edge effects (i.e. signal gated off when beam is at the edge of the rastered area) and at an ambient pressure such that increasing the pressure by at least one order of magnitude of a reactive gas does not influence the photon emission. Taken together, no report on photon emission induced by ion bombardment would satisfy these criteria. The second criterion, although more readily accessible, has not often been reported in the literature and when it has, only rarely do the intensity enhancement curves with reactive gas contamination show a plateau region at low exposure.

An alternative criterion may be developed whereby a "clean" surface may be defined as one where the arrival rate of beam ions exceeds the arrival rate of background gas atoms/molecules by at least a factor of 100. The arrival rate of beam ions may be easily deduced from the beam current density, and the arrival rate of background gas particles, γ, may be estimated as [13,14]:

$$\gamma = 3.535 \times 10^{22} \frac{P}{\sqrt{MT}} \text{ atoms/cm}^2\text{/sec} \qquad (2.1)$$

where P is the pressure in torr, M is the molecular weight in amu and T is the absolute temperature (°K). The cleanliness factor (C.F.) then becomes:

$$\text{C.F.} \approx \frac{x}{P} \cdot 1.3 \times 10^{-8} \qquad (2.2)$$

where x is the beam current density in $\mu A/cm^2$ and the cleanliness factor has been calculated using water vapour contamination (a common residual vacuum component) at room temperature. For a beam current density of 100 $\mu A/cm^2$, this requires that the base pressure be at least as low as 1×10^{-8} torr.

Justification of the boundary condition for a cleanliness factor of 100 (or about 1% of a monolayer coverage of contaminant) will be further discussed in section 3.2.

It is evident from the reviews of photon emission [1-5] and those of secondary ion emission [15,16], that there are similarities between the characteristics of the two emissions. That the enhancement of the photon emission with surface oxygen contamination was similar to the corresponding secondary ion enhancement, was pointed out by Kerkdijk et al. [17] and Blaise [18]. Martin et al. [19] attempted to correlate secondary ion and excited atom (and ion) yields as the incident beam sputtered through a Si/SiO_2 interface, although analysis of the ions and excited particles proceeded in different experimental chambers. Similar measurements were also made for oxygen adsorption upon Cr [20].

Shimizu et al. [21] improved upon these measurements by simultaneously monitoring the photon, secondary ion and Auger electron signals for 10 keV O_2^+ bombardment of Aℓ. The transient curves for ion and photon emission following oxygen exposure were found to be very similar and it was suggested that the mechanisms for excitation and ionisation were closely related.

Martin et al. [22] demonstrated a correlation between the AℓI channelling patterns, obtained by the bombardment of single crystal Aℓ with Ar^+, with the high energy component (100 eV) of the secondary ion yield. Brozdowska-Warczak et al. [23] claim some contrary results to the correlation of photon and ion yields when monitoring the sputtering yield and photon yields as a function of target temperature for 8 keV Ar^+ bombarded GaAs. Although the sputtering yield changed by about a factor of three, the GaI emission remained constant. However, caution must be stressed in the interpretation of these results as the surface contamination conditions may have changed with target temperature (Cleanliness Factor of 0.03) and the photon yield should have been correlated with the *ion* yield to provide information on the excitation/ionisation processes, rather than the sputtering yield (sum of the sputtered neutrals and ions).

Perhaps the greatest impetus to examine both photon and secondary ion yields together has been the "Local Thermodynamic Equilibrium" model of secondary ion emission. The LTE model was proposed by Andersen and Hinthorne [24] as an analytical method for the interpretation of sputtered ion intensities. The ion bombarded interaction volume was

assumed to be a region in LTE and the equilibrium concentrations to follow the Saha equations. The concentration of a given element in the target could then be calculated using the Saha-Eggert equation:

$$\frac{n^+ n_e}{n_0} = \frac{Z^+(T)}{Z_0(T)} \times \frac{2(2\pi mkT)^{3/2}}{h^3} \exp[-(E_r - \Delta E_r)/kT] \qquad (2.3)$$

where n^+, n_e and n_0 represent the concentrations of ions, electrons and neutrals, $Z^+, 2, Z_0$ are the respective partition functions, k is Boltzmann's constant, h is Planck's constant, E_r is the ionisation potential and T the plasma temperature. ΔE_r is the correction term arising from the depression of the ionisation potential in the plasma. The two unknowns, n_e and T, have been determined by measuring n^+ for two elements of known concentration in the target. The model has had success in SIMS analysis.

With the model enjoying some attention for secondary ion studies, its application to photon emission followed. Spectral analysis, assuming that the source of excitation was on LTE plasma, was first attempted by Kato et al. [25] in 1974 for Aℓ bombarded by 14 keV Ar^+. The temperature of a plasma in LTE may be determined spectroscopically by two methods [26]. Both methods are based upon the measurement of the emission lines which, for an LTE plasma, are given by

$$I_{ij} = A_{ij} h \nu_{ij} n g_i Z^{-1} \exp(-E_i/kT) \qquad (2.4)$$

where A_{ij} is the transition probability from the level i to the lower level j, ν_{ij} is the frequency of the resultant

radiation, n is the density of excited particles, g_i is the statistical weight of the level i (= 2J+1) and E_i is the excitation energy. Re-arranging and using relative intensity I_{ij} and relative transition probability we then have:

$$\ln (I_{ij}/g_i A_{ij} \nu_{ij} h) = \ln(n/Z) - E_i/kT . \qquad (2.5)$$

For constant n and Z, the plasma temperature may then be determined by a plot of $\ln(I/gA\nu)$ vs E_i for a selection of emission lines of the same type. Alternatively, the temperature may be derived by the measurement of the relative intensity of two emission lines and using equation (2.4) to solve for T. This method is subject to large errors unless the difference in excitation energies is large.

This latter method was used by Kato et al. [25] to obtain a plasma temperature characteristic of the Aℓ I emission of the order of 4000°K for Aℓ and 7000°K for $Aℓ_2O_3$. Martin and MacDonald [27] used the former technique for 55 keV Ar^+ bombarded Fe and Zn and obtained effective temperatures of the order 4000°K and 5450°K for Fe and Zn respectively. Excitation temperatures were also determined for Ar^+ bombarded Cr, Ni, Cu and Sn and were in the range 3300 - 5450°K. These "temperatures" were very similar to those derived for SIMS analysis using eq. (2.3). The straight line fit for the $\ln(I/gA\nu)$ vs E_i plots was interpreted by the authors as suggesting that the excited states of the sputtered atoms were populated as a Maxwell-Boltzmann distribution, with a characteristic excitation temperature of about 5000°K, i.e. that the probability of a species being

in an excited state with level i may be written

$$P(i) \propto g_i \exp(- E_i/kT) \quad . \qquad (2.6)$$

This characteristic temperature increased with oxygen exposure. SIMS analysis, without using standards, has also been proposed [28] by determining the plasma "temperature" spectroscopically and measuring the ion yields for use in equation (2.3).

The LTE model, however, has been strongly criticized. Snowdon [29] has criticized the model in its application to photon emission, based upon the validity conditions and establishment times for LTE to occur. There also exists some controversy as to the equivalence (or lack) of the "temperature" obtained from different elements sputtered from the same target [30 and references therein]. Detailed arguments will not be made here for or against the LTE model [see for example 5,15], however it is now believed that the model has no real physical basis as a description of the ion bombardment processes.

Unfortunately, the strong debate which surrounded the LTE model tended to obscure what were basically reasonable measurements, i.e. the population distribution of excited states. These measurements will be more closely examined in a following section. Also, the studies of the LTE model using ion and photon emissions did not produce evidence against a common excitation/ionisation process.

Recently, Williams et al. [3] have determined that the yields of secondary ions for Si and Ni are much greater than the absolute photon yields (both yields obtained under

oxygen saturation conditions). Although this result may be interpreted in terms of competing non-radiative de-excitations and electron exchange neutralisation of the ion (see next section), Williams et al. favoured a model whereby excited state formation near a surface was assumed less probable than ion formation, and that the phenomenological similarities between ion and photon emission were coincidental. This result tends to suggest that there is not a common excitation/ionisation process and that ionisation is not an extreme stage of excitation.

A conclusion from these results and those discussed in the reviews [1-5] is that, in general, the experiments so far reported have not been able to elucidate the basic processes of excitation and de-excitation. Rather, many studies have been made of interesting observations performed under far from ideal conditions. Those studies which have and are further expected to yield some information on the basic excitation and de-excitation processes are:

1) The non-radiative de-excitation processes
2) The measurement of emission functions
3) Excitation and the distribution of excited states
4) The determination of the energies of the excited states

and 5) The changes in the line emission characteristics with surface contamination.

Although the features of photon emission as outlined above are not well known, some elaborate models for photon emission characteristics have been developed. A good example of this has been the line profile modelling attempts.

The first attempt to simulate the emission line profiles for sputtered atoms was made in 1969 by van der Weg and Bierman [32]. The number of particles contributing to radiation with wavelength between λ and $\lambda + \Delta\lambda$ were taken as:

$$N(\lambda+\Delta\lambda)\partial\lambda = \iint [P_{exc}(\theta)][\sigma(\theta)][R(\theta,\alpha)]$$

$$[\delta\left(\frac{V_\beta}{C} - \frac{\Delta\lambda}{\lambda}\right)] \cdot 2\pi \sin\theta \, d\theta \, d\gamma \, d\lambda \qquad (2.7)$$

where V_β is the component of the particle velocity in the direction of observation (angle β to beam), θ is the scattering angle of the recoiled target atom, $P_{exc}(\theta)$ is the probability for excitation, $\sigma(\theta)$ is the differential cross-section, $R(\theta,\alpha)$ is the probability for non-radiative decay, α is the target angle and γ the azimuthal scattering angle. The difficulties, summarized in 1-4 above, are immediately apparent in equation (2.7). The excitation probability, P_{exc}, was assigned the form $P_{exc} \propto c_1 \cos^n(\theta)$ with $n = 0$, 1 or 2. The differential cross-section was approximated from a two body recoil sputtering event to be of the form : $\sigma(\theta) = c_2 \cos^{-2}\theta$. The non-radiative de-excitation term was taken in the form (see next section): $R(\theta,\alpha) = \exp\,[-\,(A/a\, v_n)]$.

The experimentally determined line profile for the CuI 324.7 nm line obtained by 80 keV Ar^+ bombardment of copper with $\beta = 90°$ and $\alpha = 30°$ was compared to that computed using equation (2.7). Reasonable agreement was obtained between the two profiles when $P_{exc}(\theta)$ was used in the form: $P_{exc}(\theta) = c_1 \cos\theta$ and the A/a value was used as the fitting

parameter with value $A/a = 2 \times 10^6$ cm/sec. These simulations were extended to other target materials using the same approach by Hippler et al. [33] although reasonable agreement between the measured and calculated profiles could not be found. Hippler et al. concluded that the assumption for the differential cross-section as used by van der Weg and Bierman needed to be modified to include a collision cascade sputtering component.

Considerable effort has also been spent in attempting to predict the emission line profiles for scattered projectile atoms [34 - 40]. The first attempt was by Parilis [34] in 1969, using an expression similar to (2.7). This model was later extended by Warczak et al. [35] to take into account thermal vibrations, double scattering of the incident ion and scattering from the second layer below the surface. No comparison with experimentally determined line profiles were made. The first attempt to compare predicted and measured emission profiles from scattered particles was made by Kerkdijk and E. Thomas [36] in 1973. The model for determining the line shapes was based upon two body scattering and a probability for excitation to a particular state equal to unity. This model was subsequently modified by Baird et al. [37,38] using the backscattering theory of McCracken and Freeman [41]. A non-radiative de-excitation term ($\alpha \exp(-A/a\, v_n)$) was included and the A/a value was used as a fitting parameter to produce reasonable agreement with the observed line profiles. Again, the probability for the incoming ion

to be neutralised into an excited state was assumed to be a constant. Olander et al. [39,40] have developed a more physically rigorous and complex model for the line shapes of the Doppler broadened lines. Again reasonable agreement was found between the experimentally determined line profiles and the predicted curves for appropriate choice of the A/a fitting parameter. The probability for excitation was taken from thin foil excitation studies and was assumed to be energy dependent and of the form

$$p(E) = 1/(1 + 0.028E) \qquad (2.8)$$

where E is the energy of the emerging particle in keV.

The initial hope that the measurement of the line profiles and comparison with theoretical predictions would elucidate the mechanisms for excitation and yield valuable information on the energy of particles, was not realised. An experimental reason for this is that observation of line profiles necessarily involves an integration over emission angle and energy distributions, thereby losing much information. More importantly, the models for determining the emission line profiles have all had significant weaknesses, particularly in the choice of the probability for excitation. Several different choices for the probability of excitation have been mentioned above and each of these choices has implied an equal population distribution over excited states. The distributions of excited states will be discussed in section 2.2.3. By the use of a very strong fitting parameter, $(\exp(- A/a\ v_n))$, agreement has usually been able to be made between

experimental and predicted line profiles.

These approaches would seem of little benefit until more basic information on the excitation processes for sputtered and scattered particles is understood. Each of the parameters related to the excitation process (1-5 as listed above) need to be thoroughly investigated. These are now discussed in detail.

2.2 PARAMETERS RELATED TO THE EXCITATION PROCESS

2.2.1 *The de-excitation processes*

The only method by which an experimental study of the bombardment induced excitation processes may occur is through the observation of the de-exciting particles. Radiative de-excitation may be described through the familiar decay law

$$I = I_0 \exp (- s/v \tau_i) \qquad (2.9)$$

where I_0 is the intensity observed at the point of excitation (surface), s is the distance travelled before radiative de-excitation, v is the excited particle velocity and τ_i is the lifetime of the excited state.

Photon emission may not be the only way in which the excited atom decays. It has been suggested that electron exchange transitions are a competing non-radiative de-excitation of the excited particles. Application of the electron exchange transitions model to sputtered excited atoms was first proposed by van der Weg and Rol [42,43] in

1965. The electron exchange processes have been discussed in detail by Hagstrum [44] and their application to photon emission studies has been discussed in reviews [1,2,3,5]. Although these processes have been described elsewhere [1,2,3], a brief outline of the different transitions will be included here.

Hagstrum [44] considered four possible transitions for a low energy (tens of eV) charged or excited particle approaching a surface: Resonance ionisation of an excited atom, Resonance neutralisation of an ion, Auger de-excitation of an excited atom and Auger neutralisation of an ion. These processes are shown schematically in Figure 2.1. The resonance transitions are a one electron exchange process whereby an electron from the particle tunnels to an unoccupied level in the surface electronic state (ionisation) or an electron from the fitted states of the metal is able to tunnel to an available state of the atom (neutralisation). The Auger processes are two electron transitions which may proceed via an exchange of electrons (de-excitation) or by non exchange of electrons (ionisation). Combinations of these processes have been proposed by Hagstrum and Becker [45] although the probability of multistage processes was expected to be less than that of any of the transitions shown in Figure 2.1.

The total transition rate for these processes has been approximated by the exponential form [46]

$$R_t(s) = A \exp(-as) \qquad (2.10)$$

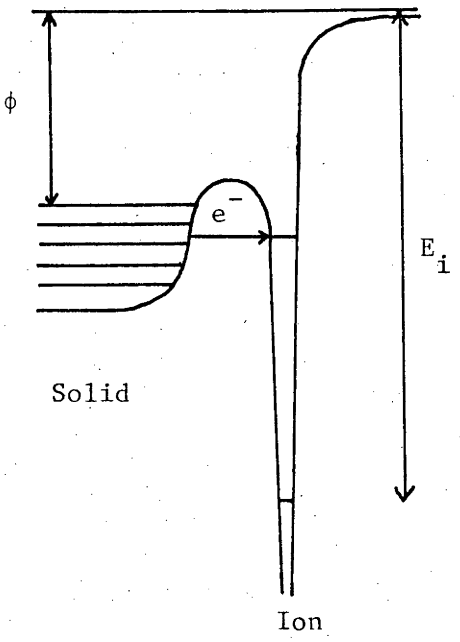

Resonance Neutralisation

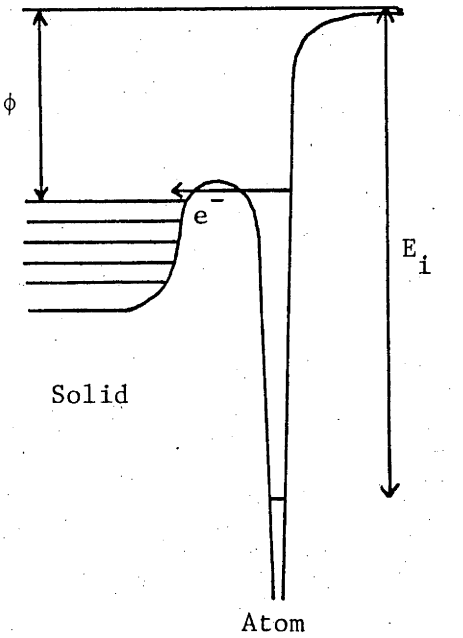

Resonance Ionisation

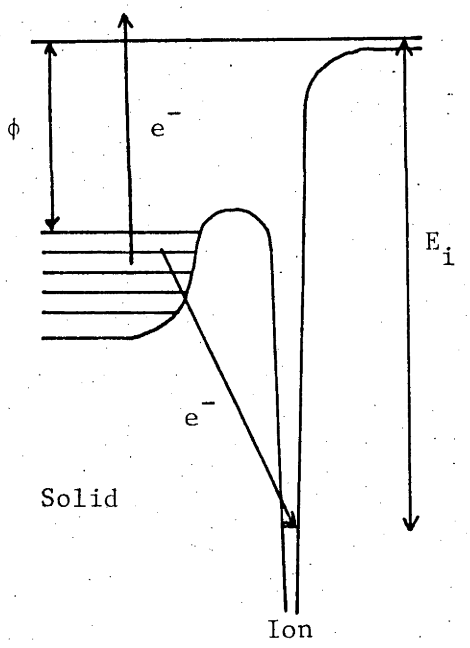

Auger Neutralisation

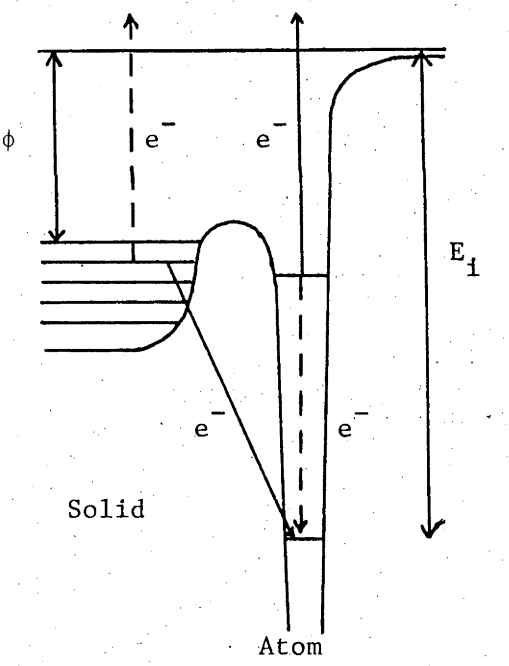

Auger De-excitation

Figure 2.1. The principal charge exchange processes after Hagstrum [44]. ϕ is the work function of the solid and E_i is the ionisation energy of the atom/ion.

where A and a are constants characteristic of the particular transition. The probability P for a particle with velocity component v_n normal to the surface escaping from the surface without undergoing a non-radiative transition then follows, [42]:

$$P(v_n) = \exp(-A/a\ v_n) \quad . \qquad (2.11)$$

Theoretical values for A(sec^{-1}) and a (cm^{-1}) have been determined for the different processes [46,47] and these are summarized in Table 2.1. The high values for A

TABLE 2.1

A and a values calculated for the different non-radiative transitions

Process	A(sec^{-1})	a(cm^{-1})	A/a (cm/sec)
Resonance transitions	$1-5\times10^{19}$	$2-3\times10^{8}$	5×10^{10}
Auger neutralisation	6×10^{14}	4×10^{8}	1.5×10^{6}
Auger de-excitation	1×10^{17}	7×10^{8}	1.4×10^{8}

for the non-radiative transitions when compared to the lifetimes for radiative decay ($10^{7}-10^{9}$ sec^{-1}), indicate that the non-radiative transitions would be expected to be the dominant process when energetically possible.

More recently, Grozdanov and Janev [48] have calculated A/a values for the resonance ionisation transition of several excited states near a Cu surface. H, He and Cu excited states were considered and the derived

A/a values were in the range 3×10^6 cm/sec for the CuI $4P^3P_{\frac{1}{2}}$ state to 6.9×10^8 cm/sec for the H(4s) excited state. The derived A/a values were found to vary with the excited state considered, for the same atom. These values were very similar to those determined by line profile calculations. The A/a value for the CuI $4P^2P_{3/2}$ state determined by van der Weg and Bierman [32] for 80 keV Ar^+ bombardment of Cu was 2×10^6 cm/sec, which is very similar to that found for another CuI line by Grozdanov and Janev. Agreement was also found between the calculated value for the He 4^3D state when compared to that derived by line profile simulation by Baird et al. [38]. The agreement between the two values for the He 3^3D state, however, was poor. It should be emphasized that the use of the A/a term for non-radiative transitions is a powerful fitting parameter, particularly for large angles of incidence. By varying the A/a value by as little as 50%, the position of the calculated intensity peak has been found to shift by up to 0.4nm, with the resulting line profile bearing little resemblance to that measured experimentally [38].

2.2.2 *Emission function measurements*

Few measurements have been made to determine the behaviour of the photon emission from sputtered particles with changing incidence energy. The measurement of these emission functions for several sputtered species was first made in 1971 by White and Tolk [49]. Several more recent measurements have also been made [50,51,52]. The measured

emission functions for the CuI 324.7 nm line for Ar^+ and N_2^+ bombardment of Cu at 45° incidence are shown in Figure 2.2. Similar curves to Figure 2.2 were also found for SrI and SiI emission functions for Ar^+ bombardment. An excitation threshold was observed at low incident energies and reactive gas bombardment was found to change the observed emission function.

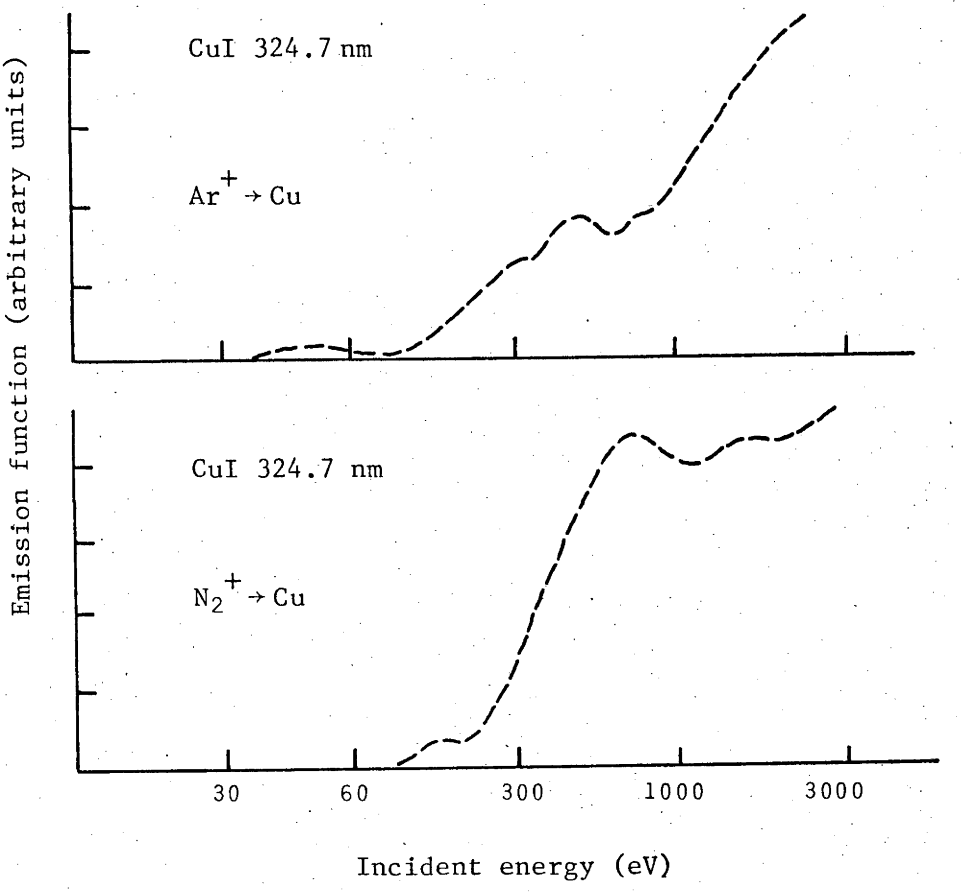

Figure 2.2. Emission functions for the CuI 324.7 nm line produced by ion-surface collision (a) $Ar^+ \rightarrow Cu$ and (b) $N_2^+ \rightarrow Cu$. The curves are plotted independently in arbitrary units [49].

The excitation function behaviour was modelled by White and Tolk using a sputtering model based upon binary collision sputtering, assuming the probability for excitation was a constant and that non-radiative transitions may influence the excited sputtered particles. The high energy part of the emission function could be simulated using an A/a value of 2×10^6 cm/sec for the CuI line (similar to that determined by line profile simulation). The deviation between the predicted and observed emission functions was concluded to represent a change in the excitation function. The derived excitation function was proposed to have a low energy peak around 100 eV incident energy and to decrease with increasing energy. The form of the derived excitation function, however, is then critically dependent upon a model for predicting the emission function which contains many strong assumptions.

No attempt was made by White and Tolk to determine the influence of varying the incidence energy. The experimental conditions for the study were unlikely to have been sufficient for a clean surface and the cleanliness factor was probably between 0.05 and 6.

Bhattacharya et al. [50] also measured emission functions although incident energies far higher than expected threshold values were used. Some of these curves for SiI, II and III are shown in Figure 2.3(a). The measurements were made for normal incidence bombardment. The emission functions for the SiI, II and III lines are shown to be different and are also different for lines of the same species. By contrast, the behaviour of the emission

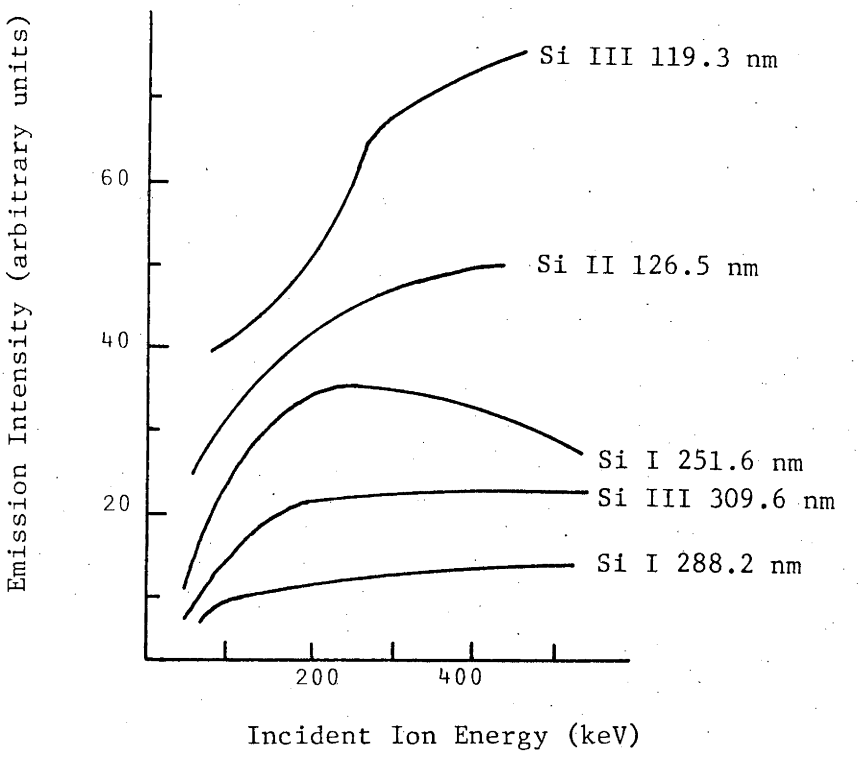

Figure 2.3(a). Emission function measurements for various Si emission lines for Ar^+ ions at normal incidence (from [50]).

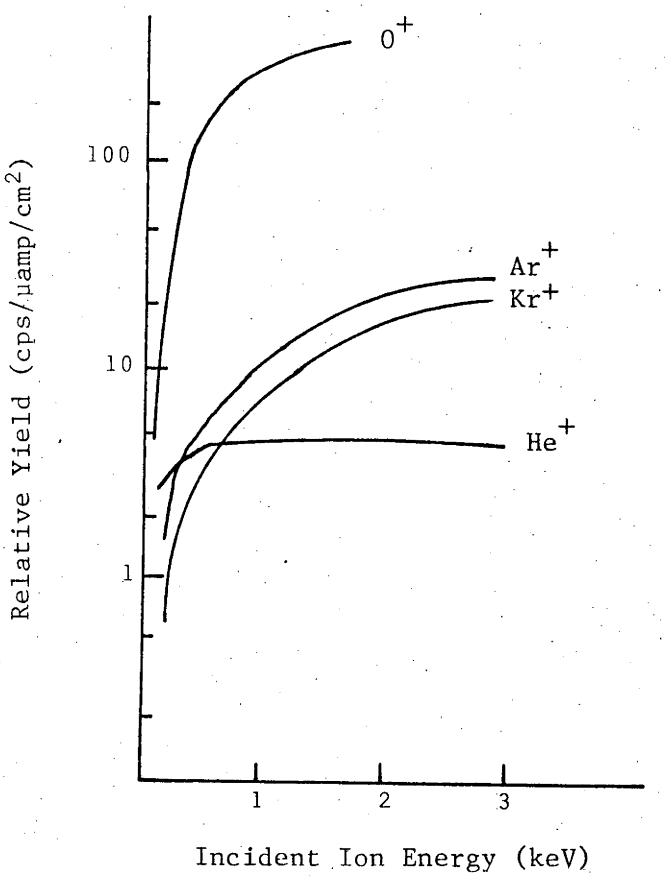

Figure 2.3(b). Emission function measurements for the Be I 234.6 nm line for various normally incident ions (after [52]).

functions for the BeI and BeII lines for normal incidence bombardment by Kr^+,Ar^+,Ne^+ and He^+ were found to be very similar [51]. He^+ bombardment was found to produce significantly different emission function curves than Kr^+,Ar^+ or Ne^+ over the energy range as shown in Figure 2.3(b) [52]. The surface conditions during bombardment for these studies were expected to be clean. Wright et al. [52] found that the BeII emission function for contaminated surface conditions showed a distinct "hump" (similar to Figure 2.2(b)), whereas under clean surface conditions, a smoothly increasing emission function was found.

The measurement of emission functions for the sputtered excited states in the incident energy range near that of the threshold and under UHV conditions would appear to be particularly important. Similarly, the influence of the incidence angle on the emission function threshold and shape may also be of importance in yielding information on the excitation processes.

The measurement of the emission function for excited scattered particles has been more thoroughly studied [36-38,53-58]. The basis for such measurements is that the emission coefficient, γ_{ij}, for the decay from state i to state j, is related to the absolute yield of photons of wavelength $\lambda(J_{ij})$ via:

$$J_{ij} = \gamma_{ij} \cdot I_B \qquad (2.12)$$

where I_B is the beam current. In the absence of non-radiative transitions, the absolute yield of photons of wavelength λ may be related to the excitation coefficient

γ_i via:

$$J_{ij} = \gamma_i . I_B . b_{ij} \qquad (2.13)$$

where b_{ij} is the branching ratio which determines the probability of the decay from state i to state j over the probability for all allowed decays to lower states from level i. It is usual to consider only the emission function as there are considerable difficulties in deriving the excitation function.

The emission functions for photon emission from scattered particles have been found to depend upon the angle of incidence, the incident projectile energy and the target species. Examples of these dependencies are shown in Figure 2.4. Kerkdijk and Thomas [36] found that the emission functions for the H_α, H_β and H_γ lines produced by H^+ bombardment of Cu at 45° incidence showed very different behaviour over the energy range 4 - 10 keV (base pressure 2×10^{-9} torr). In contrast to this result, Leung et al. [57] found that the emission functions for the H_α, H_β, H_γ, H_δ and H_ε lines for H^+ and H_2^+ bombardment of Mo at normal incidence were very similar over the energy range 1 - 6 keV per nucleon, although the emission coefficient decreased in magnitude for the successive lines: $\alpha > \beta > \gamma > \delta > \varepsilon$ (base pressure 10^{-10} torr). Leung et al. found that the emission was particularly sensitive to the surface contamination and this, together with the different incidence angle used, may account for the discrepancy with the earlier work.

The emission coefficients were found to be characteristic of the incidence energy per nucleon of the

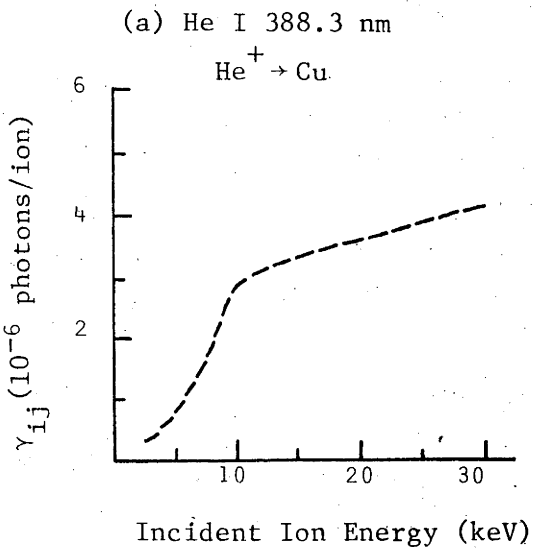

Figure 2.4(a). Emission function for the He I 388.3 nm line for $He^+ \rightarrow Cu$. The incident angle was 45° (from [38]).

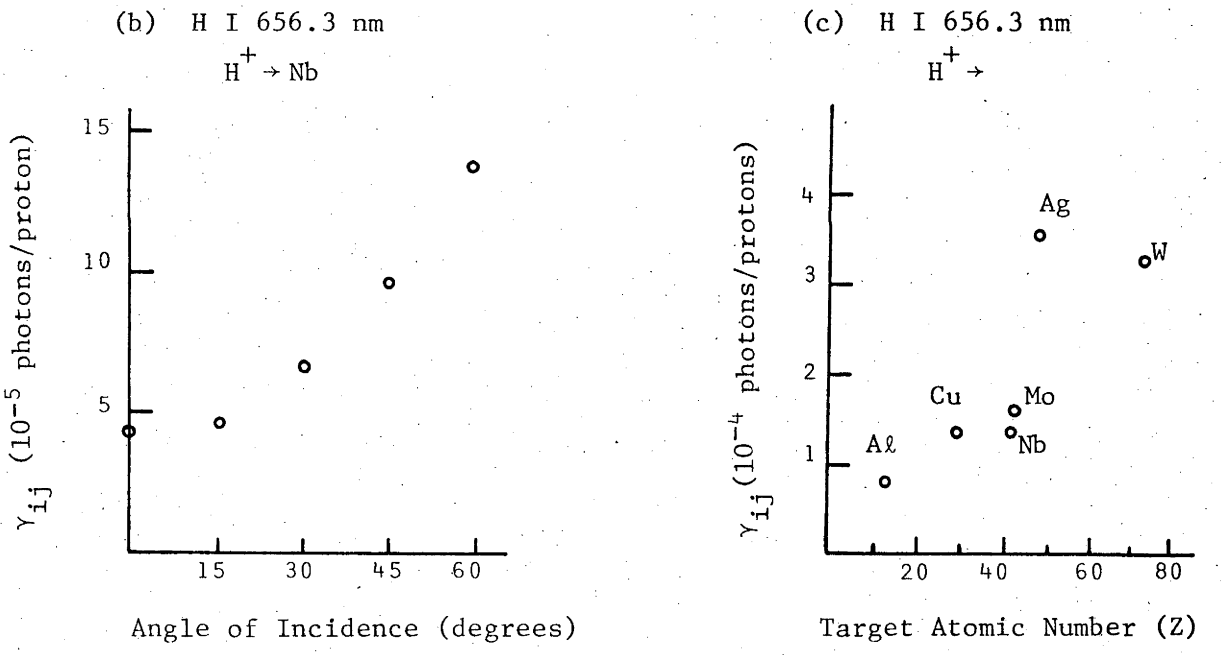

Figure 2.4 (b) Emission coefficients for the H I 656.3 nm line for 25 keV $H^+ \rightarrow Nb$ for varying incidence angle [38].

(c) Emission coefficients for the H I 656.3 nm line for 25 keV $H^+ \rightarrow$ different target elements [38].

bombarding species and independent of the incident charge (H^+ and H^- were used) and incident mass (H^+, H_2^+, and H_3^+ were used) [57]. This behaviour was also noted by Rausch and Thomas [55]. No oscillatory behaviour was found for the HeI 388.2nm emission function as has been found for the ion yield of scattered He^+ from a lead target [58].

Emission function measurements have not been, as yet, extended down to incident energies at which a threshold may be expected. Such measurements would be of interest.

2.2.3 *Excitation and the distribution of excited states*

The report by Martin and MacDonald [27] that the ion bombardment induced excitation appeared similar to the excitation produced by a plasma in Local Thermodynamic Equilibrium provoked strong response and debate [28-30, 59-72]. Tsong [59] correctly pointed out that when using a photomultiplier detector, the intensity must be expressed as $Nh\nu$ to conform to energy units where N is the detected count rate. Equation (2.5) then becomes

$$\ln\left(\frac{N}{g_i A_{ij}}\right) = \ln\left(\frac{n}{Z}\right) - \frac{E_i}{kT} \quad . \qquad (2.14(a))$$

This may also be expressed in terms of oscillator strengths (f_{ji}) as the oscillator strengths are more frequently tabulated than the A_{ij} values. (2.14(a)) then becomes

$$\ln\left(\frac{N\lambda^2}{g_j f_{ji}}\right) = \ln\left(\frac{n}{Z}\right) - \frac{E_i}{kT} \quad . \qquad (2.14(b))$$

This correction was found to result in less scatter of the data points in the $\ln\left(\frac{N}{gA}\right)$ vs E_i plots [28].

Kelly et al. [62,63] have been critical of this method for specifying the photon yield and have preferred to consider the total yield from a given upper state to all possible lower states using the expression

$$\text{Total yield} \propto P(i) \tag{2.15}$$

where P(i) is determined using equation (2.6). By plotting $\ln(\text{Total yield}/g_i)$ as a function of the excitation energy, Kelly et al. were able to determine "temperatures" for a variety of bombarded targets which were in the range 3700 - 4600°K. This temperature range was also consistent with that determined using secondary ion studies.

Snowdon [66] and Loxton et al. [72] have shown that the method of Kelly et al. was similar to that of Martin and MacDonald [27] but had one fundamental difference. Martin and MacDonald assumed that both excitation and de-excitation occurred within the plasma volume thought to be in LTE, whereas Kelly et al. have assumed the excitation source as one in LTE and that the de-excitation occurs in free space outside the plasma region. The observation of decay curves extending well in front of the target surface indicates that the de-excitation occurs away from any "LTE plasma source", as the "plasma" density away from the surface would be insufficient to allow LTE [66].

Following Loxton et al. [72], the relative initial population of level i from the sputtering source of excitation (assuming an LTE plasma is formed), n_i^s, will be:

$$n_i^s = n^s \times (\text{probability for an excited atom to be in the excited state i})$$

$$= n^s P(i) \qquad (2.16)$$

where n^s is the total number of sputtered atoms in excited states. Assuming that the population distribution of excited states follows a Boltzmann distribution, (2.16) becomes

$$n_i^s = n^s g_i \exp(-E_i/kT) . \qquad (2.17)$$

The photomultiplier count rate for the line emission with wavelength λ_{ij} will then be

$$N = n^s g_i \exp(-E_i/kT) b_{ij} \qquad (2.18)$$

where the branching b_{ij} is defined as

$$b_{ij} = A_{ij}/\Sigma_k A_{ik} = A_{ij} \tau_i \qquad (2.19)$$

and $\tau_i = 1/\Sigma_k A_{ik}$ is the natural mean lifetime of the upper level i.

It may be necessary to correct for cascading processes repopulating the level i from higher levels by the expression:

$$n_i = n_i' - \Sigma_h n_h' \cdot b_{hi} \qquad (2.20)$$

where n' is the relative initial population of the level uncorrected for cascades. Equation (2.18) reduces to the following after substituting (2.19) and re-arranging:

$$\ln\left(\frac{N}{g_i A_{ij} \tau_i}\right) \propto -E_i/kT . \qquad (2.21)$$

By summing the photon emission from all decays from the

upper level i, in the manner of Kelly et al. [62,63], the branching ratio term is removed from equation (2.18) leaving:

$$\sum_k N_{ik} = \text{Total Yield} \propto P(i) \quad ,$$ which is the expression used by Kelly.

The derived plots (denoted "reduced intensity plots" hereafter) using (2.15) are subject to difficulties imposed by the observation of all transitions from the upper level (some may occur outside the detection limits of the system used) while those using (2.21) require the knowledge of accurate branching ratios for each of the levels used in the plot.

An alternative method of determining an excitation "temperature" is to study the vibrational and rotational levels of sputtered molecules. G. Thomas et al. [71] have made such a measurement for the rotational and vibrational population distributions in the $A^2\Delta - X^2\pi$ CH radical transition sputtered by 10 keV Kr^+ bombardment of an acetone chemisorption layer on Si. An apparent temperature of 4500°K was obtained.

The criticisms of the LTE model as applied to the sputtering source of excitation have previously been outlined. As a consequence, the values of the apparent "temperatures" obtained from the LTE plots and studies of the vibrational and rotational population distributions are merely fitting parameters with no physical basis in an LTE model. This representation of the excited state distribution is certainly not unique, nor is the distribution over excited states characteristic only of the sputtering source in ion bombardment interaction.

Snowdon et al. [67,68] have shown that for 50 keV Ar^+ bombarded Zn, the plot of ln (statistical weight normalised relative level population) vs the excitation energy of the Zn I level, could be fitted to a Boltzmann relation with parameter T=5450°K or to an E_i^{-x} relation with x = 13. Over the limited range of excited levels of Fe, similar plots could be modelled using atom-atom excitation equations such as

$$n_i \propto g_i (n_i^*)^{-x} \tag{2.22}$$

where n_i^*, the effective quantum number, is defined through $E_i = - Z_c^2 R(n_i^*)^{-2} + E_\infty$, with E_∞ the binding energy of the state, Z_c is the total core charge, R is Rydberg's constant and x is thought to be related to wave function normalisation. Alternative expressions could also be modelled to the data [67]. Additionally, Snowdon et al. [69] were able to fit the relative level populations of Zn I levels excited by $Zn^+ \rightarrow Ar$ and $Zn^+ \rightarrow Zn$ gas phase single collisions at energies of 50 keV and 25 keV to that obtained by the sputtering source. Gas phase single collisions could certainly not be described in LTE terms.

Jensen and Veje [73] were able to obtain curves for the relative level populations of LiI excited by 50 keV Xe^+ bombardment of Li as a function of the principal quantum number n as shown in Figure 2.5. It was noted that similar curves were also obtained when the relative level populations were plotted as a function of the effective quantum number or the excitation energy. Andersen et al. [74] have found that plots of the relative population versus

the effective quantum number and also the orbital angular momentum number ℓ, are strikingly similar for Mg II lines excited by 50 keV Xe^+ bombardment of Mg and by 40 keV Mg^+ → He collisions. Andersen et al. concluded that excitation could be pictured as arising from the ejection of ions from the solid followed by the capture of one or more electrons from the "Sommerfeld electron gas" which may follow the ion on its outward journey.

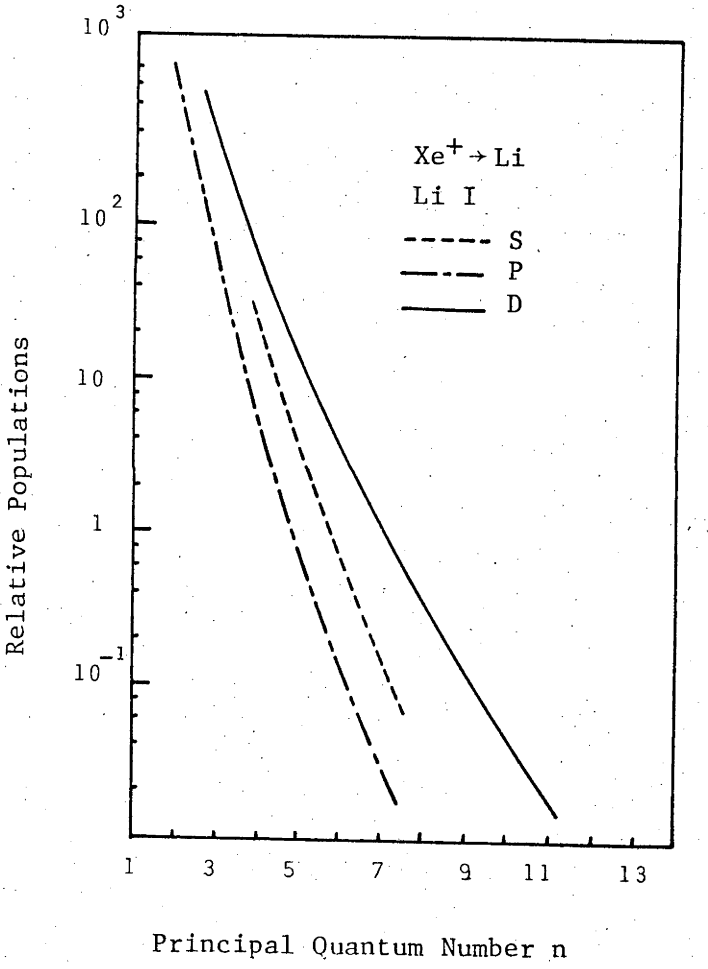

Figure 2.5. The relative level populations in Li I, corrected for cascades, as a function of the principal quantum number n [73].

Comparison of the excitation for sputtering and for gas phase collisions and similar excitation sources would seem particularly appropriate in terms of the "quasi-molecule formation" model for excitation by level crossings. Emission function measurements and excitation processes for atom-atom collisions are then also of relevance [see for example, 75].

Leung et al. [57] have studied the relative excited state populations for scattered particles (hydrogen). The dependence of the excited state populations on the principal quantum number n was noted to be very close to an n^{-6} behaviour. The reason for this dependence was not known. Again comparison may be made with other excitation sources. Andresen et al. [76] have studied beam-foil excited Li, Be and Mg projectiles and found that the relative population for different Rydberg levels of the same term series decreases, in most cases, near $(n^*)^{-3}$. This behaviour is also noted in ion-atom single collision studies. The relative populations of levels of the same charge state and with the same core configuration were unaffected by changing projectile energy. Level populations had been earlier found to depend upon the foil angle [77]. The dependence of the excited state populations on levels of the scattered atoms has not been investigated to compare with that obtained from beam-foil excitation. Obviously there is a need for further information on the dependence of the excited level populations on such parameters as the incidence energy and angle for both scattered and sputtered particles to facilitate further

comparisons with these other excitation sources.

Comparison of sputtering and scattering excitation with beam-foil excitation has recently led to the observation that the emission from scattered particles may be polarised. This is particularly evident as grazing incidence [78,79 and references therein]. Polarised emission results from excitation leading to non-statistical populations of sublevels resulting in circularly or linearly polarised emission. The search for polarised emission from sputtered atoms [57,80] and the initial results from scattered particles [36-38] have observed negative results. Andrä [81] reported the observation of circularly polarised light for Ar II emission from Ar^+ bombardment of Cu in 1975. The observation and incident beam geometry were such that the detector viewed asymmetrical excitation, resulting in the observation of polarised emission. Although the excitation leading to the uneven populations of the sublevels is not understood, polarisation studies have the potential to contribute significantly to the understanding of the excitation process. The models which have been proposed to account for the observed polarised emission indicate that the excitation occurs at the last collision as the incident particle leaves the surface.

It is now generally believed that excitation of the sputtered particle also takes place at the surface (perhaps at the last collision) or as the escaping particle passes through the field of the target surface. The

existence of excited states within the solid (i.e. excitation takes place within the solid and the particle subsequently escapes from the solid retaining its excitation) may be rejected for all but the most tightly bound states on the grounds of the dimensions of the excited particle.

The excitation process has usually been considered to be modified by the non-radiative de-excitation process as discussed in section 2.2.1. The $\exp(-A/a\ v_n)$ term has been used as a fitting parameter in modelling line profiles and emission functions for sputtered excited particles, modelling the SIMS energy spectra of secondary ions [28] and in determining the yields of scattered ions in ISS studies [82]. A survey of the A/a values obtained from the photon emission studies shows a striking similarity over the range of excitation levels, incident energies and projectile and target combinations used. Leung et al. [57] have shown that the A/a values obtained by H^+ bombardment of clean Mo for the different excited states of H with principal quantum number from $n = 3$ to $n = 7$ are the same. Baird et al. [37,38] found that the A/a values obtained for the H_α Balmer line for bombardment of Cu, Nb and Mo were all very similar and were of the same value as that obtained for the He I 587.6 nm line for the He^+ bombardment of the same targets. The A/a values for the He I 587.6 nm and He I 447.2 nm lines for He^+ bombardment of Nb were found to be 1.3×10^8 and 0.8×10^8 cm/sec respectively although the two excitation levels are separated by 0.7 eV. This lack of sensitivity to the

excitation state, excited species and target/projectile combination for the observed A/a values is surprising.

However, it has not been established that the excitation and de-excitation events preceeding photon emission may be separated. Indeed it may be expected ~~that~~ for the close distances from the surface over which the non-radiative process are expected to be important (Table 2.1) that the excited state may not have evolved from the atomic states characteristic in the solid. In the case of the quasimolecule formation model, evolution of the excited state may occur at distances from the surface which are large enough to be free of the influence of non-radiative transitions. An attempt has been made to depict the excitation event along the lines of an exponential velocity excitation [83]. Such an approach would obviate the need to introduce the non-radiative processes, but requires further justification through, for example, impact parameter dependence measurements for the excitation process.

2.2.4 *The kinetic energies of the excited particles*

Emission line profiles and wavelength shifts of the Doppler broadened lines and the intensity decay curves in front of the target surface, contain information on the velocities of the particles contributing to the observed radiation. Unfortunately, observation of the photon emission involves an integration over the energy distribution

and the sputtering trajectories of the excited particles and this obscures much of the information which otherwise may be obtained.

Although line profile simulation has yielded little information on the kinetic energies of the excited particles [section 2.1], measurement of the line profiles and line shifts may provide some information on the trends of the kinetic energies of the excited particles. Van der Weg and Bierman [32] have measured the wavelength shifts and line profiles of the CuI 324.7 nm line for changing angle of incidence and these are shown in Figure 2.6. The wavelength shifts and the wings of the Doppler broadened lines shown in Figure 2.6 demonstrated that high kinetic energy particles contribute significantly to the observed emission. The 0.04 nm line shift shown in Figure 2.6(b) corresponds to 450 eV excited Cu atoms. Excitation was proposed to occur in a binary collision event leading to the ejection of the excited Cu atom. It should be noted that these measurements were made for high angles of incidence (i.e. more towards grazing). Figure 2.6(b) was then interpreted in terms of an increasing probability for binary collision sputtering as the incidence angle approached grazing, resulting in an increased wavelength shift and line width.

Two contributions to the kinetic energy distributions of sputtered excited atoms may be considered. The first contribution is that from the binary collision sputtering as mentioned above, where the sputtered particle has a high kinetic energy of the order of several keV, for medium energy ion bombardment. The second contribution may arise

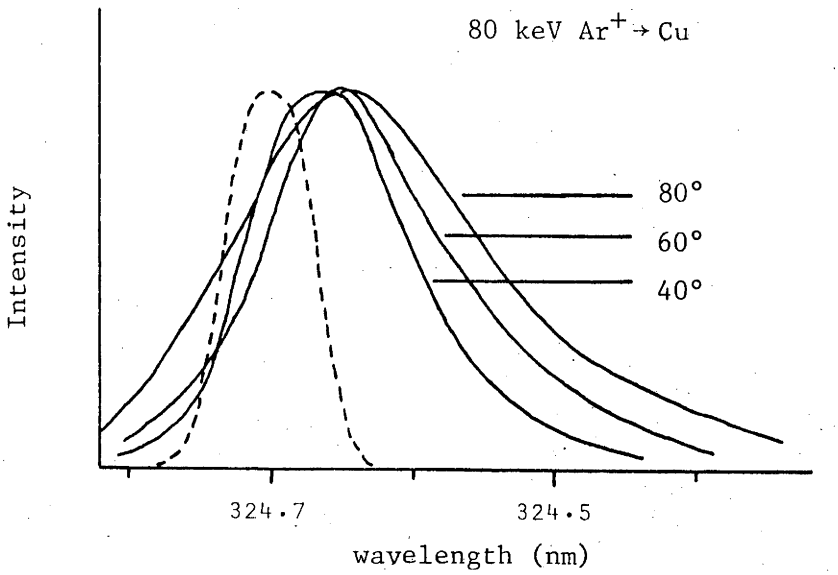

Figure 2.6(a). Line shapes of the CuI 324.7 nm line for different incident angles. The intensities are normalised and the lines compared to the unshifted reference line [32].

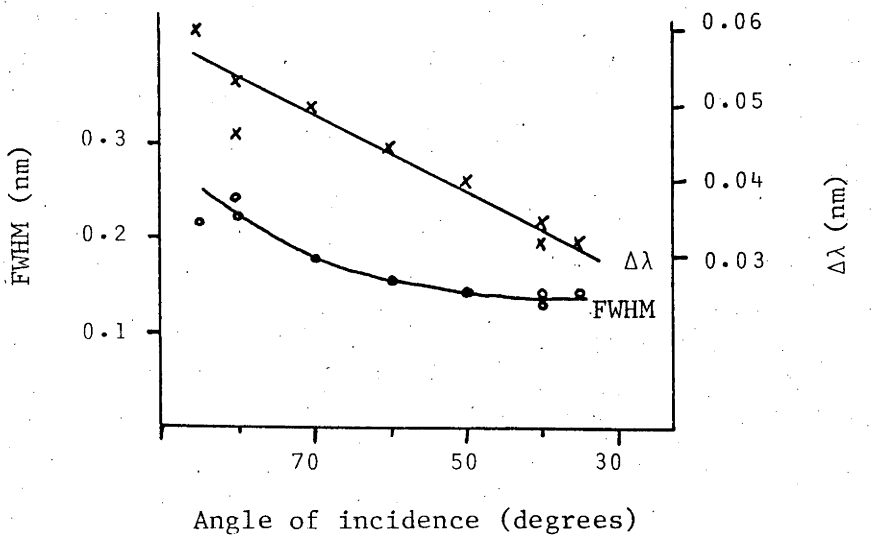

Figure 2.6(b) The derived wavelength shift ($\Delta\lambda$) and FWHM of the CuI 324.7 nm line with different angles of incidence [32].

when the collision cascade initiated by the primary knock-on atom intersects the target surface and passes enough energy to the surface atom for it to escape from the surface. Sputtered atoms from the collision cascade may have energies from several eV up to high energies, where the energy distributions are expected to follow an E^{-2} dependence (see section 1.2.2). The energy distribution of sputtered *excited* atoms may not necessarily follow this dependence. Van der Weg and Bierman [32] assumed that low energy excited particles sputtered by collision cascade processes did not contribute to the observed radiation, due to the high probability for non-radiative decay for these slower atoms (equation 2.5).

The collision cascade component contributing to the observed emission is shown by the channelling patterns for the bombardment of single crystal targets [22,84]. By measuring the channelling depth and width, van der Weg et al. [84] concluded that the particles emitting atomic lines originated from a larger depth, on average, than the particles contributing to the ionic emission lines. Martin et al. [22] also observed a channelling pattern for the Aℓ single crystal, even when the surface was expected to be covered with an amorphous oxide layer. It was concluded from this observation that the sputtered neutrals originated from below the surface amorphous oxide layers.

The energies of particles contributing to the observed emission have also been estimated by observing the photon intensity decay in front of the surface. A method for analysis of these curves was initially borrowed

from beam-foil spectroscopy where it was used to measure the lifetimes of the excited states. The intensity distribution at a distance x downstream of the foil is given by:

$$N(x) = N_0 \exp (- x/v \tau_i) \qquad (2.23(a))$$

where N_0 is the intensity at the foil surface and v is the excited particle velocity. For a sputtering source where the observation of photon emission integrates over the energy distribution and exit angles of the excited particles, the expression is used in modified form:

$$N(x) = N_0 \exp(- x/\bar{v} \tau_i) \qquad (2.23(b))$$

where x is the perpendicular distance from the surface and $\bar{v}$ is an "effective" velocity term. The decay curve analysis using (2.23(b)) may be severely influenced by cascading effects.

By measuring photon decay curves for several TiI lines emitted during bombardment of Ti by 20 keV Ar^+ and by applying equation (2.23(b)), Gritsyna et al. [85,86] concluded that the TiI spectrum was emitted by two different groups of titanium atoms. The first group of atoms had an effective energy of about 5 keV and were responsible for the emission from the more highly excited levels of Ti, whereas the second group of atoms had an effective energy of about 10-100 eV and corresponded to those atoms with upper energy level less than the first group. These results were interpreted using the resonance ionisation process discussed in section 2.2.1.

The excited levels of the atoms giving rise to the emission by "slow" Ti atoms were proposed to lie opposite the filled conduction band of the Ti metal, while the excited levels of the "fast" group of Ti atoms were proposed to lie opposite the empty conduction band. The resonance ionisation process, which would be expected to remove the excitation of the low energy particles, would be blocked for the states opposite the filled conduction band but not for the states opposite the empty conduction band. A "slow" and a "fast" average velocity would then be expected for the two types of excited atoms depending upon their excitation energy. Gritsyna et al. estimated that the Fermi level for Ti would lie between the excitation energies of the two groups of particles, i.e. between 3.8 - 4.15 eV. This value was consistent with that obtained by other measurements. Using a similar method, the widths of the conduction bands of CaO, NaCℓ and LiF have also been estimated [85,87].

Braun et al. [8] measured the decay curves in front of the Aℓ target for the Aℓ I 396.2 and 309.2 nm lines and the 358.7 nm Aℓ II line induced by 300 keV Xe^+ bombardment. Over the larger range of distance from the target used, the decay curves did not show straight line fits, but exhibited a strong concave upwards curvature. Departures from linearity on the semi-logarithmic plot had been observed previously [85] and this departure had been attributed to the influence of cascading. Braun et al. considered that these concave curves could represent a sum of exponentials although it may have been related to the energy distributions of the excited

atoms. The tails on the decay curves were attributed to excited atoms created by binary collision type sputtering.

Recently there have been several models proposed to include the estimated energy and angular distributions of the excited particles in the decay curve method for determining the energies of the excited particles. These models have been based upon a collision cascade sputtering model. Each has used a similar approach, considering an isotropic distribution of sputtered particles resulting from bombardment at normal incidence. Mladenov and Braun [88] simulated the decay curve by summing the contributions of 50, 100, 500, 10^3, 5×10^3 and 1×10^4 eV particles, to the photon emission with the assumptions of (i) cosine distribution of sputtered excited atoms, (ii) E^{-2} kinetic energy distribution of excited particles and (iii) the excited levels were depopulated according to $\exp(- s/v\tau)$. The derived curve showed qualitative agreement with the experimental curve and it demonstrated that high kinetic energy particles dominate the decay at large distances from the surface.

Carter et al. [89] used the surface normal energy distribution function, $F(E_\perp)dE = \frac{dE}{(E_\perp + U)^2}$, and have included radiative and non-radiative de-excitation to calculate both the integral photon yield (for the situation where all the space in front of the target surface is observed) as well as the differential photon yield (where observation is through a small slit). By using the surface normal energy distribution function, the angular distribution of sputtered

particles was included in the calculation. The photon yield was determined as a function of the parameter z, where z is proportional to the normal distance x from the target. A functional form for the decay curve was obtained. A principal assumption was that the sputtered particle must surmount the potential energy barrier U to escape the substrate.

This analysis also showed qualitative agreement with the experimental curves and additionally, the potential energy barrier U could be determined from the derived z vs x curves. Dzioba et al. [90] have extended this model, essentially by replacing U by the parameter E^*, where E^* is the minimum energy of excited particles *escaping from the surface*. E^* may be determined from the z vs x curves and is mathematically similar to U.

Dzioba et al. have used an excitation function which is a step function at energy E^*, similar to the step function at 50 eV used by Mladenov and Braun [88]. However, E^* was then treated as a variable, characteristic of each transition studied. The energy distribution of the sputtered particles was taken as proportional to E^{-2} rather than in the full form: $2E/(E+U)^3$ [89]. This approximation is valid where $E^* >> U$. Including the radiative and non-radiative de-excitation terms in their usual forms, the integral photon yield for the case where the target is viewed over an edge is then [40]:

$$Y^{int} = K \int_{E^*}^{\infty} \int_{0}^{\pi/2} E^{-2} . \exp\left(- \frac{a + \gamma_i \, xm^{3/2} \, 2^{1/2}}{E^{1/2} \cos\theta} \right) \sin\theta \cos\theta \, d\theta \, dE \qquad (2.24)$$

where a is associated with non-radiative processes, γ_i is the

radiative decay rate constant (equal to $1/\tau$) and K includes all terms independent of θ and E. Equation (2.24) has the normalized analytical solution:

$$Y^{int}(z) = z^{-2}\{1 - \exp(-x) - 3z\, E_4(z)\} \qquad (2.25)$$

where $z = \gamma_i x m^{\frac{1}{2}} 2^{\frac{1}{2}} / E^{*\frac{1}{2}}$ in the absence of non-radiative decay. In the case of observation of the decay with a sufficiently narrow slit, the normalized differential form is

$$Y^{diff}(z) = \left(\frac{3}{2z^2}\right)\left[\frac{1}{z} - \left(1 + \frac{1}{z}\right) \exp(-z) - zE_3(z)\right] \qquad (2.26)$$

The curves $Y^{int}(z)$ and $Y^{diff}(z)$ are shown in Figure 2.7.

This model also shows qualitative agreement with the experimental curves and furthermore yields the value of E^* from the slope of the z vs x curve interpreted from the measured decay curve.

Equation (2.26) is a specific solution for the more generalised form for the differential photon yield determined by Wright and Gruen [91].

More recently, Dzioba and Kelly [92] have extended this model by considering different forms for the excitation probability P(E). Four different forms were discussed, these being (i) the step function used to obtain (2.25) and (2.26), (ii) the step function with $P(E) \alpha E^{\frac{1}{2}}$, (iii) the step function with $P(E) \alpha (E - E^*)^{\frac{1}{2}}$ and (iv) $P(E) \alpha$ constant and using the full form of the sputtered energy distribution. The different forms for the excitation probability are shown in Figure 2.8.

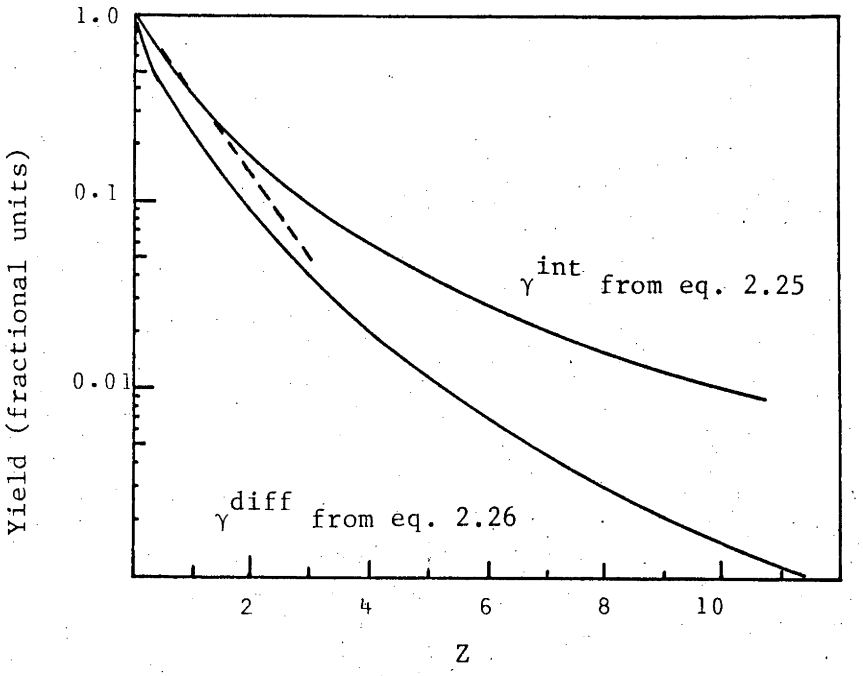

Figure 2.7 The integral yield and differential yield decay curves from equations (2.25) and (2.26). The dotted curve gives the decay similar to equation (2.23(b)).

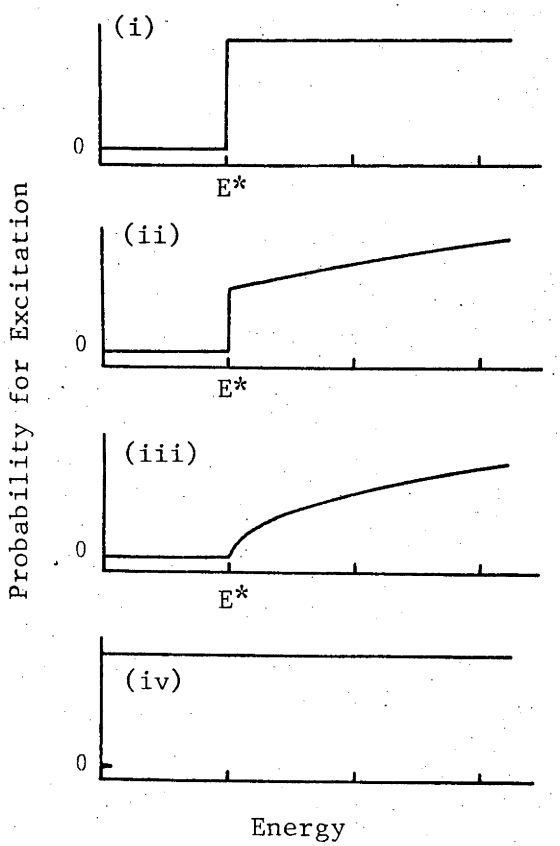

Figure 2.8 Different forms for the excitation probability used by Dzioba et al. [92]. (i) step function, (ii) step function with $P(E) \propto E^{\frac{1}{2}}$, (iii) step function with $P(E) \propto (E-E^*)^{\frac{1}{2}}$ and (iv) $P(E) \propto$ constant.

Each form of the excitation function used in solving for Y^{int}, predicted the concave decay curve observed experimentally. The corresponding $Y^{diff}(z)$ curves were all very similar.

The model of Dzioba et al. [90] has been applied to Li, LiF and NaCℓ [90], group IIA flourides [92] and Si, Ba, Na, Ni and Cr oxide glasses [93]. Each analysis has used the differential form of the yield equation (2.27) and linear z vs x plots were obtained except when cascading apparently contributed to the emission. The values of E^* obtained ranged from 10-100 eV in the case of Li and Na, 40-3000 eV for Mg, Ca, Sr and Ba fluorides and 100-2300 eV for the oxide glasses. Different excitation levels of the same element have usually had different E^* values and these may vary by up to a factor of five or more [90].

The different forms of the differential yield corresponding to the different P(E) functions discussed in [92], were also applied to the group IIA fluorides. In each case the value of E^* obtained depended consistently upon the differential yield function used although the values differed by only about a factor of two. Linear plots of z vs x were obtained for each of the forms of Y^{diff}. No experimentally preferred form of P(E) could be determined from these results.

Although the model of Dzioba et al. [90,92] has been based upon strong assumptions, there have been no attempts to check that the values of E^* were "reasonable" when compared to other experimental data. Tsong et al. [93] have compared the values of E^* with the energy parameter

determined by using the exponential fit (equation 2.23(b)), however the lack of agreement between the values is hardly surprising considering the even stronger assumptions made in obtaining (2.23(b)).

Sigmund [94] has criticized the excitation threshold model used by Dzioba et al. [90,92] and concluded that although the low energy peak for excited atoms was less than that for all of the sputtered atoms, the low energy atoms dominate the sputtered distribution of excited atoms. Sigmund then proceeded to include a more heavily weighted excitation process at energies close to threshold, using the basic assumption that excitation occurs in the bulk, and that the excited states survive until sputtered. This assumption could be criticized but is again based upon our lack of understanding of the excitation mechanism itself and illustrates the difficulty in applying any theory to sputtered excited atoms until the excitation is understood.

The influence of the incidence angle and observation angle should be stressed. E^* values are determined for normal incidence bombardment whereas line profile measurements have been made for many incidence angles. Single collision sputtering may only occur when non normal incidence bombardment is used allowing the recoiling target atom to have a probability for recoil velocity away from the target surface. This probability for single collision sputtering increases with incidence angle (see Figure 2.4). Comparison between E^* values and those estimated from line profile measurements may be invalid unless the same incidence angles have been used.

2.2.5 *Contamination induced changes in the line emission*

Contaminants, particularly oxygen, nitrogen, carbon and carbon monoxide, have been shown to significantly alter the characteristics of the observed photon emission, whether present as a surface contaminant or in the bulk [1-3]. The most basic measurements of the influence of surface contamination are those which monitor the changes in intensity as a function of surface coverage. These curves for sputtered particles, should show an initial region in which the intensity does not change with increasing background pressure (i.e. clean surface initially) followed by a section in which the intensity may change. For type I emission, this second section usually shows an intensity increase. Additionally, a third region for the type I intensity changes, in which the intensity peaks and then decreases [20], has been observed for Cr. This intensity decrease has been proposed to be associated with the decrease in the sputtering yield with oxygen coverage [20]. The exposure curves may then be used to qualitatively predict the behaviour of transient measurements for given exposures. Type II and III emissions do not necessarily follow the trends of the type I emission [8,20].

For the emission from scattered particles, these exposure curves have generally shown an increase for the type I emission with coverage, followed by a plateau region at high exposure [55,56]. In contrast to these observations, Martin et al. [95] observed an increase, followed by a peak region and then a decrease in intensity

for the H_α emission with oxygen coverage, for 50 keV H_2^+ scattering from Nb. Martin et al. also observed that the polarisation of the emitted light was particularly sensitive to the surface cleanliness with the polarised fraction decreasingly with coverage for the H_α line.

The first attempts to explain these changes in intensity used the band structure model. The standard procedure is as shown in Fig. 2.9 where the energy levels for the SiI, II and III levels are compared to the bulk energy levels for Si and SiO_2. Oxygen coverage of the Si is assumed to tend toward a SiO_2 target. The observed changes in intensity are then assumed to result from different de-excitation mechanisms occurring at the two types of surface. Thus, from Figure 2.9, an increase in the SiI 288.2 nm line may be expected with oxygen exposure as the SiO_2 band gap would inhibit the resonance ionisation process shown for this level. Strong increases in intensity for this line with oxygen exposure were observed. A corresponding, but lesser, increase for the type II line (385.6nm) and marginal decrease for the SiIII 254.2 nm line were also observed [19].

From the observation that the Si^+ yields almost followed the SiI yields, resonance ionisation as a de-excitation process for excited neutrals was proposed not to influence the excited states. A decrease in the ion yield would be expected if the resonance process was blocked (see Figure 2.1). This was also the conclusion by Meriaux [97] from the study of changes in the NiI

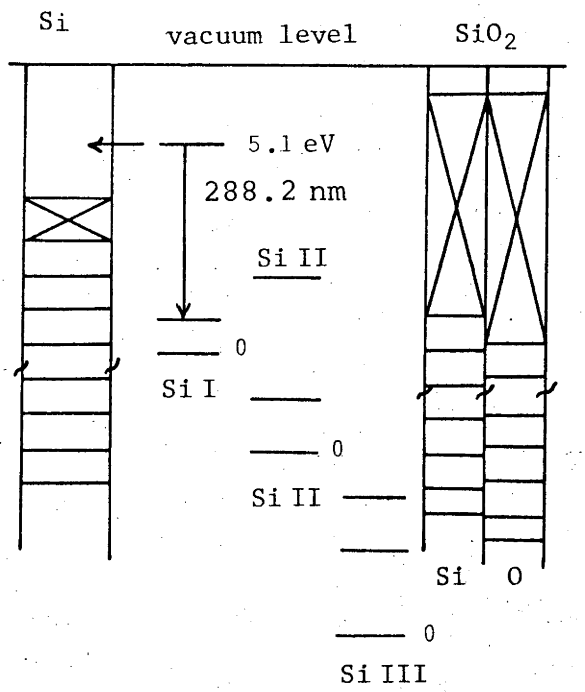

Figure 2.9. The energy level diagrams of the Si and SiO_2 solids compared to the SiI atom and SiII and SiIII ions, referred to the vacuum level at E = 0 eV. The energy levels of the excitation states are shown. The cross hatched regions are the band gaps [19].

yields with oxygen exposure, where Auger processes were concluded to dominate the observed results. The model involving Auger transitions could not, however, be extended to interpret the oxygen contamination induced changes in the Aℓ I or Mo I emission by Meriaux et al. An alternative explanation for the intensity changes was proposed involving a thermodynamic model. The band structure model has continued to be used as it was found to qualitatively explain the emissions from other ion bombarded targets [97].

Non-radiative transitions influencing the excited states in the manner assumed in equation (2.11) would be expected to change the velocity distributions of the excited particles which escape from the surface and decay radiatively. Changes in the non-radiation processes induced by surface contamination would consequently be evident in changed line profiles and decay curves. The most widely cited example has been the changes in line profile observed between bombarded Si and SiO_2 by White et al. [98]. The line profiles were found to change from 0.5 nm for the 55 KeV Ar^+ bombarded Si, to 0.1 nm for the bombarded SiO_2 under identical conditions. These changes are shown in Figure 2.10. The line profiles were interpreted using the band structure model as outlined above.

The width for the SiI 288.2 nm line from the bombarded Si appears excessively wide (many excited particles would have energies almost that of the maximum transferable energy) and has not been verified in the literature. The line width for the same SiI emission obtained by 55 keV Ar^+ bombardment of Si at 45° incidence by Martin [6] could not reproduce this result.

The line widths of Be I lines have been found to be not influenced by oxygen contamination of the bombarded Be surface [88]. Notwithstanding this result, the available line profile and decay curve measurements [8,32,43,97] indicate that the kinetic energies of the radiating atoms are lower from the bombarded oxygen contaminated surface than from the clean surface.

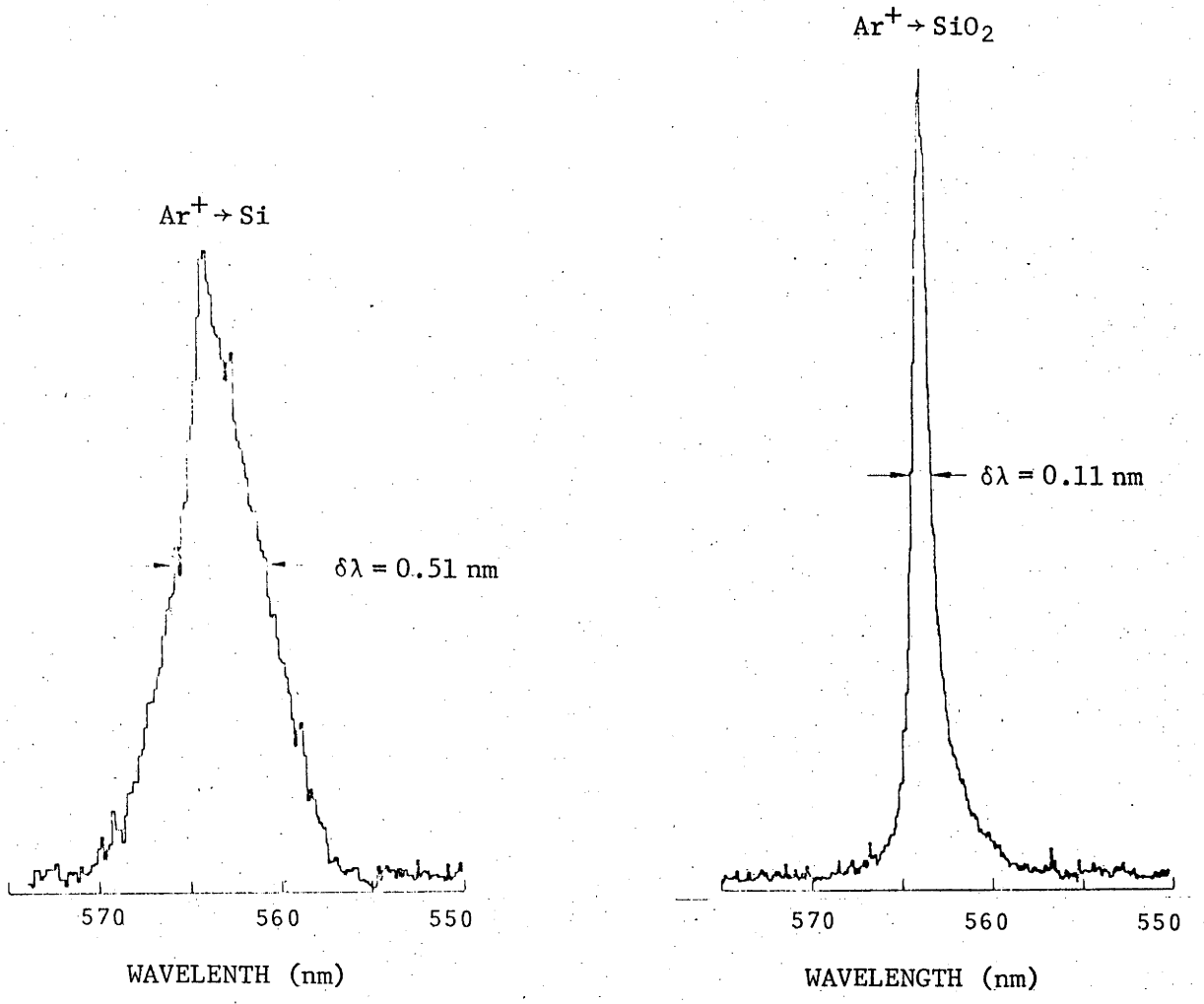

Figure 2.10. Line profiles of the Si I 288.2 nm emission line induced by 80 keV Ar^+ bombardment of Si and SiO_2. The instrument was ~ 0.1 nm (after White et al. [98]).

Despite the qualitative agreement in some cases for the band structure model, there exists further evidence to suggest that the simple resonance model, at least, does not seem to influence the excited states. G. Thomas and de Kluizenaar [99] have deliberately changed the position of the Fermi level of Cu by Cs adsorption to exclude the possibility of a resonance ionisation process in the band structure model assumption. The work function of the cesium covered surface is known to decrease by about 2.5 eV, locating the excited states adjacent to the filled states of the metal rather than the empty states for the uncoated surface. A decrease, instead of the increase in intensity as predicted by the blocking of the resonance process, was observed. It was concluded that the resonance ionisation process may not be responsible for the lower photon yield from Cu metal as compared to the oxide. The increase in intensity with oxygen adsorption was interpreted in terms of an alternative model involving excitation due to the breaking of metal-oxygen bonds [100]. A similar result for Aℓ was also observed [99]. In disagreement with this interpretation, Yu [101] has suggested that the resonance process may be possible, even in the presence of a Cs layer, due to the raising of the excited levels of the neutral atom relative to the Fermi level by image potentials. There has been criticism of the band structure model in the assumption of the existence of a band structure during ion bombardment [see, for example, 16].

Attention has been turned to alternative models to explain the enhancements usually observed with surface oxygen coverage. These have included the bond-breaking model [100] and curve crossing after quasi-molecule formation [4,18] and the surface polarisation model [16].

The bond breaking models rely upon the breaking of metal-oxygen bonds in the excitation process. Initial sputtering of the M-O system is followed by bond breaking and excitation by curve crossings. The number of excited atoms and the population distribution of the excited states is then determined by the evolution of the electronic states in the colliding and subsequently separating "quasi-molecule". The early proposal by Blaise [18] predicted an upper limit on the excitation energy of the metal atom to be of the order Δ, where $\Delta = V_1 - A_1$ and V_1 and A_1 are the ionization energy and electronegativity of the metal atom respectively. Tsong [4] has outlined a model for excitation and ionization based upon these earlier attempts and is shown in Figure 2.11. The ΔV_I term is due to the Coulomb interaction between the surface polarisation of the solid and the "quasi-molecule". The surface polarisation concept was introduced [16] to propose adsorption of oxygen either above or below the solid surface resulting in a surface dipole. This surface dipole may then modify the surface potential barrier, increasing the barrier when the oxygen (or most electro-negative) atom is above the surface and decreasing the potential barrier when the oxygen is incorporated below the surface. Transient measurements with oxygen exposure

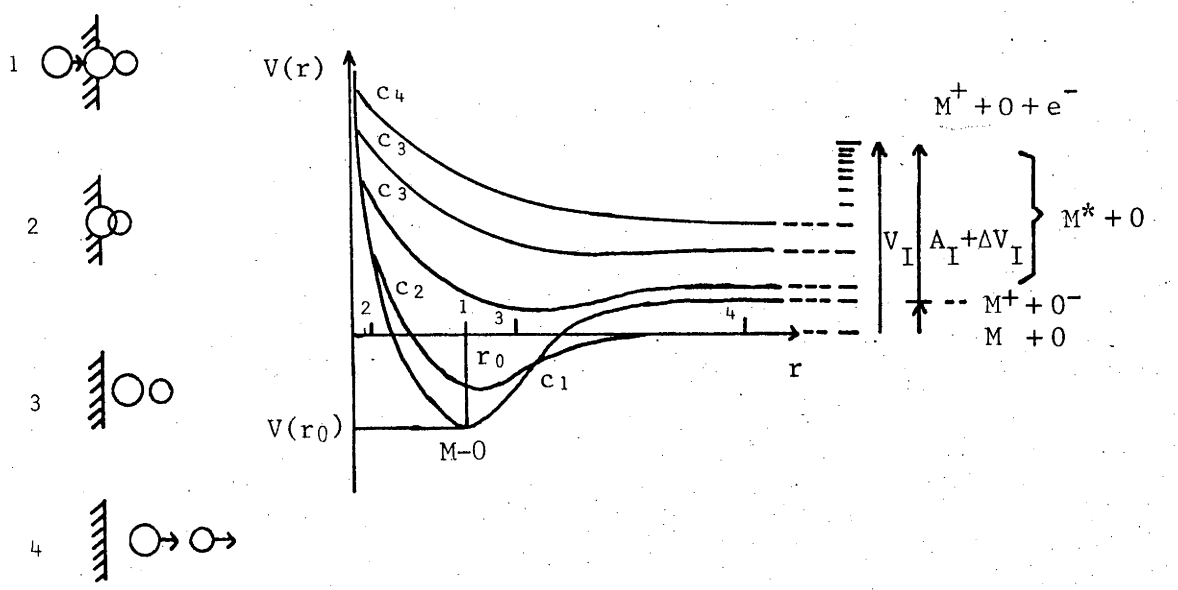

Figure 2.11. Illustration of the sputtering of an M-O quasimolecule and a schematic potential energy diagram of the M-O system during its dissociation, with increasing distance r, from the surface. The crossing points $C_1, C_2 \ldots$ are shown. V_I is the ionisation energy of M. A_I is the electron affinity of O and ΔV_I is the ionisation energy depression due to the interaction with the surface [4].

have also been explained in terms of the surface polarisation model [102].

In summary, there remains considerable difficulty in explaining the intensity changes and energy distributions of the excited atoms when contaminants are incorporated in the bulk or on the surface of the bombarded target. There remains a need for good experimental data for different contaminant and surface combinations while the experimental conditions, in particular the surface cleanliness and

influence of edge effects, need more consideration than has previously been given.

2.3 CONTINUUM AND BAND EMISSION

Considerable interest has been shown in continuum emission observed during the bombardment of several metals such as Ti,Cr,Zr,V,Mo,Nb,Ta,W,Pt [103-112]. Rausch et al. [109] have concluded that this continuum is associated with surface contamination and it was proposed that the origin of the continuum emission is sputtered excited target oxides, i.e the source is molecular. The origin of this emission had been a source for some speculation.Under the cleanest conditions of Rausch et al. (cleanliness factor of 130), the continuum emission from 23.5 keV Ar^+ bombarded Mo almost disappeared. Bombardment of MoO_3 or Mo under oxygen contamination conditions reproduced the continuum spectra similar to those found previously by Kerkdijk et al. [107] and White et al. [105] where the cleanliness factors were less than 10. Rausch et al. found that the continuum spectra for Mo produced by O_2 and CO adsorption were very similar and that the continua for different metals were different.

The proposal by Rausch et al. [109] that sputtered metal oxide molecules were responsible for the continuum emission has been criticised by Kiyan et al. [110] based upon the findings of Belykh et al. [112]. Belykh et al. [111,112] studied continuum emission from 3.5 keV Cs^+ bombardment of Ta under "clean" and oxygen rich environments.

It was reported that the intensity of several selected features of the Ta continuum spectra exhibited a net decrease in intensity when the oxygen partial pressure was increased, a result not consistent with the model of continuum emission resulting from sputtered metal oxides. Furthermore, supposed cleaning of the Ta target did not decrease the continuum intensity and consequently C and O contamination resulting in continuum emission was ruled out. However, the cleanliness factor for these works was of the order 30 - 80 and this would suggest that the surfaces may not have been sufficiently clean. A more positive criticism by Kiyan et al. [110] was that the observed continuum spectra did not correlate well with known band spectra of diatomic molecules [113]. The radiation, however, may arise from MO_n for n = 1,2,3,... and the spectra from these more complex molecules is often not known. Kiyan et al. [110] observed that the continuum spectra from the transition metals were almost independent of the metal target species.

Surface contamination during ion bombardment has also resulted in the observation of molecular emissions. One of the first molecular emissions to be found was the CH $A^2\Delta - X^2\pi$ band (edge at 431.2 nm) [8], present due to the poor target cleanliness used for this study. Jensen and Veje [73] also observed CH radiation as well as molecular radiation attributed to BeH ($^2\pi - {}^2\Sigma$ transition at 499 nm) and the MgO Green system ($'\Sigma - '\Sigma$ between 490-520 nm). Again these emissions were due to poor surface cleanliness (surface cleanliness factor about 0.1). By increasing the oxygen background pressure during the bombardment of Cu and

Aℓ, G. Thomas et al. [114] were able to observe the appearance of CuO band heads and the AℓO Green system respectively. H_2O vapour contamination in the case of the bombardment of Aℓ, lead to the appearance of the AℓH ($A'\pi - X'\Sigma^+$) transition. Identification of these molecular emissions has often been particularly difficult due to the absence of good molecular wavelength tables, especially for more complex systems.

To overcome the difficulties in identification of the emitting species, G. Thomas et al. [115] compared a high resolution scan of Kr^+ bombarded Si with H_2O vapour contamination with that obtained using the same monochromator for the OH bands from an oxy-acetylene flame. The close similarities of the spectra enabled the identification of the sputter bands as emission from the OH radical.

Although molecular ion emission of the type M_n^+ has been observed in SIMS studies, photon emission from these molecular species has not been identified.

2.4 APPLICATIONS OF PHOTON EMISSION

Despite the lack of understanding of the processes leading to photon emission, several fields of application using the emitted photons have emerged. Observation of line emission appears suitable for depth profiling of layers over substrates [116] and also for analysis of hydrogen in solids [117]. It is often not possible to detect hydrogen by other methods and SIMS and photon emission appear suited to this purpose. Line emission has also been used for

qualitative and quantitative analysis [118,119]. Most of the quantitative analysis has been used with doped glasses and insulators, where the band gap has been assumed to exclude non-radiative transitions, allowing all excited states to decay radiatively. The analysis is made qualitative through the identification of the spectral lines (sensitivity then rests on the absolute yields for that level of the element and possible spectral overlap with other constituents) and quantitative by comparison with standards. Meriaux [120] has reported the analysis of Cu/Ni alloys where the line intensities were found to be proportional to the bulk concentrations. The conditions for the study, however, were probably insufficient to maintain surface cleanliness.

Recently Taglauer et al. [121,122] have shown that the changes in the line emission intensities may be used to derive desorption coefficients.

2.5 CONCLUSIONS

There is an evident need for better definition of experimental aims in photon emission studies to obtain more information to compare with models for an excitation process. Also evident is the lack of adequate models which may be used in any more than a basic qualitative manner. Attempts in obtaining such a model have been hampered in trying to correlate reports in the literature which have been done with many different experimental parameters and under varying surface cleanliness conditions.

Any model to account for the photon emission would need to be able to explain (i) the distribution of excited states, (ii) the kinetic energies of the excited atoms, (iii) the changes induced by surface contamination and (iv) the sensititivity to the particular excited state. There is a need, therefore, for a detailed study of a particular system with regard to these parameters. Such a study has been made here for the Ti system and is reported in Chapter 4. Application to other systems is discussed in Chapter 5. Expected areas of interest such as the emission function determination (section 2.2.2) have not been experimentally possible in this study.

REFERENCES

[1] W.F. van der Weg, in: Proc. NATO Summerschool on Material Characterization using Ion Beams, Corsica, 1976 (Plenum Press, 1977)

[2] C.W. White, E.W. Thomas, W.F. van der Weg and N.H. Tolk, in: Inelastic Ion-Surface Collisions eds. N.H. Tolk, J.C. Tully, W. Heiland and C.W. White (Academic Press, 1977)

[3] G.E. Thomas, Surface Sci. 90 (1979) 381

[4] I.S.T. Tsong, presented at: Third International Workshop on Inelastic Ion-Surface Collisions, Feldkirchen, Westerham, W. Germany, 1980

[5] R.J. MacDonald, C.M. Loxton and P.J. Martin, presented at: Third International Workshop on Inelastic Ion-Surface Collisions, Feldkirchen, Westerham, W. Germany, 1980

[6] P.J. Martin, Thesis, Australian National University (1976)

[7] A.R. Knudsen, D.J. Nagel, J. Comas and K.W. Hill, Nucl. Instr. Methods 149 (1978) 507

[8] M. Braun, B. Emmoth and I. Martinson, Physica Scripta 10 (1974) 133

[9] K.-H. Schartner, H.J. Flaig, D. Hasselkamp and A. Scharmann, Nucl. Instrum. Methods 168 (1980) 419

[10] C.B. Kerkdijk and R. Kelly, Radiation Effects 38 (1978) 73

[11] R. Kelly, S. Dzioba, N. Tolk and J. Tully, Surface Sci. 102 (1981) 486

[12] A.R. Striganov and N.S. Sventitski, Tables of Spectral Lines of Neutral and Ionized Atoms, (Plenum, New York, 1968)

[13] N.W. Robinson, The Physical Principles of UHV Systems and Equipment (Chapman and Hall Ltd, 1968)

[14] S. Dushman, Scientific Foundations of Vacuum Technique, 2nd Edition, ed. J.M. Lafferty (John Wiley and Sons, 1966)

[15] K. Wittmaack, Inelastic Ion-Surface Collisions, eds. N.H. Tolk, J.C. Tully, W. Heiland and C.W. White (Academic Press, 1977)

[16] P. Williams, Surface Sci. 90 (1978) 588

[17] C.B. Kerkdijk and R. Kelly, Surface Sci. 47 (1975) 294

[18] G. Blaise, Surface Sci. 60 (1976) 65

[19] P.J. Martin, A.R. Bayly, R.J. MacDonald, N.H. Tolk, G.J. Clark and J.C. Kelly, Surface Sci. 60 (1976) 349

[20] R.J. MacDonald and P.J. Martin, Surface Sci. 67 (1977) 237

[21] R. Shimizu, T. Okutani, T. Ishitani and H. Tamura, Surface Sci. 69 (1977) 349

[22] P.J. Martin and R.J. MacDonald, Radiation Effects 32 (1977) 177.

[23] B. Brozdowska-Warczak, L. Gabla, R. Pedrys, M. Szymónska and A. Warczak, Surface Sci. 75 (1978) 61

[24] C.A. Andersen and J.R. Hinthorne, Anal. Chem. 45 (1973) 1421

[25] M. Kato, R. Shimizu and T. Ishitai, Technology Reports of the Osaka University, vol. 24, no. 1199 (1974) 451

[26] P.W.J.M. Boumans, Theory of Spectrochemical Excitation (Hilger and Watts, London, 1966)

[27] P.J. Martin and R.J. MacDonald, Surface Sci. 62 (1977) 551

[28] R.J. MacDonald and R.F. Garrett, Surface Sci. 78 (1978) 371

[29] K.J. Snowdon, Radiation Effects 40 (1979) 9

[30] I.S.T. Tsong and N.A. Yusuf, Surface Sci. 90 (1979) 417

[31] P. Williams, I.S.T. Tsong and S. Tsuji, Nucl. Instr. Methods 170 (1980) 591

[32] W.F. van der Weg and D.J. Bierman, Physica 44 (1969) 206

[33] R. Hippler, W. Krüger, A. Scharmann and K.-H. Schartner, Nucl. Instr. Methods 132 (1976) 439

[34] E. Parilis, Atomic Collision Phenomena in Solids, p.517, eds. D.W. Palmer, M.W. Thompson and P.D. Townsend (North Holland, 1970)

[35] A. Warczak, B. Brozdowska-Warczak, P. Pedrys and L. Gabla, Acta Phys. Pol. A 47 (1975) 543

[36] C. Kerkdijk and E.W. Thomas, Physica 63 (1973) 577

[37] W.E. Baird, M. Zivitz, J. Larsen and E.W. Thomas, Phys. Rev. A 10 (1974) 2063

[38] W.E. Baird, M. Zivitz and E.W. Thomas, Phys. Rev. A 12 (1975) 876

[39] D.R. Olander, C.B. Kerkdijk and C. Smits, Surface Sci. 49 (1975) 28

[40] C.B. Kerkdijk, C.M. Smits, D.R. Olander and F.W. Saris, Surface Sci. 49 (1975) 45

[41] G.M. McCracken and N.J. Freeman, J. Phys. B (Atom. Molec. Phys.) 2 (1969) 661

[42] W.F. van der Weg and P.K. Rol, Nucl. Instr. Methods 38 (1965) 274

[43] C. Snoek, W.F. van der Weg and P.K. Rol, Physica 30 (1964) 341

[44] H.D. Hagstrum, Phys. Rev. 96 (1954) 336

[45] H.D. Hagstrum and G.E. Becker, Phys. Rev. B 8 (1973) 107

[46] A. Cobas and W.E. Lamb, Phys. Rev. 65 (1944) 327

[47] S.S. Schekhter, JETP 7 (1937) 750, Zh. Eksperim. i. Teor. Fiz. 1 (1930) 386

[48] T.P. Grozdanov and R.K. Janev, Phys. Lett 65A (1978) 396

[49] C.W. White and N.H. Tolk, Phys. Rev. Letters 26 (1971) 487

[50] R.S. Bhattacharya, D. Hasselkamp and K.-H. Schartner, J. Phys. D: Appl. Phys. 12 (1979) L55

[51] R.B. Wright and D.M. Gruen, Nucl. Instr. Methods 170 (1980) 577

[52] R.B. Wright and D.M. Gruen, J. Chem. Phys. 73 (1980) 664

[53] W.E. Baird, M. Zivitz and E.W. Thomas, Nucl. Instr. Methods 132 (1976) 445

[54] E.O. Rausch and E.W. Thomas, Phys. Rev. A (1976) 1912

[55] E.O. Rausch and E.W. Thomas, Nucl. Instr. Methods 149 (1978) 511

[56] E.W. Thomas, H. Inouye and E.O. Rausch, J. Appl. Phys. 49 (1978) 2911

[57] S.Y. Leung, N.H. Tolk, W. Heiland, J.C. Tully, J.S. Kraus and P. Hill, Phys. Rev. A 18 (1978) 447

[58] E. Taglauer, W. Heiland, R.J. MacDonald and N.H. Tolk, J. Phys. B: Atom. Molec. Phys. 12 (1979) L533

[59] I.S.T. Tsong, Surface Sci. 69 (1977) 609

[60] R.J. MacDonald, R.F. Garrett and P.J. Martin, Surface Sci. 75 (1978) L155

[61] I.S.T. Tsong, Surface Sci. (1978) L159

[62] R. Kelly, C.J. Good-Zamin, M.T. Shehata and D.B. Squires, Nucl. Instr. Methods 149 (1978) 563

[63] C.J. Good-Zamin, M.T. Shehata, D.B. Squires and R. Kelly, Radiation Effects 35 (1978) 139

[64] T. Okutani and R. Shimizu, Surface Sci. 88 (1979) 51

[65] K.J. Snowdon, Radiation Effects 42 (1979) 185

[66] K.J. Snowdon, B. Andresen and E. Veje, Radiation Effects 40 (1979) 19

[67] K.J. Snowdon, B. Andresen and E. Veje, Radiation Effects Letters 43 (1979) 205

[68] K.J. Snowdon, G. Carter, D.G. Armour, B. Andresen and E. Veje, Radiation Effects Letters 43 (1979) 201

[69] K.J. Snowdon, G. Carter and D.G. Armour, Surface Sci. 90 (1979) 429

[70] K.J. Snowdon and R.J. MacDonald, Nucl. Instr. Methods 170 (1980) 351

[71] G.E. Thomas and B.R. de Konig, Chem. Phys. Letters 55 (1978) 418

[72] C.M. Loxton, R.J. MacDonald and P.J. Martin, Surface Sci. 93 (1980) 84

[73] K. Jensen and E. Veje, Z. Physik 269 (1974) 293

[74] N. Andersen, B. Andresen and E. Veje, - presented at: Symposium on Sputtering, Vienna, 1980

[75] K.-H. Schartner, Surface Sci. 90 (1979) 482
V. Kempler, Surface Sci. 90 (1979) 461
E.W. Thomas, Excitation in Heavy Particle Collisions (Wiley Interscience, New York, 1972)

[76] B. Andresen, S. Hultberg, B. Jelenkovic, L. Liljeby, S. Mannervik and E. Veje, Z. Physik A293 (1979) 181

[77] B. Christensen, E. Veje and P. Hvelplund, Phys. Rev. A 18 (1978) 2042

[78] H.G. Berry, Inelastic Ion Surface Collisions, eds. N.H. Tolk, J.C. Tully, W. Heiland and C.W. White (Acadmic Press, New York, 1977)

[79] H.J. Andrä, R. Fröhling and H.J. Plöhn, Inelastic Ion Surface Collisions, eds. N.H. Tolk, J.C. Tully, W. Heiland and C.W.White (Academic Press, New York, 1977)

[80] L. Gabla, M. Szymonski and M. Szulkin, Physica 81C (1976) 193

[81] H.J. Andrä, Phys. Letters 54A (1975) 315

[82] E. Taglauer and W. Heiland, Appl. Phys. 9 (1976) 261

[83] R.J. MacDonald and M.W. Thompson - preliminary work.

[84] W.F. van der Weg, N.H. Tolk, C.W. White and J.M. Kraus, Nucl. Inst. Methods 132 (1976) 405

[85] V.V. Gritsyna, T.S. Kiyan, A.G. Koval' and Ya.M.Fogel', Radiation Effects 14 (1972) 77

[86] T.S. Kiyan, V.V. Gritsyna and Ya.M. Fogel', Z. Physik A 285 (1978) 257

[87] T.S. Kiyan, V.V. Gritsyna and Ya.M. Fogel', Nucl. Instr. Methods 132 (1976) 435

[88] G.M. Mladenov and M. Braun, Phys. Stat. Sol.(a) 53 (1979) 631

[89] G. Carter, G. Fischer, R. Webb, S. Dzioba and R. Kelly, Radiation Effects 45 (1979) 45

[90] S. Dzioba, O. Auciello and R. Kelly, Radiation Effects 45 (1980) 235

[91] R.B. Wright and D.M. Gruen, J. Chem. Phys. 72 (1980) 235

[92] S. Dzioba and R. Kelly, Surface Sci. 100 (1980) 119

[93] I.S.T. Tsong and N.A. Yusuf, Nucl. Instr. Methods 170 (1980) 357

[94] P. Sigmund; presented at 3rd Intern. Workshop on Inelastic Ion-Surface Collisions, Feldkirchen-Westerham, W. Germany (1980)

[95] P.J. Martin, L. Berzins and R.J. MacDonald, Surface Sci. 95 (1980) L277.

[96] J.P. Meriaux, R. Goutte and C. Guillaud, Appl. Phys. 7 (1975) 313

[97] M. Braun, Physica Scripta 19 (1979) 33

[98] C.W. White, D.L. Simms, N.H. Tolk and D.V. McCaughan, Surface Sci. 49 (1975) 657

[99] G.E. Thomas and E.E. de Kluizenaar, Nucl. Instr. Methods 132 (1976) 449

[100] G.E. Thomas, Radiation Effects 31 (1977) 185

[101] M.L. Yu, Surface Sci. 90 (1979) 442

[102] I.S.T. Tsong and S. Tsuji, Surface Sci. 94 (1980) 269

[103] W.F. van der Weg and E. Lugujjo, Atomic Collisions in Solids (Plenum Press, New York, 1975)

[104] T.S. Kiyan, V.V. Gritsyna, Yu, E. Logachev and Ya.M. Fogel', Sov. Phys. JETP Lett. 21 (1975) 77

[105] C.W. White, N.H. Tolk, J. Kraus and W.F. van der Weg, Nucl. Instr. Methods 132 (1976) 419

[106] T.S. Kiyan, V.V. Gritsyna and Ya. M. Fogel', Nucl. Instr. Methods 132 (1976) 415

[107] C.B. Kerkdijk, K.-H. Schartner, R. Kelly and F.W. Saris, Nucl. Instr. Methods 132 (1976) 427

[108] C.W. White and N.H. Tolk, J. Nucl. Materials 63 (1976) 506

[109] E.O. Rausch, A.I. Bazhin and E.W. Thomas, J. Chem. Phys. 65 (1976) 4447

[110] T.S. Kiyan, V.V. Gritsyna and Ya.M. Fogel', Sov. Phys. JETP 47 (1978) 730

[111] S.F. Belykh, V.I. Veksler, R.N. Evtukhov, L.B. Kudryashova and B.A. Tsipinyuk, Sov. Phys. Solid State 20 (1978) 2018

[112] S.F. Belykh, V.I. Veksler, R.N. Evtukhov and Kh.A. Usmanov, Interation of Atomic Particles with a Solid, Pt. 2, Khar'kov (1976) p.198 (in Russian)

[113] R.W.B. Pearse and A.G. Gaydon, The Identification of Molecular Spectra (Chapman and Hall, London, 1963)

[114] G.E. Thomas and E.E. De Kluizenaar, Inter. J. Mass Spect. Ion Phys. 15 (1974) 165

[115] G.E. Thomas, E.E. de Kluizenaar and M. Beerlage, Chem. Phys. 7 (1975) 303

[116] C.W. White, Nucl. Instr. Methods 149 (1978) 497

[117] I.S.T. Tsong and R.B. Liebert, Nucl. Instr. Methods 149 (1978) 523

[118] C.W. White, D.L. Simms and N.H. Tolk, Characterization of Solid Surfaces ed. by P.F. Kane and G.R. Larrabee (Plenum, New York, 1974)

[119] I.S.T. Tsong and A.C. McLaren, Spect. Act. 30B (1975) 343

[120] J.P. Meriaux, Thesis, University Claude Bernard, Lyon, France (1971)

[121] E. Taglauer, W. Heiland and R.J. MacDonald, Surface Sci. 90 (1979) 661

[122] R.J. MacDonald, W. Heiland and E. Taglauer, Applications of Surface Sci. 5 (1980) 197

CHAPTER THREE

EXPERIMENTAL METHOD

The experiments described in the following chapters were performed on either of two experimental systems. These systems were available for medium energy (up to 100 keV) or for low energy (up to 5 keV) ion bombardment. In the first section of this chapter, the experimental equipment and method will be discussed with reference to the ion sources, vacuum systems and experimental chambers for the two different systems and the data gathering and data analysis. The second section will report on an examination of the influence of the measurement technique on a selection of the observed data. The relation to previous reports in the literature will be discussed.

3.1 THE EXPERIMENTAL EQUIPMENT AND METHOD

The experimental equipment and method section will be subdivided into sections on the medium and low energy ion accelerator systems, the targets and target preparation methods, data measurement and finally, the method for data collection and analysis.

3.1.1 *The medium energy ion accelerator system*

The medium energy ion accelerator system is shown schematically in Figure 3.1(a). An Ortec 350 duoplasmatron ion source was used to produce He^+,Ne^+, Ar^+ or Kr^+ ions.

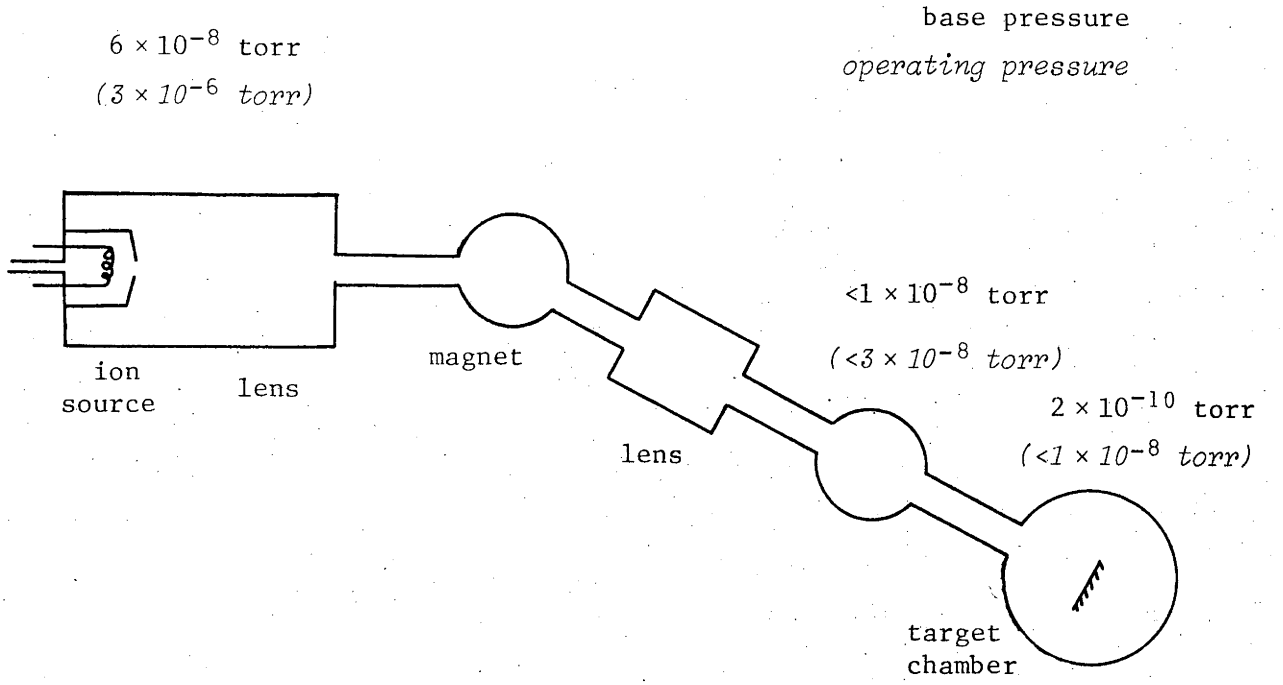

Figure 3.1(a). Schematic diagram of the medium energy ion accelerator system.

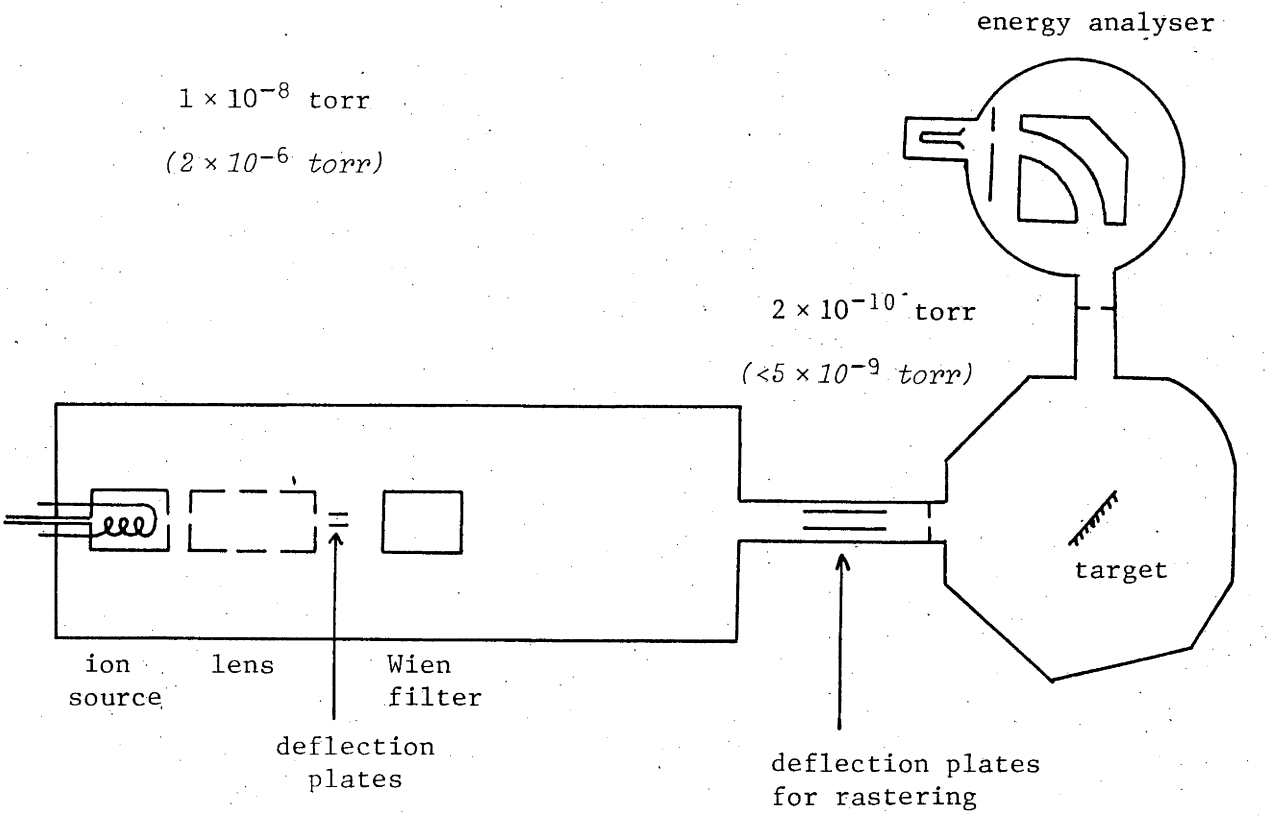

Figure 3.1(b). Schematic diagram of the low energy ion accelerator system.

O_2^+ beams could be produced using an inert gas/air mixture in the source and by selecting the appropriate mass beam with the selecting magnet M. The selecting magnet and angle in the beam line had the advantages of removing neutral and ionised components of the total ion beam from the source which were not wanted and in preventing light emission produced in the source region from possibly reaching the detector by reflection from the target. After passing through the magnet, the ion beam could be further steered and focussed by an electrostatic triplet quadrapole lens mounted inside the beam transport line. Final steering plates were mounted in the differential pumping chamber to deflect the beam through an aperture and onto the target. The final aperture, mounted at the front of the experimental chamber, was usually of 5 mm diameter. Other circular apertures of varying diameter could be placed in the same position when required.

The source, magnet and electrostatic lens regions were pumped by two oil diffusion pumps with water cooled baffles. The differential pumping chamber (used to isolate the ion source region, with its high inert gas load during operation, from the experimental chamber) was also diffusion pumped and was liquid nitrogen trapped when experiments were in progress. The base and operating pressures in these regions are indicated in Figure 3.1(a). A turbomolecular pump was used with the UHV experimental chamber to maintain an oil free vacuum of base pressure 2×10^{-10} torr. The chamber pressure was monitored with a nude ionisation gauge.

The targets were mounted on a Vacuum Generators 3 axis goniometer which allowed X,Y and Z movement, axial rotations and also (for single crystal target studies) azimuthal rotation. The beam current could be monitored directly from the bombarded target. For more accurate beam current measurements, the target could be biased to +70 eV to suppress secondary electron emission. Although the beam current density varied with the ion and the acceleration energy used, it was usually in the range 200 - 1000 $\mu A/cm^2$. The beam was not rastered.

High purity oxygen (Linde Gases, 99.99% pure) could be introduced into the experimental chamber through a leak valve to controlled pressures between mid 10^{-9} torr and mid 10^{-5} torr. The arrival rate of oxygen molecules at the surface was estimated using equation (2.1).

3.1.2 *The low energy ion accelerator system*

The low energy ion accelerator system, shown schematically in Figure 3.1(b), used a "Colutron" hot cathode, electron bombardment ion source. This type of ion source is capable of producing inert gas ion beams with very little energy spread. The ions produced in the source region were extracted and focussed by an einzel lens and accelerated by up to 5 kV. To remove any charged beam impurities, the beam was passed through a Wien Filter consisting of crossed electric and magnetic fields. Although neutral particles were able to pass through the filter and on to the target, this beam component was measured to have negligible influence on the results obtained.

A second einzel lens was mounted at the entrance to the experimental chamber with deflector plates positioned after the lens. This einzel lens was able to focus the beam down to a spot size at the target of about 1 mm diameter or less. The deflector plates allowed final positioning of the beam spot to the centre of the experimental chamber. A "3M" beam raster unit was used to supply appropriate voltages to the deflector plates to raster the beam in a rectangular grid over the target surface.

The source region was evacuated with a liquid nitrogen baffled oil diffusion pump to the base and operating pressures as indicated in Figure 3.1(b). The stainless steel experimental chamber was mounted directly above a turbomolecular pump. A base pressure of 2×10^{-10} torr could be obtained in the chamber after overnight baking at 200°C. The pressure in this chamber was measured with a nude ionisation gauge.

Targets were mounted on a Varian precision goniometer which allowed X, Y and Z movements and rotation about the goniometer axis. The goniometer could hold four targets; each target having separate heaters to allow target heating by electron bombardment to about 900°C. The incident beam current could be estimated directly from the target, or measured when the target was biased to suppress secondary electron emission. Beam current densities of the order $50 - 200\,\mu A/cm^2$ were obtained, although this current was proportionately less when rastering the beam.

High purity O_2 or CO (Matheson, 99.9% pure) could be admitted into the experimental chamber in controlled

flows between low 10^{-9} torr and 10^{-5} torr. The arrival rate of background gas molecules was again estimated from equation (2.1).

3.1.3 *Targets and target preparation*

All the targets used, with the exception of the Ti compounds and the Nb-V alloys, were high purity rods (99.999% pure) supplied by Materials Research Corporation. The TiO crystals were supplied by Balzers (99.5% pure) and the TiO_2 crystals by Tioxide International (99.9% pure). Sintered powder targets of TiO and TiO_2 were also supplied by Tioxide International. The TiN, TiC and TiB were high purity samples supplied by E. Taglauer (Max-Planck Institüt für Plasma Physik, Garching bei München, FDR), with the TiN and TiC grown on Stainless Steel and Titanium substrates respectively. The Nb-V alloys were high purity samples supplied by W.O. Hofer (K.F.A., Jülich, FDR).

In all cases, target preparation was the same. The targets were cut using a diamond saw and then polished with diamond pastes to a 1 micron finish before degreasing with acetone and placing in the vacuum system. Where possible, the targets were cleaned by heating to about 900°C with simultaneous Ar^+ ion bombardment. When target heating was not possible on the medium energy ion accelerator, the targets were initially mechanically rastered using the Y and Z goniometer movements, to reduce edge effects. In each run, bombardment commenced at least one hour before data was taken, to allow the signals to stabilize as surface contaminants were removed.

3.1.4 *Data measurement*

Using the medium energy ion accelerator, observation of the emitted photons produced by the ion bombardment could be made through a sapphire window mounted at any of the ports in the plane of the incoming beam. The window was usually mounted such that the observation was at 90° to the incoming beam unless otherwise stated. Light passing through the window was collected by a 15cm focal length quartz lens, which then focussed the light into a scanning monochromator. In addition, a slit arrangement was usually used to define the observation volume. These slits were mounted 25mm from the target and could be continuously varied from outside the vacuum system to obtain slit widths between 0 and 20mm. The lens could be moved to allow for measurement of limited volumes of the emitting region (differential yield measurement - lens position 1 of Figure 3.2(a)), or for observation of the whole of the emitting region (integral yield measurement - lens position 2 of Figure 3.2(a)). For differential yield measurements, the observation region is slightly trapezoidal in shape. This is not so important, particularly if allowance is made for this in the interpretation of the results.

When making differential yield measurements, the intensity of the emission was critically dependent upon the value of X, the position of the target in the incoming beam direction. The intensity peaked sharply as the target surface was moved through the observation region. In contrast to this, during integral yield measurements the intensity

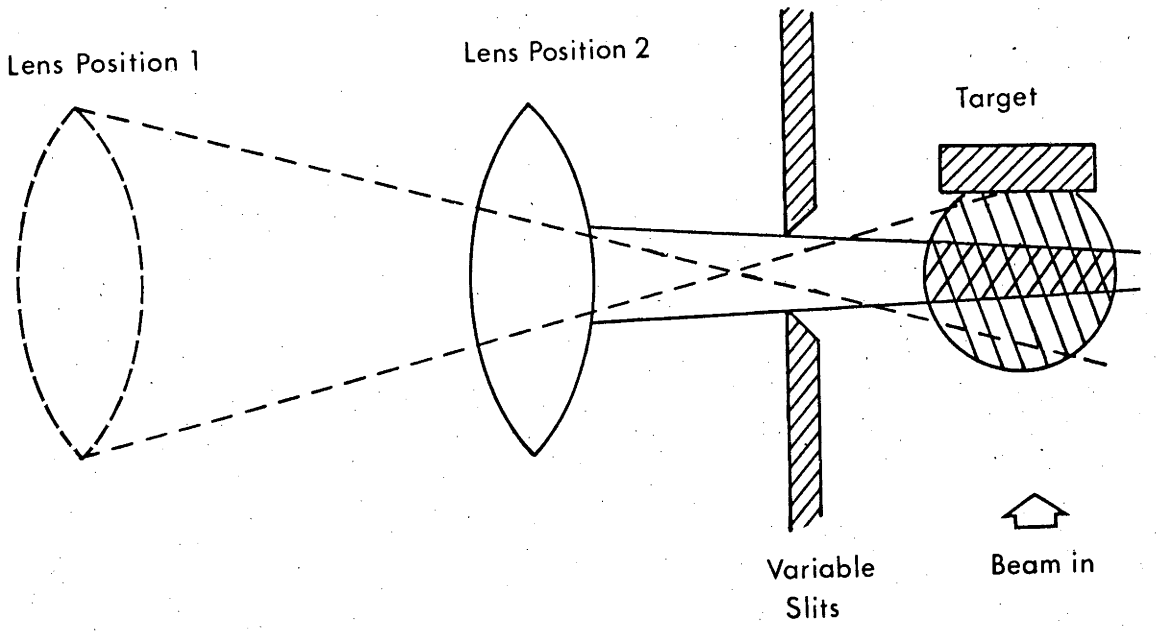

Figure 3.2(a). Experimental arrangement used with the medium ion accelerator system, showing the lens position and observation volume for integral yield measurement (position 1) and differential yield measurement (position 2).

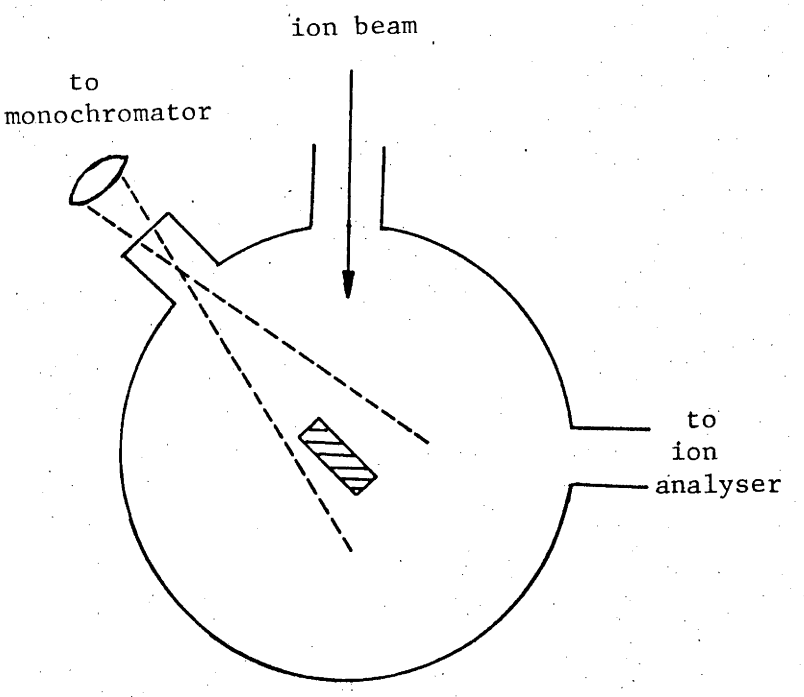

Figure 3.2(b). Observation geometry used with the low energy ion accelerator.

was found to peak and then become independent of further target position movement. These simple checks were always made to verify differential versus integral yield measurements.

Photon emission from low energy ion bombardment was observed through a sapphire window mounted at 45° to the incident beam, with the target either normal to the beam, or at 45° so that observation was parallel to the target surface as shown in Figure 3.2(b).

All photon counting experiments discussed here were performed with either a Jarrel-Ash 82-010 0.5 metre Ebert scanning monochromator, or a Bausch and Lomb 0.5 metre 33-86-45 scanning monochromator, depending upon the resolution required. The Bausch and Lomb monochromator had an effective aperture of f/4.4 with a 1200 line per mm. grating blazed for 300.0 nm in first order. It had an optimum resolution of 0.3 nm and the resolution could be varied by adjustment of the entrance and exit slit widths. With its low f number and the resolution set at about 0.8 nm, the Bausch and Lomb monochromator was particularly useful in observing weak and broad emissions. The low incidence energy experiments were done exclusively with the Bausch and Lomb monochromator.

The Jarrel-Ash scanning monochromator had an effective aperture of f/8.6 and was fitted with a 1180 line per mm grating. It was supplied with three sets of fixed entrance and exit slits, of widths 10, 25 and 50 microns. By assuming that the natural widths of emission lines from a hollow cathode lamp were far less than the instrument resolution,

the instrument line widths at half intensity were measured as 0.019, 0.039 and 0.072 nm respectively for the three sets of slits. With this good resolution, the Jarrel-Ash monochromator was used for all line width studies, using either the 10 or 25 micron entrance and exit slits.

The linear wavelength drives on both monochromators were modified by the addition of a precision stepper motor (Calderon Limited, size 14 or 15) and gearbox (Weyers Limited, 1000:1, 100:1 or 15:1). These stepper motors were driven by a MacLeans stepper motor controller which could supply selected pulse rates between 1 and 400 per second. The motors required 12 pulses per revolution. For line profile measurements, the Jarrel-Ash drive was coupled to a 100:1 gearbox resulting in a minimum step size of 1/1200 nm. Other measurements using the Jarrel-Ash monochromator were made with a 15:1 gearbox coupled to the drive resulting in a minimum step size of 1/180 nm. The Bausch and Lomb monochromator drive was coupled only to a 1000:1 gearbox with a minimum step size of 1/120 nm.

An EMI 9789 QB a photomultiplier was mounted in a light proof housing at the exit slit of both monochromators for photon detection. These tubes were specially selected for their exceptionally low dark current which was characteristically of the order of 1 count per second at room temperature. Cooling of these tubes was not necessary to lower the dark current. The photocathode was of the K-Cs type, sensitive to ultra-violet radiation as well as the visible range. The 13 stage dynode chain was wired according to [1].

The relative detection efficiency of the monochromator,

photomultiplier, lens and window detection assembly was determined for each counting system in order to compare the relative intensities of the spectral lines. This calibration was made by comparison of the transmitted intensity with a radiation standard. A Phil ips W2 KGV 221 tungsten ribbon lamp fitted with a silica window was used as this standard. The lamp was calibrated by the CSIRO National Standards Laboratory (Aust.) and the conditions for these calibrations were reproduced to attain the same lamp output. To overcome saturation of the counting system when the lamp was observed directly by the detector, the lamp output was reflected from a fresh $BaSO_4$ powder through the detection system. The reflectance of the $BaSO_4$ was taken from [2]. The calibration was then obtained from the ratio of the observed reflected radiance (with the appropriate correction to obtain energy conversion from the photomultiplier output) to the calibrated lamp output. Due to the rapid decrease in emissivity of the tungsten lamp at shorter wavelengths, a correction term for the effect of stray light in the monochromator was added in the manner of van der Bos et al. [3]. The stray light correction was made using a glass filter to absorb radiation below 330 nm and assuming that the glass transmits 85% of the light above 400 nm. Comparison of the measured signals with and without the glass filter gives the stray light correction. The relative detection efficiency measured for the Jarrel-Ash monochromator and detection system is shown in Figure 3.3. A similar relative detection

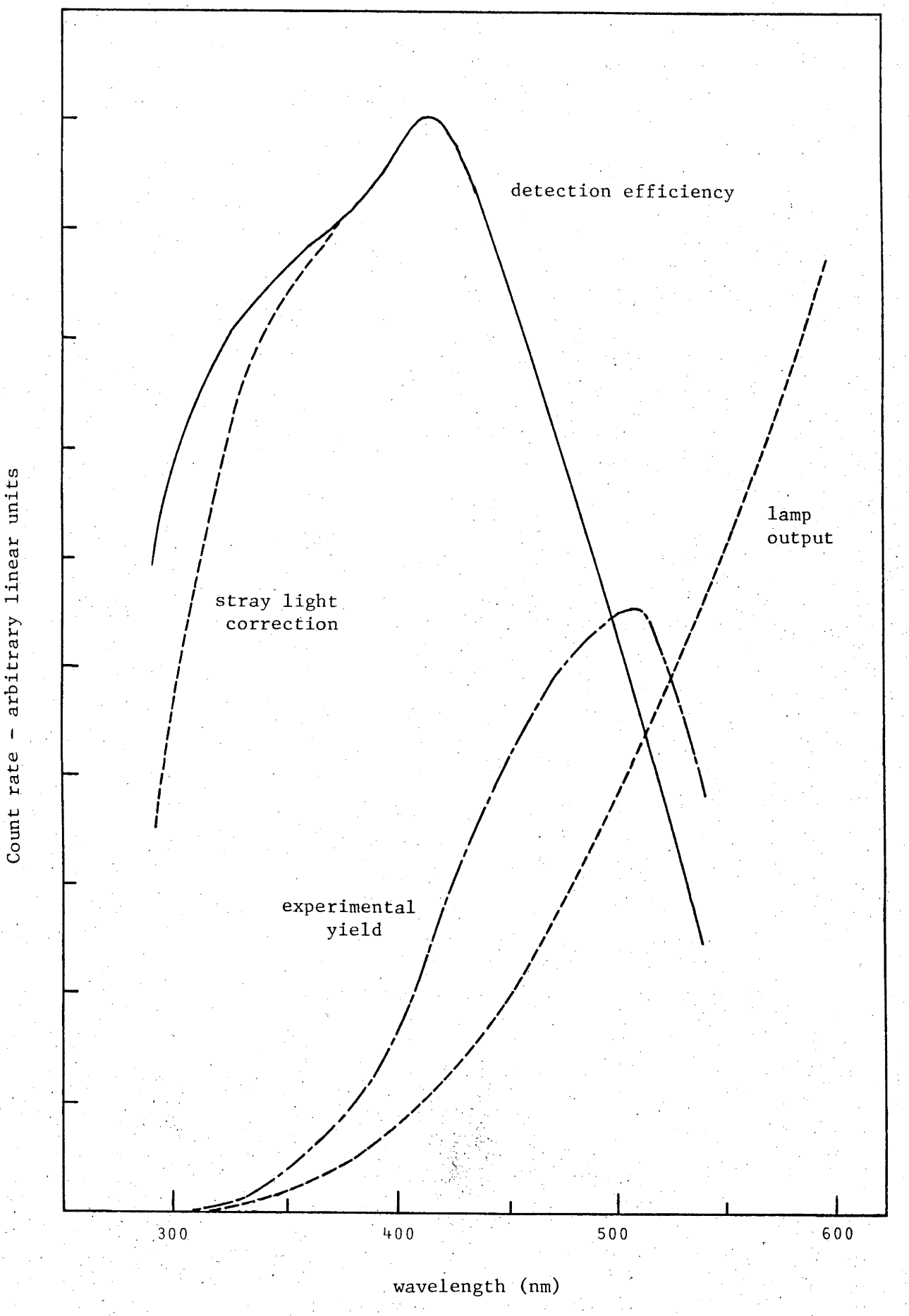

Figure 3.3 Transmission curve derived for the Jarrel-Ash monochromator and associated optical system.

efficiency for the Bausch and Lomb monochromator with the detection system has been measured previously by Martin [4].

A basic SIMS analyser could be used simultaneously with photon detection for medium energy ion bombardment. The SIMS analyser consisted of a stainless steel housing for the quadrupole rods with a shield at the front to stop neutral particles and photons from reaching the detector. The detector was a Channel Electron Multiplier operated in pulse counting mode with 3kV on the multiplier entrance. The RF voltages for the quadrapole were supplied by an EAI Model 450 residual gas analyser controller. The SIMS analyser was designed to accept low energy particles and was capable of mass analysis to 500 amu. Resolution was sufficient for isotope separation.

The low energy ion accelerator system also had facilities for Ion Surface Scattering (ISS) measurements. The analyser, shown in Figure 3.1(b), was a 90° hemispherical electrostatic energy analyser designed for resolution better than 1% [5]. The radii of the inner and outer hemispheres were 4.40 and 5.50 cm respectively. The detector was a bakeable Channel Electron Multiplier operated in pulse counting mode. An operating potential of 3.5 kV was applied to the entrance of the multiplier to accelerate the incoming ions and hence overcome energy dependent efficiency characteristics. The energy analyser was calibrated as within 2% of that expected [5].

3.1.5 *Data Collection and Analysis*

The stepper motors for the wavelength drive of the monochromators could be operated in continuous stepping mode or in unit stepping mode. In continuous stepping mode, the wavelength increases or decreases continuously and this is most useful when using a pen chart (or other continuous) recorder. Unit stepping mode could be most usefully used with a multi-channel-analyser (MCA), such that pulses from the photomultiplier could be accumulated into the MCA for a preset time or ion dosage per wavelength interval. The wavelength interval could be selected using the MacLean stepper motor controller. Pulses from the photomultiplier were passed to a pre-amplifier (Ortec 9301) and then to an amplifier (Ortec 451) before passing to the internal single channel analyser of the MCA (Ortec 6240, 4096 channel). The pulses into the MCA could be gated off by a timer/scaler system after the preselected time or ion dose. During the signal gated off period, the wavelength drive of the monochromator was activated to change to the next wavelength interval. This technique was particularly useful for low count rate situations to measure a count rate versus wavelength curve.

The method for accumulating counts for either the ISS system or the SIMS system was very similar with the wavelength drive replaced by a voltage programmer, which supplied increasing voltage to the hemispherical energy analyser plates or the quadrapole rods respectively.

As mentioned previously, the low energy ion accelerator system had the additional capability for beam rastering. When rastering, the amplifier output was gated off when the beam was outside a preset area, which ranged from 100% to 0% of the total rastered distance in both the Y and Z directions. In this manner, edge effects could be eliminated by choosing a gated area less than the total rastered area so that there was no signal contribution when the beam was at the edge of the rastered area. The gated signal could then be passed to the internal single channel analyser of the MCA.

With the counts versus wavelength (or energy, or time) spectra stored in the MCA, the data could then be taken to a tape punch for hardcopy, or passed directly to a Hewlett Packard 2100 series computer for plotting and analysis.

3.2 THE INFLUENCE OF THE MEASUREMENT METHOD

It will be shown in this section that the measurement technique and experimental geometry may have a strong influence on the results obtained. The main points to be discussed here are (i) the influence of the observation area with particular reference to the measured line profiles and the determination of E^* values using the model of Dzioba et al. [6], and (ii) the influence of the incidence energy and angle on the photon emission, particularly for surface contamination induced intensity changes. There are many other types of results which may be influenced by the experimental method and these will be discussed,

wherever relevant, in the following chapters. The two points discussed here are basic to the experimental method and discussion of these later chapters.

It is evident that surface cleanliness and any edge effects will also play a role in determining the photon emission characteristics in the manner discussed previously in Chapter Two. The cleanliness factors (see section 2.1) for the experiments discussed here and in the following chapters have usually ranged between 700 and 10,000, which are considered sufficient to maintain "clean" conditions. Artifacts in the observed data relating to insufficient cleaning of the target are not considered very probable for the experiments reported here.

3.2.1 *The influence of the observation area and observation geometry*

Publications dealing with photon emission from ion bombarded surfaces have usually (but not always!) reported the observation geometry; but little effort has usually been made to accurately determine the observation area. Examples of the observation geometry used by several groups are shown in Figure 3.4, with some indication of the observation volume (where possible). The proportion of the decay observed will depend upon the viewing geometry, the observation volume and the radiating volume for that particular emission. The radiating volume is determined by the velocity of the particles contributing to the radiation and the level lifetime, through the familiar

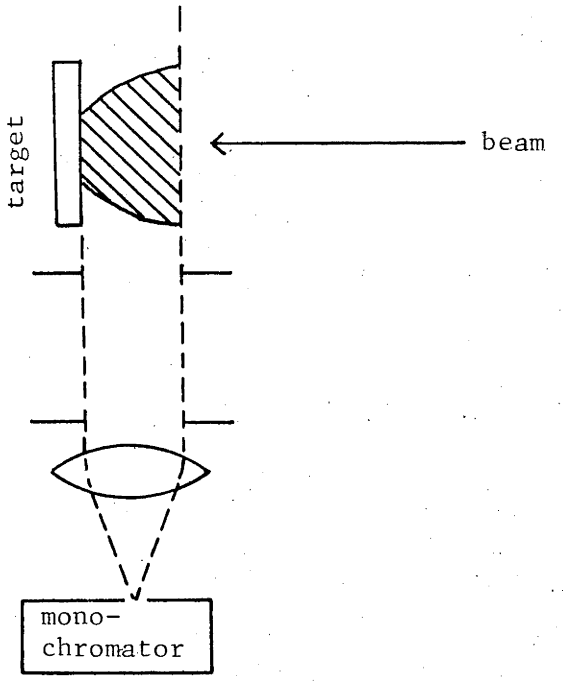

Figure 3.4(a). Experimental geometry used to measure decay curves and E^* values [6-10]. The decay region observed is shown.

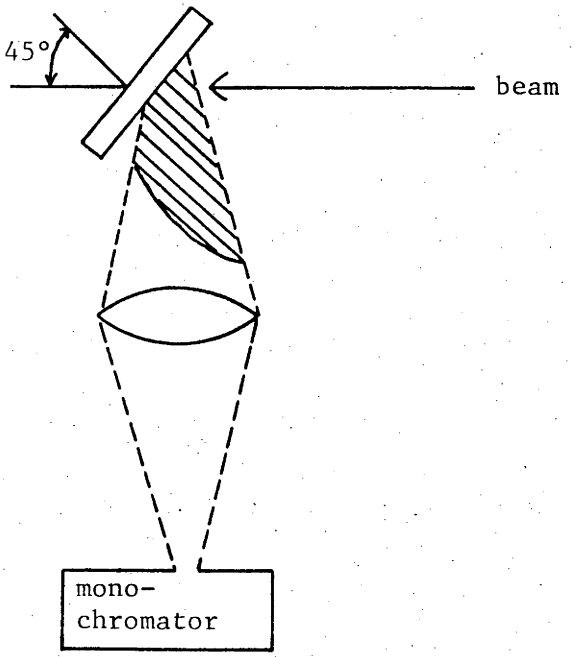

Figure 3.4(b). Experimental geometry used by Martin and MacDonald [11] to measure the relative level populations.

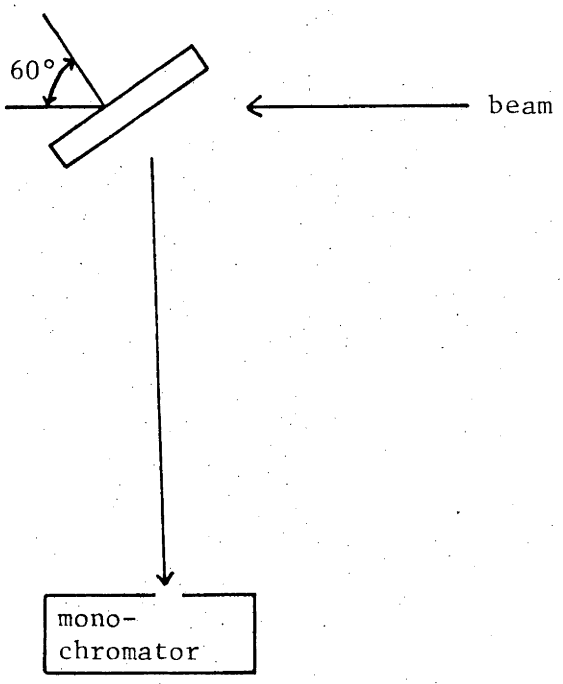

Figure 3.4(c). Experimental geometry used by van der Weg and Bierman 12 to measure line profiles.

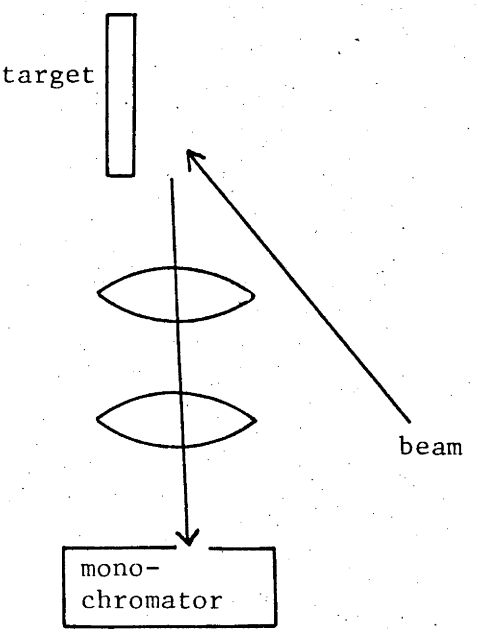

Figure 3.4(d). Experimental geometry used by MacDonald et al. [13] to measure intensity changes with CO exposure.

decay law $I = I_0 \exp\left(-s/v\tau_i\right)$, where s is the distance travelled, v is the particle velocity and τ_i is the lifetime of the level. Integration over the excited particle energy distribution and the sputtering exit angle gives the radiating volume which is characterized by some decay length, defined as the perpendicular distance from the surface over which the intensity falls to a given fraction of the initial intensity. This decay length is particularly important for the geometry shown in Figure 3.4(a), where differential yield observation close to the surface discriminates against particles with high perpendicular velocities which decay further away from the surface. Observation with 45° incidence, as shown in Figure 3.4(b), smears out some of this influence, as a much wider distribution of energies and exit angles is sampled. However, the decay proportion viewed using this geometry is more difficult to define in cases where not all of the radiating volume is observed, than for the case of normal incidence bombardment. The application of differential yield analysis and the influence of the observation volume on the measurement of population densities has been discussed by Snowdon [7].

For integral yield measurements, use of a lens is required to image the whole of the radiating region. It has the disadvantage that an integration over the whole of the radiating region may disguise effects such as cascading, which would become increasingly important at larger distances from the surface. The influence of cascading may be more carefully checked using differential

yield measurements, where the use of observation volume defining slits is needed. The use of slit systems without lenses restricts the use of differential yield measurements to situations where high count rates are found, i.e. most intense lines and often with oxygen contamination to enhance the signals. When using a lens with a slit system for differential yield measurements, as used in this study, great care must be taken to determine the observation volume. Differential yield measurements have the disadvantage that should the radiating volume change (for example, through surface contamination (see 4.1.5)) then the changed proportion of the observed radiation will also influence the yields obtained. Differential yield measurements have the advantage that they may contain information on the changes in yields or other emission characteristics which have not been smeared out by integration over the whole of the radiating volume. The geometry and observation volume (and position) influence on the observed emission line profiles illustrates this.

Line profiles

Consideration of the angular distribution of the sputtered excited particles leads to the conclusion that the position of the spectrometer with respect to the incident beam and target normal will have a large effect on the observed emission line profile and shift. In the case of normal incidence bombardment where a cosinal distribution of sputtered particles is expected, and of sputtered excited

atoms is assumed, observation at 90° to the beam would produce a symmetrical line shape with peak intensity unshifted from the expected wavelength position. Observation at any other forward angle will produce a Doppler shifted line with wavelength shifted to the blue, due to the excited particle velocity component predominantly toward the detector. There may also be an additional peak corresponding to light which has been reflected from the target (which will then be red shifted). The peak shifts may yield additional information provided that the reflected component may be subtracted. Similar arguments may also be applied for cases when the target is not bombarded at normal incidence, remembering that the intensity distribution peaks toward the forward reflection angle [14]. This has been shown in Figure 2.1 and need not be repeated here. Line profiles were usually measured here for normal incidence bombardment, obviating the need for wavelength shift measurements and the need to account for the reflected component.

The line profiles have been measured as a function of perpendicular distance, X, from the target, using differential yield measurements. Changes in the line profile were determined for a line where cascading was not expected to be important (Ti I 399.8 nm) and for the case where the emission line was expected to be influenced by cascading from upper levels (Al I 308.2 nm). These lines are of particular importance to the discussion in Chapters 4 and 5. The experimental arrangement is that shown in Figure 3.2(a). The measured line profiles as a function

of the perpendicular distance from the target are shown in Figure 3.5(a),(b). The line profiles are found to broaden with distance from the target for both the Ti I and Al I lines. The increase in the line width for the Ti I line with distance from the target would not be related to cascading effects but would be expected to be associated with an increase in the average energy of the excited particles, as the lower energy particles decay closer to the surface.

Comparison of line profiles obtained using an integral yield measurement with those in Figure 3.5 have revealed that the emission lines from integral yield measurement were most similar to, but showed a greater contribution to the line wings than, the differential yield measurement at the target surface. This is consistent with the observed rapid decrease in intensity with distance from the target, so that although the line profiles are broader at greater distance from the target surface, the contribution to the total integrated profile is much less than the contribution from particles decaying near the surface.

Line profile data reported in the following chapters were measured using integral yield analysis and these would then be related to an average energy parameter parallel to the surface.

Decay curves

A measurement which depends critically on the observation volume is that of the intensity decay curves

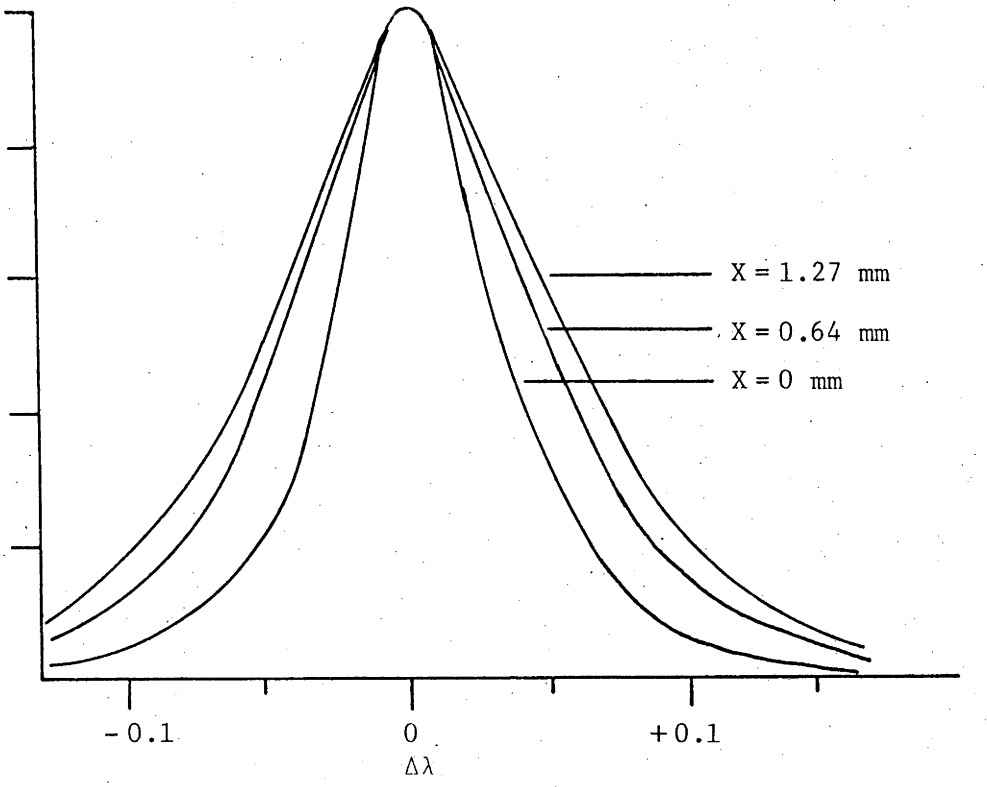

Figure 3.5(a). Line profiles for the Ti I 399.8 nm line measured at different distances from the target. The profiles were obtained for 55 keV $Ar^+ \rightarrow$ Tr at normal incidence under UHV conditions using an instrument resolution of 01039 nm.

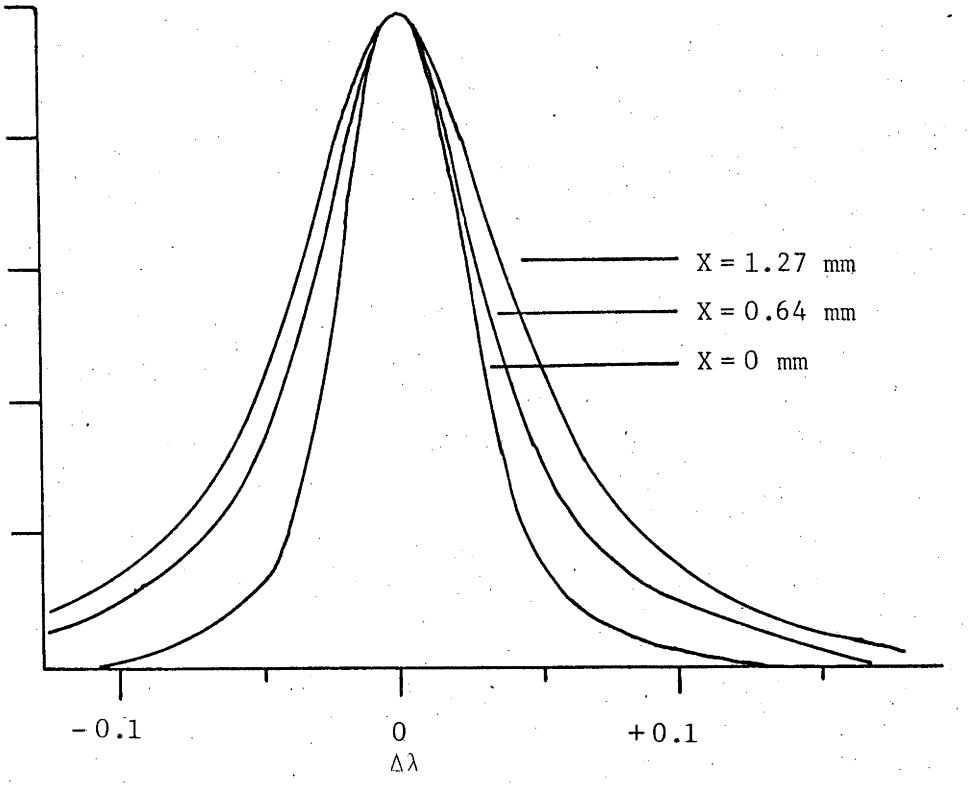

Figure 3.5(b). Line profiles for the Aℓ I 309.2 nm line measured at different distances from the Aℓ target. The experimental parameters were the same as used for (a).

in front of the target. These decay curves may be analysed using the model of Dzioba et al. [6] to determine an energy parameter E^* which is related to the minimum energy of the sputtered excited particles. Evaluation of E^* may proceed via the measurement of the decay curves using a differential yield analysis or integral yield analysis and equation (2.26) or (2.25) respectively. Differential yield measurements have been made in all previous studies with observation volume widths (required to be "sufficiently narrow" [6]) of 0.2mm (Dzioba et al. [6,8]) and 0.15mm (Tsong [9]), defined by fixed observation slits as in Figure 3.4(c).

The influence of the observation volume on the values of E^* obtained will be discussed for a short and a long lived excited state for Ti I (399.8 and 521.0 nm respectively) and an excited state of Al I where cascading is expected to be important (308.2 nm). The internal consistency of the model for predicting the same E^* value for integral and differential yield measurements will also be examined.

The observation volume was determined by the slit width as shown in Figure 3.2(a), where its width is shown to be slightly less than the slit width and slightly trapezoidal in cross section. The influence of the slit width on the E^* value obtained will obviously be related to a characteristic length, L, associated with each transition such that for slit widths greater than this length, the analysis will tend towards an integral yield instead of a differential yield measurement. This characteristic length will be determined by the velocity of the excited particle and the lifetime of the excited state through the

intensity decay law, integrated over the energy distribution and emission angles of the excited particles.

The slit widths were varied between 0.2mm and 4.0mm with the lens in position 2 as shown in Figure 3.2(a) and the target translated in the x direction to obtain differential yield measurements of the decay curves. Measurements were made for the Ti I 521.0nm (τ = 193 nsec [15]) and 399.8nm (τ = 22 nsec [16]) lines and the Al I 308.2nm (τ = 6.5 nsec [17]) line. The decay curves and derived z vs x curves using the differential yield analysis are shown for the Ti I lines from bombarded Ti in Figure 3.6(a),(b). Similar curves for the Al I line from bombarded Al metal are shown in Figure 3.7(a),(b).

Figure 3.7(b) shows a clearly defined break in the curve and this is probably due to cascading influence from the $4p^2p^0$ state ($\tau \sim 50$ nsec [17]). Decay curves obtained for slit widths up to 1.0 mm were essentially the same; however, with slit widths greater than 1.0 mm the initial decay which is dominated by the short lived $4s\ ^2S$ state cannot be resolved. The characteristic length L appears to be about 1 mm for this particular Al state.

The influence of the slit width on the E^* values for Ti I obtained from Figure 3.6(b) using the differential yield analysis is shown in Table 3.1. The values are essentially the same but show a tendency to increase with increasing slit width. This tendency would be expected from consideration of the $Y^{diff}(z)$ and $Y^{int}(z)$ curves [6], as the increased slit width should tend towards an integral yield measurement. The behaviour of E^* with slit width

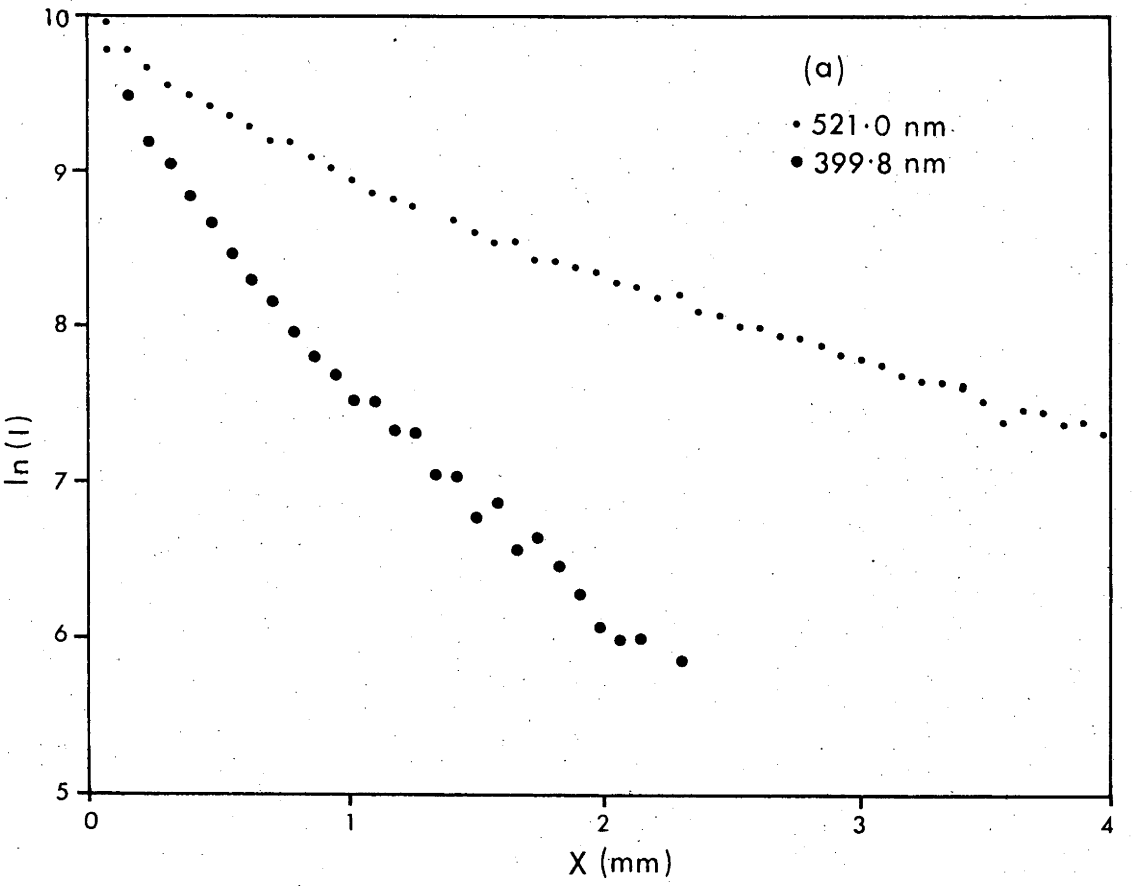

Figure 3.6(a). Differential decay curves for the Ti I 399.8 nm and 521.0 nm lines from Ar^+ bombarded Ti. A 0.4 mm slit width was used although all slit widths from 0.2 mm to 4.0 mm produced identical curves.

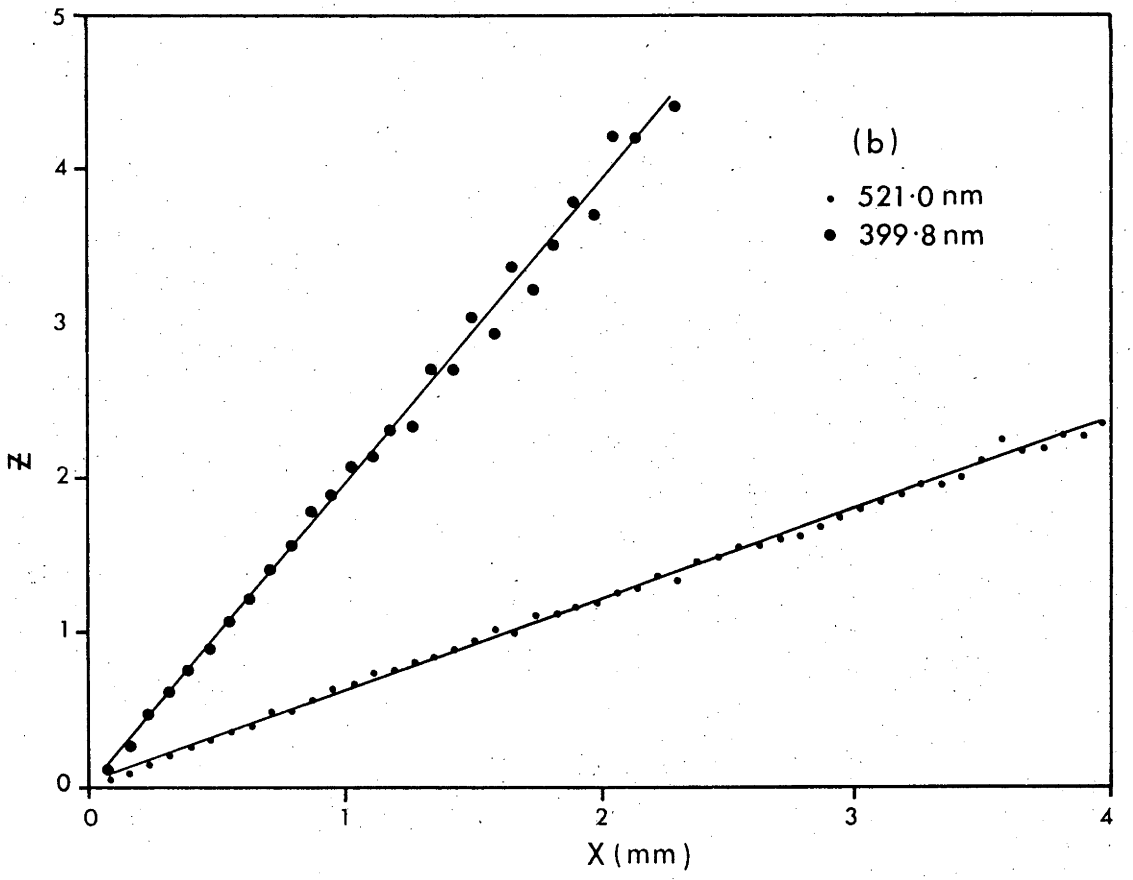

Figure 3.6(b). The z vs x curves derived from (a) using eq. (2.26).

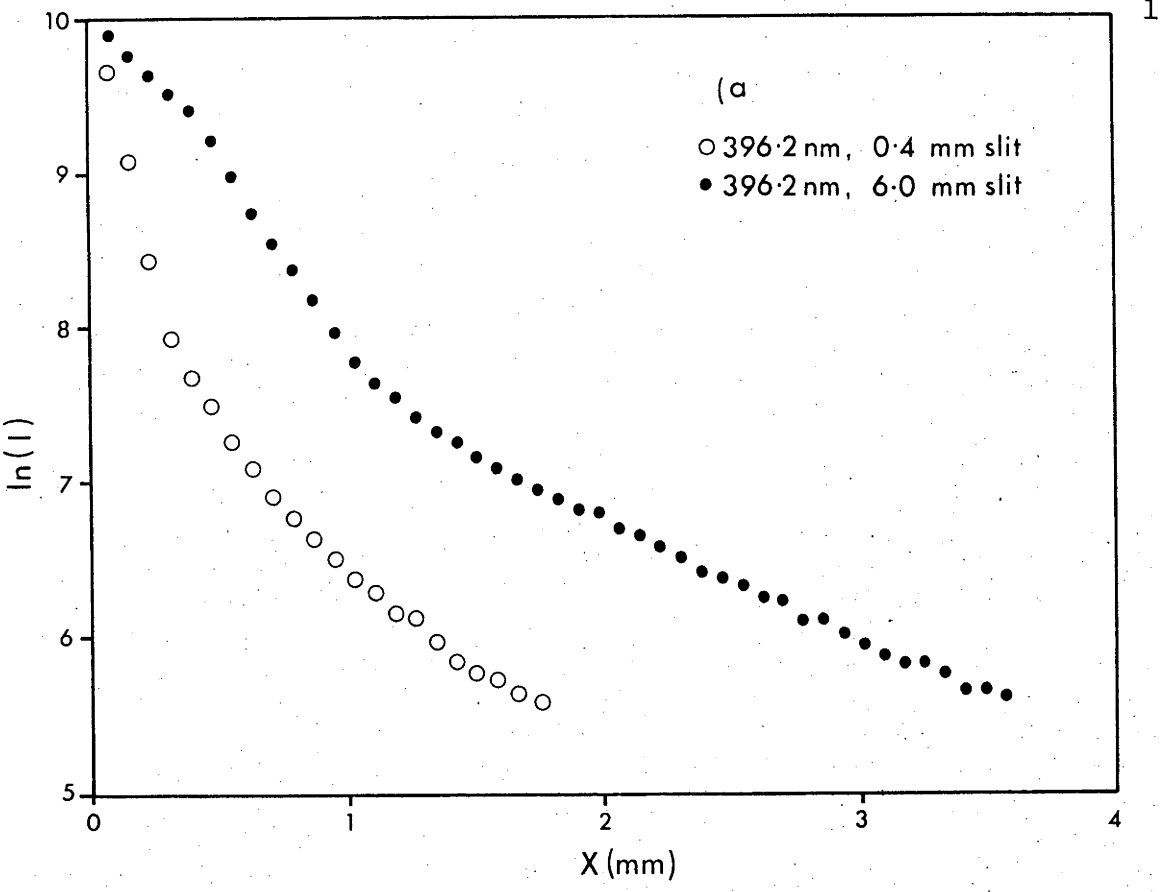

Figure 3.7(a). Differential decay curves for the Aℓ I 396.2 nm line from Ar^+ bombarded Aℓ for the slit sizes 0.4 mm and 6.0 mm. Slit sizes from 0.2 mm to 1.2 mm produced the same normalized decay curves.

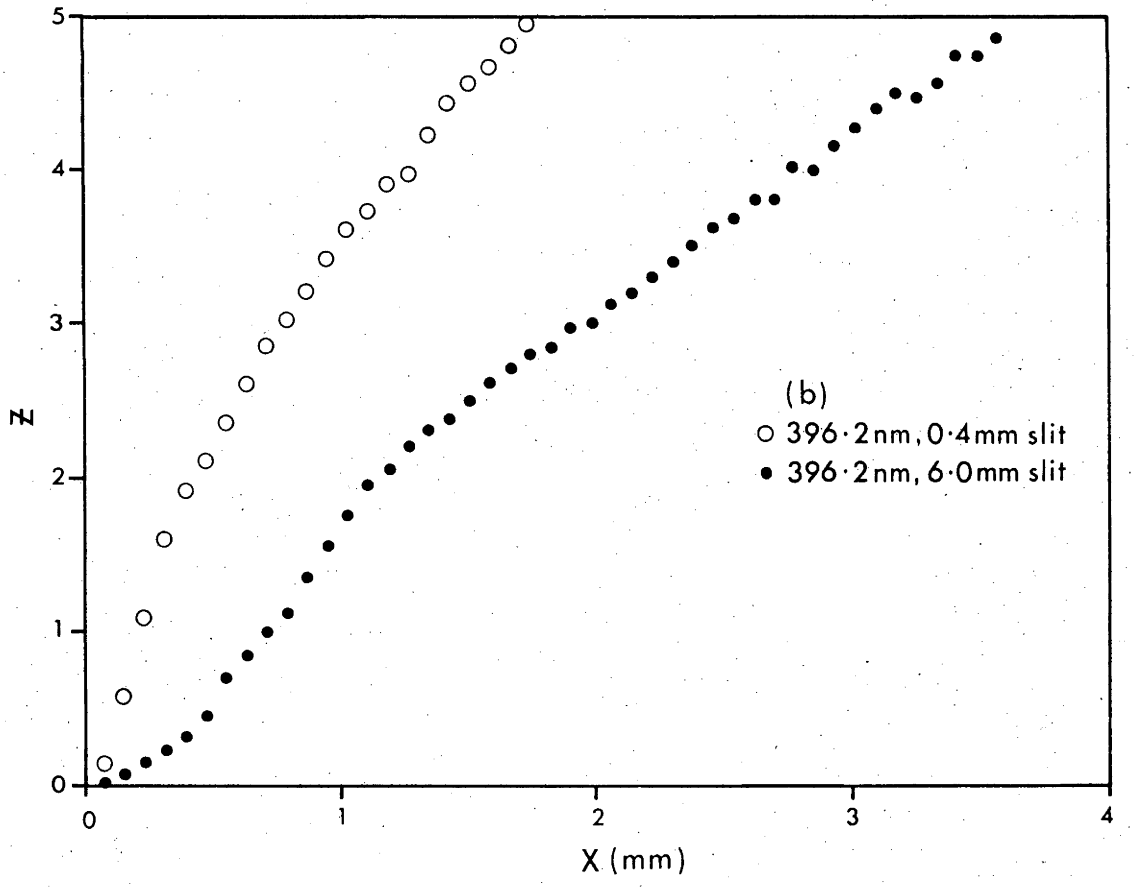

Figure 3.7(b). The z vs x curve derived from (a) using equation (2.26).

is similar for both lines and from Table 3.1 the characteristic lengths for both lines would be expected to be of the order 1-2 mm. It must be remembered that for the lens in position 2 of Figure 3.2(a), the observation volume is slightly narrower than the actual slit width shown in Table 3.1.

TABLE 3.1

The Effect of Slit Width on the Derived Value of E^* for Ti I line emission.

Slit Width	E^*(eV)	
	521.0 nm	399.8 nm
0.2	18.5 ± 0.5	161 ± 10
0.4	18.9 ± 0.5	150 ± 10
0.8		157 ± 10
1.0	19.6 ± 0.5	
1.2		152 ± 10
4.0	21.9 ± 0.5	174 ± 15

To contrast these measurements, the E^* values obtained using the integral form of the decay curve and the differential form for the same curve may be compared. This has been done for the slit width of 4.0 mm which may be expected to approach an integral yield measurement. The z vs x curve derived from Figure 3.6(a) using $Y^{int}(z)$ is shown in Figure 3.8. Importantly, both the integral and

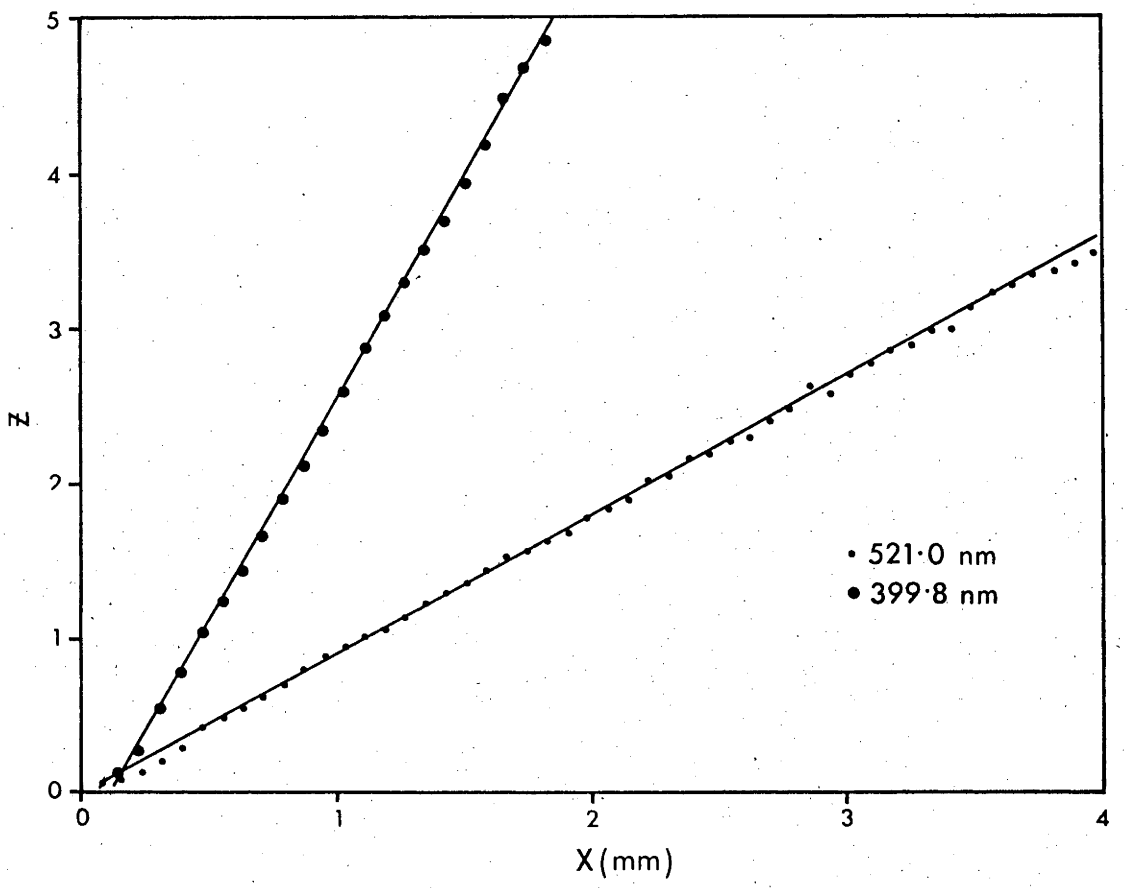

Figure 3.8. The z vs x curves derived from the differential yield measurements shown in Figure 3.6(a) using the integral yield analysis from equation (2.25).

the differential yield analyses produce a linear fit for the z vs x curves and consequently, the fit of the data may not be used for determining a length scale for the experiment. The results of the two analyses for the same experimental data are shown in Table 3.2. The errors shown do not include the contribution from the uncertainty in the level lifetime. The analysis using the integral yield curve predicts a value of E^* significantly lower than the value predicted using the differential yield curve, although the wider slit width used would be expected to tend towards the integral yield measurement. The difference in values, however, is no greater than those derived using the differential yield analysis and different forms of P(E) [10]. This demonstrates the relative insensitivity of using the experimental data to infer the correctness or otherwise of equations (2.26) and (2.25).

TABLE 3.2

Comparison of the use of $Y^{diff}(z)$ and $Y^{int}(z)$ curves to analyse the data of Fig. 3.6(a) using a slit width of 4.0 mm

Ti I λ(nm)	E^*(eV) using $Y^{diff}(z)$	E^*(eV) using $Y^{int}(z)$
521.0	29.9 ± 0.5	8.6 ± 0.5
399.8	174 ± 15	57 ± 12

In order that the model be internally consistent, the values of E^* obtained using a differential analysis of the decay curve and an integral analysis should be the same. To determine the integral yield curve the lens was placed as in position 1 of Figure 3.2(a), where the observation volume was far greater than previous measurements. In this position, the intensity peak was relatively insensitive to target position. The decay curves obtained were used to derive z vs x plots using the $Y^{int}(z)$ curve, to compare with the differential yield measurements shown in Figures 3.6(b) and 3.7(b). The z vs x curves are compared for the Ti and Al lines in Figure 3.9(a),(b). The E^* values are compared for the Ti I lines in Table 3.3. Again the initial Al curve could not be resolved using the integral measurement. For the Ti I lines the results are now almost identical. To allow comparison, the errors shown do not include that due to the uncertainty in the lifetimes of the levels.

TABLE 3.3

Comparison of the E^* values obtained using integral and differential yield measurements for Ti

Ti I λ(nm)	E^*(eV) using integral analysis	E^*(eV) using differential analysis
521.0	22 ± 1	18.5 ± 0.5
399.8	137 ± 15	150 ± 13

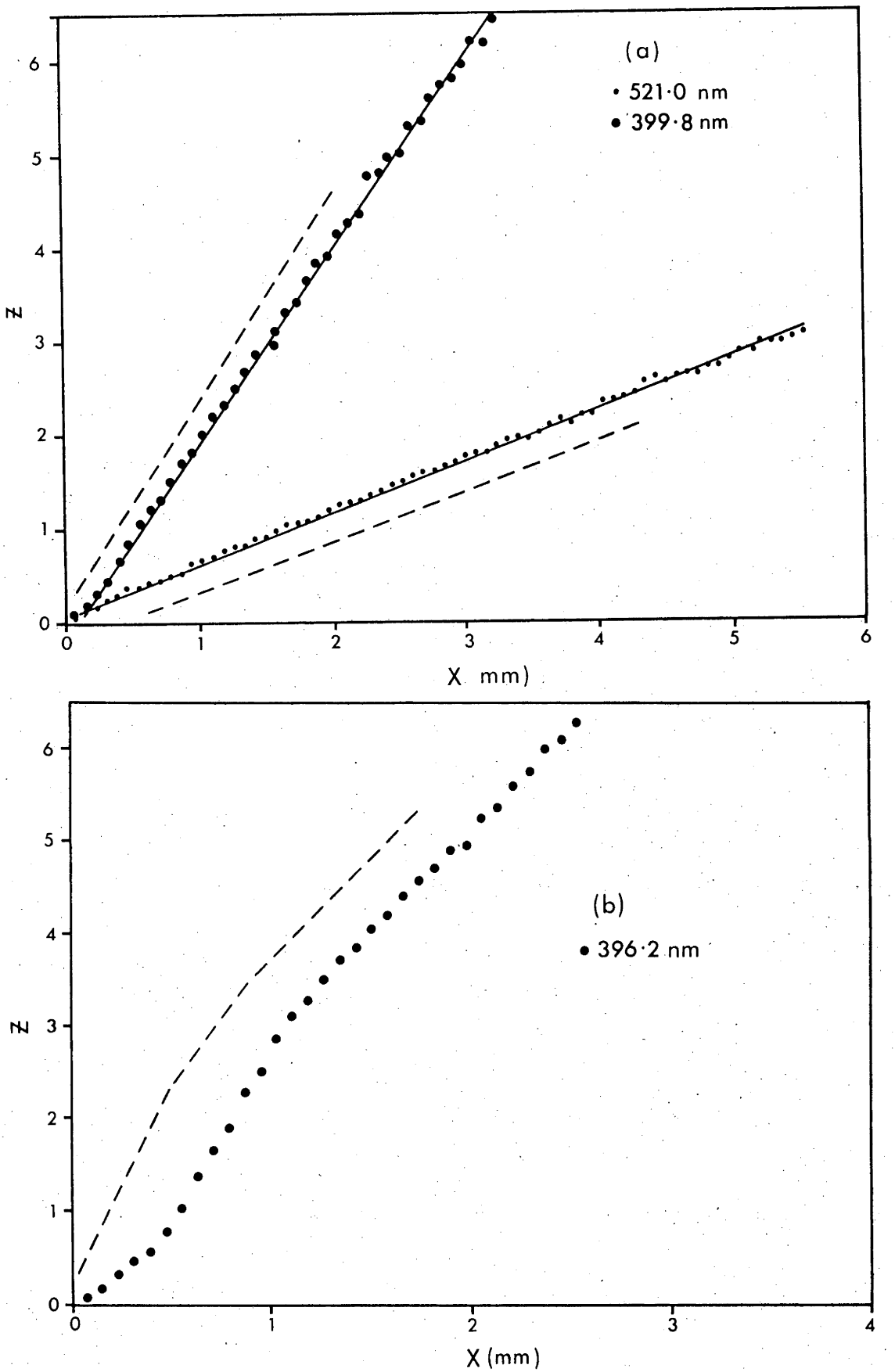

Figure 3.9. The z vs distance curves obtained from integral yield measurement and analysis (solid lines) for (a) Ti I 399.8 nm and 521.0 nm lines and (b) Aℓ 396.2 nm line. The differential yield curves from Figures 3.6(b) and 3.7(b) are shown for comparison (dashed lines).

3.2.2 *The incidence energy and angle*

The influence of the energy and angle of the incident beam on the changes in photon emission intensity with surface contamination has been investigated. The influence of these experimental parameters on the emission line profiles will be discussed in Chapters 4 and 5 with reference to the excitation event. Discrepancies between previous observations of contamination induced intensity enhancements have been discussed in section 2.5 and although the initial surface cleanliness may contribute to these discrepancies, no attempt has been made to investigate the influence of other experimental parameters.

Enhancement of the emission at 399.8 nm by CO contamination for 4 keV Ar^+ bombarded Ti has been measured for three different angles of incidence. The viewing geometry was similar to that shown in Figure 3.4(d) with an integral yield analysis made at 45° to the incident beam. The Bausch and Lomb monochromator was used which is sensitive to continuum emission (due to its modest resolution). No attempt was made to subtract the continuum emission component, although this was found to be between 20 - 40% of the total emission at high exposure. The observed intensity enhancements for the different incidence angles are shown in Figure 3.10, where it can be noted that the enhancement with CO contamination is significantly higher at increased incidence angle. At larger incidence angles, the CO contamination has greater influence at lower exposures and this would be related, in part, to the decreased beam current density. The continuum emission

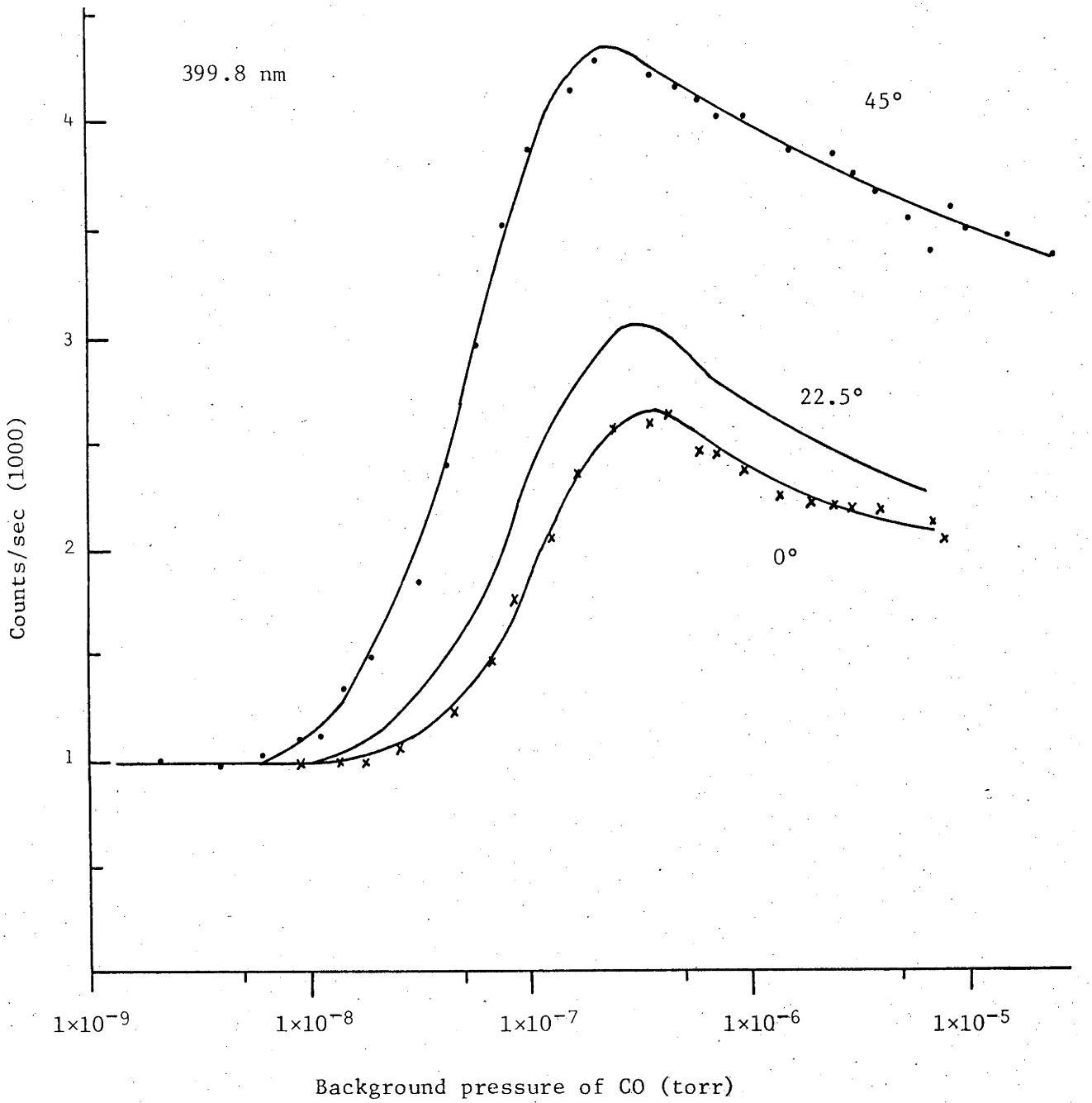

Figure 3.10. Changes in the intensity of emission at 399.8 nm with CO exposure at different incidence angles for 4 keV Ar^+ bombardment of Ti. The curves have been normalised at the cleanest conditions.

component was also noted to change with the incidence angle and exposure. Further discussion of continuum emission changes with surface contamination will be made in Chapter 6.

Similar changes in intensity of the emission at 399.8 nm due to oxygen exposure have been measured for Ar^+ bombarded Ti with different incidence energies of 4 keV and 55 keV. The observed intensity changes are shown in Figure 3.11. Normal incidence bombardment and integral yield measurements were made in both cases. The relative enhancements were monitored by the Bausch and Lomb monochromator for 4 keV bombardment and the Jarrel-Ash monochromator for 55 keV bombardment. The Jarrel-Ash monochromator, with its higher resolution, is not as sensitive to continuum emission as the Bausch and Lomb monochromator. No attempt was made to subtract continuum emission in either case. The continuum emission component for the case of 4 keV Ar^+ incident on Ti was about 30% at the intensity peak and the corresponding component for 55 keV Ar^+ bombardment was about 2-5%. This difference would not account for the discrepancy in the two curves of Figure 3.11.

Different incident energy Ar^+ bombardment of Ni showed similar behaviour for the Ni I 325.4 nm emission to that found for Ti where the enhancement with surface contamination was found to vary with the incidence energy. The difference between the enhancement of the Ni I 325.4 nm line with O_2 exposure for 4 keV and 55 keV Ar^+ bombardment was particularly pronounced and warrants further investigation.

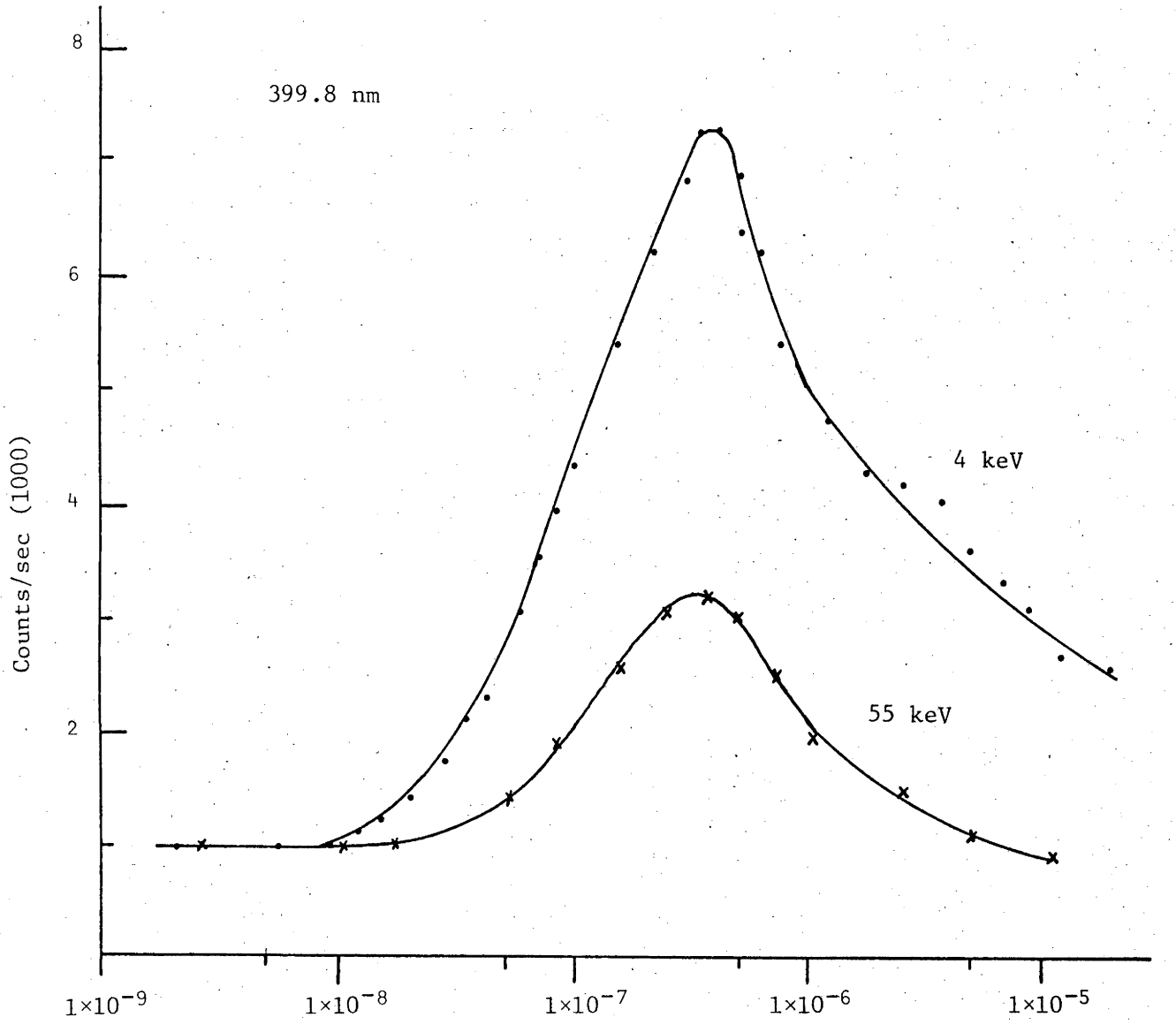

Figure 3.11. Changes in the intensity of emission at 399.8 nm with O_2 exposure for 4 keV and 55 keV Ar^+ bombardment of Ti at normal incidence. The curves have been normalised at the cleanest conditions and the curve for 55 keV Ar^+ bombardment has been shifted to make the intensity peaks coincide (the curves were measured on different systems).

From Figure 3.11, the exposure at which the relative intensity begins to increase for the Ti I 399.8 nm line corresponds to a ratio of arrival rates of background oxygen molecules to incoming beam ions of about 30 (determined using equation (2.1)). This value would lend support to the proposal (section 2.1) that a cleanliness criterion may be established with a boundary condition for cleanliness at a cleanliness factor of 100, at least for Titanium.

3.2.3. *Discussion and conclusions*

A brief study of the relationship between the observed data and the method of measurement has shown that, unless considerable care is taken, the data may be strongly influenced by the experimental method. The need to accurately define and state the experimental parameters has been demonstrated.

The observation volume has been shown to be critically important in the measurement of decay curves and their subsequent analysis using the model of Dzioba et al. [6]. Disregarding for the moment the validity or otherwise of this model, its internal consistency has been shown for the use of either integral or differential yield measurements to be used to derive a parameter E^*. However, care needs to be exercised in ensuring that the expected integral yield measurement does observe the whole radiating region and that the observation volume is less than the characteristic

decay length for differential yield measurement. The linear fit of the data in the derived z vx x form does not indicate that these conditions have been satisfied.

Influences on the measured line profiles and contamination induced enhancements have also been examined. The emission line profiles were found to change by up to 50% with observation volume position for normal incidence bombardment and differential yield analysis. Integral yield measurements of the line profiles were found to be similar to the differential yield measurements made at the target surface. Contamination induced enhancements of the photon emission were found to change in magnitude with varying angle of incidence and incidence energy of the bombarding beam. The preliminary nature of the investigation shown in Figures 3.10 and 3.11 should be emphasized and a thorough experimental investigation of the influence of the incidence angle and energy is needed.

The influence of the monochromator used, has also been mentioned. This is particularly important for continuum emission studies where a higher resolution monochromator will discriminate against weaker broad emissions.

The results illustrate that care must be made in comparing and attempting to apply photon emission models to the results of different experiments where different experimental parameters and methods were used.

REFERENCES

[1] M.R. Zatzick, Application Note 71021, SSR Instruments Co. (1970).

[2] F. Grum and G.W. Luckey, Appl. Optics 7 (1968) 2289.

[3] J. van der Bos, G.J. Winter and F.J. de Heer, Physica 40 (1968) 357.

[4] P.J. Martin, Thesis (1976) Australian National University.

[5] D.J. O'Connor, Thesis (1978) Australian National University.

[6] S. Dzioba, O. Auciello and R. Kelly, Radiation Effects 45 (1980) 235.

[7] K.J. Snowdon, Radiation Effects 42 (1979) 185

[8] S. Dzioba and R. Kelly, Surface Sci. 100 (1980) 119.

[9] I.S.T. Tsong and N.A. Yusuf, Nucl. Instr. Methods 170 (1980) 357.

[10] S. Dzioba and R. Kelly, Surface Sci. to be published.

[11] P.J. Martin and R.J. MacDonald, Surface Sci. 62 (1977) 551.

[12] W.F. van der Weg and D.J. Bierman, Physica 44 (1969) 206.

[13] R.J. MacDonald, E. Taglauer and W. Heiland, Applications of Surface Sci. 5 (1980) 197.

[14] H. Kerkow, Phys. Stat. Sol. (a) 10 (1972) 501.

[15] W.L. Wiese and J.R. Fuhr, J. Phys. Chem. Ref. Data 4 (1975) 263.

[16] B.L. Cardon, P.L. Smith and W. Whaling, Phys. Rev. A 20 (1979) 2411.

[17] K. Jensen and E. Veje, Z Physik 269 (1974) 293.

CHAPTER FOUR

PHOTON EMISSION FROM ION BOMBARDED Ti AND ITS COMPOUNDS

In this chapter, a detailed study of Ti I photon emission from sputtered Ti atoms has been made. A thorough study of the band structure model and its application to the Ti system has been discussed in section 4.1. Reference has been made to the relative population of the excited levels, the energies of the emitting atoms and the changes observed with oxygen contamination. Other factors influencing the results are also discussed. Section 4.2 has concentrated on the measurement of kinetic energy related parameters for the emitting Ti atoms sputtered from Ti and several Ti compounds. An attempt has been made to discuss these findings with relation to possible excitation processes.

The Ti I emission lines of particular importance in this chapter are shown in the Ti I energy level diagram, Figure 4.1.

4.1 THE INFLUENCE OF NON-RADIATIVE TRANSITIONS ON Ti I EMISSION

4.1.1 *Introduction*

The application of the band structure model and interpretation using non-radiative transitions in competition to photon emission, has been discussed in section 2.2.4. The band structure model has found qualitative agreement for some

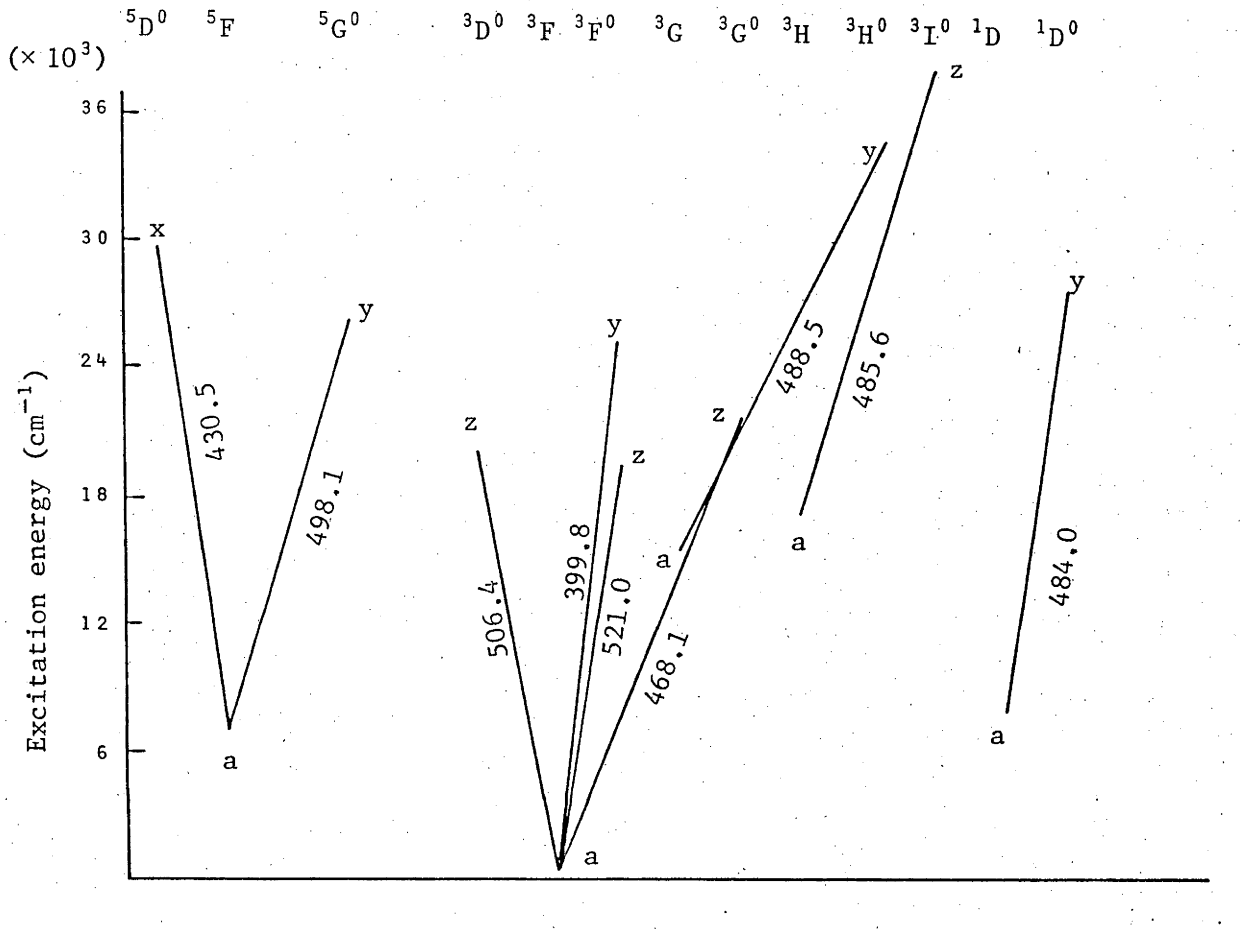

Figure 4.1 Partial Grotrian diagram for Ti I showing the transitions of importance to the discussion in this Chapter. The wavelengths for the transitions are in nm.

bombarded elements but has not been able to predict the behaviour of the photon emission with oxygen contamination in some other cases.

No thorough investigation has been reported for excited states which lie opposite filled, empty and forbidden regions of the conduction band, to determine the intensity changes for these three groups of excited atoms due to changes in the band structure. Thomas and De Kluizenaar [1] report results for states opposite the empty conduction band of Cu, but other quantitative studies have not rigorously tested the predictions of the charge exchange model. Usually an oxide-like structure has been assumed,although this may not be realistic under bombardment conditions and a more accurate surface characterization is required.

A detailed study of photon emission from a system where the upper energy levels of the excited states of the atom span the occupied and unoccupied states of the conduction band and forbidden states of the bombarded material should yield detailed information on the role of exchange processes. Ti and its oxides are such a system, where the wide range of upper levels for Ti I span the three mentioned regions of the metal, and furthermore, there are a large number of spectral lines in a practical wavelength region for study.

The non-radiative processes are expected to influence the intensities and the velocities of the particles contributing to the radiation. It would be expected that any electron exchange process which competes

with and reduces photon emission should influence the observed Boltzmann-like distribution of excited states. In the case of the reduced intensity plots for Fe [2], all the upper energy levels of the lines considered lie opposite the same region of the band structure and no influence on the reduced intensity plots would be expected using the resonance ionisation model. For Ti, where the wide range of excitation energies span a large region of the band structure, a discontinuity in the reduced intensity plot at the Fermi level would be expected using this model for excited states above and below the Fermi level. Boundaries between unoccupied and forbidden regions in the band structure would be expected to be similarly indicated.

Atom energy levels are expected to be broadened at the small distances from the surface at which the non-radiative processes are important [3]. However, choosing a system with a relatively wide range of excitation levels should result in differences between the non-radiative processes influencing these levels.

4.1.2 *Reduced intensity plots*

All reduced intensity plots were obtained using photon intensities measured by scanning the monochromator through the wavelength range from 300 - 522 nm. Photon spectra for Ar^+ bombarded Ti and TiO_2 are shown in Figure 4.2. Observation was made parallel to the target surface with an observation volume close to the integral yield analysis method shown in Figure 3.2(a). As the

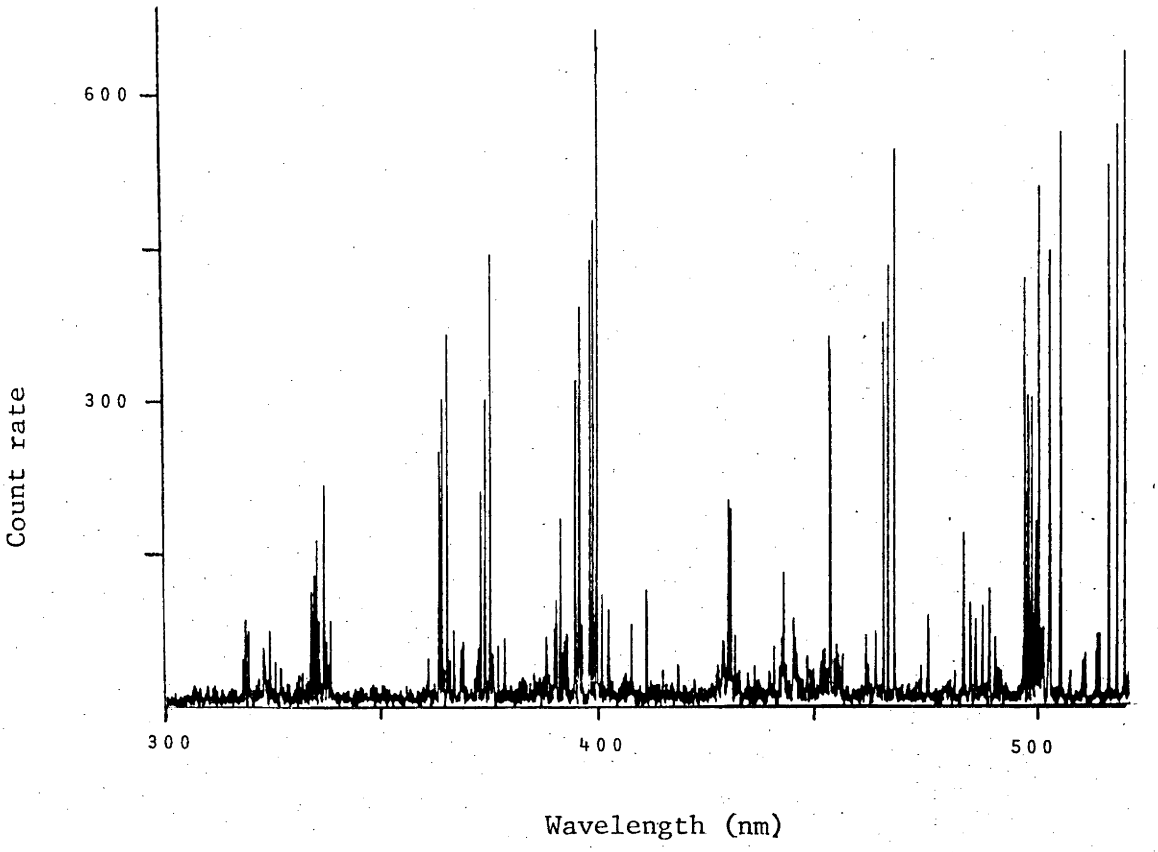

Figure 4.2(a). Emission spectrum from Ar^+ bombarded Ti under UHV conditions.

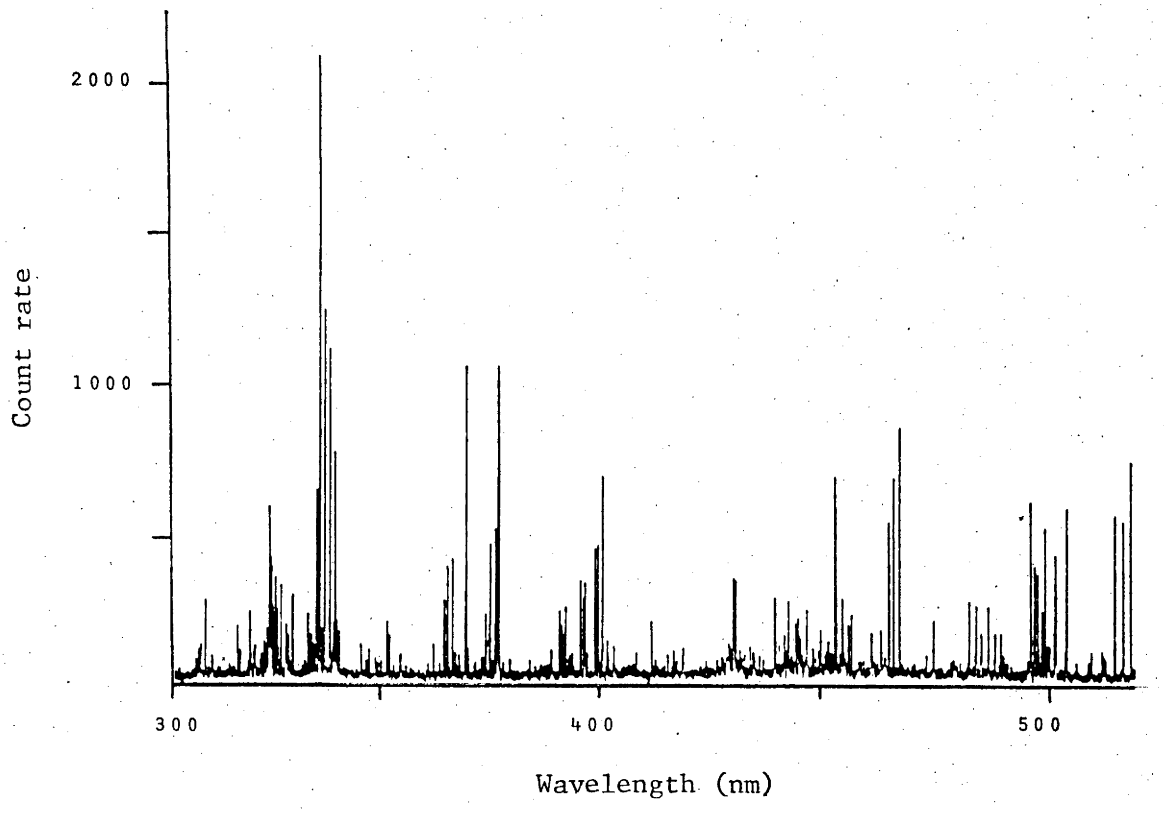

Figure 4.2(b). Emission spectrum from Ar^+ bombarded TiO_2. Ti II emission lines around 330 nm dominate the spectrum.

entire decay region was not viewed, lifetime effects will play some part in determining the number of photons observed. Excitation levels with longer lifetimes will have a larger proportion of radiative decay outside the observation region (this will be discussed in a later section). No corrections have been made for this, as only relative changes between bombarded targets are of interest.

The derived reduced intensity plot for Ti from 55 KeV Ar^+ bombarded Ti using equation (2.21) is shown in Figure 4.3. To contrast this plot, the reduced intensity curve derived through the plasma approximation, equation (2.14(a)), is also shown. The g_i and A_{ij} values are from [4]. The influence of the added term for the branching ratio in the case of Ti I is shown to be particularly strong, with the "slope" of the guide line changing dramatically. Using the LTE model, this would change the derived "T" parameter from about 4500°K to around 8000°K, higher than that normally found as a fitting parameter for SIMS data [5]. However, it is clearly difficult to accurately determine the lifetimes and branching ratios (equation (2.19)) as some of the A_{ik} values are not known. Obvious corrections to the branching ratios used in obtaining Figure 4.3 need to be made.

For example, the 411.2 nm line does not lie on the line shown in Figure 4.3(b), however the lifetime calculation for this level does not include contributions from the 1055.18 nm, 794.92 nm and 407.64 nm lines which are alternative radiative decay channels. From intensity tables [6], the relative A_{ik} values for this excited state

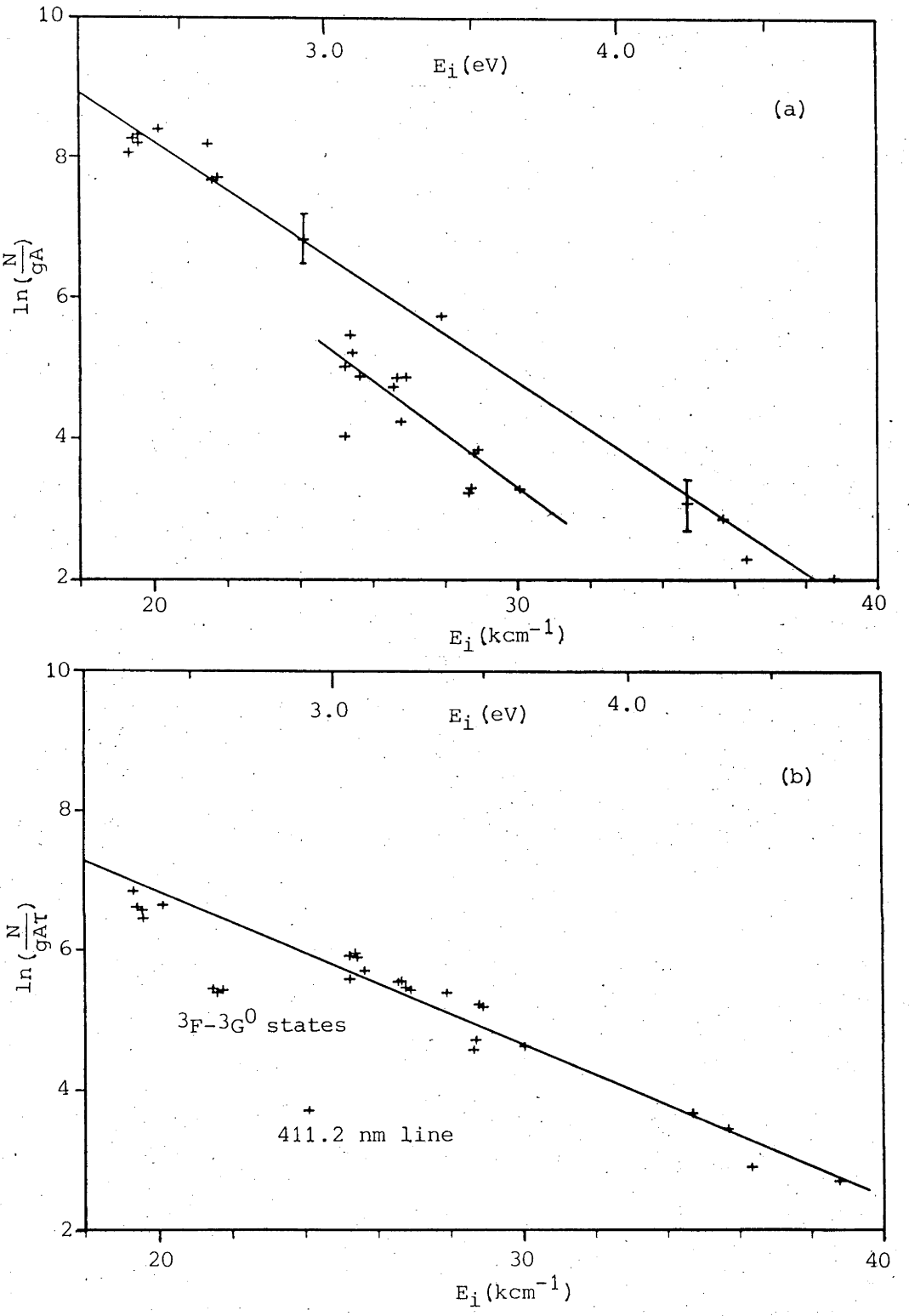

Figure 4.3(a). Reduced intensity plot for Ti I emission from 55 keV Ar^+ bombarded Ti under UHV conditions and using the plasma approximation, equation (2.14(a)).

4.3(b). Reduced intensity plot for Ti I for similar experimental conditions but using equation (2.21).

may be estimated and a decrease of about 50% in the calculated lifetime would be expected. This would shift the point up closer to the line of Figure 4.3(b). Similar arguments may be applied to the transitions between the $^3F - {}^3G^0$ states in Figure 4.3(b) causing these points to shift slightly upward. Another important factor is that these two examples have lifetimes significantly longer than other lines and hence more of their radiation will occur outside the observation volume. The extent of these lifetime corrections will be discussed in a later section.

It has previously been shown [7,8] that cascading from higher levels to the excitation level studied, may be of importance. A correction of the form of expression (2.20) for the 521.0 nm line of Ti I with $E_i = 19574$ cm^{-1}, which would be influenced by cascading from the 456.3 nm and 547.7 nm lines, has been estimated assuming a Boltzmann distribution of excited states and is of the order of 6%. This would not be significant on the reduced intensity plots shown.

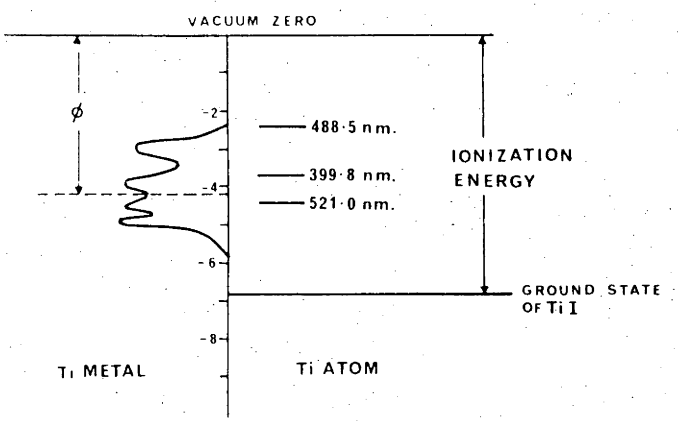

Figure 4.4 A schematic comparison of the energy levels of Ti metal with selected Ti I lines. The three Ti I lines have been found to be typical of the Ti I lines which lie below, opposite and above the empty conduction band of Ti metal as shown and have relatively strong intensities for observation. ϕ is the work function.

The corrected plot, Figure (4.3(b)), may be compared with the band structure of Ti as shown in Figure 4.4, where selected excited states of the Ti atom are shown for comparison. The shape of the density of states function is taken from the calculations by Welch and Hygh [9], and is located such that the Fermi level corresponds to the work function for Ti [10]. It can be noted from Figure 4.4 that there are excited states with excitation level opposite the empty conduction band. These levels should be susceptible to a resonance ionisation process as proposed by Gritsyna et al. [11]. This competing process should decrease the intensity of photon emission from these levels, however no discontinuity in Figure 4.3(b) is observed which may be attributed to this process. The discontinuity in the region of the Fermi level and the top of the empty conduction band as shown in Figure 4.3(a) disappears when the branching ratio term is included.

Ti I emission from bombarded TiO_2 (single crystal but with random orientation) has also been studied for comparison with that obtained from the bombarded metal. Reduced intensity plots for 55 keV Ar^+ and O_2^+ bombardment of Ti and TiO_2 are shown in Figure 4.5. Also shown are the reduced intensity plots for Ar^+ bombarded Ti and TiO_2 under dynamic oxygen exposure conditions, the oxygen partial pressure being mid 10^{-6} torr.

Similar experiments have also been performed with TiO targets and the spectra,reduced intensity plots and line profiles obtained from bombardment of TiO and TiO_2 have been found to be identical. Sintered powder TiO_2 samples were

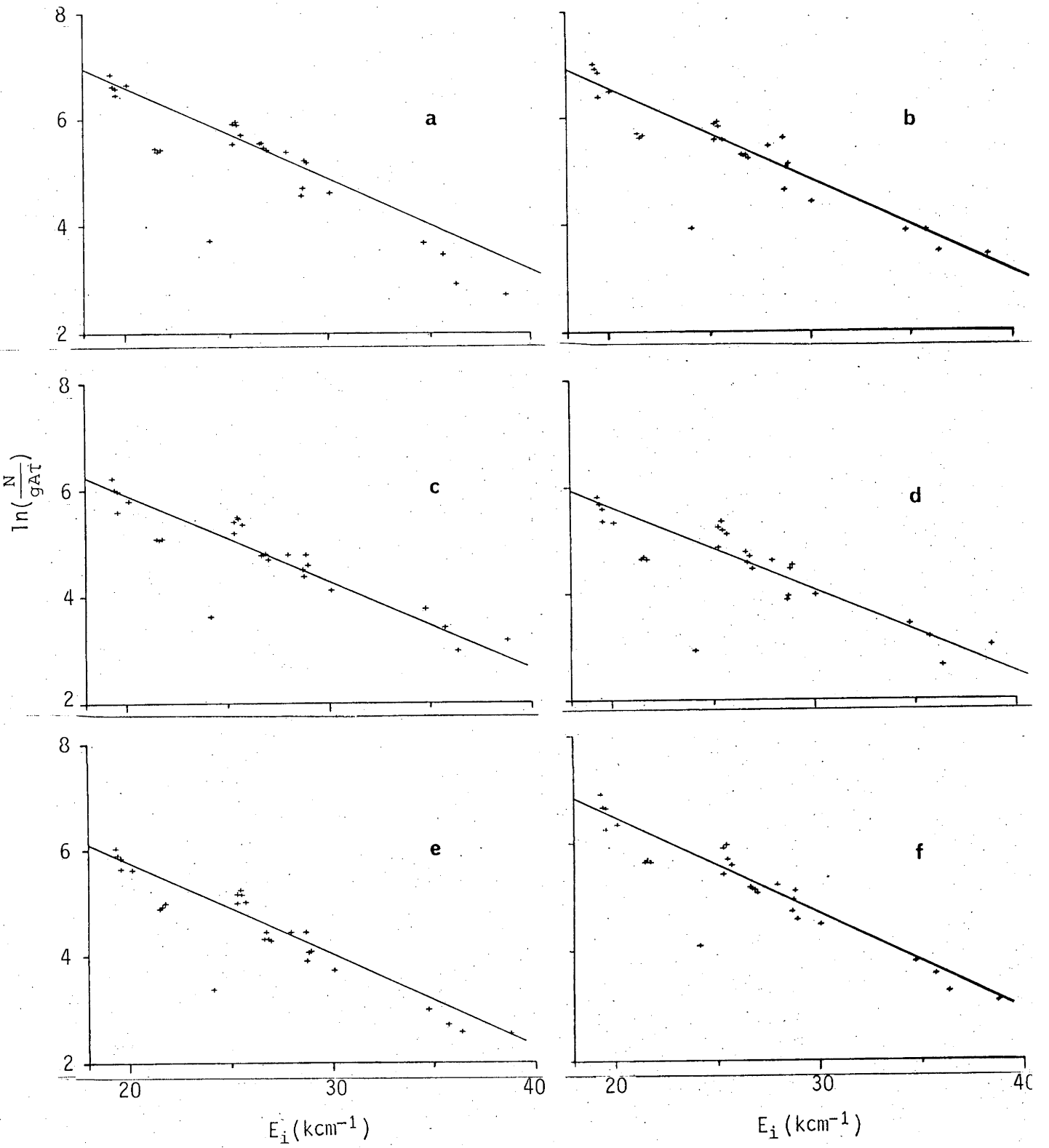

Figure 4.5 Reduced intensity plots using equation (2.21) for TiI for (a) $Ar^+ \rightarrow Ti$, (b) $Ar^+ \rightarrow TiO_2$, (c) $\rightarrow Ti + O_2$, (d) $Ar^+ \rightarrow TiO_2 + O_2$, (e) O_2^+ Ti and (f) $O_2^+ \rightarrow TiO$. All measurements were made under UHV conditions except for (c) and (d) where the oxygen partial pressure was 6×10^{-6} torr. The incidence energy was 55 keV. For comparative purposes, the straight line fits have been drawn such that all lines are parallel to that for $Ar^+ \rightarrow TiO_2 + O_2$.

found to change colour after irradiation to that of the unbombarded TiO sintered powder target. This suggests, as found by others [12 - 15], that the TiO_2 target is reduced to a TiO_x (where $x < 2$), or possibly Ti_2O_3 [12] surface under Ar^+ bombardment.

4.1.3 *The influence of oxygen exposure on the photon intensity*

The main use of the band structure model has been to attempt to explain, in a qualitative manner, the changes in the photon emission intensity with oxygen exposure. A study has been made here of the changes in photon yield as a function of oxygen exposure for the three lines shown in Figure 4.4. Intensity changes for these lines with oxygen exposure from Ar^+ bombardment of TiO_2 have also been monitored. These results are shown in Figure 4.6. The Ti sputter yield variation with oxygen exposure for Ar^+ bombardment measured by Hofer and Martin [16], is also indicated for comparison. However, it must be noted that a different beam energy of 11 keV has been used by Hofer et al. The photon intensity changes are summarized in Table 4.1.

It must be pointed out that the data points at the lowest oxygen to ion bombardment ratio are taken where the increasing pressure due to oxygen leakage begins to alter the gauge reading. As the residual gas before leaking is oxygen is principally Ar (from the beam), the plateau region probably extends down at least one order of magnitude below that shown. No reliable estimate of the ratio

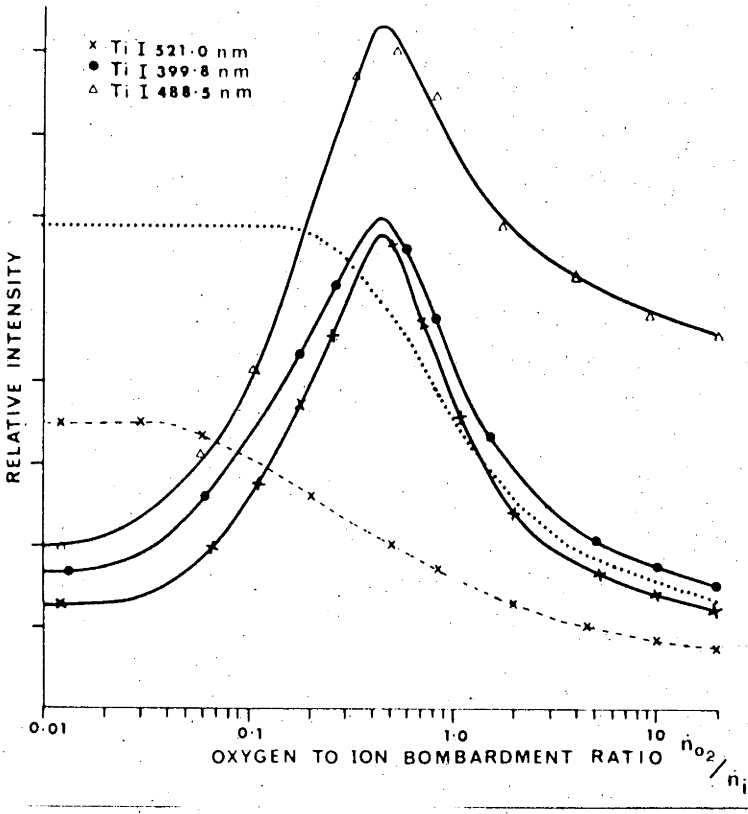

Figure 4.6. The variation of Ti I photon yield with oxygen exposure for 55 keV Ar^+ bombarded Ti. Oxygen exposure is expressed in terms of the ratio of the rate of arrival of oxygen to the surface ($\dot{n}_0$) to the rate of arrival of the beam current ($\dot{n}_i$). The solid lines represent the variation in intensity for the bombarded metal and the dashed line shows the variation for the bombarded dioxide. The dotted line shows the variation of the sputtered yield of Ti with oxygen exposure for comparison [16]. The curves from the bombarded metal have been normalized at $\dot{n}_0/\dot{n}_i \simeq 0.01$ and have been vertically shifted for clarity.

TABLE 4.1

Changes in photon intensity with the ratio of of oxygen to ion arrival rate $\dot{n}_0/\dot{n}_i$. Intensities are relative to that at $\dot{n}_0/\dot{n}_i \simeq 10$ for each line

λ (nm)		$(\dot{n}_0/\dot{n}_i < 0.01)$	$(\dot{n}_0/\dot{n}_i \simeq 0.45)$	$(\dot{n}_0/\dot{n}_i \simeq 10)$
521.0	Ar^+ on Ti	1.0	3.9	1
399.8		1.0	3.3	1
488.5		0.4	1.8	1
521.0	Ar^+ on TiO_2	4.3	2.4	1
399.8		4.1	2.5	1

of arrival rates for contaminant and beam could be made in this region and only the observed increase in pressure has been included in Figure 4.6.

It has been noted previously for Cr [17] that the intensity of neutral lines initially increased with oxygen exposure to a maximum and then decreased, with the decrease being attributed to the change in the sputtering yield. The photon intensity from Ti I behaves in a similar manner to the Cr result. Figure 4.6 indicates the similarity in the photon decrease and the change in sputtering yield as measured by Hofer and Martin. It can be clearly seen that the variation of the photon emission with oxygen exposure for the 488.5 nm line is different.

4.1.4 *The kinetic energies of the particles contributing to radiation*

As demonstrated in section 2.2.4, the emission line profiles may yield information on the non-radiative processes which are able to influence the excited atoms. The lines studied by the high resolution scanning monochromator are again those shown in Figure 4.4. A summary of the line profile data is given in Table 4.2.

As noted earlier with the intensity changes for oxygen exposure, the 521.0 nm and 399.8 nm spectral lines show similar behaviour, both showing a decrease in FWHM of about 25% for oxygen exposure. These changes for the 521.0 nm line are shown in Figure 4.7. The $\Delta\lambda/\lambda$ values for these two lines are also different with oxygen exposure. The 488.5 nm line is different to both of the other lines, being much wider, although its behaviour with oxygen is similar.

In summary, the 521.0 nm and 399.8 nm lines show similar behaviour in relation to intensity and line profile changes with oxygen exposure. The 488.5 nm line appears to behave differently to these. The line profiles decrease in width with oxygen contamination until saturation, after which further changes in intensity (a decrease) are not accompanied by a change in the line profile.

To compare with the data of Gritsyna et al. [11], an attempt has also been made to estimate the kinetic energies of the excited atoms by measuring the decay curves in front of the target. Only the initial region of the decay has been observed (the target movement was less than 2.0 mm, with an integral viewing geometry as shown in

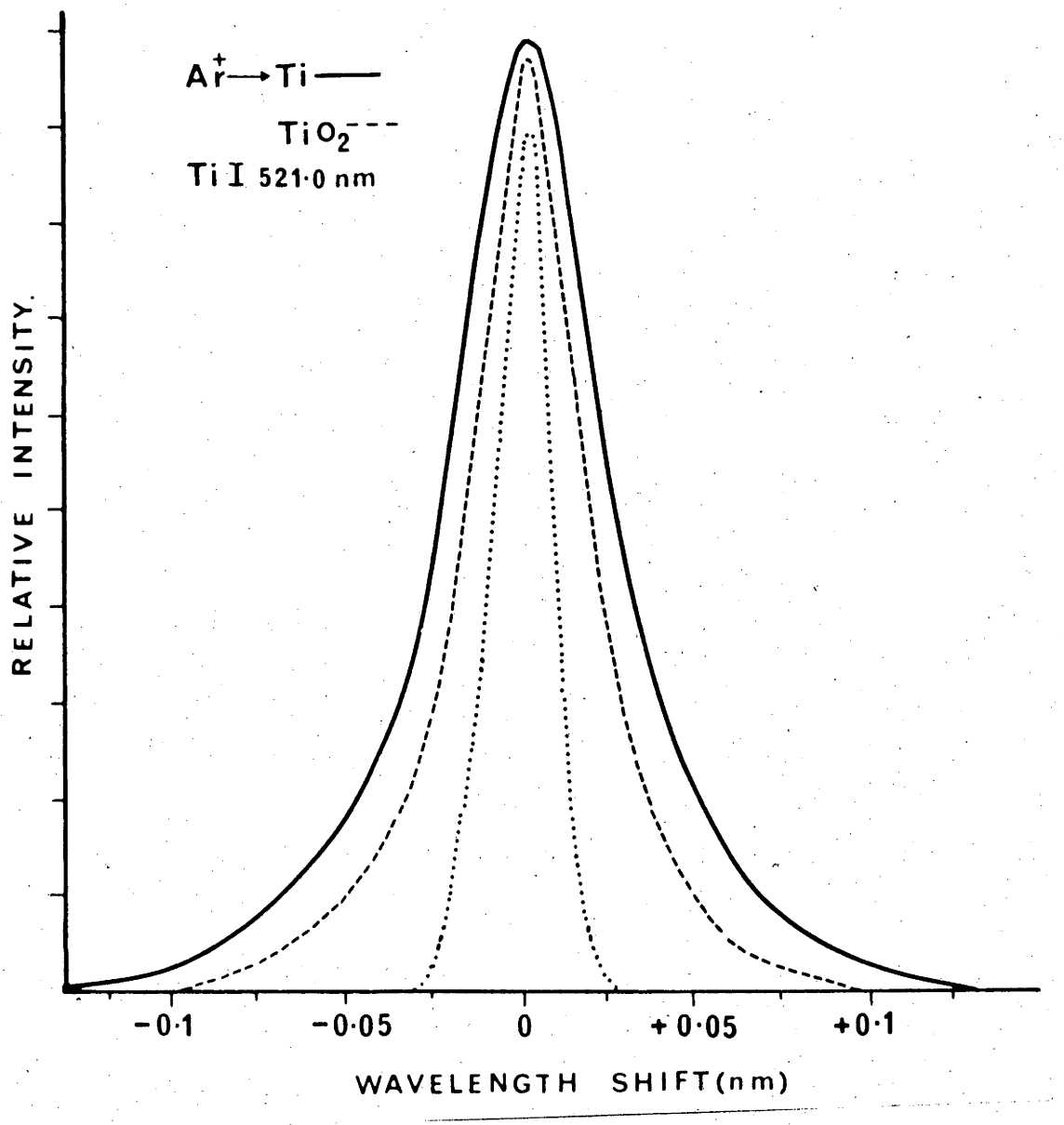

Figure 4.7. Line shape of the 521.0 nm Ti I line from Ar^+ bombarded Ti, compared with the same line from Ar^+ bombarded TiO_2 (dashed line). These may be compared with the dotted reference line emitted by a hollow cathode lamp indicating the instrumental resolution.

TABLE 4.2

The FWHM and $\Delta\lambda/\lambda$ values of the 521.0, 3.99.8 and 488.5 nm lines from bombarded Ti and TiO_2

Conditions		TiI 521.0 nm		TiI 399.8 nm		TiI 488.5 nm	
		FWHM (nm)	$\Delta\lambda/\lambda$ ($\times10^{-4}$)	FWHM (nm)	$\Delta\lambda/\lambda$ ($\times10^{-4}$)	FWHM (nm)	$\Delta\lambda/\lambda$ ($\times10^{-4}$)
Ar^+ on Ti	($\dot{n}_0/\dot{n}_i < 0.02$)	0.053	1.02 ± 0.10	0.057	1.43 ± 0.13	0.097[a)]	2.2 ± 0.2
	($\dot{n}_0/\dot{n}_i \simeq 0.45$)	0.037	0.71	0.044	1.10		
	($\dot{n}_0/\dot{n}_i \simeq 5$)	0.039	0.75	0.042	1.05	0.067	1.37 ± 0.12
O_2^+ on Ti	($\dot{n}_0/\dot{n}_i < 0.02$)	0.049	0.98	0.047	1.17		
Ar^+ on TiO_2	($\dot{n}_0/\dot{n}_i < 0.02$)	0.038	0.73	0.044	1.10	0.065	1.33 ± 0.12
	($\dot{n}_0/\dot{n}_i \simeq 5$)	0.038	0.73	0.041	1.03	0.062	1.27 ± 0.12
O_2^+ on TiO_2	($\dot{n}_0/\dot{n}_i < 0.02$)	0.037	0.71	0.047	1.17		

a) Estimated from measurement with 25 μm slits.

Figure 3.2(a)) and the analysis has proceeded through equation (2.23(b)), i.e. Yield $\propto \exp(-x/\bar{v}\tau)$. The variation of ln (counts) as a function of the perpendicular distance from the target for the three lines shown in Figure 4.4, is shown in Figure 4.8 for Ar^+ bombarded Ti and TiO_2. It can be seen from Figure 4.8 that the decay occurs closer to the target surface for the bombarded oxide than the bombarded metal under UHV conditions.

The line profile and decay curve data suggest that the average velocity of excited particles contributing to radiation decreases with oxygen contamination.

4.1.5 *Decay length effects - the influences of level lifetime and particle velocity.*

The intensity decay curves shown in Figure 4.8 are a consequence of the excited state lifetime and the velocities of particles with that particular excited state, i.e. the lifetime τ_i, the surface normal velocity $v_\perp$ and $\phi.\phi$ is the angle between the surface normal and the outgoing path of the excited particle. The decay lengths (distance over which the intensity falls to some fraction of the initial intensity) may influence some of the measurements of the photon emission characteristics and care must be taken to account for such influence. This will be a result of the observation volume used and the observation position. For an ion-bombardment source, the relative strength for wavelength λ_{ij}; $N_{\lambda_{ij}}$, would be:

$$N_{\lambda_{ij}} = n_i.b_{ij}.F(\lambda, \text{observation volume and position}) \qquad (4.1)$$

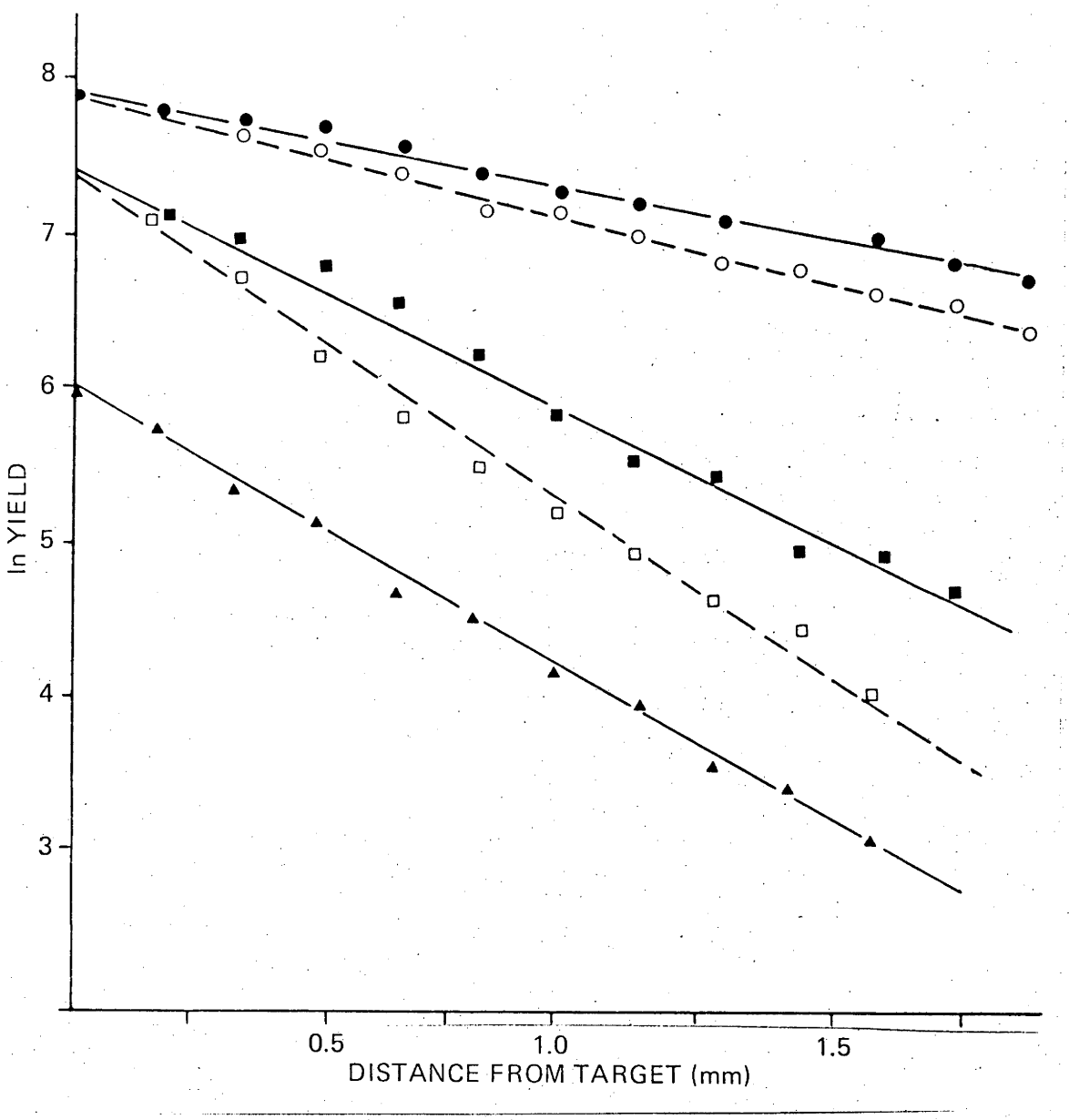

Figure 4.8. Plot of ln (photon yield) with perpendicular distance of observation from the target for the (●) 521.0 nm, (■) 399.8 nm, and (▲) 488.5 nm Ti I lines from Ar^+ bombarded Ti. The dashed lines are similar plots for the (○) 521.0 nm and (□) 399.8 nm Ti I lines from Ar^+ bombarded TiO_2. The metal and dioxide curves are normalized to the same initial value.

where n_i is the relative population of level i, b_{ij} is the branching ratio and F is an instrument and collection efficiency factor. For the situation where less than the whole radiating region is observed, F will be collection efficiency dependent upon each different transition, through the family of curves similar to Figure 4.8.

As an example of the dependence upon observation position, the reduced intensity plots for TiI from Ar^+ bombarded Ti (similar to Figure 4.3(b)) have been found to change as a function of x, the perpendicular distance from the surface. The slope of the guide line for the reduced intensity plot becomes more negative with distance from the target. This is a consequence of the points at low excitation energy ($< 24000\,cm^{-1}$) having, in general, relatively large decay lengths.

It is also clear that the observation volume will influence the photon count rates and consequently the reduced intensity plots. As an example of this influence, the reduced intensity plots have been determined using an integral yield measurement and using a differential yield measurement where the observation volume has been estimated to be 0.5 mm wide. These reduced intensity plots have been determined for only a selection of the lines used in Figure 4.5. To determine the correction term for the small observation volume, the decay curves for these lines were measured and the decay lengths for the intensity to fall to $I_0/6$ were determined. The observation factor, K, for the 0.5 mm observation area, was determined from the decay curves as:

$$K = \frac{\Sigma \text{ intensity over the decay curve in the observation volume}}{\Sigma \text{ intensity over the whole decay curve}} \qquad (4.2)$$

Decay lengths and the observation factors for selected TiI lines, obtained from Ar^+ bombarded TiO_2, are shown in Table 4.3. The observed intensities for the differential yield measurement using the 0.5 mm observation volume should be multiplied by the factor K to correct for the smaller observation volume. The derived uncorrected and corrected reduced intensity plots are shown in Figure 4.9, where it can be seen that the correction term from Table 4.3 is able to account for the changes in the observation volume. However, this correction requires the measurement of the decay curves for each line and knowledge of the observation volume. It would be an experimentally better practice to ensure that an integral yield measurement were made. The larger decay lengths for the lines used here with low excitation energies (coincidental) are shown in Table 4.3, illustrating the point made above that the observation position dependence is dominated by these lines.

The observation volume used may also have an influence on the surface contamination induced enhancement. Figure 4.8 shows that the decay lengths are decreased with oxygen contamination when compared with the pure metal. Consequently, when using a differential yield measurement to determine the intensity changes with oxygen exposure, the measurement technique may result in an increased yield due to more of the total decay occurring inside the observation volume. The

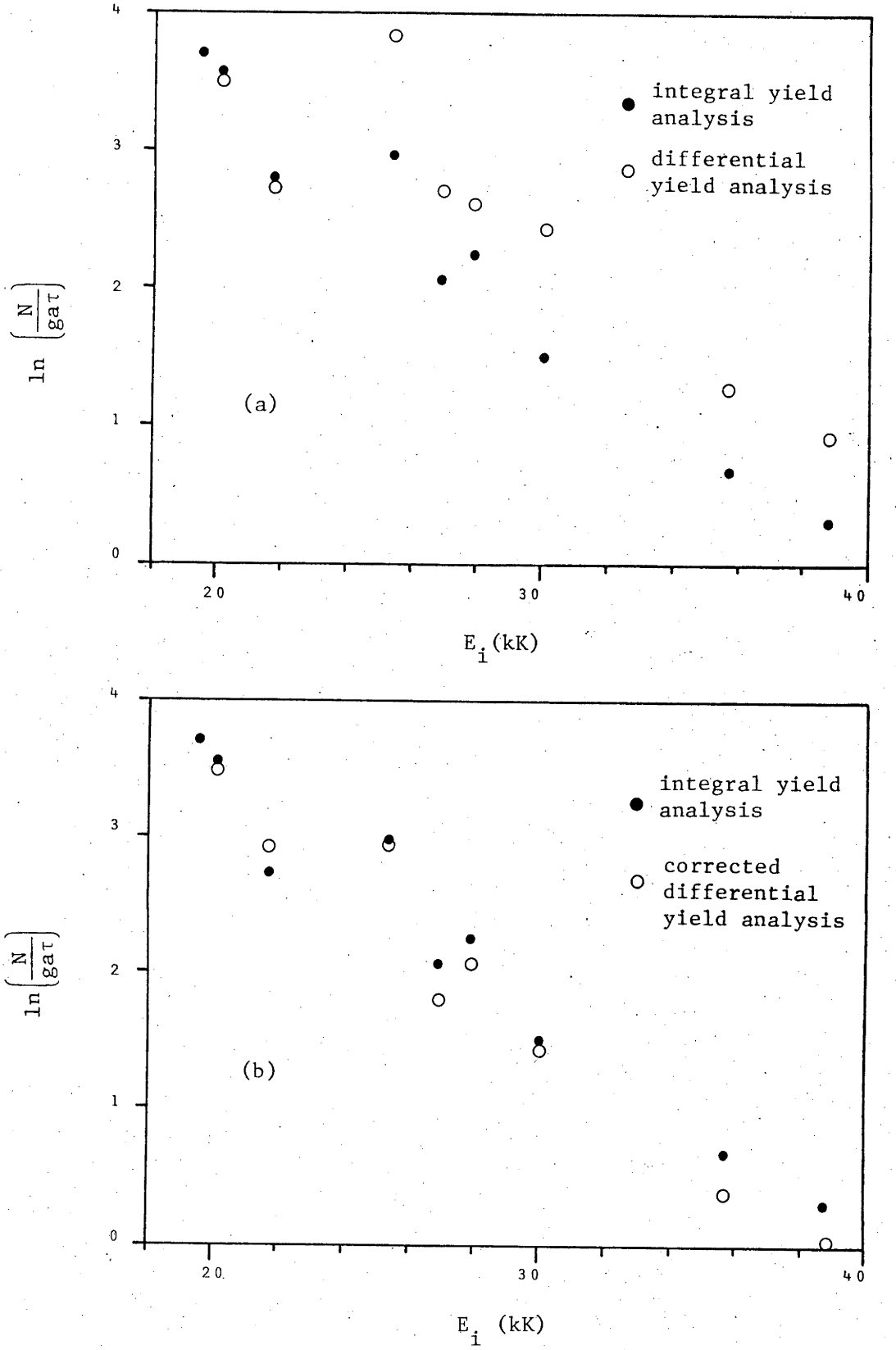

Figure 4.9 Reduced intensity plots for TiI emission from Ar^+ bombarded Ti measured using integral and differential (0.5 mm slit) yield measurements. The comparison of the measurements is shown in (a) while (b) shows the comparison for the corrected differential yield analysis using Table 4.3.

TABLE 4.3

Decay lengths for the line intensities to fall to $I_0/6$ for selected TiI lines, and the Observation volume factor, K, for an observation volume of 0.5 mm. The factor K is normalised to 1 for the 399.8 nm line.

λ(nm)	Decay length (mm)	K	$E_i(cm^{-1})$
521.0	2.46	2.4	19574
506.4	2.38	2.4	20126
468.1	3.18	3.0	21740
399.8	0.67	1.0	25388
498.1	0.64	1.0	26911
484.0	1.23	1.4	27907
430.5	0.44	0.9	30060
488.5	0.64	1.0	35685
485.6	0.64	1.0	38780

magnitude of this influence will decrease as the observation volume approaches that of an integral yield measurement.

An example of the magnitude of this influence has been estimated for the case of a differential yield measurement using a 0.5 mm observation volume. The intensity enhancement for the TiI 399.8 nm line was correlated with the different proportions of the total decay observed in a 0.5 mm observation volume from the bombarded Ti and from the TiO_2 as shown in Figure 4.8. It was estimated from the summation of the relative intensities for the different decay curves over this observation volume, that the differential yield measurement would result in a 25% larger intensity enhancement than the integral yield measurement. This difference is solely attributed to the change in the decay length with oxygen contamination of the surface.

These examples show that care must be taken in making the measurement and in the interpretation of the data to account for any spurious effects resulting from the observation volume and position.
Provided that these parameters are known, the above examples show that these influences may be accounted for.

4.1.6 *The influence of surface morphology on the intensity changes with surface oxygen contamination*

It has been found that bombardment of metal surfaces by ion beams may result in the formation of surface features such as cones, pyramids and ridges (for pictures of these topography changes, see, for example [18]). This surface morphology may have some influence on the angular distribution and total yield of sputtered particles [19, and references there in]. Whitton et al. [19] found that bombardment of Cu by 40 keV Ar^+ resulted in an overall sputtering yield from the pyramid covered surface ~ 50% greater than from the flat surface.

The surface morphology of the Ti target bombarded by 55 keV Ar^+ was examined using a scanning electron microscope for the different conditions corresponding to the initial plateau, peak region and decrease regions for the intensity changes with oxygen exposure shown in Figure 4.6. Comparison was also made between Ti targets bombarded under UHV conditions and at an exposure of 6×10^{-6} torr O_2 during bombardment for equivalent time/dose rates. The targets were initially polished to a 1 micron finish using diamond pastes.

The Ti target bombarded by Ar^+ under UHV conditions ($\sim$ 100 $\mu A/cm^2$ for 1 hour) displayed very sharp and pronounced cone and ridge formation. For similar bombardment dose at a background pressure of 6×10^{-6} torr of oxygen, the surface morphology was found to be quite smooth by comparison, showing only a few ill developed ridges. This observation is in agreement with that found previously [20] where O_2^+ and, to a lesser extent, N_2^+ bombardment produced less surface structure than Ar^+ bombardment. Detailed study of the surface corresponding with the three regions mentioned previously, indicated that the changes in surface morphology were far slower than the short time intervals during which the photon yields were able to change. Although the energy distributions of the sputtered particles were not measured by Whitton et al. [19], their results would suggest that the photon intensity should decrease (providing all factors such as the excitation probability remained constant) with oxygen contamination as the surface becomes smoother. Certainly this study cannot rule out that the surface morphology does not, to some extent, influence the changing intensities with oxygen contamination. However, it is expected that this influence is only of minor importance and would not be responsible for the increase or, in particular, the subsequent decrease in intensity shown in Figure 4.6. These intensity changes may then be ascribed to changes in the excitation or de-excitation processes.

4.1.7 *Discussion*

The different conditions as shown in Figure 4.5, have been used in an attempt to change the band structure and the Fermi level from that of clean Ar^+ bombarded Ti. Using the charge exchange model, these changes would be expected to be reflected in the reduced intensity plots due to intensity changes from blocking of non-radiative de-excitations. Although the band structure and Fermi level changes have not been simultaneously monitored here, an estimate of the trends may be taken from the literature.

Blaise and Slodzian [21] have studied work function changes with oxygen exposure under bombardment conditions and found that oxygen exposure induces a work function change for Ti metal from 3.9 eV to 5.2 eV, the latter being similar to that of TiO_2 [13]. Oxygen bombardment of the metal would be expected to follow a similar trend.

UPS studies of TiO_2 have been made under UHV conditions for the (100) and (110) faces of a single crystal before and after 2 keV Ar^+ bombardment [13]. It was found that the Ar^+ bombardment induced preferential sputtering of oxygen from TiO_2, which was accompanied by pronounced changes in the work function and band structure. The work function of the clean well ordered (100) and (110) surfaces was found to change from 5.5 to 4.6 eV for the bombarded surface. It was further noted that the work function decreased monotonically with surface oxygen concentration. However, oxygen ion bombardment produced no observed change and it was suggested that a disordered TiO_2 surface layer was formed.

Studies of oxygen chemisorbed on TiO_2 single crystal surfaces [22,23] have found a change of +0.3 eV in the work function for 2 keV Ar^+ bombarded TiO_2 with 10^5 L O_2 exposure. Some increase in the work function would thus be expected for the oxygen exposure of TiO_2 described here. A summary of the work function changes expected for the conditions used in this study is shown schematically in Figure 4.10.

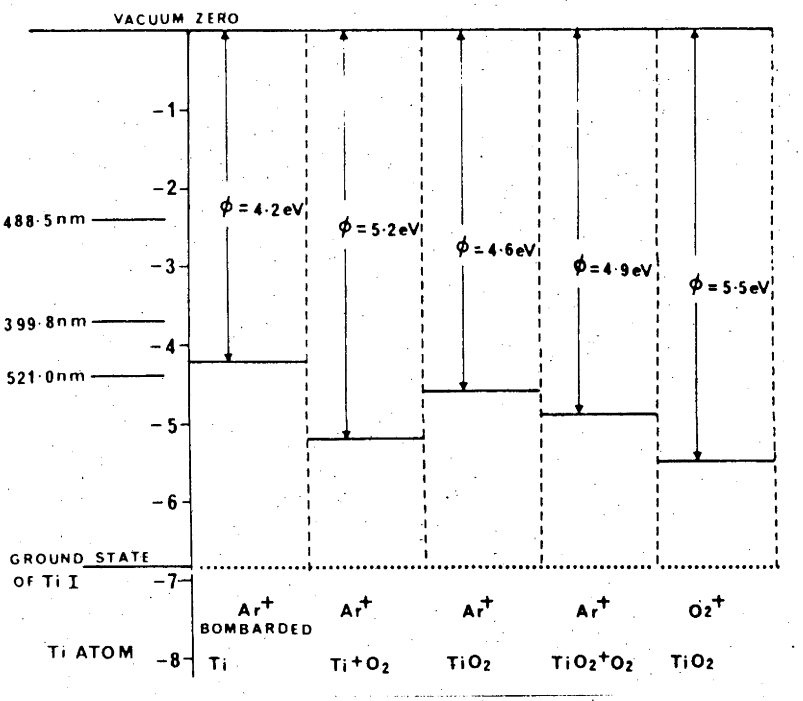

Figure 4.10 Comparison of the Ti I energy levels of selected lines and the work function changes for various bombardment conditions. The work function data have been obtained from references [10,13,14,22,23].

Using the resonance ionisation model, a difference in the charge exchange processes influencing the 521.0 and 399.8 nm Ti I lines is expected for Ar^+ bombarded Ti, as

the Fermi level lies between the excitation energies of the two lines. A resonance ionisation would be predicted for the upper level but would be blocked for the lower level. With the increased work function for Ar^+ bombarded Ti under oxygen exposure conditions or from bombarded TiO_2, the two excitation energies would lie opposite the same region of the band structure and the charge exchange processes influencing both lines would be expected to be the same. A difference between the reduced intensity plots for Ar^+ bombarded Ti and for the oxygen exposure conditions would then be predicted in the excitation energy region corresponding to the Fermi level of Ti. The reduced intensity plots, however, show minimal differences in this region (see Figure 4.5).

Although the log plots are relatively insensitive to intensity changes, a 50% variation in relative intensity should be readily observed. The resonance process, if it occurs, should be a preferred and strong interaction with a high reaction rate [13]. Thus, the failure to observe any change in the reduced intensity plots corresponding to this process, suggests that it does not influence the excited atoms leaving the surface.

From equation (2.8) the intensity of an emission line may be written as the expected intensity I_0 at the surface modified by the probability for escape from the surface without undergoing a charge exchange process:

$$I = I_0 \exp (- A/av) \ . \qquad (4.3)$$

The A/a values for the charge exchange processes have been theoretically calculated (see section 2.2.1), and are of the order 1×19^9 m/s for a resonance process and 1×10^6 m/s for an Auger de-excitation. Any change in the band structure which would block a resonance ionisation process would thus cause a large intensity increase from excitation levels no longer influenced by this process.

In predicting intensity changes for Ar^+ bombarded Ti with oxygen exposure, the work function changes as shown in Figure 4.10 must be considered. The band gap of TiO_2, however, is not known under bombardment conditions. Assuming that oxygen exposure induces an oxide-like band structure with work function as shown in Figure 4.10 and a band gap of approximately 2-3 eV [13], this resonance ionisation process(proposed as an alternative de-excitation for the upper level of the 399.8 nm line) will be blocked with oxygen exposure. A corresponding increase in intensity for the 399.8 nm line should then occur. If such a band gap is not present under bombardment then the opposite should be expected as a resonance ionisation process will become possible for the upper state of the 521.0 nm line. The point is that the behaviour of the 399.8 and 521.0 nm lines would be expected to be different with oxygen exposure, and that any change should occur to a large extent.

However, Figure 4.6 shows that both lines similarly increase in intensity with oxygen exposure by a factor of only 3-4. Similarly, the energy distributions of particles contributing to radiation are not strongly changed with oxygen

exposure, as shown in Figure 4.8 and by the reduced line widths.

The decrease in intensity with oxygen exposure is similar to the falling sputtering yield of Ti with oxygen exposure determined by Hofer and Martin [16]. It can be seen from Table 4.2 that there is no change in the line profile from the peak of the photon intensity at $\dot{n}_0/\dot{n}_i \simeq 4.5$ to the upper exposure limit of $\dot{n}_0/\dot{n}_i \simeq 5$. This suggests that there is no change in the velocity distribution of atoms contributing to radiation and that the decrease is not due to a change in the charge exchange process. This supports the explanation suggested for Cr [17], that the decrease in intensity after the initial increase for oxygen exposure is due to the falling metal atom sputtering yield.

Provided that the lifetime τ_i is known for a given level, then the mean perpendicular velocity, which is necessarily an integrated velocity term over the angular and velocity distributions, may be determined using eq. (2.23(b)) and Figure 4.8 in the manner of Gritsyna et al. [11,24,25]. It must be remembered, however, that cascading may have a profound effect upon the curves. For this determination of the mean perpendicular velocity, $\bar{v}_\perp$, the lifetimes of the excited states giving rise to the 521.0, 399.8 and 488.5 nm lines have been calculated as 1.93×10^{-7}, 2.12×10^{-8} and 1.89×10^{-8} s, respectively [4].

These values are in agreement within 10% for the lifetimes calculated and measured by others [26-28]. The value $\bar{v}_\perp$ may then be compared with that obtained from the

line profile studies. An estimate of the average energy of atoms contributing to radiation $\bar{v}_{\parallel}$, is calculated from the Doppler shift of the wavelength at the FWHM of the line after the instrument broadening has been taken into account. The results of the two types of calculation are shown in Table 4.4.

TABLE 4.4

Estimates of the average velocity and energy for the atoms contributing to radiation using the intensity decay curves (A) and the line profiles (B)

	λ (nm)	A		B	
		$\bar{v}_{\perp}$ (m/s)	$\bar{E}_{\perp}$ (eV)	$\bar{v}_{\parallel}$ (m/s)	$\bar{E}_{\parallel}$ (eV)
Ar^+ on Ti	521.0	3.3×10^4	250	1.4×10^4	40
	399.8	1.2×10^5	3000	2.0×10^4	85
	488.5	1.1×10^5	2500	2.9×10^4	185
Ar^+ on TiO_2	521.0	2.8×10^4	150	9.5×10^3	20
	399.8	9.1×10^4	1800	1.4×10^4	40
	488.5	8.8×10^4	1700	1.9×10^4	80

The values of the energies obtained in this work using the decay curves and the method of Gritsyna et al. are similar to the results of Gritsyna et al. [11], although the values of the lifetimes used for their calculations were not indicated. The 521.0 nm line with excitation energy below the Fermi level for Ti, has a much lower calculated

energy than the other lines and this tends to support the hypothesis proposed by Gritsyna et al. that a resonance ionisation may be blocked for this level. Ar^+ bombardment of TiO_2 reduces the energy values obtained, however the large difference between the calculated energies of the atoms giving rise to the 521.0 and 399.8 nm lines remain, although the band structure and Fermi level are expected to change from that of the bombarded metal.

The large difference in energy between the atoms giving rise to the 521.0 and 399.8 nm lines, calculated using this method, should be reflected in the line profiles which are dominated by Doppler broadening. In contrast to this result, the line profiles indicate no such large difference between the atoms contributing to the 521.0 and 399.8 nm lines. The ratio of the energies between these groups is only 1:2 as compared to 1:13 calculated using the method of Gritsyna et al. This difference and the failure to indicate the changed Fermi level for Ar^+ bombarded TiO_2 cast some doubt upon the latter method. The inconsistent values obtained using this method would be attributed to the averaging over the angular and energy distributions of the particles contributing to the radiation.

The line profiles obtained from Ar^+ bombarded Ti show distinct changes for the three lines considered as shown in Tables 4.2 and 4.4. These lines show a reduced line width and reduced average velocity with oxygen exposure. The line profiles and average energy for the 521.0 and 399.8 nm lines are different, however their

relative changes and the previously observed intensity changes with oxygen exposure are similar. If a charge exchange process occurs then a similar change in these processes could be expected for the two excited states. Equation (2.17) indicates that the probability of an atom escaping from the surface without undergoing an exchange process is strongly velocity dependent. Minor velocity changes calculated from the line profiles between lines, and for oxygen exposure, suggest little change in the charge exchange processes. Blocking of an exchange process such as a resonance ionisation process would not be consistent with these velocity changes. The 488.5 nm line may be influenced by an additional process indicated by the significantly higher average velocity and intensity change with oxygen exposure.

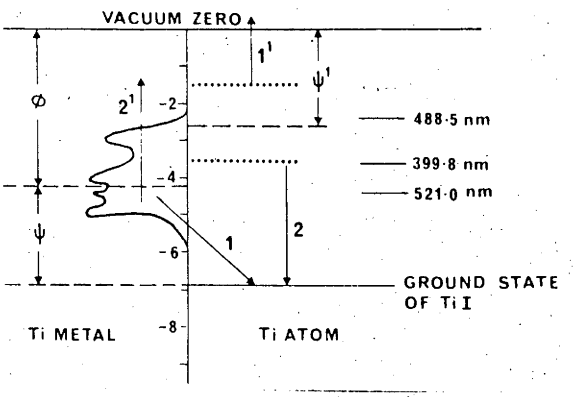

Figure 4.11 Proposed Auger de-excitation processes 1,1' and 2,2' which may influence the excited states of Ti I. The dotted lines represent possible excitation levels of Ti I.

Although the resonance ionisation process does not appear to influence the excited states of Ti, an Auger

process as shown in Figure 4.11 may be possible. The Auger de-excitation 2,2' shown in Figure 4.11 will influence all states. However, it may be possible to differentiate between it and the process, 1,1', as for electron 1' to gain sufficient energy to be ejected to the vacuum level in the latter process then $\psi' \leq \psi$.

The differences in the line profiles between lines such as the 521.0 and 399.8 nm remain difficult to reconcile with the charge exchange model. It may be possible to introduce a model based upon the probability for excitation to account for the differences between the behaviour of different excitation levels and the marked changes with oxygen exposure without using the charge exchange model.

It should be stressed that although the charge exchange model using the processes of Hagstrum [13] has been used many times to explain results of experiments on ion bombardment induced photon emission, there exists no *direct* evidence for the occurrence of such processes. Most of the evidence consists of either predictions based upon comparisons of energy band structures with isolated atom energy level diagrams, or comparisons of experimental data with fitted curves using an exp(-A/av) fitting parameter. The former takes no account of modifications of atomic energy levels near a surface, while the latter involves a powerful fitting parameter which may simply indicate mathematical strength rather than physical validity.

There have been other attempts to explain the mechanisms of excitation and ionisation. The plasma model has been found

not to survive rigorous testing although it appears to be a qualitative fitting. Oxygen induced effects, discussed in section 2.2.5, have been variously described using bond-breaking models and quasimolecule formation models. However, these models do not suggest a mechanism for the formation of excited atoms (or ions) from a clean surface. Without knowledge of the excitation itself, we may be able to write:

$$\begin{pmatrix}\text{Yield of excited atoms}\\ \text{per incident ion in the}\\ \text{energy range E to E+dE}\end{pmatrix} = \begin{pmatrix}\text{Number of atoms}\\ \text{sputtered in energy}\\ \text{range E}\rightarrow\text{E+dE}\end{pmatrix} \times \begin{pmatrix}\text{Cross-section}\\ \text{for}\\ \text{excitation}\end{pmatrix},$$

$$Y(E)dE = \eta(E)dE\cdot\sigma(E_{ex},E_{kin}). \qquad (4.4)$$

where the cross-section for excitation is a function of the excitation energy and the kinetic energy of the particle (and perhaps the exit angle ϕ). Equation (4.4) may be applied to ionisation by the appropriate replacements. The total yield of excited atoms is then an integral over exit energies (and ϕ) of equation (4.4). For photon emission studies of different emission lines, the $\eta(E)dE$ component is the same for each excitation level of the atom and hence the E_{kin} dependence of σ is the same and the excited level distribution merely indicates the dependence on E_{ex}. For many different metals the $\eta(E)dE$ component is similar and again the excitation cross-section depends only upon E_{ex}.

When oxygen is adsorbed on the surface, the yield change may reflect a change in the $\eta(E)dE$ component (changes in the energy spectrum of sputtered particles with oxygen

adsorption is well established) and hence some change in the E_{kin} component of σ. The role of changes in the energy spectrum due to binary components in the cascade should be capable of experimental investigation. This would require that the two components in the alloy or compound do not segregate. Should excitation occur with the last collision event as the surface atom is sputtered, different collision partners may produce different excitations. Furthermore, the cascade can be modified by varying the angles of incidence or exit and this should allow investigation of the E_{kin} dependence of $\sigma(E_{ex},E_{kin})$. It is obvious that information on the energies of the particles contributing to the observed radiation is of much importance. The main point is that it may not be necessary to invoke electron exchange processes to account for the experimental results such as those reported here and elsewhere (section 2.2).

4.1.8 *Conclusions*

The study of 55 keV Ar^+ and O_2^+ bombardment of Ti and TiO_2 has shown that the excited states of Ti atoms, which span an energy range of 2.5 eV, appear to have a Boltzmann-like distribution as reported for other bombarded species [29]. These reduced intensity plots have been shown to change markedly when the more physically correct equation is used to describe the level decays (2.21), rather than the plasma excitation and de-excitation equation used by Martin et al. [29]. The reduced intensity plots are also shown to be critically dependent on the observation volume

and position used to measure the line intensities. There exists considerable difficulty in deriving the reduced intensity plots due to the lack of knowledge of the branching ratios and the influence of cascading for many of the lines required to include in these plots. In view of these difficulties, and the non-uniqueness of the fit which may be used with the data (see for example, [30]) the value of such measurements is questionable beyond the observation that the population of the excited states appears similar to $\exp(-k.E_{ex})$ over the energy ranges usually considered.

In agreement with previous studies for Cu and Al, and Cr [31,32], the resonance ionisation process does not appear to influence the excited states of Ti when sputtered from Ti and TiO_2 by Ar^+ and O_2^+ bombardment. The resonance ionisation model cannot be used to interpret the changes of intensity with oxygen contamination for three Ti I states with widely varying excitation energy, nor is its influence seen in the relative population distributions. Correlations with band structure, however, are difficult as the band structures need to be taken from the literature and there is considerable doubt that these may be applicable under ion bombardment conditions. The simple band structure theory as often used,certainly does not apply here. Indeed, a proposal that changes in the photon emission characteristics be modelled only upon the sputtered atom distributions and the cross section for excitation has been discussed and further tests of such a model have been suggested.

The two-electron Auger de-excitation processes, however, cannot be excluded as a means of explaining the changes in line intensity, line profile and intensity decay curves with exposure to oxygen. It is not clear if these processes could explain the differences observed in the behaviour of different excitation levels.

The line widths (and hence a related energy distribution) have been found to decrease with oxygen contamination. The surface oxygen contamination is also accompanied by an intensity increase. Further exposure leads to a peaking of the intensity enhancement followed by a decrease not accompanied by any change in line profile. These observations regarding the intensity decrease and the comparison with the sputtering yield measurements with oxygen contamination by Hofer et al. [16], suggest that the decrease in intensity is related to the falling sputtering yield.

It has been shown that the method used by Gritsyna et al. [11,24,25] for estimating the mean velocities of emitting particles from the intensity decay curves, does not produce results which are consistent with the observed line profiles of the Ti I emission. There is an evident need for information on the energies of particles contributing to the radiation and such information may help in describing the excitation process. Measurements of the kinetic energies of the particles contributing to radiation for selected Ti I lines are discussed in section 4.2.

4.2 THE MEASUREMENT OF KINETIC ENERGY RELATED PARAMETERS FOR Ti ATOMS

Information on the kinetic energies of particles contributing to radiation may be determined through measurements of the decay curves and the emission line profiles (and line shift) as discussed in Chapter 2. In this section, the results of such measurements will be reported for the three Ti I lines so far examined. Changes in these kinetic energy distributions will also be examined for different chemical environments of the target Ti atom, changes in the incidence energy of the beam and as a function of the excitation energy levels of the sputtered atom. Possible implications of the results of these measurements will be discussed.

4.2.1 *Estimates of the kinetic energies of excited particles using the Dzioba model compared with other techniques.*

There are three experimental energy parameters which may be determined to compare with various models and propositions for excitation. In order to compare these, the parameters which may influence the energy distributions, such as the angle of incidence and the surface contamination conditions, must be kept constant. The measurement and interpretation of two of these energy parameters, E^* (using the decay curve model of Dzioba et al. [33,34]) and $\bar{E}_\perp$ (using the exponential decay curve approximation of Gritsyna et al. [24]) require normal incidence bombardment and observation at 90° to the beam. The third energy parameter, derived

from the measurement of line profiles, is then an averaged energy term with component parallel to the surface - $E_{||}$.

The E^* values determined here have been obtained with 0.4 mm slit sizes (the observation volume, shown in Figure 3.2(a), is slightly smaller) and the analysis of the measured decay curve has proceeded through equation (2.26), where the constant step function probability for excitation is assumed. There appears no experimental evidence to prefer other forms for the excitation probability as discussed in [34]. The variation of the values of E^* obtained using these other assumptions is no more than a factor of 2 [34]. Derived values of E^*, the minimum energy of particles contributing to the radiation, would be slightly lower than the related average energy for an E^{-2} distribution of sputtered excited atoms.

Differential decay curves for the 521.0, 399.8 and 488.5 nm lines have been measured for 55 keV Ar^+ bombardment of Ti and TiO_2. The measured decay curves for these lines obtained from the bombarded Ti under UHV conditions are shown in Fig. 4.12(a). It may be noted that the differential yield curves, measured over long decay distances to obtain Figure 4.12(a), show a pronounced curvature unlike the approximately linear curves shown in Figure 4.8. By a comparison of Figure 4.12(a) with the curve representing equation (2.27), (Figure 2.9), z vs x curves have been derived and are shown in Figure 4.12(b). Similar curves were obtained from the bombarded TiO_2, showing the same trends evident in Figure 4.8, i.e. that the intensity decayed more quickly with distance from the oxide than from the metal.

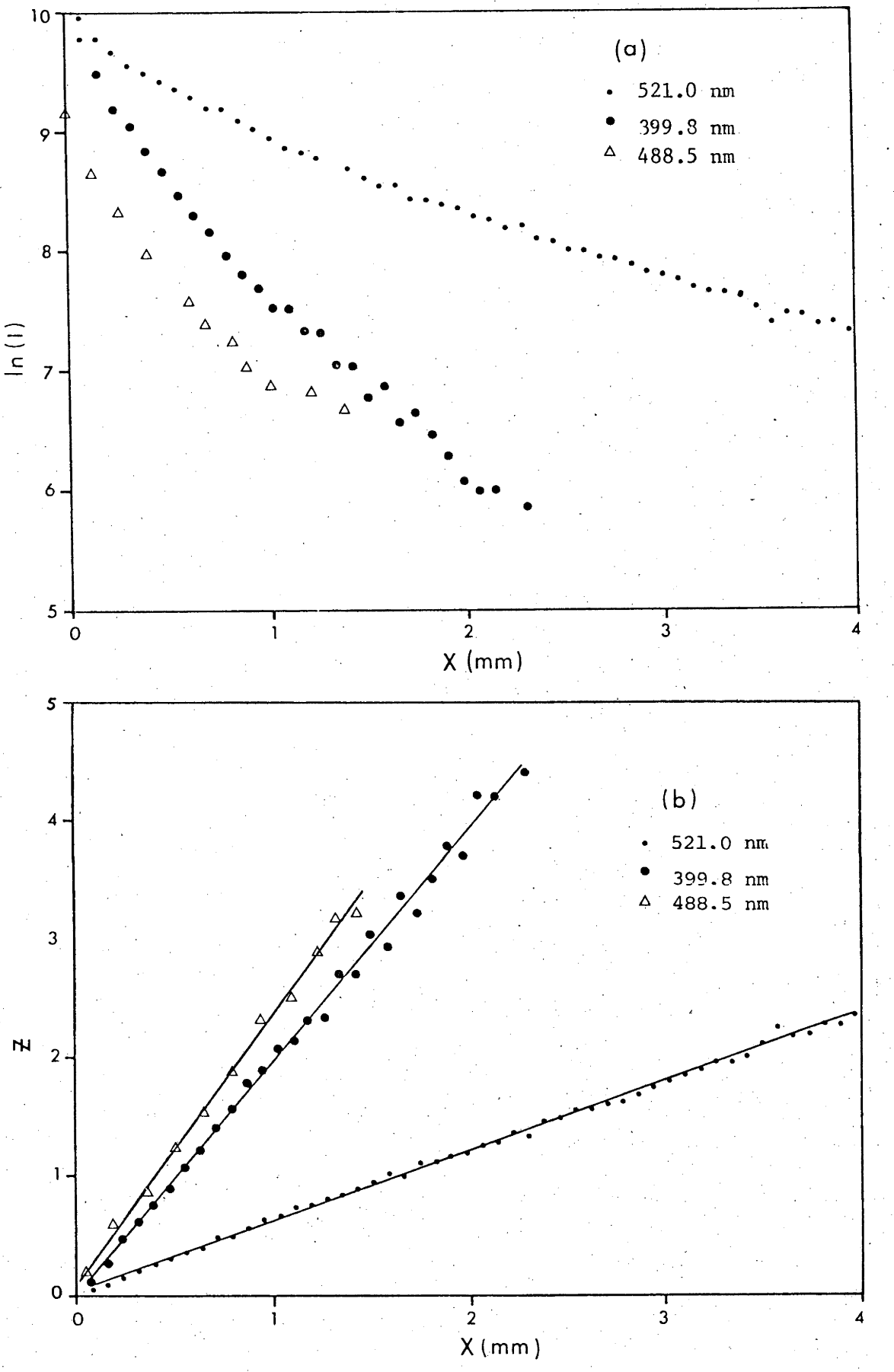

Figure 4.12. Measured decay curves (a) and derived z vs x curves (b) for differential yield analysis of the TiI 521.0 nm, 399.8 nm and 488.5 nm lines. The slit width was 0.4 mm.

The values of E^* were derived from the slope of the z vs x curves, where the slope $\frac{dz}{dx}$ is given by: $\frac{dz}{dx} = \gamma_i m^{\frac{1}{2}} 2^{\frac{1}{2}} / E^{*\frac{1}{2}}$. These values for the three Ti I lines are compared with the estimates of the energies of the emitting particles, determined in section 4.1, in Table 4.5.

TABLE 4.5

Comparison of the kinetic energy parameters $E_\perp$, E^* and $E_\parallel$ derived from the decay curves using equation (2.23) ($E_\perp$); the decay curves using the model of Dzioba et al. (E^*) and the emission line profiles ($E_\parallel$).

λ(nm)	Target	$E_\perp$ (eV)	E^* (eV)	$E_\parallel$ (eV)
521.0	Ti	250	18	40
	TiO_2	150	12.5	20
399.8	Ti	3000	150	85
	TiO_2	1800	64	40
488.5	Ti	2500	160	185
	TiO_2	1700	101	80

4.2.2 *Influence of changing the incidence energy of the beam*

The decay curves for the 521.0 nm line from Ar^+ bombarded TiO_2 have been determined for a range of different incident energies to determine any possible dependence upon the amount of energy deposited in the collision cascade. The values of E^* obtained from these curves are summarized

in Table 4.6. It may be noted that the values are very similar over the incidence energy range used. The errors shown do not include the contribution from the lifetime of the excited state and, therefore, are an indication of the relative changes in the determined E^* values. Differential yield measurements were taken for each incidence energy with the resolution of the monochromator significantly degraded to detect the line at low incident energies where the beam current densities were lower.

TABLE 4.6

The E^* values obtained from the Ar^+ bombarded TiO_2 for the Ti I 521. nm line using differential yield measurements, as a function of the incidence beam energy.

Incidence Energy (keV)	E^*(eV)
63.0	13.0 ± 1.5
53.0	13.5 ± 1.5
43.0	13.0 ± 1.5
33.0	12.0 ± 1.5
22.5	11.5 ± 1.5
18.0	11.0 ± 1.5
12.5	10.5 ± 1.5
7.5	11.0 ± 1.5
5.0	8.5 ± 2.5

4.2.3 *The influence of different chemical environments.*

The influence of different chemical environments on the characteristics of photon emission and the excitation process of Ti I has also been examined. Decay curves have

been measured for 55 keV Ar^+ bombardment to Ti, TiO_2, TiN, TiC and TiB for the 521.0, 399.8 and 488.5 nm lines using differential yield measurements and the z vs x curves have been obtained from these decay curves using equation (2.26). E^* values have been derived from these z vs x curves and have been compared in Figure 4.13 with the $(\Delta\lambda/\lambda)^2$ values obtained by measurement of the emission line profiles, for the same group of targets. The $(\Delta\lambda/\lambda)^2$ values have had the instrument resolution de-convoluted and are related to an average energy parallel to the target surface. The behaviour of the two sets of data are very similar with each measurement technique following the previously observed trend that the kinetic energies of particles contributing to radiation increases with the excitation energy of the level. This result will be examined in more detail in the following section.

Reduced intensity plots were also determined for the Ar^+ bombarded TiN, TiC and TiB and were found to be almost the same as those obtained for bombarded TiO_2.

4.2.4 *Excitation energy dependence of the kinetic energies of the excited atoms*

To verify the observation so far made that the kinetic energies of the excited particles appears to increase with the energy of the excitation level of the Ti atom, several other Ti I lines have been studied for 55 keV Ar^+ bombardment of TiO_2. The titanium oxide was used for this study as the photon emission is stronger than from the pure metal - an

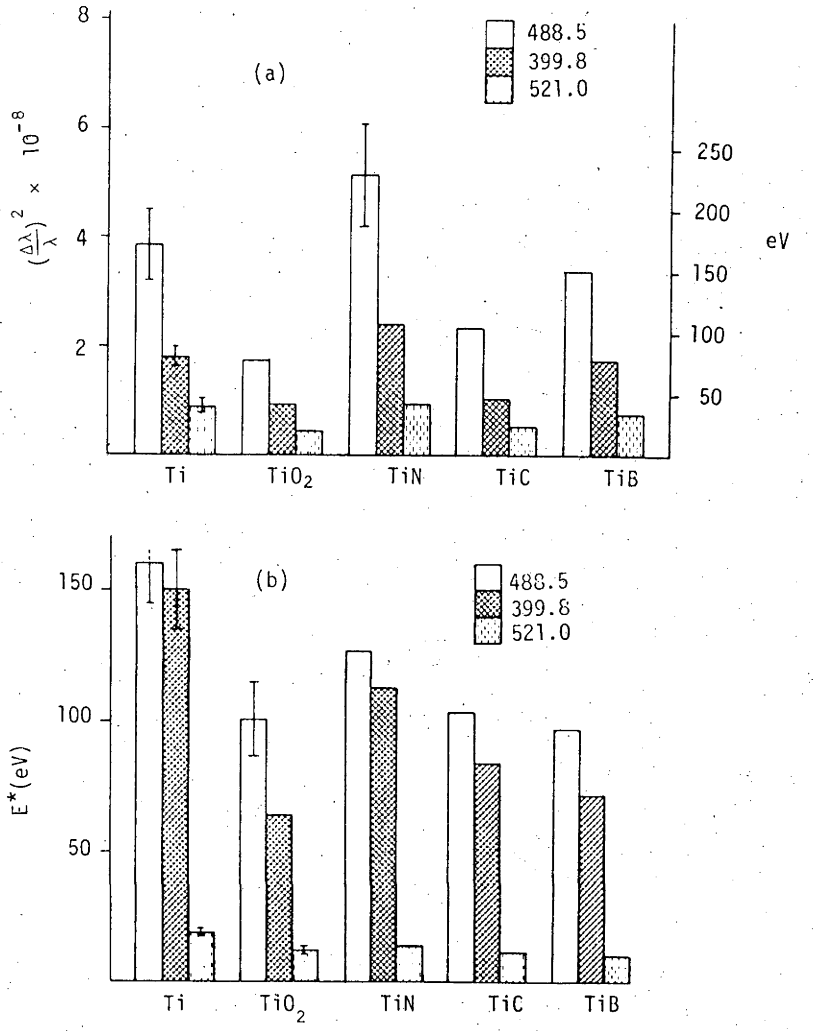

Figure 4.13. (a) The $(\Delta\lambda/\lambda)^2$ values obtained by line profile measurements for the TiI 521.0, 399.8 and 488.5 nm lines from the Ar^+ bombarded Ti compounds. (b) The E^* values for the same lines obtained by decay curve measurements using 0.4 mm slits and the expression for the differential yield, equation (2.27). In both cases the beam was incident normal to the surface and the observation angle was kept at 90° to the beam.

advantage in making measurements of relatively weak lines. Differential decay curves were measured for those selected Ti I lines (which range over 2.5 eV excitation energy) with a 0.4 mm slit to obtain E^* values. These energy values have been compared in Table 4.7 with the energy parameter $E_{\|}$, obtained from line profile measurements under normal incidence bombardment.

TABLE 4.7

The E^* and $E_{\|}$ values obtained by measuring decay curves and line profiles from TiO_2

Ti I λ (nm)	E^* (eV)	$E_{\|}$ (eV)	τ_i (ns)	$E_{ex}(cm^{-1})$
521.0	12 ± 4	20 ± 5	193[a]	19574
506.4	12 ± 4	30 ± 5	194[a]	20126
468.1	8 ± 3	30 ± 5	333[a]	21740
399.8	64 ± 20	40 ± 10	21[b]	25388
498.1	60 ± 16	60 ± 10	15[b]	26911
484.0	36 ± 20	50 ± 15	48[a]	27907
430.5	110 ± 35	60 ± 10	9[a]	30060
488.5	103 ± 35	80 ± 20	19[a]	35685
485.6	93 ± 30	120 ± 30	17[a]	38780

a [4]
b [26-28]

The trend towards higher kinetic energy particles contributing to higher excited states is also shown in Table 4.7. This would suggest that the trends shown in Figure 4.13 for the different excitation levels is real, and not an artifact of the uncertainty in the level lifetime

values. This would tend to support the hypothesis (equation (4.4)) that the cross-section for excitation is dependent upon (at least) the excitation energy.

4.2.5 *Discussion.*

The E^* values obtained for Ti I in this study are generally of the same order as those obtained in previous applications of the model for sputtered excited atoms [33-36]. These values are higher than the peak energy for secondary ion emission but are not of the order of keV which have been found in some studies [33-36]. The values obtained here, however, are consistent with measurements of another energy parameter derived from line profile measurements and consequently appear physically reasonable. Both energy parameters are found to decrease in about the same ratio with oxygen contamination. Considering the differences in the physical interpretation of the $(\Delta\lambda/\lambda)^2$ and E^* values, the energy parameters have a striking similarity.

The similar magnitudes of E^* and the energy parameter determined from the line profile measurements add credence to the model of Dzioba et al. within the limitations of the threshold form of the excitation function (see ref. [34]). Certainly the similar magnitudes of the energy parameters obtained would not lend experimental support for any particular form of the various excitation probability proposed in [34] to be favoured. It is immediately evident from Table 4.5 that this model is physically much more

reasonable than the exponential decay law (2.23(b)).

It is interesting to note that excited states giving the highest E^* values in this and other studies, are generally those with the shortest lifetimes. This may reflect the need for narrower slit widths to observe lines with short lifetimes, provided that the influence of cascading can be neglected. Tsong [36] has recently attempted to answer this criticism by using an OMA to observe the intensity decay in front of the target, resulting in vastly improved spatial resolution ($\sim 5\mu m$). For a supposedly cascade free Ba I line, the E^* value was still found to be of the order of 1-2 keV. To look for a possible breakdown in the model for these lines, it is important that such a result is cross-checked by (for example) line width data. Alternatively, such a high E^* value should be reflected in emission function measurements, where no radiation should be seen with an incidence energy of similar magnitude to E^*. These experiments would be relatively simple, and indicate the need for good emission function data to be obtained (as stressed in Chapter 2).

The magnitudes of the energy parameters determined are also of interest in discussions of the excitation processes. There have been two main propositions regarding the energies of particles contributing to radiation: (i) that the excited sputtered particles are those from the high energy tail of the sputtered energy spectrum which result from direct or near-direct recoils from ion-surface atom collisions and (ii) that the sputtered particles are excited when a surface atom is ejected after the collision

cascade intersects the surface. The atoms are therefore emitted with lower average energies. Measurements of the excited particle energies have been discussed in terms of either of these two propositions or alternatively, in terms of a combination of the two. The absence of the lower energy component of the excited atom energy distribution, has been attributed to the influence of non-radiative processes (these arguments, and references,are detailed in section 2.2.3 and 2.2.4). The low to medium kinetic energies obtained here for the levels of Ti under normal incidence bombardment would suggest that a major part of the excitation could be a result of proposition (i) above, rather than direct recoil collisions. There is a near direct recoil component, as evidenced by the wings of the Doppler broadened emission lines, but this is estimated to be of lesser importance then proposition (i) for normal incidence bombardment. Consequently, the value of E^* obtained would be expected to be relatively independent of the incidence energy, a trend which is evident in Table 4.6, although the incidence energy difference is only a factor of 8. These arguments immediately suggest that further experiments are required to extend the range of incidence energies and also to investigate the relative importance of propositions (i) and (ii) as a function of the angle of incidence. Delaney [37] has suggested a means of estimating their relative importance through the modelling of the emission line profiles, however the difficulties and inherent assumptions in line

profile modelling have been fully discussed in section 2.1 and would limit such an approach.

It was proposed at the end of section 4.1 that should the excitation occur at the last collision when the collision cascade intersects the surface, different excitations may be experimentally investigated by using alloys or compounds to alter the final collision partners. A preliminary study of this proposition has been made here for Ti and its compounds. The different chemical environments have been shown to lead to decreased E^* values when compared with emission from the clean metal. This behaviour has been shown to occur for each of the Ti I excitation levels studied, in about the same ratio. The line profile data also mirrors this behaviour. No significant trends are seen with the changing masses of the non-titanium element in the compound with relation to, for example, the maximum transferable energy in a head on collision for the two elements. A thorough study in terms of the quasi-molecule curve crossing excitation model, although difficult for a particularly complex system like Ti I, may provide more positive information.

The similarities in the behaviour of the magnitude of the E^* values obtained from Ti and the Ti compounds also supports the previous conclusion that band structure effects play little part in determining the Ti I photon yields.

Although there is a trend for higher E^* values for higher excited Ti I states, insufficient transitions have been studied over a suitable excitation energy range to find any form of dependence for the E^* values. It is

interesting, however, to consider the number of sputtered atoms contributing to radiation with energy $E > E^*$, with respect to the apparent success in matching the excited state populations with a Boltzmann-like distribution [see for example, references 29, 38 and section 4.1], or other functions [30,39].

With an energy spectrum of the form

$$f(E)\,dE = \frac{2E\,dE}{(E+U)^3} \tag{4.5}$$

it may be shown that the number of particles with energy greater than E^* is [33]:

$$n'(E) = \frac{2E^*U + U^2}{(E^* + U)^2} . \tag{4.6}$$

For an ion-bombardment excitation source

$$N_{\lambda_{ij}} = n_i\, b_{ij}\, F(\lambda, \text{ Observation volume}) \tag{4.7}$$

where $N_{\lambda_{ij}}$ is the relative signal strength for the radiative transition between levels i and j, n_i is the relative population of level i, b_{ij} is the branching ratio for level i and $F(\lambda_1$, Observation volume) is an instrument and collection efficiency factor. Also included in F is the factor for the proportion of the decay observed when the whole of the decay region is not viewed (see Figure 4.9).

The relative population of the levels may then be determined to obtain a reduced intensity plot.

The derived E^* and $E_{\|}$ values shown in Table 4.7 may be used to determine a similar plot of the relative population of the levels by considering the number of atoms contributing to the radiation. The constant step function model of excitation is assumed with step at E^*, using the values which have previously been experimentally determined. The use of a constant step function is a major simplification which implies that high kinetic energy atoms may be counted more than once, i.e. a high kinetic energy atom is included in each summation in evaluating n' for each excitation level, resulting in some overlap of the integrated regions for the different excitation levels. This will overestimate the number of excited atoms with higher excitation energy.

The relative population of the level i, n_i, is taken as

$$n_i = g_i\, n'(E_i^*) \qquad (4.8)$$

where g_i is the statistical weight of the level i (= 2J+1). Using equations (4.5), (4.6) and (4.8) and the E^* and $E_{\|}$ values from Table 4.7, the predicted level populations may be estimated. The statistical weight normalized populations derived using the E^* and $E_{\|}$ values are compared with experimentally determined populations for integral yield measurements from Ar^+ bombarded TiO_2 in Figure 4.14. The fit obtained, in terms of these reduced intensity plots, is reasonable in view of the simplicity of the assumptions made.

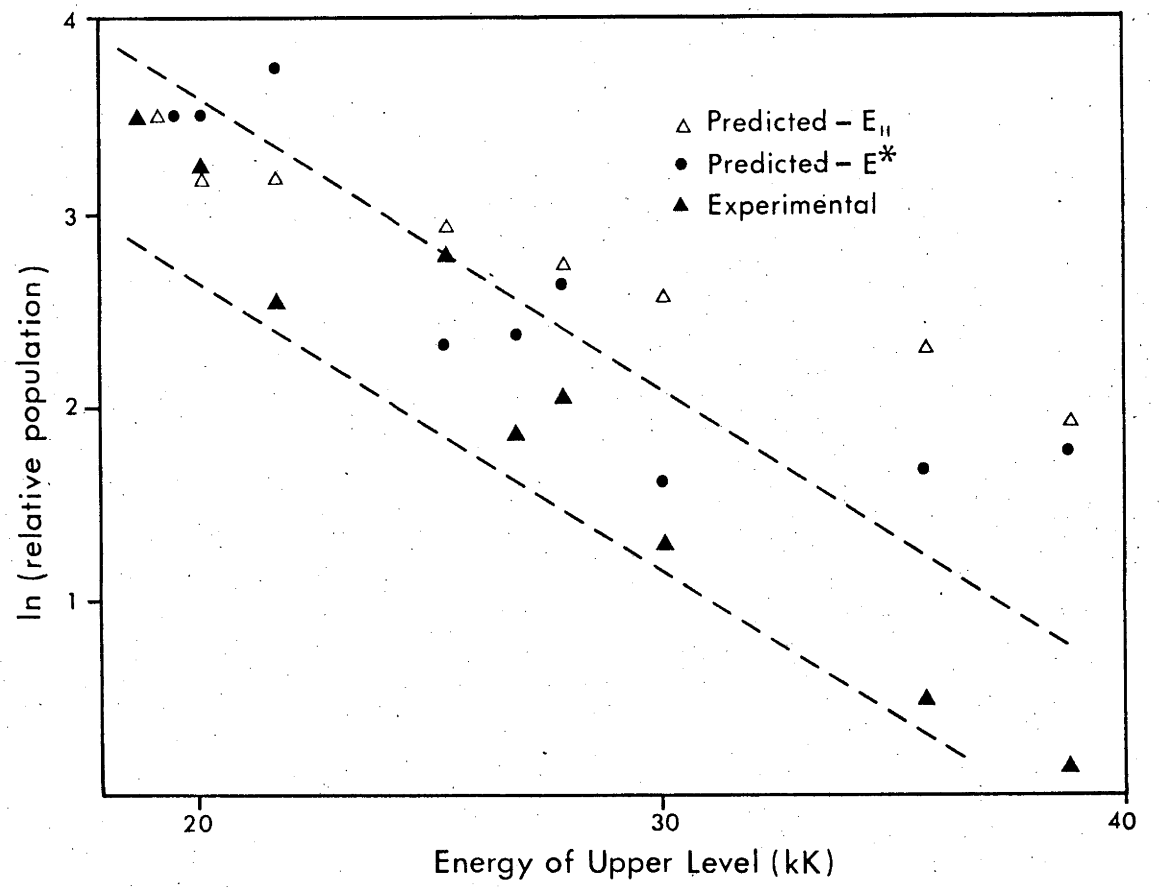

Figure 4.14. The statistical weight normalized relative level populations plotted against the excitation energy for the experimentally determined and predicted values for TiI from Ar^+ bombarded TiO_2. The dashed lines represent the scatter of the experimentally determined values for measurements on other lines (see Figure 4.5).

Although the reduced intensity plots may then only reflect the number of particles with $E > E^*$ able to contribute to the radiation, these measurements of the reduced intensity plots are of limited value until the processes responsible for the E_{ex} dependence of excitation are known. This same criticism also applies to the possibility that the changes in the photon intensity for Ti I lines may only reflect the decrease in the E^* value, allowing more particles to radiate. Indeed, estimates of the increase in the numbers of particles able to contribute to radiation for the changes in E^* and $E_{\|}$ values for the 521.0, 399.8 and 488.5 nm lines through equations (4.5), (4.6) and (4.7) would suggest increases of about 170%, 220% and 160% respectively. These are of the same order as those found experimentally (Figure 4.6). The important point, however, is *why* and *how* the E^* values decrease with surface contamination and this model does not indicate the mechanisms for these changes. The E^* values are then starting points for a more complete understanding of the excitation processes.

4.2.6 *Conclusions*

The model of Dzioba et al. [33,34] for analysing the decay curves for excited sputtered atoms has been shown to deduce values for an E^* value, related to the minimum kinetic energy of particles contributing to radiation, which are consistent with measurements of another energy parameter derived through line profile measurements, for Ti I. This consistency adds credence to the model of Dzioba et al. within

the limitations of the threshold forms of the excitation probability and is demonstrated here for the first time. The values of E^* obtained are generally higher from the sputtered clean metal than when the Ti atom is sputtered from a variety of compounds involving Ti and O,N,C and B. Higher excited levels of the Ti atom have been found to yield higher values of the energy parameters E^* and $E_{\|}$. Furthermore, the low to medium energy E^* and $E_{\|}$ values obtained suggest excitation resulting mainly from the collision cascade rather than in direct recoil collision sputtering, for normal incidence. This is also evidenced by the lack of dependence on the incidence energy.

The step function excitation model, where the particles contributing to radiation are those in the emitted energy spectrum with $E > E^*$, has been shown to be physically reasonable when compared with the experimental observations for Ti. Specifically, these observations are the average energy of the excited particles as determined from line profile measurements and, to a limited extent, the distribution of excited states. Changes in the E^* values may be related to different excitation processes at the surface and this may be via different curve crossings when foreign atoms are placed into the cascade, as in the case of contamination. This difference has previously been ascribed to non-radiative de-excitation processes. However, there appears no experimental evidence here to support the latter explanation for Ti, at least for the resonance ionisation process.

However, the E^* values may be only a fitting parameter which characterises the emission and for a more complete understanding of the photon emission process, the excitation event itself must be determined. The experimental data has been unable to be used to determine a preference for the form of the excitation process. In summary, any excitation model proposed for the creation of excited sputtered particles must be consistent with the intensity and average kinetic energy changes with oxygen, the differences in average kinetic energy for different energy levels and the distribution of excited states. This has been shown to be close to a straight line when plotted assuming a Boltzmann distribution. Curve crossing excitation cannot be ruled out for this excitation mechanism.

4.3 SUMMARY

Several important observations have been made for Ti I photon emission from bombarded Ti and Ti compounds. These observations relate to the distributions of the excited states, the kinetic energies of the excited atoms and the changes in the photon emission characteristics induced by surface oxygen contamination.

The distribution of excited Ti I states has been observed to be approximately of the form $\exp(-k.E_{ex})$ for the range of excited states considered. This form for the excited state distribution was not found to change to any marked extent when the Ti atom was sputtered from either clean Ti metal or a variety of Ti compounds.

Measurement of kinetic energy related parameters, $E_{\|}$ and E^*, have shown these to be similar for several Ti I lines sputtered from a variety of Ti compounds and from pure Ti. This is the first independent check of the model of Dzioba et al. in deriving energy parameters consistent with methods other than decay curve analysis. The values of average kinetic energy parameters characteristic of the Ti I lines examined were in the range 10 - 190 eV. These were found to decrease when the Ti atom was sputtered from a Ti compound involving N,O,C or B,or from an oxygen contaminated Ti surface. The E^* and $E_{\|}$ values were also found to increase with the excitation energy of the Ti I level.

Moderate enhancement factors were found for Ti I emission with surface contamination of oxygen (enhancements between 3-4). These enhancements were found to vary for different excitation levels.

Care has been taken to account for factors influencing the emission yields such as the observation volume and position and surface morphology changes with irradiation. It has been concluded that the important changes reflecting the differences between excited states, with different excitation energies and from different surface conditions, are in the excitation and/or de-excitation processes. Resonance ionisation as a de-excitation process has been found, at least here for Ti, not to influence the Ti I emission. To further investigate the excitation and de-excitation processes, an examination of the trends observed in the Ti I emission for other bombarded materials would be useful.

REFERENCES

[1] G.E. Thomas and E.E. de Kluizenaar, Nucl. Instr. Methods 132 (1976) 449.

[2] R.J. MacDonald and R.F. Garrett, Surface Sci. 78 (1978) 371.

[3] H.D. Hagstrum, Phys. Rev. 96 (1954) 336.

[4] W.L. Wiese and J.R. Fuhr, J. Phys. Chem. Ref. Data 4 No.2 (1975) 263.

[5] R.J. MacDonald and R.F. Garrett, to be published (1981)

[6] See, for example, A.R. Striganov and N.S. Sventitski, Tables of Spectral Lines of Neutral and Ionized Atoms (Plenum, New York, 1968)

[7] K. Jensen and E. Veje, Z. Physik 269 (1974) 292.

[8] J. Azencot and R. Goutte, Nucl. Instr. Methods 157 (1978) 99.

[9] R.M. Welch and E.H. Hygh, Phys. Rev. B 4 (1971) 4261

[10] See, for example, American Institute of Physics Handbook, 2nd ed. (McGraw-Hill, New York, 1963)

[11] V.V. Gritsyna, T.S. Kiyan, A.G. Koval and Ya.M. Fogel, Radiation Effects 14 (1972) 77.

[12] T. Parker and R. Kelly, in: Proc. Inter. Conf. on Implantation in Semiconductors and Other Materials (Plenun, New York, 1973) p.551.

[13] Y.W. Chung, W.J. Lo and G.A. Somorjai, Surface Sci. 64 (1977) 588.

[14] V.E. Henrich, G.D. Dresselhaus and H.J. Zeiger, Phys. Rev. Letters 36 (1976) 1335

[15] R. Holm and S. Storp, Appl. Phys. 12 (1977) 101.

[16] W.O. Hofer and P.J. Martin, Appl. Phys. 16 (1978) 271

[17] R.J. MacDonald and P.J. Martin, Surface Sci. 67 (1977) 237.

[18] R. Shimizu, Jap. J. Appl. Phys. 13 (1973) 228

[19] J.L. Whitton, W.O. Hofer, U. Littmark, M. Braun and B. Emmoth, Appl. Phys. Letters 36 (1980) 531.

[20] K. Tsunoyama, T. Suzuki and Y. Ohashi, Jap. J. Appl. Phys. 15 (1976) 349.

[21] G. Blaise and G. Slodzian, Surface Sci. 40 (1973) 708

[22] W.J. Lo, Y.W. Chung and G.A. Somorjou, Surface Sci. 71 (1978) 199

[23] V.E. Henrich, G. Dresselhaus and H.J. Zeiger, J. Vacuum Sci. Technol. 15 (1978) 534

[24] V.V. Gritsyna, T.S. Kiyan, R. Goutte, A.G. Koval and Ya. M. Fogel, Izv. Akad. Nauk SSSR, Ser. Fiz. 35 (1971) 578

[25] T.S. Kiyan, V.V. Gritsyna and Ya.M. Fogel, Nucl Instr. Methods 152 (1976) 435

[26] B.L. Cardon, P.L. Smith and W. Whaling, Phys. Rev. A 20 (1979) 2411

[27] J.R. Roberts, T. Andersen and G. Sørensen, Astrophy. J. 181 (1973) 567

[28] W. Whaling, J.M. Scalo and L. Testerman, Astrophys. J. 212 (1977) 571

[29] P.J. Martin and R.J. MacDonald, Surface Sci. 62 (1977) 551
I.S.T. Tsong, Surface Sci. 69 (1977) 609
C.J. Good-Zamin, M.T. Shehata, D.B. Squires and R. Kelly, Radiation Effects 35 (1978) 139

[30] K.J. Snowdon, B. Andresen and E. Veje, Radiation Effects Letters 43 (1979) 205

[31] G.E. Thomas and E.E. de Kluizenaer, Nucl. Instr. Methods 132 (1976) 449

[32] R.J. MacDonald and P.J. Martin, Surface Sci. 67 (1977) 237

[33] S. Dzioba, O. Auciello and R. Kelly, Radiation Effects 45 (1980) 235

[34] S. Dzioba and R. Kelly, Surface Sci. 100 (1980) 119

[35] I.S.T. Tsong and N.A. Yusuf, Nucl. Instr. Methods 170 (1980) 357

[36] I.S.T. Tsong, Third Intern. Workshop on Inelastic Ion-Surface Collisions, Feldkirchen-Westerham, FDR (1980)

[37] P.A. Delaney, Thesis, Australian National University (1977)

[38] C.M. Loxton, R.J. MacDonald and P.J. Martin, Surface Sci. 93 (1980) 84

[39] K.J. Snowdon, G. Carter, D.G. Armour, B. Andresen and E. Veje, Radiation Effects Lett. 43 (1979) 291

CHAPTER FIVE

PHOTON EMISSION FROM OTHER SOLIDS

A detailed study of the characteristics of photon emission from ion bombarded Ti has revealed some trends in the data. Specifically these have been (i) the kinetic energy parameters of excited atoms differ with excitation energy, (ii) the value of the kinetic energy parameters were of the order of tens to hundreds of eV for normal incidence bombardment, (iii) the kinetic energy parameters decreased with oxygen exposure and (iv) the intensities increased with oxygen exposure until a saturation occurred, followed by an intensity decrease with further exposure. A study has been made here for other Ar^+ bombarded targets to determine whether these are general characteristics of photon emission for all elements. The influence of changing the incidence angle has also been examined. A further test of the proposal that different collision partners may give different excitations (begun during the study of Ti I emission from Ti compounds) has been made for a series of Nb/V alloys. This result has application for photon emission chemical analysis. The influence of oxygen exposure on the emissions from the alloys (and hence the chemical analysis) has also been examined.

5.1 THE KINETIC ENERGY PARAMETERS FOR EXCITED PARTICLES

Kinetic energy parameters for normal incidence bombardment may be derived through the measurement of

decay curves and the analysis using the model of Dzioba et al. [1] (E^*), or through the measurement of the emission line profiles ($E_{||}$) as shown in section 4.2. A major disadvantage in the former method is the need to know the lifetime of the excited state. Measurement of the line profiles may be hampered by the resolution required for low kinetic energy excited particles. Cascading will, of course, influence both techniques. The line profile method has been favoured here and has been shown to yield similar results to the E^* values for the Ti I system (section 5.2). The kinetic energy parameters have been investigated for a variety of bombarded elements for type I, II and III emission, as a function of the excitation energy of the same species and as a function of the incidence angle of the target.

5.1.1 *The E_{ex} dependence for the kinetic energy parameter*

The $E_{||}$ kinetic energy parameter has been determined for a series of bombarded elements for excited levels with different excitation energies. In each case, integral yield analysis was used to determine the line profiles and the measurements were made with the Jarrel-Ash monochromator with optimum resolution 0.019 nm. The energy parameter $E_{||}$ was estimated from the half line width of the FWHM of the line profile and assuming that this half width represents an "average" Doppler shift of the emitted line. In cases where the line profile was insufficiently wide to estimate the contributions due to the Doppler broadening and the instrument line width (i.e. the measured

FWHM was of the same order as the instrument FWHM) then only the measured line width has been discussed. In such cases, the $E_{\|}$ parameter is expected to be of the order of several eV or less.

The E_{ex} dependence of the kinetic energy parameter has been investigated in detail for the Cr I and Ni I line emissions. The results of the line profile measurements on the Ni I emission lines are shown in Table 5.1 and for the Cr I emission lines are shown in Table 5.2.

TABLE 5.1

The measured FWHM of Ni I emission lines and derived $E_{\|}$ parameters for different excitation energies. The line profiles were measured with an instrument FWHM of 0.039 nm. 55 keV Ar^+ bombardment at normal incidence was used with ultra high vacuum conditions.

Ni I λ(nm)	Measured FWHM (nm)	$E_{\|}$ (eV)	E_i (cm^{-1})
352.4	0.052	65 ± 25	28569
351.5	0.049	49 ± 25	29321
361.9	0.062	120 ± 50	31031
305.0	0.070	250 ± 75	32973
300.2	0.062	177 ± 90	33501
300.3	0.082	395 ± 90	34163
305.7	0.069	238 ± 90	34409
301.2	0.073	285 ± 75	36601

Tables 5.1 and 5.2 show similar trends to those found for Ti: the energy parameter $E_{\|}$ increases for states having higher excitation energy. The values of the $E_{\|}$ parameter for Cr excited atoms are very similar to those obtained from bombarded Ti and the Ni values are also

TABLE 5.2

The measured FWHM of Cr I emission lines and derived $E_{||}$ parameters for different excitation energies. The line profiles were measured with an instrument FWHM of 0.019 nm. 55 keV Ar^+ bombardment at normal incidence was used with ultra high vacuum conditions.

Cr I λ (nm)	Measured FWHM (nm)	$E_{||}$ (eV)	E_i (cm^{-1})
425.4	0.038	36 ± 14	23499
427.4	0.043	49 ± 14	23389
520.6	0.042	32 ± 16	26796
520.8	0.044	35 ± 16	26788
357.8	0.046	83 ± 22	27935
435.1	0.073	159 ± 25	31280
464.6	0.071	131 ± 25	29825
391.9	0.068	168 ± 25	33816

similar, although higher than that found for Ti excited atoms. The measurements for Ni, however, were made with an instrument resolution not as good as that used for the measurement of the Cr I and Ti I line widths. Cascading is not expected to strongly influence the excited states examined here [2]. It is interesting to note that equivalent excitation energy levels for Ti, Ni and Cr are characterised by similar $E_{||}$ values. Ti, Ni and Cr are all transition metals of similar mass and each has an unfilled 3d shell in the electronic configuration.

To further investigate these similarities between the $E_{||}$ values from Ti, Ni and Cr, several other target species have been bombarded and the emission line profiles measured. The results of these measurements are shown in Table 5.3.

TABLE 5.3

The measured FWHM of atomic emission lines and derived $E_{||}$ parameters for different elements bombarded at normal incidence under ultra high vacuum conditions by 55 keV Ar^+. The line profiles were measured with an instrument FWHM of 0.019 nm.

Species	λ(nm)	Measured FWHM(nm)	$E_{||}$ (eV)	E_i (cm^{-1})
Zn I	307.5	0.029	~ 30	32502
	213.8	0.022		46745
	481.0	0.025		53672
	328.2	0.027	~ 20	62769
Mg I	285.2	0.024		35051
Aℓ I	396.2	0.043	30 ± 7	25348
	308.2	0.033	24 ± 7	32435
Si I	288.2	0.035	34 ± 9	40992

It may be noted from Table 5.3 that the emission line profiles from Zn I and Mg I studied here for normal incidence bombardment are of the same order as the instrument FWHM. This would indicate that the kinetic energy parameters for atoms with these excited states would be very low.

The observation previously noted, that excited states of Ti, Ni and Cr atoms yield similar $E_{||}$ values, does not apply to the elements studied here. In the case of Zn, where the excitation energies for several of the lines studied are far higher than those studied for Ti, Ni and Cr, even the highest excitation level studied has a very low $E_{||}$ value.

The $E_{||}$ values for the Aℓ I lines are also low, however, these values are expected to be influenced by cascading (see Figure 3.7(b)). The values shown may then be slightly higher than would be obtained without cascading influencing the level. The low value of $E_{||}$ obtained for the Si I 288.2 nm line is also of interest. It could be expected from the results of White et al. [3] (see also Figure 2.10) that a particularly high value for the kinetic energy parameter would be obtained under UHV conditions. The conclusion [3] that only excitation through binary collision sputtering contributes to the emission would not seem to be valid here, although not all of the experimental parameters are the same.

5.1.2 *Kinetic energy parameters for ionised atom emission*

Kinetic energy parameters have also been determined for ionised particle emission to compare with those obtained from neutral atom emission. $E_{||}$ values, obtained by integral yield line profile measurement, are shown in Table 5.4.

The $E_{||}$ values for the Mg II 280.3 nm line are expected to be strongly influenced by cascading from upper levels. One of these upper levels is responsible for the 279.1 nm line which is observed to be about 25% of the intensity of the 280.3 nm line. Consequently, at least one quarter of the total emission of the 280.3 nm line must arise through states which were previously in the excited state with E_i = 71491 cm^{-1} but have decayed by emitting radiation of wavelength 279.1 nm, to the

TABLE 5.4

The measured FWHM of ionised atom emission lines and derived $E_{\|}$ parameters for different elements bombarded at normal incidence under ultra high vacuum conditions by 55 keV Ar^{+}. The line profiles were measured with an instrument resolution of 0.019 nm.

Species	λ(nm)	Measured FWHM (nm)	$E_{\|}$ (eV)	E_i (cm^{-1})
Mg II	280.3	0.045	60 ± 10	35669
	279.1	0.050	78 ± 10	71491
Aℓ II	281.6	0.041	52 ± 12	95348
Aℓ III	360.1	0.073	120 ± 40	143712
Si II	385.6	0.049*	46 ± 18	81252
Si III	254.2	0.048	96 ± 20	122215

* estimated from measurement with instrument resolution 0.039 nm.

---

excited state with $E_i = 35669\ cm^{-1}$. This would then hamper any attempt to use the model of Dzioba et al. to determine E^* values for this state. The derived z vs x curve from decay curve measurements for the Mg II 280.3 nm line is shown in Figure 5.1. The break in the curve indicates that cascading level feeding is important. At greater distances from the target, the curve is dominated by the cascading transitions from the upper states with $E_i = 71491 cm^{-1}$ and $E_i = 69805\ cm^{-1}$.

The derived $E_{\|}$ values shown in Table 5.4 appear higher than values obtained from the neutral atom emission lines. However, the difference is not as large as may be expected for the very high excitation energies found for

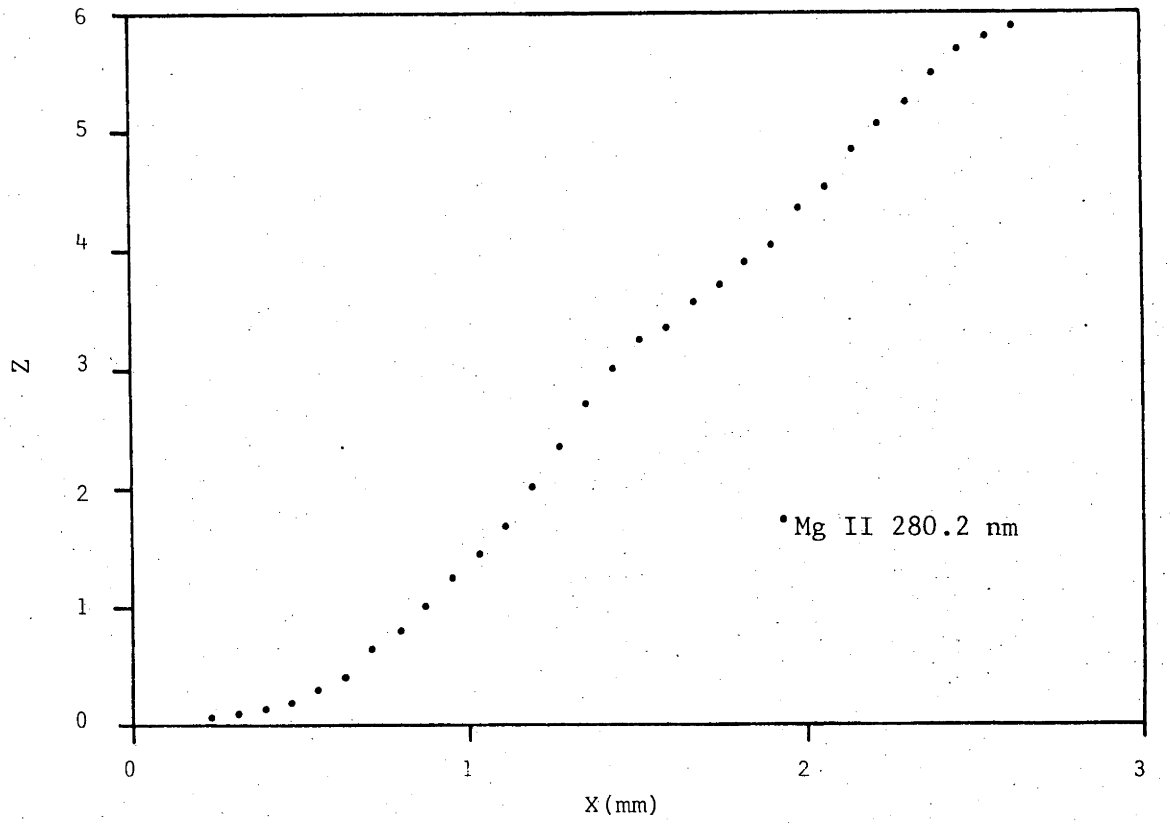

Figure 5.1. Plot of z vs x determined from integral yield decay curve measurement of the Mg II 280.3 nm line and using the analysis from equation (2.25).

several of these ionised atom emissions, where the excitation energies have ranged up to 143712 cm^{-1}.

5.1.3 *Line profile changes with the angle of incidence*

The low to medium values obtained here for the energy parameters have all been determined for normal incidence bombardment. In the case of Si I 288.2 nm emission in particular, the $E_{\|}$ value is considerably less than that expected from previous studies [3]. However,

the results for the Si I line profile measured by White et al. [3] were obtained using an angle of incidence other than normal incidence. The binary collision sputtering component of the total sputtered yield is expected to increase as the angle of incidence increases. This has been shown previously in Figure 2.6 where the angle of incidence influences the emission line profiles. The profiles broaden with increasing angle of incidence.

The Si I 288.2 nm emission line profile has been studied here as a function of the angle of incidence of the 55 keV Ar^+ beam. The observation angle was at 90° to the incident beam and integral yield measurements were made. An instrument resolution of 0.039 nm was used for this study. To increase the emission intensity, the line profiles were measured under a high oxygen exposure and with the target positioned for maximum signal strength. Towards grazing incidence where the emission may extend further downstream of the bombarded spot, the viewing geometry may no longer be an integral yield measurement. At these higher incidence angles there may also be a contribution to the measured line profile from the bombardment of the leading edge of the target. Care was taken to ensure that such emission was kept to a minimum by re-positioning the target.

The changes in the Si I 288.2 line profile are shown in Figure 5.2. The line profiles are shown to broaden considerably with increasing incidence angle and eventually

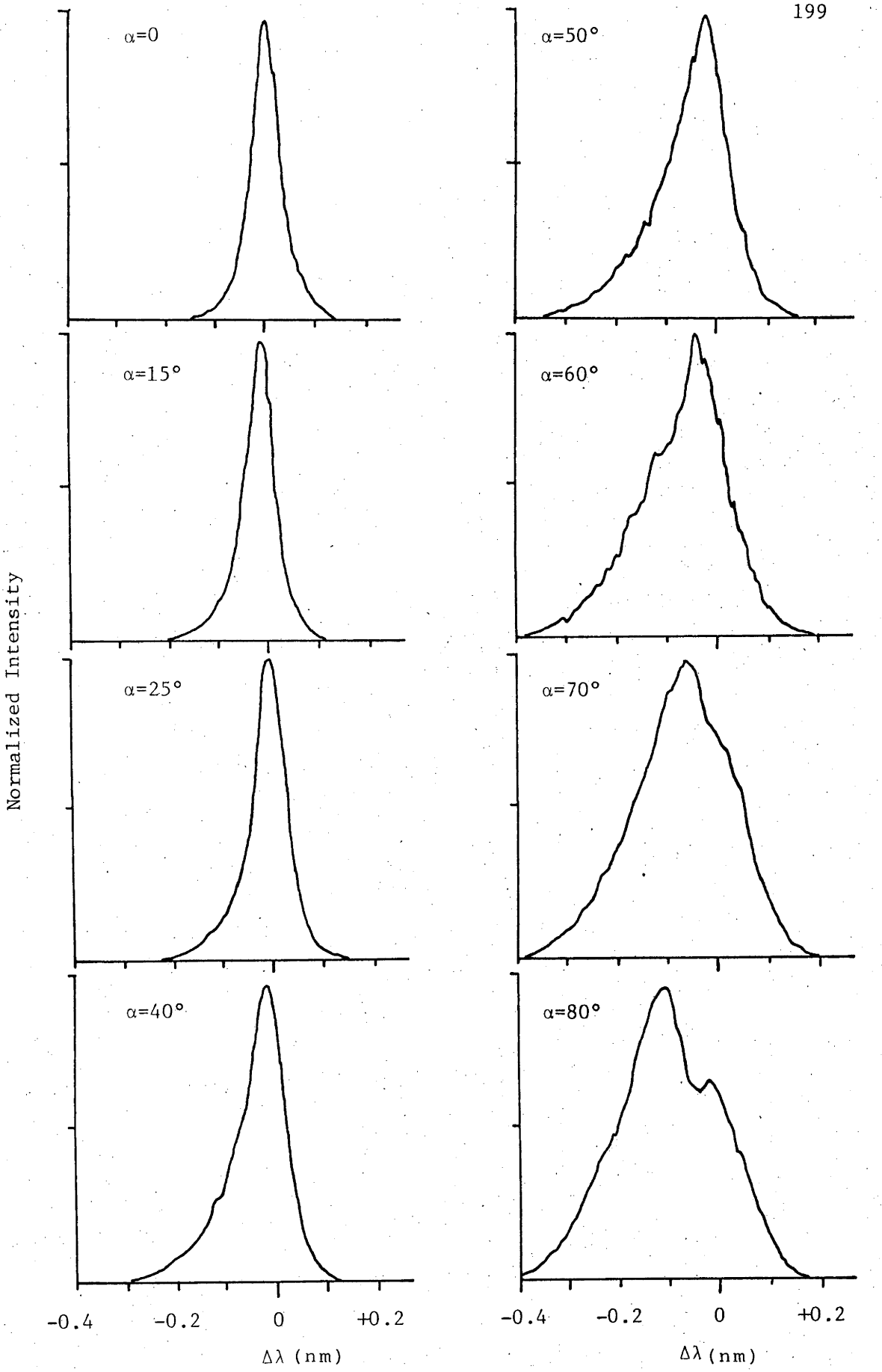

Figure 5.2. Normalised line profiles for the SiI 288.2 nm line for different incidence angles, α, of the 55 keV Ar^+ beam. Oxygen exposure was used to enhance the signals. The instrument resolution was 0.039 nm.

become up to 0.3 nm wide at half intensity. The emission lines show some shift in the intensity peak toward lower wavelengths and also show pronounced asymmetry at higher incidence angles. This "blue" shift and broadening is a result of sputtered atoms having a velocity component toward the detector. The extent of the broadening shown in Figure 5.2 suggests that higher kinetic energy particles are of increasing importance as the incidence angle increases. This is consistent with the expected increase in importance of binary collision sputtering at higher incidence angles. For normal incidence bombardment, the recoiling target atom has no velocity component away from the surface and must undergo further collisions before contributing to the sputtered flux. The probability for the recoil target atom to have a velocity component away from the target increases with increasing angle of incidence. A greater binary collision sputtering component is then expected.

The reflected component of the observed emission is also shown in Figure 5.2 by the increased "red" shift (excited particles are moving away from the surface) with increased incidence angle.

5.1.4 *Line profiles in channelling directions*

Another method for examining the influence of the collision cascade versus the binary collision sputtering contributions, may be through channelling studies. In a channelling direction, the collision cascade would be expected to be initiated deeper within the lattice than

in the case of non-channelled incidence directions. A decreased collision cascade component to the total sputtering yield would then be expected. Line profile measurements in and out of channelling directions have been made for 55 keV Ar^+ bombardment of a single crystal. A Ni target with a (110) surface and an Aℓ (100) target surface were used.

The Ni single crystal was set for 45° incidence and rotated about the azimuthal angle to obtain the channelling yield minimum. Observation was at 90° to the incidence beam direction and the line profiles were measured using integral yield analysis. The emission line profile for the NiI 352.4 nm line was measured for the beam incident along this channelled direction. A line profile was also measured for this line in a random (non-channelled incidence) direction, determined by azimuthal rotation of the target until an intensity maximum was observed. The two normalised line profiles for the NiI 352.4 nm line are shown in Figure 5.3.

The measured line profiles shown in Figure 5.3 are not influenced strongly by channelled and random incidence directions. Both line profiles show a small hump on the low wavelength side of the emission peak which is found to disappear for normal incidence bombardment. From the wavelength shift of this peak compared with the main intensity peak, excited atoms contributing to the emission of this second peak are estimated to have kinetic energies of the order of 2 keV. Excited particles contributing to this emission would represent the binary collision sputtering component of the total sputtering yield. The relative

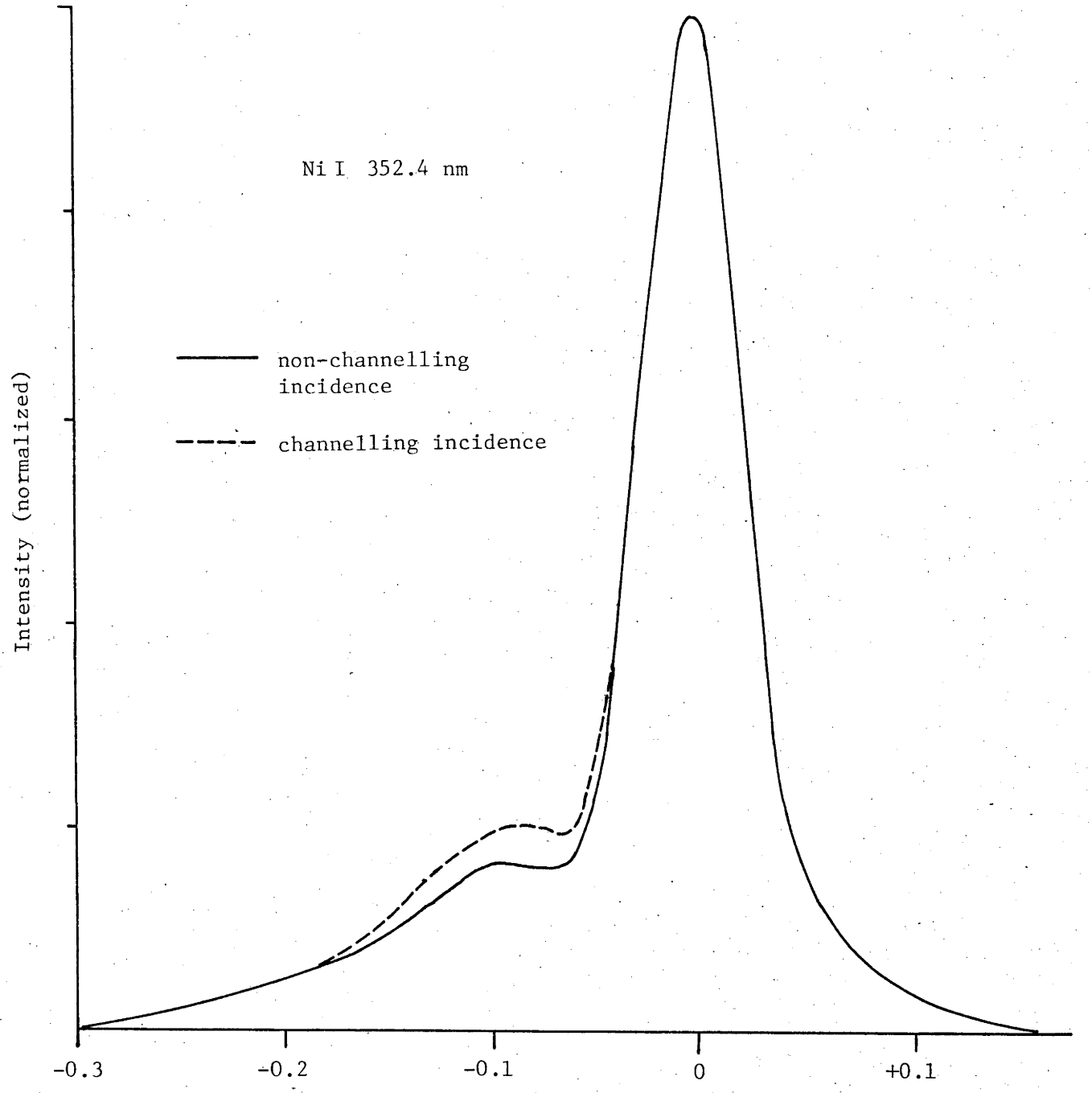

Figure 5.3 The measured line profiles for the Ni I 352.4 nm line for Ar^+ › Ni (110) in channelling and non-channelling incidence directions. The instrument resolution was 0.039 nm.

intensity of this second peak increases by 30 ± 10% with channelling incidence direction when compared with a random incidence direction. This would be expected to reflect the decreased collision cascade sputtering component for channelled incident ions which initiate the collision cascade deeper inside the lattice. Further experimental (and perhaps, simulation) investigation of these experiments for channelled versus random incidence directions are warranted. Additional results for the Aℓ I 396.2 nm emission line for channelling and random incidence directions for an Aℓ (100) surface have shown no change in the emission line profiles. However, the study was hampered by the need for increased resolution to study the narrower Aℓ I lines.

5.1.5 *Discussion*

The $E_{\|}$ values obtained here and shown in Tables 5.1 - 5.4 may be compared with E^* values obtained elsewhere [4,5] using the model of Dzioba et al. [1]. This comparison is shown in Table 5.5. In cases where the same lines have not been studied here, $E_{\|}$ values are shown for emission lines of the same species and similar excitation energy. The correspondence between the values obtained is good except for the Si I 288.2 nm and Mg II 279.8 nm lines. The derived z vs x curve used to obtain E^* for the Si I line by Tsong et al. [4] indicates that cascading may be strongly influencing the observed Si I 288.2 nm emission. This may have contributed to the discrepancy between the derived kinetic energy parameters. The lifetime used by

Tsong et al. to determine the E^* value was that for the excited level leading to the 288.2 nm emission and not the cascade feeding state. The difference between the Mg II kinetic energy parameters for similar Mg II states may be associated with spectral overlap of the 279.8 nm line used by Dzioba et al. [5]. Three emission lines occur near the 279.8 nm line [6]; these being the 279.79 nm (E_i = 35730 cm^{-1}), 279.799 nm (E_i = 71491 cm^{-1}) and 279.80 (E_i = 71491 cm^{-1}) emission lines. The Mg II 279.1 nm line used here to derive the $E_{||}$ value is not expected to have this spectral overlap.

TABLE 5.5

Comparison of $E_{||}$ values obtained here and E^* values derived through intensity decay measurements

Species	λ(nm)	$E_{||}$ (eV)	E^*(eV)
Ni I	346.1		101 ± 20 [4]
Ni I	352.4	65 ± 25	
Cr I	425.4	36 ± 14	40 ± 8 [4]
Si I	288.2	34 ± 9	684 ± 140 [4]
Mg I	285.2	< 25	15 - 40 [5]
Mg II	279.8		760 - 1600 [5]
Mg II	279.1	78 ± 10	

Certainly the $E_{\|}$ values obtained here over the (limited) range of bombarded elements studied, have not produced high kinetic energy parameter values of the order of keV's for normal incident bombardment. The E^* values are higher than the most probable kinetic energies of secondary ions but are consistent with those energies expected in the high energy tail of the kinetic energy distributions for collision cascade induced sputtering [7]. It may be premature to develop an excited atom sputtering model based upon binary collision type sputtering [8] to account for the high values of E^* sometimes derived from intensity decay curve measurements for normal incidence bombardment, particularly when such values have not been checked with, for example, line profile measurements.

That the binary collision sputtering component is important for excited atom production has been shown by the influence of the incidence angle on the emission line profiles (Figure 5.2) and, more tentatively, by the influence of the incidence direction on the line profiles from a single crystal target (Figure 5.3). As the incidence angle increases, the binary collision sputtering component and with it, the kinetic energies of the sputtered atoms, increases and this is reflected in the broadening and line shift of the Si I emission line.

Excited Ti, Cr and Ni atoms with similar excitation energies are noted to have similar $E_{\|}$ values. However, for Zn atoms with similar excitation energies, the $E_{\|}$ values are considerably less than the values for Ti, Cr or Ni.

Zn is also a transition metal element of similar mass but has a filled 3d electronic configuration. The differences between the kinetic energies of these transition metal elements indicate that the probability for excitation is not only dependent upon the excitation energy of the level and the kinetic energy distributions of the sputtered (not necessarily excited) atoms. The $E_{||}$ values obtained from ionised atoms are sometimes not different to $E_{||}$ values obtained from some neutral emissions. The excitation energies are usually considerably higher than those for neutral atom excited levels (by up to a factor of 5 for levels studied here). However, the $E_{||}$ values obtained from ionised atoms are higher than the values obtained from neutral atoms of the same species for the elements studied here.

5.2 PHOTON EMISSION FROM BOMBARDED Nb/V ALLOYS

An attempt has been made to observe "matrix effects" on photon emission from ion bombarded metal alloys. These effects would become evident in a photon emission quantitative analysis study of the metal alloy. The influence of oxygen exposure on this analysis technique has been investigated. Changes in the Nb I and V I emissions with oxygen exposure have been discussed.

5.2.1 *Photon emission analysis of Nb/V alloys*

There are several reasons why quantitative analysis using photon emission for a series of metal alloys is of importance here. Primarily, the analysis may test

the proposal (section 4.1) that should excitation occur during the final collision as the collision cascade intersects the surface, different excitations through $(M_1 \rightarrow M_2)$, $(M_1 \rightarrow M_1)$ and $(M_2 \rightarrow M_2)$ collisions may be expected where M_1 and M_2 are the masses of the binary alloy constituents. Non linearities in the photon emission intensity with alloy concentration of a particular element would result from these different excitations. Also important is that photon emission for quantitative analysis has not normally been applied to metal alloys but has been restricted to doped glasses and insulators where the band gap is assumed to exclude non-radiative transitions, thereby allowing all excited states to decay by photon emission. Oxygen (as a surface contaminent, or in the bulk) is commonly employed to enhance signal sensitivity and to exclude non-radiative transitions and the influence of the oxygen contamination on the analysis of a metal alloy is then also of interest.

In the absence of matrix effects and assuming that the competing non-radiative processes influencing the excited atoms do not change with alloy constituent concentration (or are absent), the photon yield for a particular species would be expected to follow the relation:

$$\text{Photon Yield} = K.S.\,\emptyset.P_{exc} \qquad (5.1)$$

where S is the sputtering yield, $\emptyset$ is the surface concentration, P_{exc} is the probability that the sputtered particle is in the excited state used for analysis and K includes the detection efficiency and branching ratio.

Non linearities in the photon yield with bulk concentration may then be related to either of changes in the sputtering yield, surface concentration with bombardment or the probability for excitation.

The Nb/V alloys used for analysis varied from 98% Nb to 6.5% Nb. Analysis of these Nb/V alloys using ISS, photon emission and SIMS has been reported in detail elsewhere [9] and only the photon emission results will be discussed here. The Nb/V system is a convenient system to study since atomic mass separation is sufficient to avoid mass overlap in SIMS and ISS and there are strong emission lines sufficiently separated in wavelength to avoid spectral overlap in the photon emission analysis. Sputtering yields for He^+ and Ar^+ bombardment of the pure elements are very similar [10,11] so that major preferential sputtering effects are not anticipated in the measurements. The arc melted alloys are known to form a continuous series of solid solutions [12] and consequently, segregation is not expected to influence the results, unless segregation occurs under bombardment.

Photon emission analyses were measured using UHV and oxygen background pressure environments. The UHV analysis was performed with the total background vacuum less than 10^{-9} torr and the background oxygen conditions were with an oxygen pressure of 7×10^{-6} torr. The beam current density for the incoming 55 keV Ar^+ beam in each case was 0.5 mA/cm^2. Photon emission from the sputtered particles was observed perpendicular to the target surface with the Jarrel-Ash monochromator set for

0.08 nm resolution and the targets were bombarded at normal incidence. An integral yield viewing geometry was used to encompass any change which may occur in the emitting volume for changes in the Nb:V concentrations. The Nb I 405.9 nm and V I 411.1 nm lines were chosen as reference lines, since both are free of spectral overlap from emission lines of the other element and are intense and conveniently close to facilitate fast scanning. These emission lines are shown in Figure 5.4.

All target surfaces were irradiated for at least one hour before stable signals were obtained, with long term transients in the photon emission being observed for all signals. For the previously unbombarded surfaces, an initial intensity decay occurs which would be associated with surface oxide removal, followed by a transient increase of about 30% before the signal reaches a stable level. This secondary rise is possibly due to bombardment induced heating and subsequent outgassing of the target which increases the photon emission. Similar effects have been observed when the target is heated. Heating the targets to 800°C induced long term transients in the photon emission. The long lifetimes of these transients are most probably related to the difficulty in obtaining clean surfaces of Nb. Nb is known to have a very high solubility and binding energy for oxygen, nitrogen, carbon and hydrogen [13].

The results of the analyses performed under UHV conditions for the V and Nb concentrations are shown in Table 5.6. In each case, the intensity of the line was

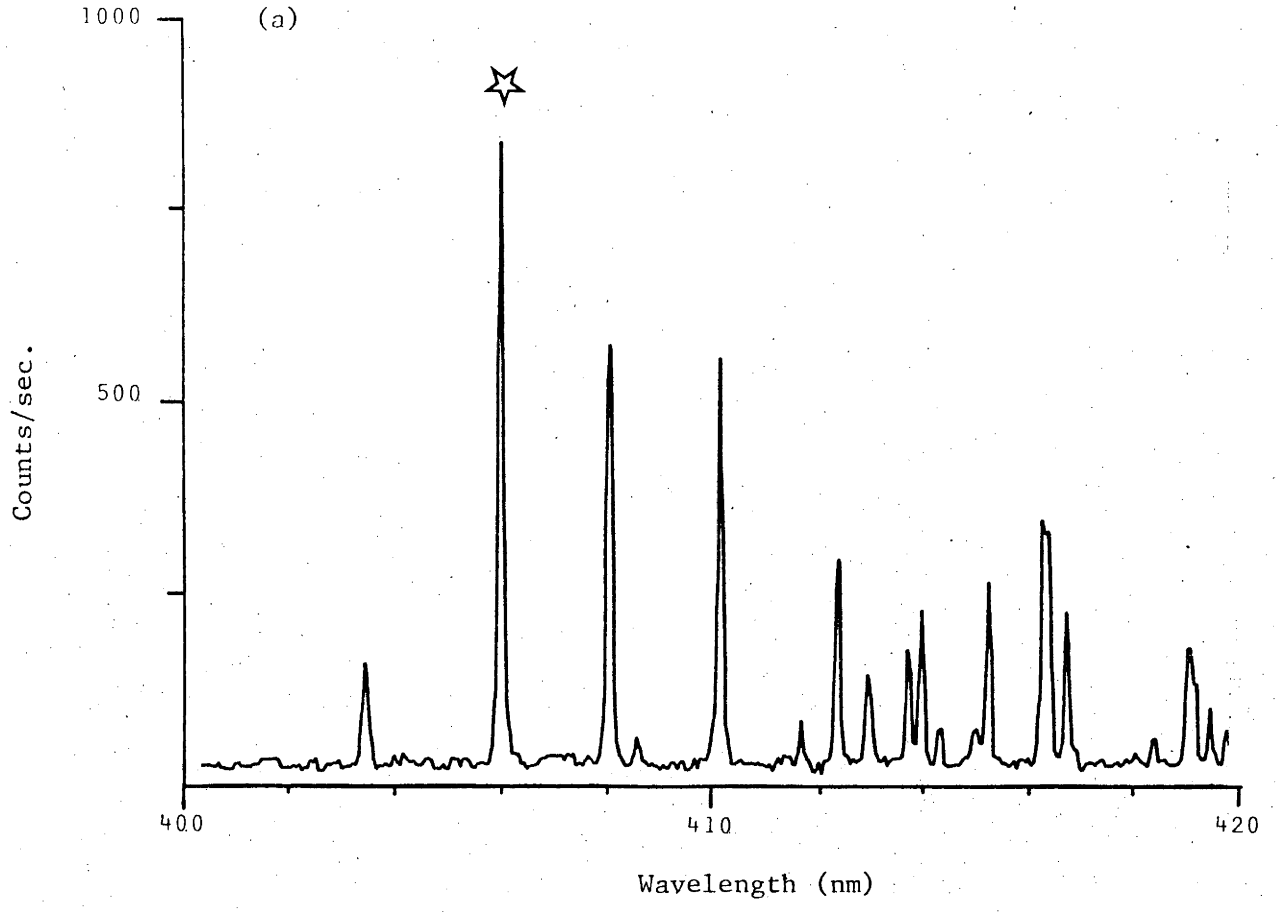

Figure 5.4(a). Wavelength scan for 55 keV Ar^+ bombarded Nb. The NbI 405.9 nm line is indicated.

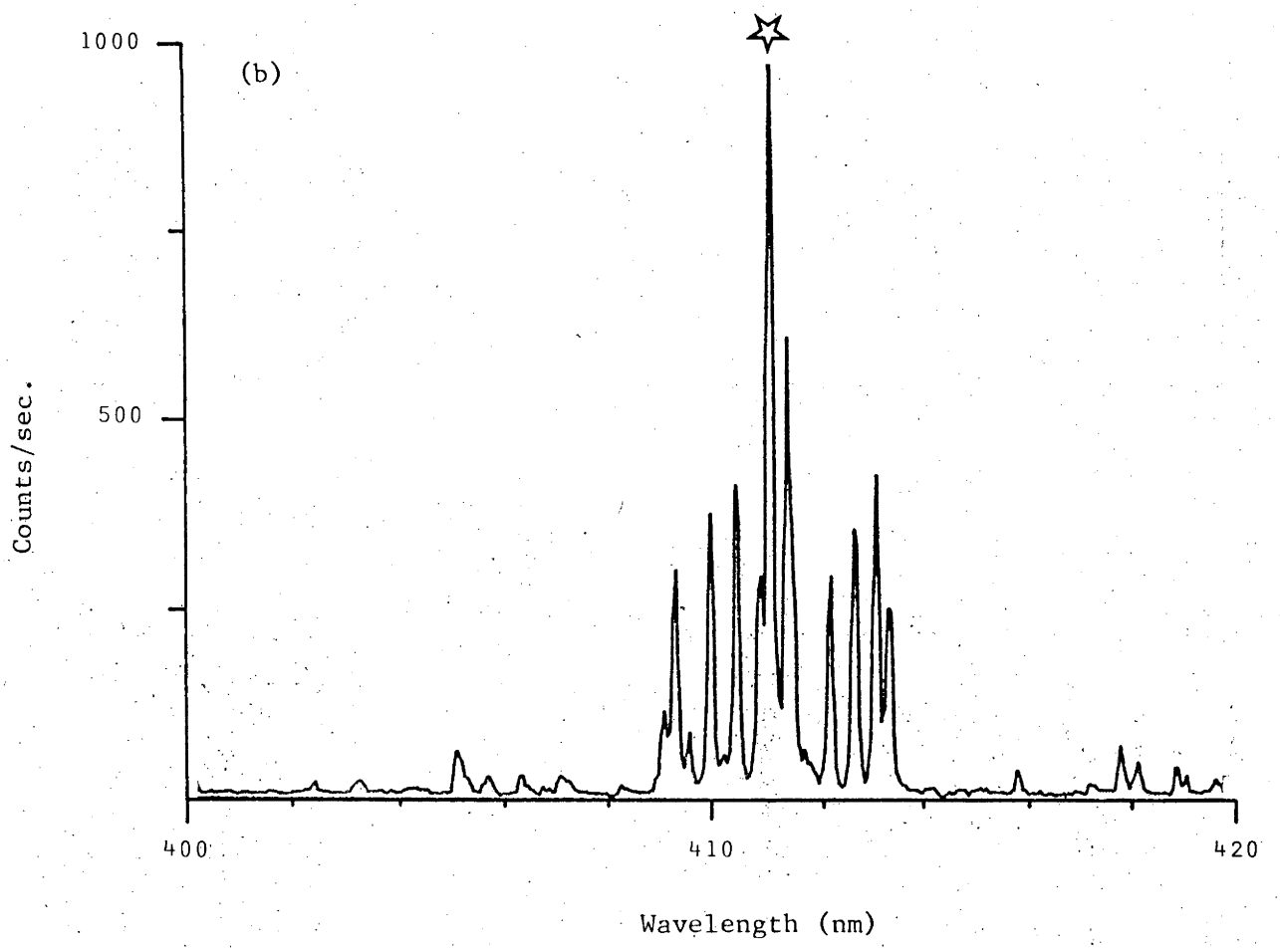

Figure 5.4(b). Wavelength scan for 55 keV Ar^+ bombarded V. The VI 411.1 nm line is indicated.

TABLE 5.6

Analysis of Nb/V alloys using the NbI 405.9 nm and the V 411.1 nm line under UHV conditions.

Target	Nb Concentration using Nb I 405.9 nm	V Concentration using V I 411.1 nm	%V + %Nb	EPMA NB Concentration
#9	98 ± 2%	2 ± 3%	100	98
#8	81 ± 2	16 ± 3	97	80
#7	55 ± 4	44 ± 4	99	45.5
#6	31 ± 4	70 ± 3	101	24
#5	17 ± 4	82 ± 2	99	13
#4	8 ± 3	91 ± 2	99	6.5

assumed proportional to the atomic concentration which was then determined by comparison with the intensity from the pure element standard. The photon emission analyses are compared with the alloy concentrations determined by electron probe analysis performed over micro and macro sections of the surface [14].

Table 5.6 shows that the photon emission analyses are very close to those obtained by the electron probe analysis (except for Alloy #7) although all appear slightly Nb rich. The analysis appears consistent, with the sum of the independently determined concentrations being close to 100%.

The photon emission analyses performed at 7×10^{-6} torr background oxygen pressure are shown in Table 5.7.

TABLE 5.7

Analysis of Nb/V alloys using the Nb I 405.9 nm line and the V I 411.1 nm line under conditions of 7×10^{-6} torr background oxygen pressure.

Target	Nb Concentration using Nb I 405.9 nm	V Concentration using V I 411.1 nm	%V + %Nb	EPMA Nb Concentration
#9	98 ± 2%	11 ± 3%	109	98
#8	64 ± 3	69 ± 3	133	80
#7	20 ± 2	79 ± 2	99	45.5
#6	12 ± 2	102 ± 2	111	24
#5	3 ±1.5	63 ± 3	66	13
#4	2 ± 1	68 ± 3	70	6.5

Agreement with the EPMA results is now poor, with the sum of the two components being in the range 66 - 133%. In general, the V atomic concentration is determined to be too high and the Nb concentration too low.

These results under oxygen contamination conditions may be understood when the behaviour of the line intensities from the alloys with oxygen exposure are considered. The intensity changes with oxygen exposure for the emission at 405.9 nm which includes continuum emission and the Nb I 405.9 nm line, from pure Nb and the #8, #7 and #5 alloys, are shown in Figure 5.5. The conditions under which the analysis measurements for Table 5.7 were made is indicated.

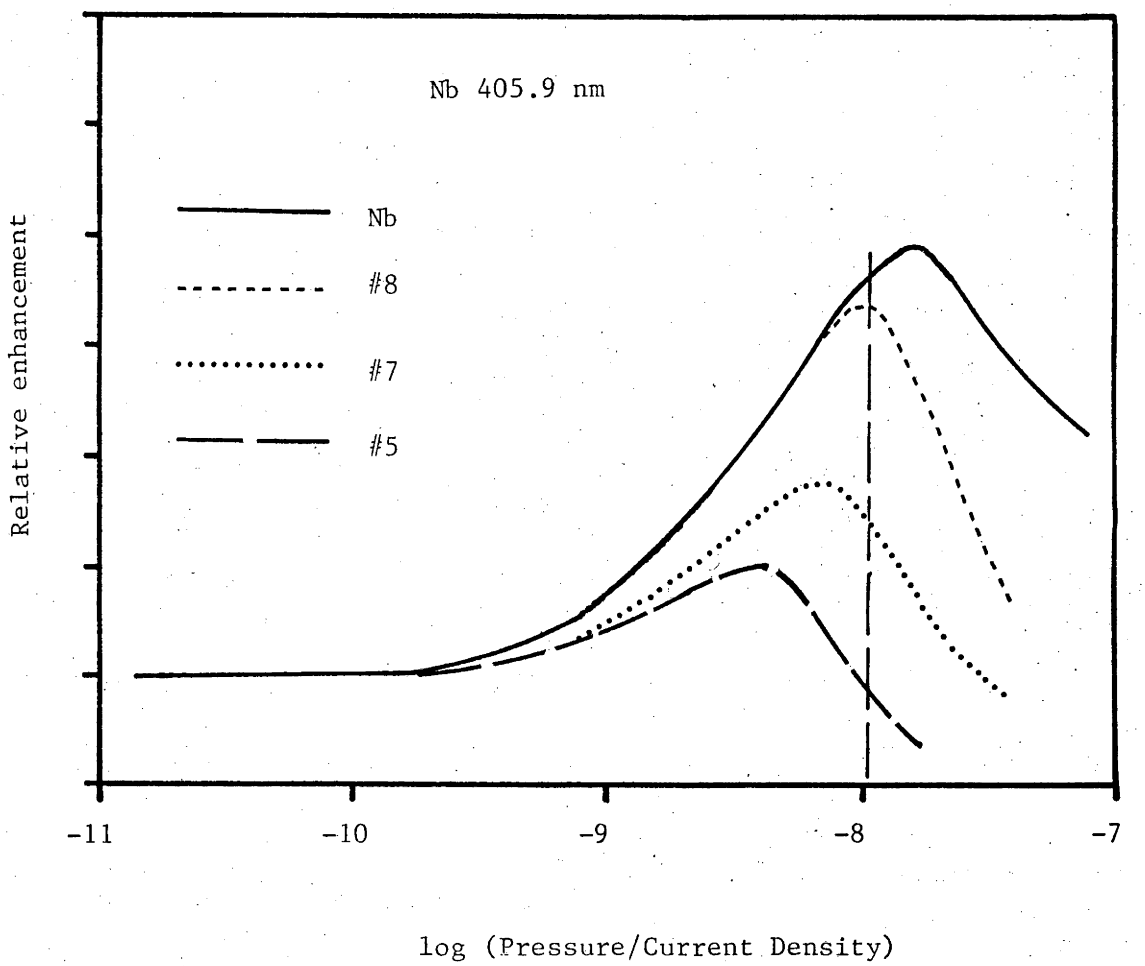

Figure 5.5. Intensity changes for the emission at 405.9 nm (no more than 10% continuum component) with oxygen exposure, from Nb and selected Nb/V alloys. The conditions used for the photon emission analysis under oxygen exposure conditions is shown (pressure in torr and current density in $\mu A/cm^2$).

Similar curves may also be obtained for the V I 411.1 nm emission (see also Figure 5.6(b)).

The enchancement curves, Figure 5.5, show that the intensity changes with oxygen exposure vary with the different bombarded alloys. Consequently, the line intensities for the condition under which the analysis was made, are no longer proportional to the alloy concentrations. To correct the analysis shown in Table 5.7, a correction term must be used which takes into account the differing enhancements with oxygen exposure. This factor for the Nb I 405.9 nm line, may be derived from the relative enhancements at the oxygen exposure used for analysis as shown in Figure 5.5. The corrected analyses using these factors determined from the enchancement curves for the Nb I and V I lines, are shown in Table 5.8.

TABLE 5.8

The analysis of the Nb/V alloys shown in Table 5.7 corrected for the varying enhancements with oxygen exposure. The correction terms have been derived from the enhancement curves for oxygen exposure.

Target	Corrected Concentration Nb (%)	V (%)	EPMA Nb Concentration
#8	71 ± 12	22 ± 6	79.7
#7	43 ± 15	50 ± 10	45.6
#5	18 ± 15	100 ± 15	12.9

The use of the correction term leads to derived concentrations consistent with those obtained by electron probe analysis, although the relative uncertainty is increased.

These results show that a correction term, to compensate for the varying enhancements with oxygen exposure, must be determined from exposure to obtain quantitative analysis of the Nb/V alloys under non UHV conditions. This requires that exposure curves are measured for every alloy to be analysed. It further requires that clean surfaces be initially produced for the measurement of these exposure curves. The increased effort and decreased accuracy associated with non UHV quantitative analysis for Nb/V alloys renders this technique unattractive. Further study would seem warranted to determine whether these matrix effects with oxygen are limited to the Nb/V system used here, or could have influenced previous photon emission analyses [see for example, 15].

5.1.2 *The influence of oxygen exposure on line emission from the Nb/V alloys.*

The intensity changes for the V I and Nb I emission lines with background oxygen pressure may now be examined in detail. These changes for the Nb I 405.9 nm and V I 411.1 nm lines are shown in Figure 5.6. In each case the contribution of background and continuum emission has been subtracted and the intensity normalised for the emission under the cleanest conditions. The background pressure divided by the beam current density is proportional to the ratio of the arrival rates of oxygen atoms to incoming beam ions.

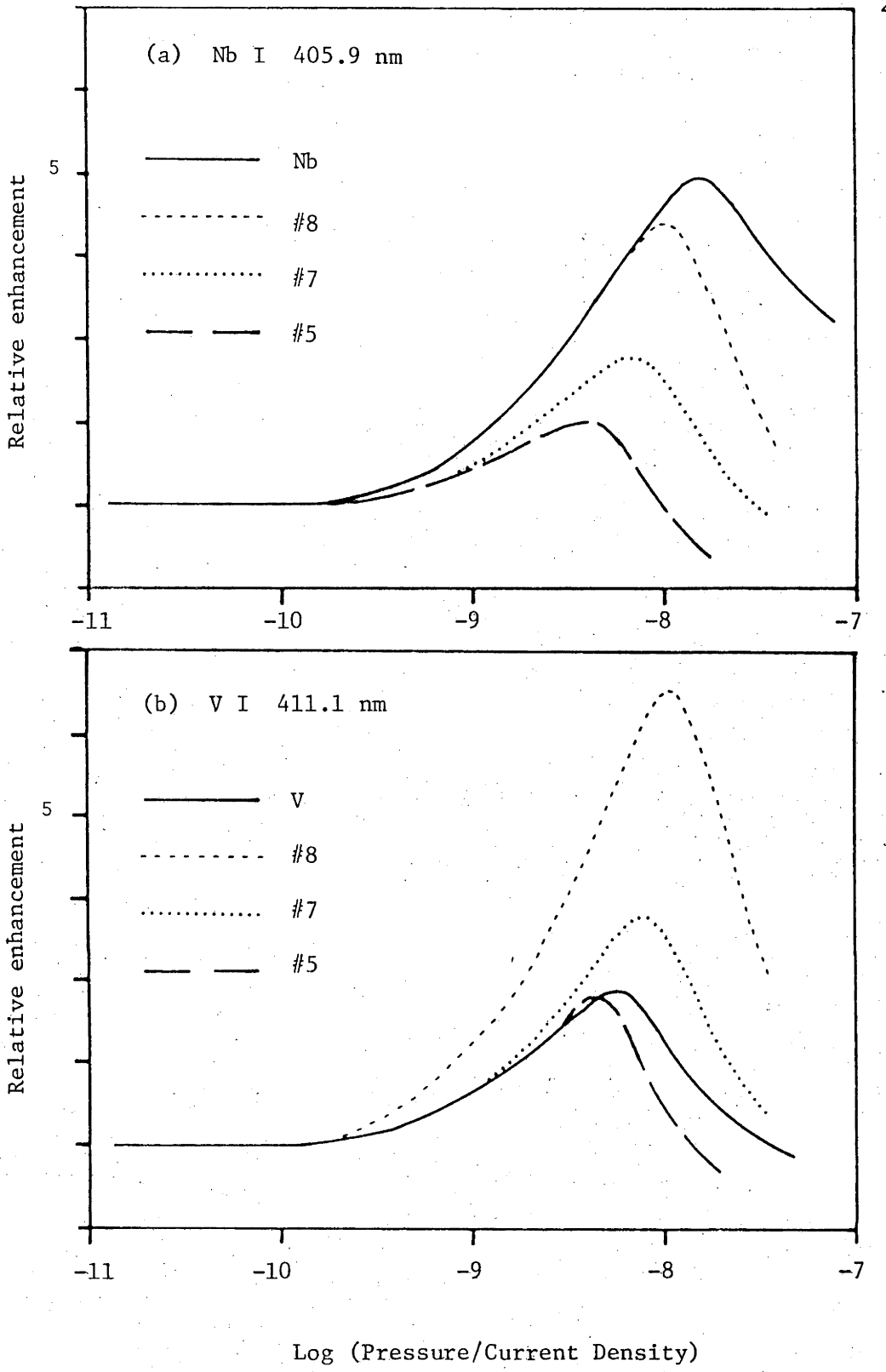

Figure 5.6 (a) The intensity changes for the NbI 405.9 nm line with oxygen exposure for the bombarded Nb and #8, #7 and #5 alloys.

(b) The intensity changes for the VI 411.1 nm line with oxygen exposure for the bombarded V and #8, #7 and #5 alloys.

(Pressure in torr and the current density in $\mu A/cm^2$. The intensities have been normalised at the cleanest conditions and background and continuum emission have been subtracted.)

The intensity changes show characteristic increases with background oxygen pressure, a peak region and then a decrease in intensity with increased oxygen pressure. A similarly observed decrease was noted for Ti emission and has to be ascribed to the decrease in the sputtering yield (section 3.1). Figure 5.7 shows that the intensity peaks for the Nb I and V I occur at different exposures from the bombarded pure Nb and V respectively. When the two elements are alloyed, the Nb I and V I lines peak at the same exposure. Furthermore, the intensity peaks shift to higher background oxygen pressure with increasing Nb concentration in the alloy. This shift is almost linear with increasing Nb concentration as shown in Figure 5.7.

The enhancement at the intensity peak is shown to be greater for the Nb I line than the V I line from the pure elements. From the bombarded alloys, the relative increase of the V I line is greater than for the Nb I line. The relative enhancement of both lines from the alloys increases with the Nb concentration as shown in Table 5.9. The enhancements of the V I line from the three alloys are in the same ratio as those for the Nb I line, although the actual values are different.

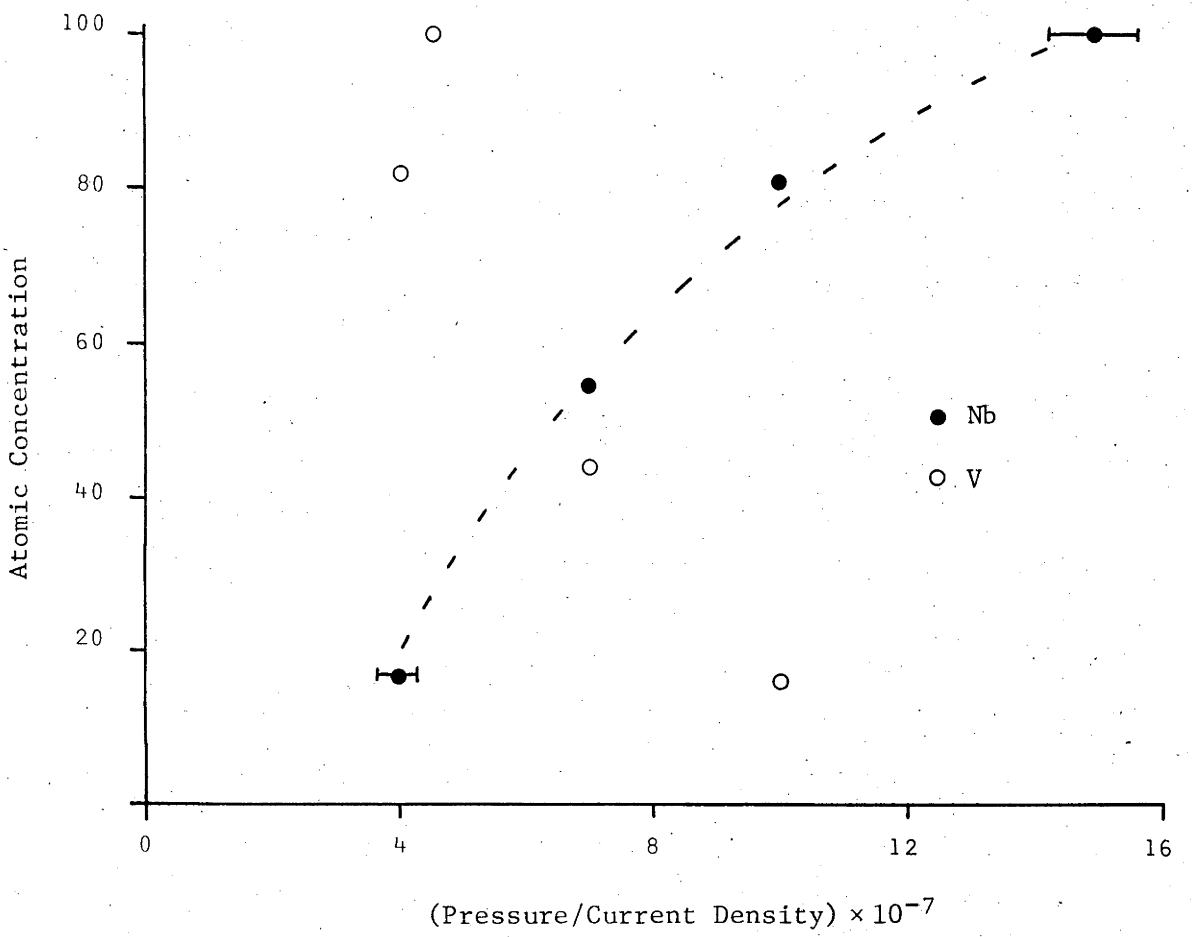

Figure 5.7 The position of the enhancement peak of the NbI (and VI) lines due to oxygen exposure as a function of the atomic concentration of Nb (and V) in the alloy. (Pressure in torr and current density in $\mu A/cm^2$.)

TABLE 5.9

Ratios of the increase in photon yield at the intensity peak above the clean yield, to that of the pure metal.

Target	Ratio of the increase for the Nb I 405.9 nm	Ratio of the increase for the VI411.1 nm	Nb Concentration
Pure Element	1.00	1.00	
#8	0.86	3.01	79.7
#7	0.46	1.52	45.6
#5	0.25	0.92	12.9

5.2.3 *Discussion*

The photon emission analysis results obtained under UHV conditions and shown in Table 5.6 show good agreement with the bulk concentrations as determined by electron probe analysis. The Nb concentration appears slightly high for V rich alloys, although internal consistency of the analysis is shown for the independently determined Nb and V concentrations. These results show that the analysis technique may be used for metal systems such as Nb/V with an expected accuracy of about ±5 atomic percent using UHV conditions. This accuracy is similar to that of SIMS analysis [9]. Non-radiative de-excitations do not influence the analysis as has been previously expected [15] and the photon yields are shown to follow the proposed relationship, equation (5.1). Oxygen exposure during the analysis, which would be expected to increase the sensitivity and inhibit non-

radiative de-excitation processes, has been found to render the measured photon yields non linear with bulk concentrations in the alloy. The analysis obtained under oxygen exposure conditions may be corrected by measuring the influence of the oxygen exposure for the line used for analysis for each of the alloys analysed.

It may be concluded from the observation that the photon yields follow equation (5.1) under UHV conditions, that band structure effects play little part in influencing the photon emission, at least for the Nb I and V I lines studied here. The electronic band structures would be expected to change with the alloy constituent concentrations and be different from that of the pure metal.

The UHV analysis result may also reveal something of the excitation process. Excitation has previously been discussed in terms of atom-atom collisions through either quasimolecule formation [16] or through other collisional excitation as the collision cascade intersects the surface. The collisions of interest in the Nb - V system under UHV conditions which may produce Nb atom excitation are:

- the primary asymmetric collisions Ar → Nb (this component is expected to be low for sputtered atoms with normal incidence bombardment)
- the secondary symmetric collisions Nb → Nb
- the secondary asymmetric collisions V → Nb
- the secondary asymmetric collisions Ar → Nb due to pre-implanted Ar.

Excitation of the Nb atomic level leading to emission of the 405.9 nm line for the bombarded alloys may be different to that from the bombarded Nb target through the additional secondary asymmetric V → Nb collisions shown above.

Should these secondary collisions be important in the excitation of the Nb atom (or the V atom for corresponding collisions of interest), then a deviation in the behaviour of the line intensities from that predicted using equation (5.1) would be expected [17]. However, there is no clear evidence for this in the analysis results apart from the slightly Nb rich analysis of alloys #7 and #6 shown in Table 5.6. Furthermore, in the assumption of excitation through quasimolecule formation, the linear variation of the peak intensity with atomic concentration indicates that the excitation is primarily through the primary asymmetrical collisions Ar → Nb (or V) [17].

Similar results were obtained for an Aℓ Auger peak height with alloy concentration by Viaris de Lesegno and Hennequin [17]. A second Aℓ Auger emission was found to follow a parabolic intensity peak height with Aℓ concentration and the excitation for this emission was interpreted through the asymmetrical collisions Ar → Aℓ and symmetrical collisions Aℓ → Aℓ together [17]. The extent of the symmetrical collision contribution was found to increase with incident energy. This quadratic behaviour was not found here for the V I or Nb I emission lines.

Nb → V and V → Nb collisions may be concluded to contribute little (if at all) to the excitation of the

Nb and V atoms. Excitation as the sputtered particles pass through the surface potential also appears of limited importance; shown by the lack of influence of the changing surface electronic structure.

The Nb enriched analysis obtained for alloys #7 and #6 under UHV conditions is not expected to be related to contamination influence from the bulk or through edge effects. Oxygen exposure has been shown to lead to V rich analysis (Table 5.7).

Photon analysis obtained under surface oxygen contamination conditions (Table 5.7) are shown not to be internally consistent and it may be concluded that factors other than surface concentration changes are also contributing to the intensity enhancements. Sputtering yield changes would be expected to influence the photon yield only at high exposures, however the photon yields shown in Figure 5.6 are influenced by low oxygen exposures. The initial changes in the photon emission with surface contamination may then be assumed to be attributed to changes in the excitation probability alone.

As the Nb concentration in the alloys increases, Nb I emission tends toward the characteristics of the emission from pure Nb with respect to the intensity enhancements and position of the intensity peak with oxygen exposure. The addition of V to Nb tends to decrease the Nb I peak intensity with oxygen exposure, whereas the addition of Nb to V tends to increase the VI peak intensity with oxygen exposure.

To examine the enhancements and peak intensity shifts with oxygen exposure, the line emission may be divided into two components: emission characteristic of the clean surface and emission influenced by the surface contamination. The second component increases in importance with oxygen exposure and coverage.

Considering firstly the quasimolecule formation model for the enhanced yield of Nb I, there will be an additional collision to those of Ar → Nb, Nb → Nb, V → Nb mentioned previously and this is the 0 → Nb collision. This extra collision may account for the enhancement from the pure Nb metal. Figure 5.6 shows that the V concentration of the alloy also influences the Nb I enhancement and consequently some other excitation process must also be changed during bombardment of the alloys. To continue to use the quasimolecule formation model, Figure 5.6 would require that oxygen exposure increases the V → Nb collision contribution to the Nb atom excitation or that the V modifies the 0 → Nb collision contribution to the Nb atom excitation, i.e. that it is now a three atom influence process.

These "matrix effects" whereby V → Nb collisions are a possible explanation for the changing photon yields, are only observed with oxygen exposure. Matrix effects observed in SIMS measurements have been previously suggested to be associated with the influence of contaminents [18]. The enhancement of the VI 411.1 nm line is greater in the case of oxygen exposure of the alloys than the pure metal and this would require that the Nb → V (+0)

collision contributes strongly to the excitation of the VI 411.1 nm upper excited state. Conversely, the V → Nb (+0) collision would be required to contribute little to the excitation of the Nb atom. Here the notation Nb → V (+0) may be interpreted as the Nb atom collides with the V and attached O producing V - O quasimolecule. V excitation then occurs through curve crossing as the sputtered V - O quasimolecule separates. The enhancement peak heights may be qualitatively interpreted as due to the Nb → V (+0) collision providing a smaller V - O internuclear distance and greater excitation probability through curve crossing than the lighter mass V collision V → Nb (+0).

The peak position is shown to move to higher exposure with increasing Nb concentration. The peak intensity for the Nb I line from the pure Nb occurs at a higher oxygen exposure than the peak intensity for the V I line from the pure V. This would be related to the sputtering yields (the changing sputtering yield is expected to be responsible for the decrease in the emission), the changing excitation probability and the desorption cross-section of the oxygen. These contributing factors make the interpretation of the changes in the position of the enhancement peak difficult. However, it should be noted that the enhancement peaks for the V I and Nb I lines from the alloys occur at the same exposure. This observation appears difficult to relate to the quasimolecule formation model involving Nb, V and O atoms.

A second possible explanation for these results [19] may be that the Nb concentration, for example, determines

the extent of the enhancement through the amount of oxygen adsorbed on the surface or the sites of the oxygen on the surface. It is not clear that this should be the case as the electronegativity values for Nb and V are similar [20], although different background oxygen exposures are required to saturate the Nb I and V I emissions from the pure metals. In the assumption of linear intensity changes with surface coverage [21] and that the changing sputtering yields with oxygen are similar, this model would account for the enhancement peaks of both lines occurring at the same exposure. The relative changes in the peak heights for the Nb I and V I lines are shown to be similar in Table 5.9. Figures 5.6 and 5.7 would suggest that the addition of V to Nb decreases the surface oxygen coverage almost linearly with V concentration, resulting in a decreasing peak enhancement with increasing V concentration. Figures 5.6 and 5.7 would further require that the addition of Nb to V results in more oxygen per V atom, even for very high oxygen exposures of the pure V, to account for the greater enhancement from the alloys than from the metal. However, this model does not suggest information on the excitation processes. Measurement of the desorption cross sections for oxygen in the manner of Taglauer et al. [21] should provide a most useful check on this second proposal. The desorption cross-sections would be expected to decrease almost linearly with increasing Nb concentration of the alloy.

5.3 INTENSITY AND LINE PROFILE CHANGES WITH SURFACE CONTAMINATION

A series of targets has been examined in an effort to classify various targets with regard to the behaviour of the photon emission from sputtered excited neutrals with oxygen exposure. Both the line profile and intensity changes have usually been monitered. A previous attempt to characterise the emission changes with oxygen exposure has used the measurement of transients [22] and interpretation using the surface polarisation model.

5.3.1 *Si*.

The changes in the line profiles for the oxidation of Si are important in view of the large changes in the line widths of the Si I 288.2 nm line from Si and SiO_2 found by White et al. [3]. Very wide Si I 288.2 nm line profiles from bombarded Si could only be reproduced in this study at high angles of incidence (Figure 5.2). Integral yield measurements of the line profile and intensity changes with oxygen exposure have been made here for the Si I 288.2 nm line produced by normal incidence bombardment of Si by 55 keV Ar^+. The line profile measurements were made with an instrument resolution of 0.039 nm at an observation angle of 90° to the incident beam.

The intensity enhancement for the Si I 288.2 nm line emission with oxygen exposure is shown in Figure 5.8. Several important features may be noted. Unlike the enhancement for Ti, Nb and V, the Si I emission shows a

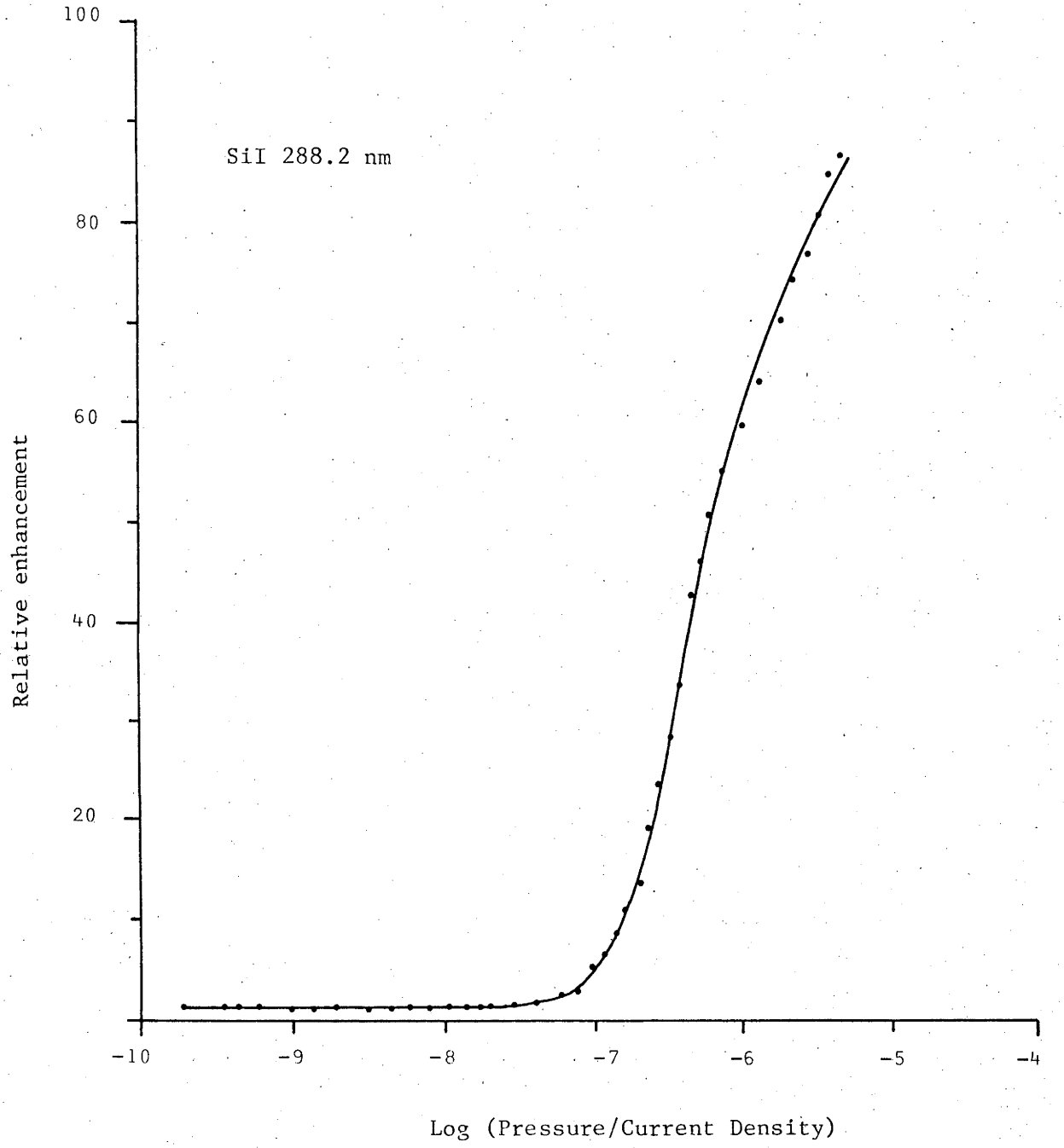

Figure 5.8 The intensity enhancement of the SiI 288.2 nm line with oxygen exposure for normal incidence bombardment of Si by 55 keV Ar^+ (pressure in torr and current density in $\mu A/cm^2$).

much higher enhancement factor (>85) which does not peak for the relatively high exposures shown. In comparison with the Nb I and V I enhancements shown in Figure 5.6, Si is also shown to require much higher oxygen exposures to induce intensity changes. The Si I emission does not begin to increase until the equivalent oxygen pressure is about two orders of magnitude higher than that needed to influence the Nb I and V I emissions.

The changes in the Si I 288.2 nm line profiles with oxygen exposure for normal incidence bombardment and for an incidence angle of 80° (where wider Si I emission lines are found, similar to that observed by White et al. [3]) are shown in Figure 5.9. Little change is noted for normal incidence bombardment, while the decrease in line width at 80° incidence bombardment is not as severe as that expected from the measurements by White et al. It has been assumed that bombardment of Si with oxygen contamination shows similar photon emission characteristics to the bombarded oxide (shown for Ti + O_2 and TiO_2 in Chapter 4). The angles of incidence used by White et al. have not been stated, although Figure 5.2 would suggest that any variation in the incidence angle between the bombardment of the Si and SiO_2 targets would have a pronounced effect. The extreme changes in line profile for the Si I line with oxygen exposure observed by White et al. could not be reproduced here.

The measured line widths (FWHM of 0.057 nm under UHV and oxygen contaminated conditions) for normal incidence bombardment indicate that the energy parameter

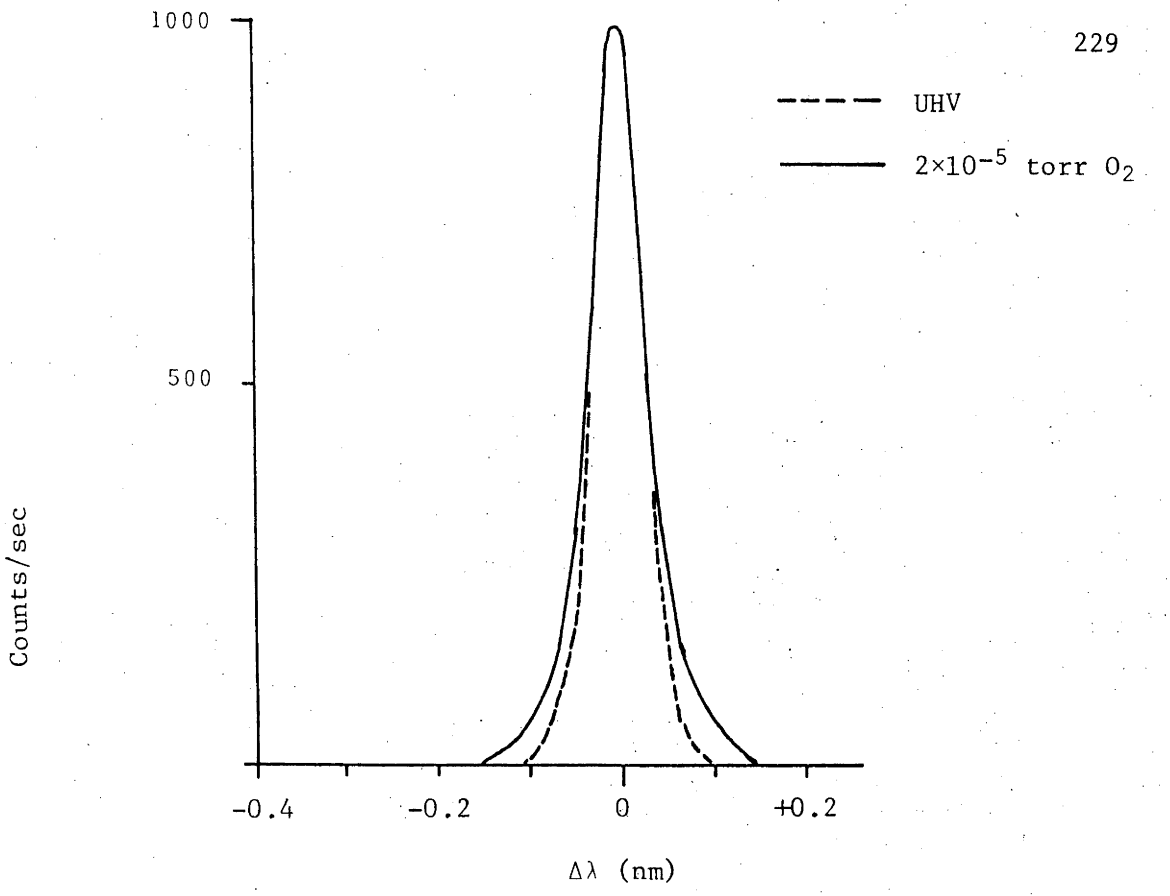

Figure 5.9(a) Normalised line profile changes for the SiI 288.2 nm line with oxygen exposure for normal incidence bombardment.

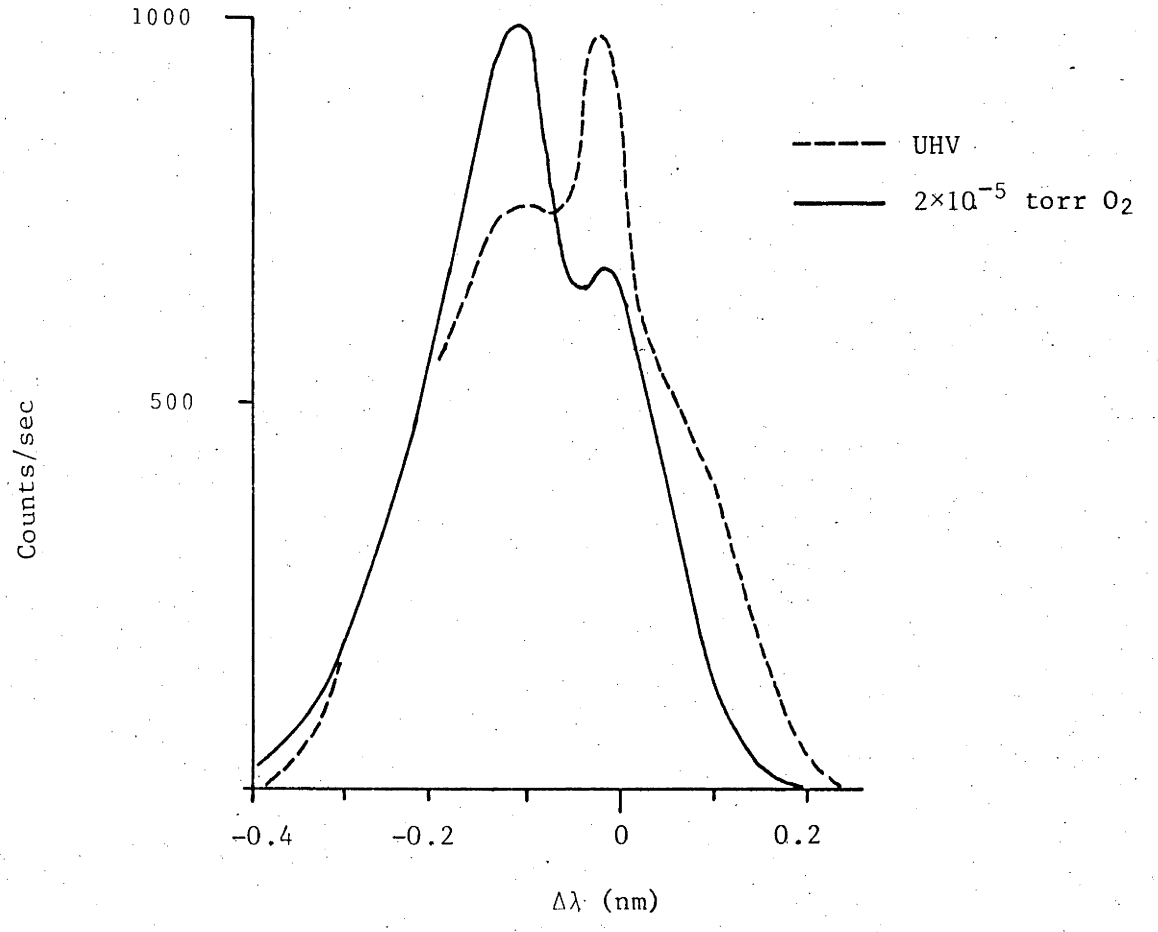

Figure 5.9(b) Line profile changes for the SiI 288.2 nm line with oxygen exposure for 80° incidence bombardment.

$E_{||}$ does not change significantly with oxygen contamination. This observation would negate the suggestion from section 4.2 that changes in the emission intensity may reflect the changes in the E^* parameter (using the step function model for the excitation probability), allowing different numbers of sputtered particles to contribute to the observed radiation. E^* values, which are expected to follow the $E_{||}$ trends (section 4.2), would remain about the same with oxygen exposure for the excited state leading to the 288.2 nm emission.

5.3.2 *Aℓ, Mg.*

Line profile and line intensity changes with oxygen exposure have also been monitered for Mg I and Aℓ I using the same experimental conditions as used for the normal incidence study of the Si line.

The intensity changes with oxygen exposure for an Aℓ I and a Mg I emission line are shown in Figure 5.10. Also shown are the intensity changes for an Aℓ III and a Mg II line. The type I emission lines for both metals show strong enhancement with oxygen exposure and no saturation level is evident in the exposure range shown. The increase for the Aℓ I 396.2 nm emission line shows a pronounced dip in the enhancement curve (at an arrival ratio of oxygen to incoming ion estimated from equation (2.1), to be about 5) which is also observed for the Aℓ I 308.2 nm line. Further oxygen exposure leads to greater enhancement. This dip is possibly associated with a second oxidation phase of the Aℓ

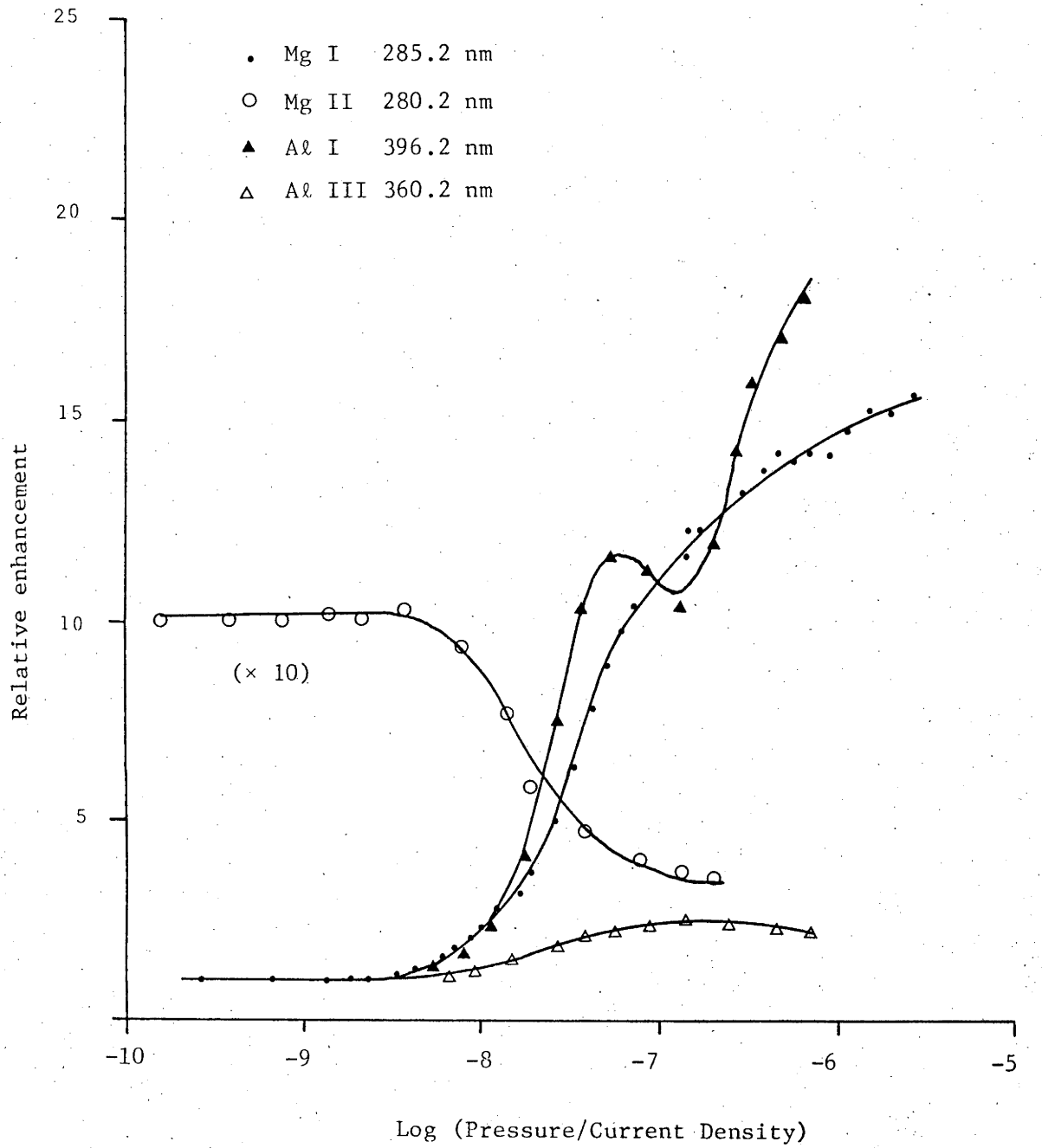

Figure 5.10 Intensity enhancements for the Mg I 285.2 nm, Mg II 280.2 nm, Aℓ I 396.2 nm and Aℓ III 360.2 nm lines with oxygen exposure for normal incidence 55 keV Ar^+ bombardment (pressure in torr and current density in $\mu A/cm^2$).

TABLE 5.10

Measured FWHM of emission lines of Mg and Aℓ under UHV and oxygen exposure conditions. The instrument resolution was 0.019 nm, and the targets were bombarded at normal incidence.

Line (nm)	UHV FWHM(nm)	UHV $\frac{\Delta\lambda}{\lambda}$ ($\times 10^{-4}$)	Oxygen Exposure FWHM	Oxygen Exposure $\frac{\Delta\lambda}{\lambda}$($\times 10^{-4}$)
Aℓ I 308.2	0.033 ± .003	1.08 ± .09	0.046 ± .003	1.49 ± .10
Aℓ I 396.2	0.043 ± .003	1.07 ± .09	0.054 ± .004	1.36 ± .15
AℓII 281.6	0.041 ± .11	1.46 ± .40	0.061 ± .11	2.17 ± .38
AℓIII 360.1	0.073 ± .017	2.03 ± .46	0.093 ± .011	2.58 ± .30
Mg I 285.2	0.024 ± .003	0.84 ± .10	0.024 ± .003	0.84 ± .10
MgII 279.6	0.047 ± .003	1.68 ± .10	0.047 ± .003	1.68 ± .10
MgII 279.8	0.047 ± .003	1.68 ± .10	0.045 ± .003	1.68 ± .10

surface. The enhancements observed for the lines from the neutral atoms are not mirrored by the ion emission lines which, for the case of the Mg II 280.2 nm line, show a decrease with oxygen exposure.

Line profile changes with oxygen exposure for the Mg and Aℓ lines are shown in Table 5.10.

Table 5.10 shows that the line profile for the Mg I 285.2 nm line does not appreciably change with oxygen exposure. It should be noted that this line is very weakly broadened and is almost at the resolution limit. This may be a factor in not being able to resolve any oxygen exposure induced changes in the line profile. The energy parameter $E_{||}$ for this line would then be very low. Oxygen exposure does not change either of the Mg II line profiles.

In contrast to all previous measurements in this report, the Aℓ I, II and III lines were all found to become *broader* with oxygen exposure. These results, together with Figure 5.10 showing the intensity increase for the same lines with oxygen exposure, are in direct contradiction to the band structure model and are perhaps the clearest evidence against this model. Again the energy parameter $E_{||}$ is expected to be low for the Aℓ I emission but is shown to increase for the more highly ionized states of Aℓ. For the Aℓ III 360.1 nm line, the $E_{||}$ value is 120 ± 40 eV obtained by normal incidence bombardment under UHV conditions and this value changes to 200 ± 50 eV for surface contamination with oxygen.

5.3.3 *Cr (Ni, Cu).*

The intensity enhancements for the Cr I 427.4 and 388.3 nm lines were also measured with increasing oxygen pressure. The experimental conditions were the same for the Si I study. The behaviour of the 388.3 nm line is of interest as the upper energy level of this transition is an autoionizing level of Cr. The enhancements of the two line emissions with increasing background pressure are shown in Figure 5.11. The behaviour of the two lines with oxygen exposure is similar with the autoionizing level line at 388.3 nm enhancing slightly more than the 427.4 nm line. The excitation energies for the two lines are 23386 cm^{-1} and 57097 cm^{-1} for the 427.4 and 388.3 nm lines respectively.

The autoionization process is important in the secondary ion emission model of Blaise [22 and previously

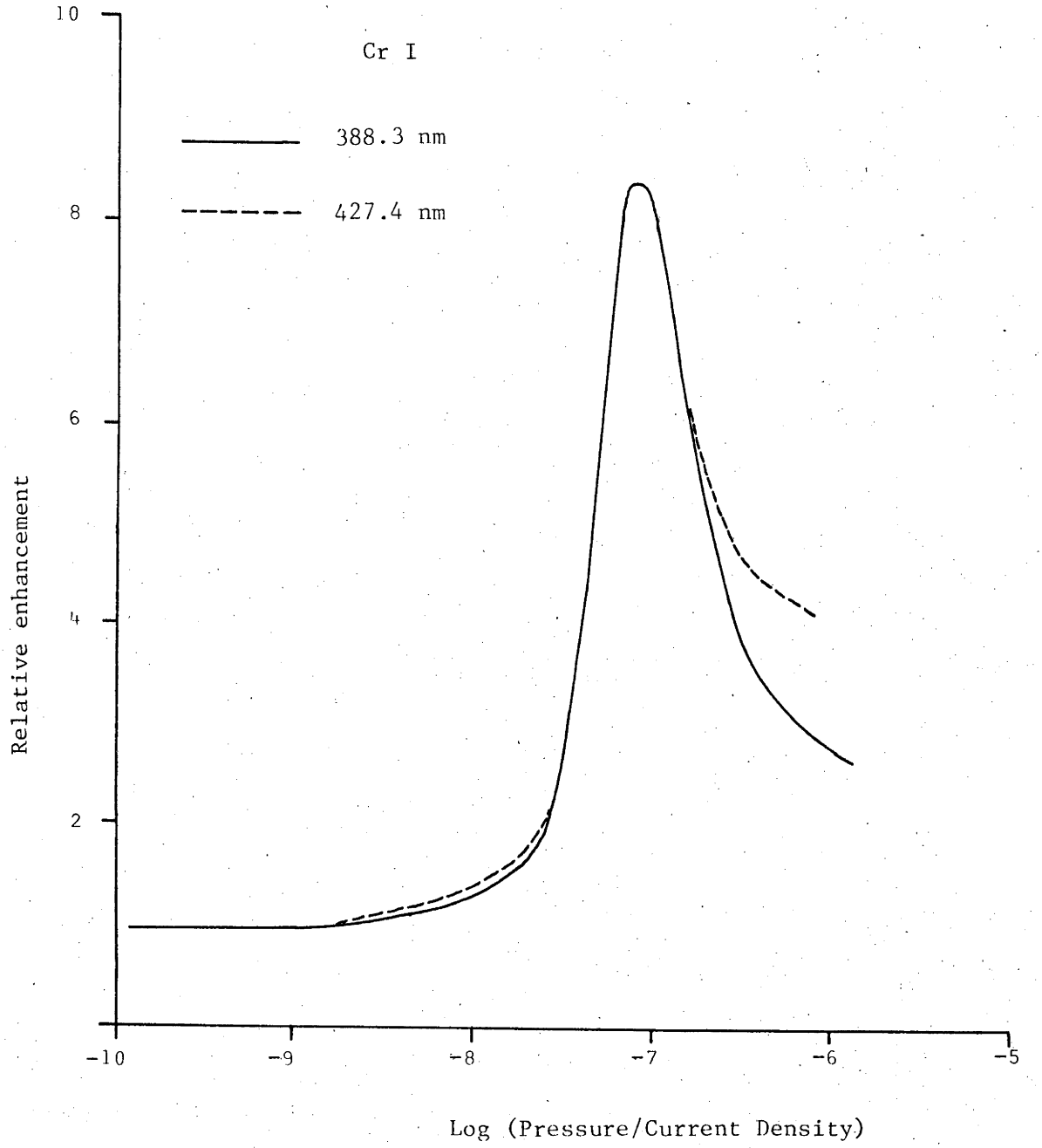

Figure 5.11 Oxygen induced enhancements for the CrI 427.4 and 388.3 nm lines (pressure in torr, current density in $\mu A/cm^2$). Normal incidence bombardment was used.

cited works therein]. Secondary ion emission is thought to proceed via an autoionization process undergone by the sputtered atom which is in an autoionizing state. The atom then decays through an autoionizing process or an Auger process, to form part of the secondary ion yield. Considering that the secondary ion emission usually enhances by a much greater factor than the photon emission [24], Figure 5.11 would suggest that the autoionization of sputtered excited atoms would not be a major contribution to secondary ion emission. The enhancements are similar to that found for Ti although a trend toward higher enhancement for higher excitation energy was also found (section 4.1).

Similar behaviour to that shown by the Cr I lines for oxygen exposure has also been shown by the Cu I 327.4 nm and Ni I 301.2 and 352.4 nm lines and are not reproduced here.

The changes induced in the measured line profiles for several selected Cr I and Ni I lines are shown in Table 5.11.

Table 5.11 shows that the behaviour of the Cr I line profiles with oxygen exposure is also very similar to that of the Ti I behaviour. Ni I, however, shows distinct differences to these other transition elements. The line profiles are shown to increase with oxygen exposure for the lower excitation levels studied, but remain constant for the higher excitation levels which have been studied. This behaviour of Ni with oxygen exposure is different to any of the other bombarded targets so far reported.

TABLE 5.11

(a)

The $\left(\frac{\Delta\lambda}{\lambda}\right)$ values measured for Cr I lines under clean and oxygen contaminated conditions. FWHM ($\Delta\lambda$) measurements were made with an instrument resolution of 0.019 nm and normal incidence bombardment.

CrI λ (nm)	UHV $\left[\frac{\Delta\lambda}{\lambda}\right] \times 10^{-4}$	Oxygen exposed $\left[\frac{\Delta\lambda}{\lambda}\right] \times 10^{-4}$	E_i (cm^{-1})
427.4	1.01 ± .11	0.66 ± .11	23386
464.6	1.53 ± .14	0.95 ± .14	29825
435.1	1.68 ± .16	0.95 ± .16	31280
391.9	1.74 ± .18	1.05 ± .18	33816

(b)

The $\left(\frac{\Delta\lambda}{\lambda}\right)$ values measured for Ni I lines under clean and oxygen contaminated conditions. FWHM ($\Delta\lambda$) measurements were made with an instrument resolution of 0.039 nm and normal incidence bombardment.

Ni I λ(nm)	UHV $\left[\frac{\Delta\lambda}{\lambda}\right] \times 10^{-4}$	Oxygen exposed $\left[\frac{\Delta\lambda}{\lambda}\right] \times 10^{-4}$	E_i (cm^{-1})
352.4	0.52 ± .03	0.72 ± .03	28569
351.5	0.49 ± .03	0.71 ± .03	29321
361.9	0.62 ± .07	0.84 ± .07	31031
305.0	0.70 ± .07	0.70 ± .06	32973
301.2	0.73 ± .10	0.81 ± .09	36601

5.3.4 *Oxygen exposure for TiC, TiN, TiB.*

The changes in intensity for the Ti I 399.8 nm line with oxygen exposure when sputtered from Ti C and Ti N are shown in Figure 5.12(a). Figure 5.12(b) shows the change in the FWHM of the emission line profile for the same line with oxygen exposure for 55 keV Ar^+ bombardment of Ti C, Ti N and Ti B at normal incidence. The intensity increases with exposure are much lower than those observed for the clean metal (Figure 4.6). The line profiles are shown to be further influenced by oxygen contamination, in addition to the changes also observed for the bulk contamination (Figure 4.13).

5.3.5 *Discussion*

All the metals so far studied show an increase in photon emission with increasing oxygen exposure. The extent of this increase (i.e. the enhancement factor) is dependent upon the excitation level for some elements. Some bombarded metals also show a peak in the intensity increase with oxygen exposure, followed by decreasing intensity for increased exposure. This behaviour was found earlier with Ti I emission and the decrease was attributed to the falling sputtering yield. There appears to be three classes of materials characterised by the behaviour of photon emission intensity with oxygen exposure. In the first class belong the elements such as Si, Mg and Aℓ which show strong increases in photon emission with oxygen exposure and which do not show a peak and subsequent

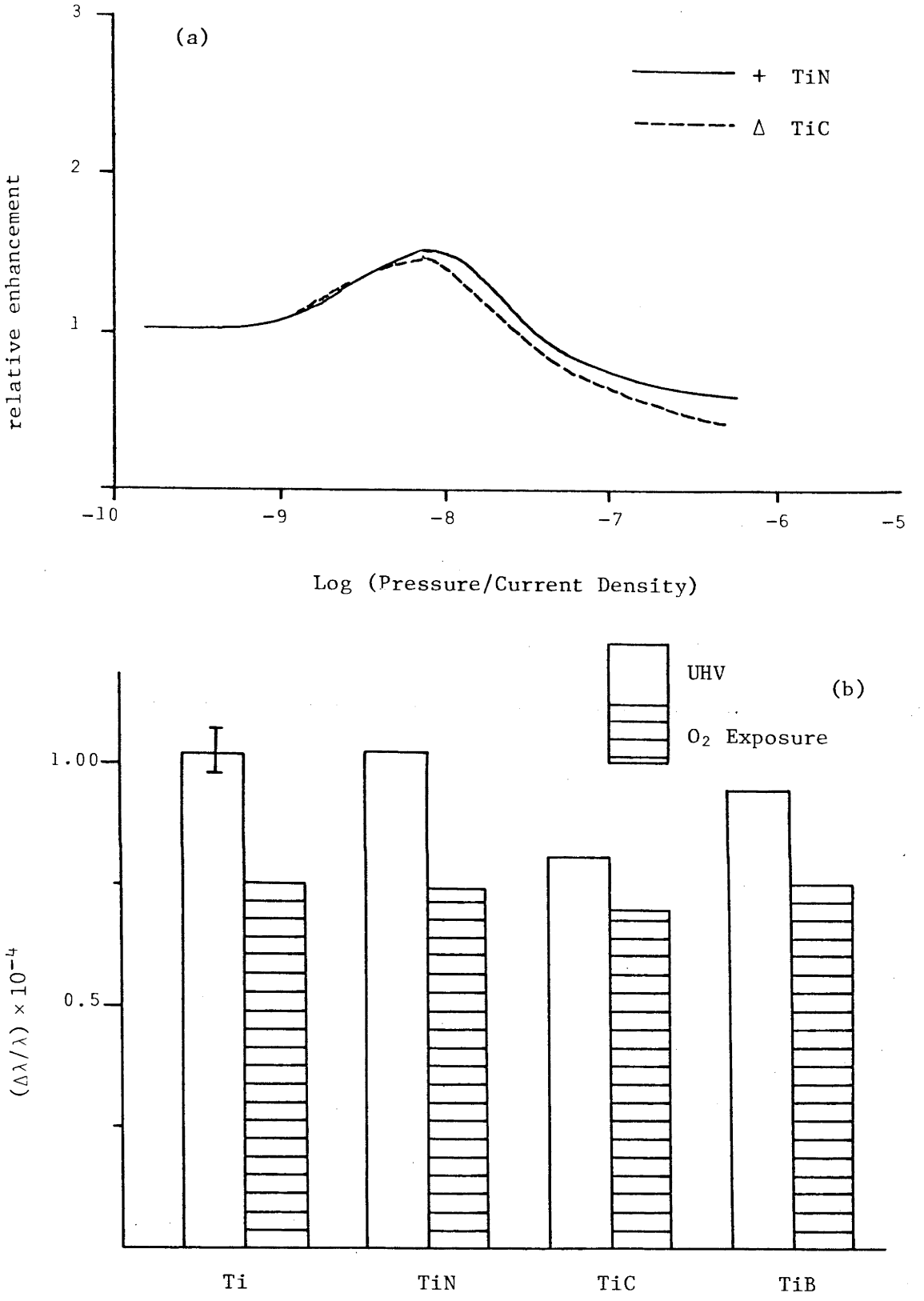

Figure 5.12 (a) Intensity changes with oxygen exposure for the TiI 521.0 nm line when sputtered from TiN and TiC (pressure in torr, current density in $\mu A/cm^2$).

(b) Measured line width changes with oxygen exposure for the TiI 521.0 nm line.

Normal incidence bombardment by 55 keV Ar^+ was used for both 5.12(a) and (b).

intensity decrease for the exposures used here. Mg and Aℓ further show two stages in the enhancement curves, suggesting a second oxide growth phase. No continuum emission is evident. The second class encompasses metals such as Ni and Cu which show moderate enhancements (usually less than a factor of 10 for normal incidence bombardment) with oxygen exposure. Again no continuum emission is observed for bombardment under oxygen exposure conditions. Finally, the third group are those elements which show moderate enhancements with oxygen exposure but which also show continuum emission. These elements include Ti, V, Nb W, Mo and Ta. Continuum emission from the strong continuum emitters, Nb and Ta, will be discussed in Chapter 6.

It does not appear possible to correlate these classes of elements with the behaviour of the changes in average kinetic energy of the excited particles (as shown by emission line profiles). Some emission lines such as the Ti I and Cr I decrease in width with oxygen exposure. Other neutral lines such as Aℓ I increase in width while others such as the Si I 288.2 nm and possibly the Mg I 285.2 nm lines are not changed by oxygen exposure. Cascading effects on the Aℓ I behaviour may be important. Finally, Ni I emission lines exhibit both types of behaviour (constant and increased widths) with oxygen exposure, depending upon the excitation energy of the level considered.

Atomic line emission changes with CO exposure are significantly different to those found for O_2 exposure (Figures 3.10 and 3.11).

Ionised line emission changes do not correlate with atomic line emission changes for O_2 exposure with respect to the intensity changes for Aℓ II or Mg II. The Aℓ II, Aℓ III and Mg II line profile changes with oxygen exposure show similar behaviour to the corresponding neutral emission lines.

5.4 CONCLUSIONS

It has been shown that photon emission may be used for quantitative analysis under UHV conditions for a metal alloy system such as Nb/V. However, photon emission analysis performed under background oxygen exposure has yielded poor results due to pronounced changes in the photon emission characteristics for the different alloys. The results obtained under the oxygen exposure conditions may be corrected by measuring the relative enhancements of the lines used for analysis for each alloy when compared with the enhancement from the pure element standard. These results imply that photon emission analysis for metal alloys, at least for Nb/V alloys, must be performed under UHV conditions.

Band structure effects on the photon emission are not shown for the V I and Nb I lines from the bombarded alloys under UHV conditions. The line intensities reflect only the changes in the constituent concentrations. Matrix effects induced by different excitational collisions involving (V - Nb) and (Nb - Nb) collisions for the Nb atom excitation, are also not found for UHV analysis. A similar

conclusion is found for the V I excitation. The excitation process under UHV conditions is not known. There is no direct evidence for quasimolecule excitation processes, nor excitation as the sputtered atom passes through the influence of the surface potential.

Excitation under UHV has been shown to lead to kinetic energy distributions which vary with the excitation energy of the excited atom and also for the ionisation state of the atom. More highly excited states of the atom are associated with higher kinetic energy particles for Ti, Ni and Cr and has also been observed in other systems, e.g. Aℓ. Ionised atoms have also been found to be associated with higher kinetic energy particles. The kinetic energy parameter, $E_{\|}$, derived through line profile measurements, has been in the range <20 to 300 eV for a variety of excited states and excited species. Although some similarities exist between $E_{\|}$ derived from similar target species (e.g. Ti, Cr, Ni) with states of similar excitation energies, differences are found between these targets and a similar transition metal, Zn. The difference between these examples of the excitation process is not known, however it may be concluded that the probability for excitation does not depend only on the excitation energy of the level and the kinetic energies of the sputtered atoms.

Changing the angle of the incident beam to the target normal has been shown to dramatically change the kinetic energy parameters of the excited states (see

Figure 5.2). At higher angles of incidence the contribution to the photon emission of excited atoms sputtered by binary collisions with the incident ion, increases. This results in a broadened Doppler shifted emission line profile. This component shows a slight relative increase for channelling incidence for a single crystal target.

Matrix effects on the Nb I and V I photon emission are observed with oxygen exposure of the Nb/V alloys during bombardment. All of the Nb, V and O atoms influence the observed line emission from the alloys with surface oxygen contamination. It is not clear whether the oxygen influences the contribution from the (Nb - V) collisions or alternatively, the V (or Nb) influences the adsorption site and coverage for the oxygen and hence the Nb I (or V I) emission. Quasimolecule formation cannot be ruled out as the excitation process from the contamination influence sputtering site.

Oxygen exposure has also been shown to influence the excited yields and usually the kinetic energy distributions of the excited states, even for atoms sputtered from substates which are influenced by bulk contaminants (e.g. Ti B, Ti C and Ti N). Bombarded elements (55 keV Ar^+ at normal incidence) were found to behave in three main classes with oxygen exposure. The first class showed very strong enhancement of type I photon emission which did not peak in the exposure range used (examples: Mg, Aℓ, Si). The second class of elements showed moderate enhancement of about a factor of 10 and no continuum emission (examples: Ni, Cu). The final class of elements

were those which showed moderate enhancement but also emitted continuum emission (examples: strong continuum emitters Ta, Nb and weaker continuum emitters Ti).

The relative enhancement of the type I lines was found to be influenced by the excitation state of the upper level of the transition and on the contamination element or compound. O_2 produced different changes in line intensity enhancement than CO contamination.

Line profile changes with contamination were found not to correlate with intensity changes for all elements as would be expected from previous studies. Ti I and Cr I lines were found to decrease in width with oxygen contamination whereas the Aℓ I lines studied were found to increase. Ni I emission lines were found to exhibit either an increase or no change with oxygen exposure, depending upon the excitation level.

A large change in the emission line profile of the Si I 288.2 nm line with oxygen exposure, as expected from previous measurements [3], was not found in this study. The $E_{\|}$ parameter determined for this line for normal incidence bombardment is of the order of tens of eV and does not change appreciably with oxygen exposure. Broadened Si I lines of the order of those previously found [3] could only be obtained here for large angles of incidence. The line profile was found to broaden with increasing incidence angle. At high incidence angle, the Si I 288.2 nm line was found to decrease in width with oxygen exposure, but not to the extent expected from the previous study. These results indicate the importance of

the incidence angle used and difficulty in attempting to compare experiments made with different experimental parameters.

Again, more thorough interpretation of the observed changes is limited by the lack of understanding of the basic excitation process. These measurements have been able to exhibit some of the consequences of the changing of the excitation process and together with those shown in Chapter 4, represent a detailed analysis of the characteristics which may help in our understanding of these processes.

REFERENCES

[1] S. Dzioba, O. Auciello and R. Kelly, Radiation Effects 45 (1980) 235

[2] A.R. Striganov and N.S. Sventitski, Tables of Spectral Lines of Neutral and Ionized Atoms (Plenum 1968)

[3] C.W. White, D.L. Simms, N.H. Tolk and D.V. McCaughan, Surface Sci. 49 (1975) 657

[4] I.S.T. Tsong and N.A. Yusuf, Nucl. Instr. Methods 170 (1980) 357

[5] S. Dzioba and R. Kelly, Surface Sci. 100 (1980) 119

[6] W.L. Wiese, M.W. Smith and B.M. Miles, Atomic Transition Probabilities, Vol.2 (U.S. Government Printing Office, 1969)

[7] P. Sigmund, Phys. Rev. 184 (1969) 383

[8] S. Dzioba and R. Kelly, to be published, Nucl. Instr. Methods

[9] P.J. Martin, C.M. Loxton, R.F. Garrett, R.J. MacDonald and W.O. Hofer, presented at: Vth International Conference on Ion Beam Analysis, Sydney, 1981

[10] J. Roth, J. Bohdansky and W. Ottenberger, IPP Report, Garching, 9/26 (1979

[11] H.H. Andersen and H.L. Bay, Sputtering by Ion Bombardment, Chapter IV, ed. R. Behrisch (Univ. Aarhus Press, 1980)

[12] H. Hansen and K. Anderko, Constitution of Binary Alloys, 2nd Edition (McGraw Hill, 1958)

[13] M. Grundner and J. Halbritter, J. Appl. Phys. 51 (1980) 397

[14] N. Ware, Research School of Earth Sciences, Australian National University

[15] C.W. White, D.L. Simms and N.H. Tolk, in: Characterization of Solid Surfaces, eds. R.F. Kane and G.R. Larrabee (Plenum, 1974)

[16] U. Fano and W. Lichten, Phys. Rev. Lett. 14 (1965) 627

[17] P. Viaris de Lesegno and J.-F. Hennequin, Surface Sci. 103 (1981) 257

[18] K. Wittmaack, private communication

[19] The initial proposal by I.S.T. Tsong is acknowledged

[20] L.C. Pauling, The Nature of the Chemical Bond (Cornell University Press, 1968) p.93

[21] E. Taglauer, W. Heiland and R.J. MacDonald, Surface Sci. 90 (1979) 661

[22] I.S.T. Tsong and S. Tsuji, Surface Sci. 94 (1980) 269

[23] G. Blaise, Radiation Effects 18 (1973) 147

[24] R.J. MacDonald and P.J. Martin, Surface Sci. 67 (1977) 237

CHAPTER SIX

CONTINUUM EMISSION

In this chapter the continuum emission from Ar^+ bombarded Nb has been examined with reference to the proposal by Rausch et al. [1] that the source of the continuum is sputtered metal oxide molecules. The influence of O_2 and of CO background pressures has also been investigated. The criticism by Kiyan et al. [2] of the proposal by Rausch et al. has also been discussed for continuum emission from bombarded Ta. Finally, continuum emission from a series of Nb/V alloys has been examined to determine whether there are any matrix effects on the emission, as noted previously for NbI and VI line emission changes with surface contamination (section 5.2).

6.1 CONTINUUM EMISSION FROM Nb, Ta AND Nb/V ALLOYS

6.1.1 *Nb continuum emission*

Continuum emission induced by 4 keV Ar^+ bombardment of Nb has been studied for several different surface conditions using integral yield measurements and the experimental geometry shown in Figure 3.2(b). An attempt has been made to correlate continuum emission with surface cleanliness conditions. The low energy ion accelerator system was used as it allows target heating and beam rastering to produce a clean surface, as well as the facility to

make ISS measurements for surface characterization. The Bausch and Lomb monochromator (resolution about 0.8nm) was used and with its low f number and modest resolution, this monochromator is particularly useful in the observation of weak and broad signals.

Nb continuum emission in the wavelength range 250-650 nm has been measured. It was found that gating the photon signals produced by rastered Ar^+ bombardment reduced the continuum emission significantly, indicating that edge effects contribute to the continuum emission. This is shown in Figure 6.1 where the photon spectra obtained from the non-rastered beam and the rastered and signal gated spectra are compared from an annealed but previously unbombarded Nb sample. The photon signal was gated so that only the emission from the inner 70% of the total Y and Z beam scans was measured. Edge effects would not contribute to the photon spectrum shown in Figure 6.1(b). By eliminating edge effects, the Nb continuum emission is shown to change markedly.

To produce a photon spectrum of Nb showing little continuum emission required many cycles of heating and Ar^+ bombardment cleaning. Nb photon spectra obtained under clean, CO saturated and O_2 background conditions are shown in Figure 6.2. Figure 6.2(a) shows a high resolution Nb spectrum obtained by 55 keV Ar^+ bombardment under UHV conditions. The high resolution study would be expected to discriminate against broad band features and it shows the NbI lines dominating the spectrum. Shown in Figure 6.3

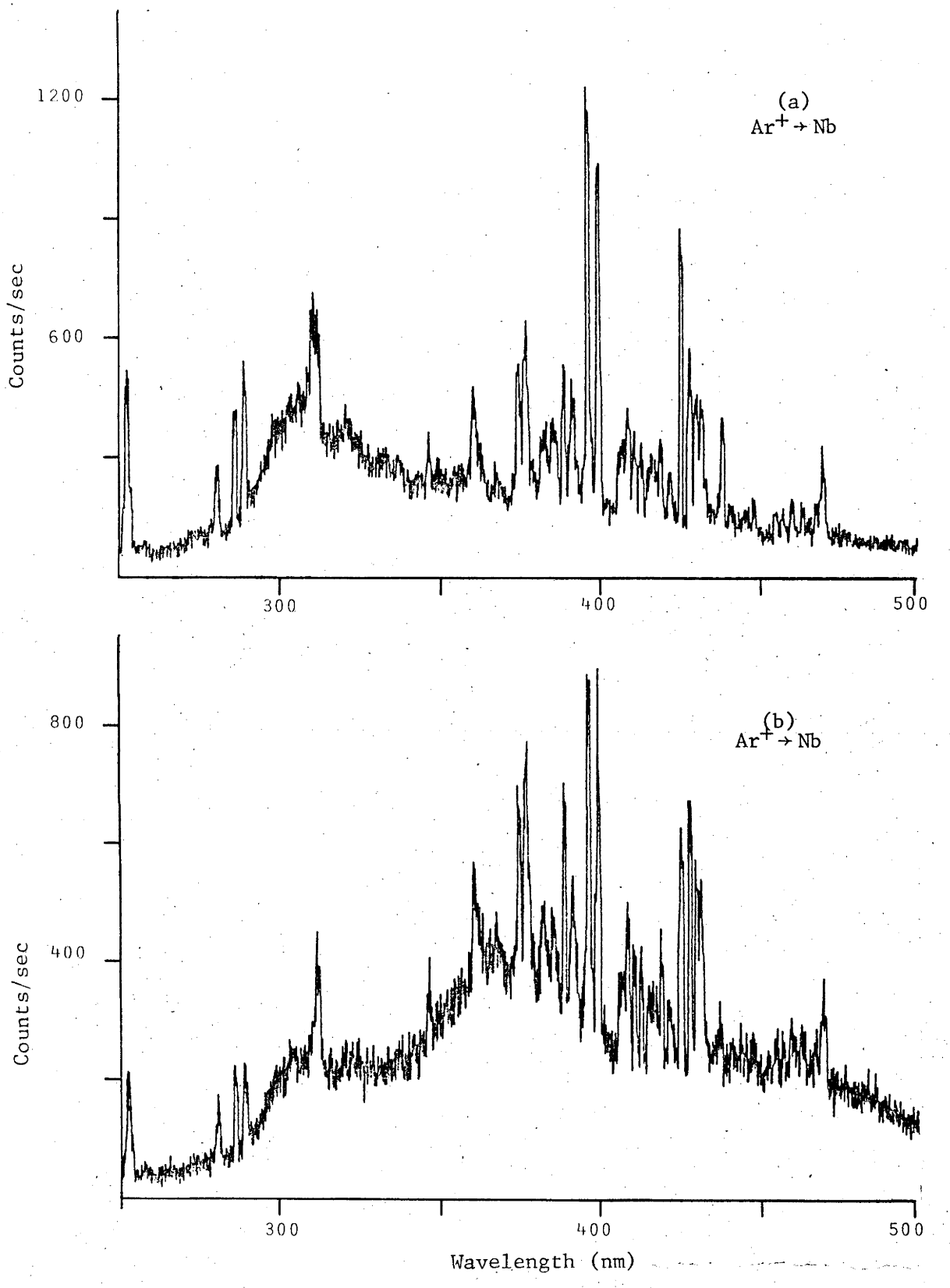

Figure 6.1 Photon spectra obtained from 4 keV Ar^+ bombardment of an annealed, but previously unbombarded Nb target with (a) no beam rastering and (b) been rastering and signal gating to exclude edge effects. The spectra have not been corrected for detection sensitivity.

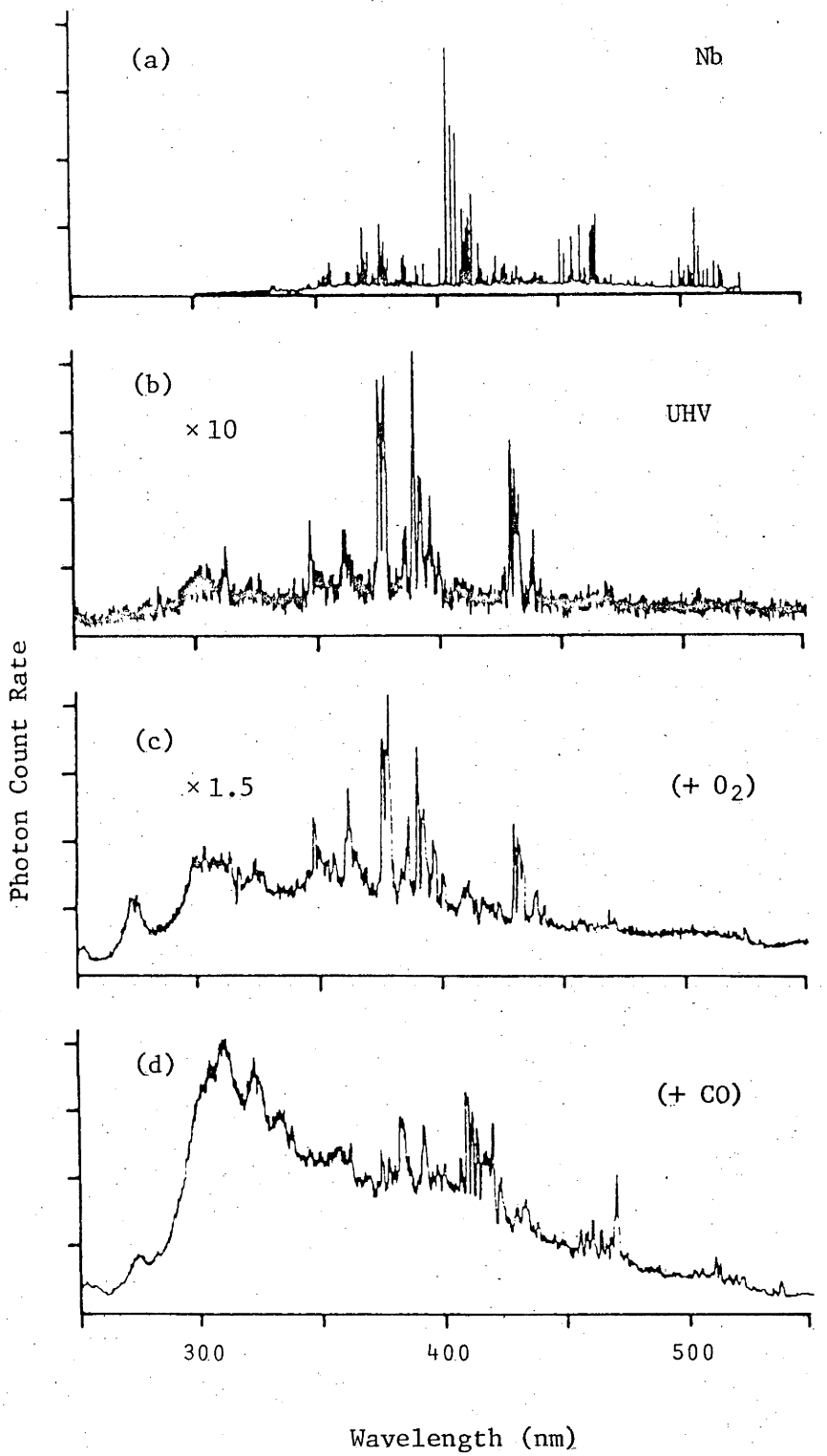

Figure 6.2. Nb photon spectra obtained under the following conditions: (a) 55 keV Ar^+ → Nb at UHV (high resolution), (b) 4 keV Ar^+ → Nb at UHV, (c) 4 keV Ar^+ → Nb with background O_2 pressure of 3×10^{-6} torr and (d) 4 keV Ar^+ → Nb with background CO pressure of 3×10^{-6} torr. The spectra have not been corrected for detection sensitivity.

are the ISS spectra obtained from the Nb under the "clean" and CO saturated conditions used in obtaining Figure 6.2.

The continuum emission at 407.0 nm for the Ar^+ bombarded Nb was found to increase with background oxygen pressure (and hence, surface contamination) until an intensity peak was observed, after which the intensity decreased (see also Figure 5.5). In contrast to this result, increasing CO background pressure induced an increase in the emission at 407.0 nm until saturation occurred, after which the intensity was independent of increased CO pressure. The two spectra shown in Figure 6.2 for background contamination conditions, were performed at the pressure at which the CO enhanced yield saturated. This corresponds to an exposure where the NbI signal was decreasing with increasing O_2 pressure. In each case the observed spectrum shown in Figure 6.2 consists of NbI lines, broad band continuum and discrete broad features.

The sensitivity of continuum emission to contamination is illustrated by the ISS spectrum shown in Figure 6.3(a) where there is no evidence for an oxygen peak or secondary ions indicating surface contamination. The ISS oxygen peak was found to disappear with the continuum emission slightly more intense than that shown in Figure 6.2(b). This relation of the ISS peak and continuum emission has also been found for Mo and Ti under similar conditions for the ISS system used here. The Mo continuum spectrum obtained was similar to that shown in [1], with characteristic broad emission around 290-295 nm.

It is evident from Figure 6.2 that CO contamination

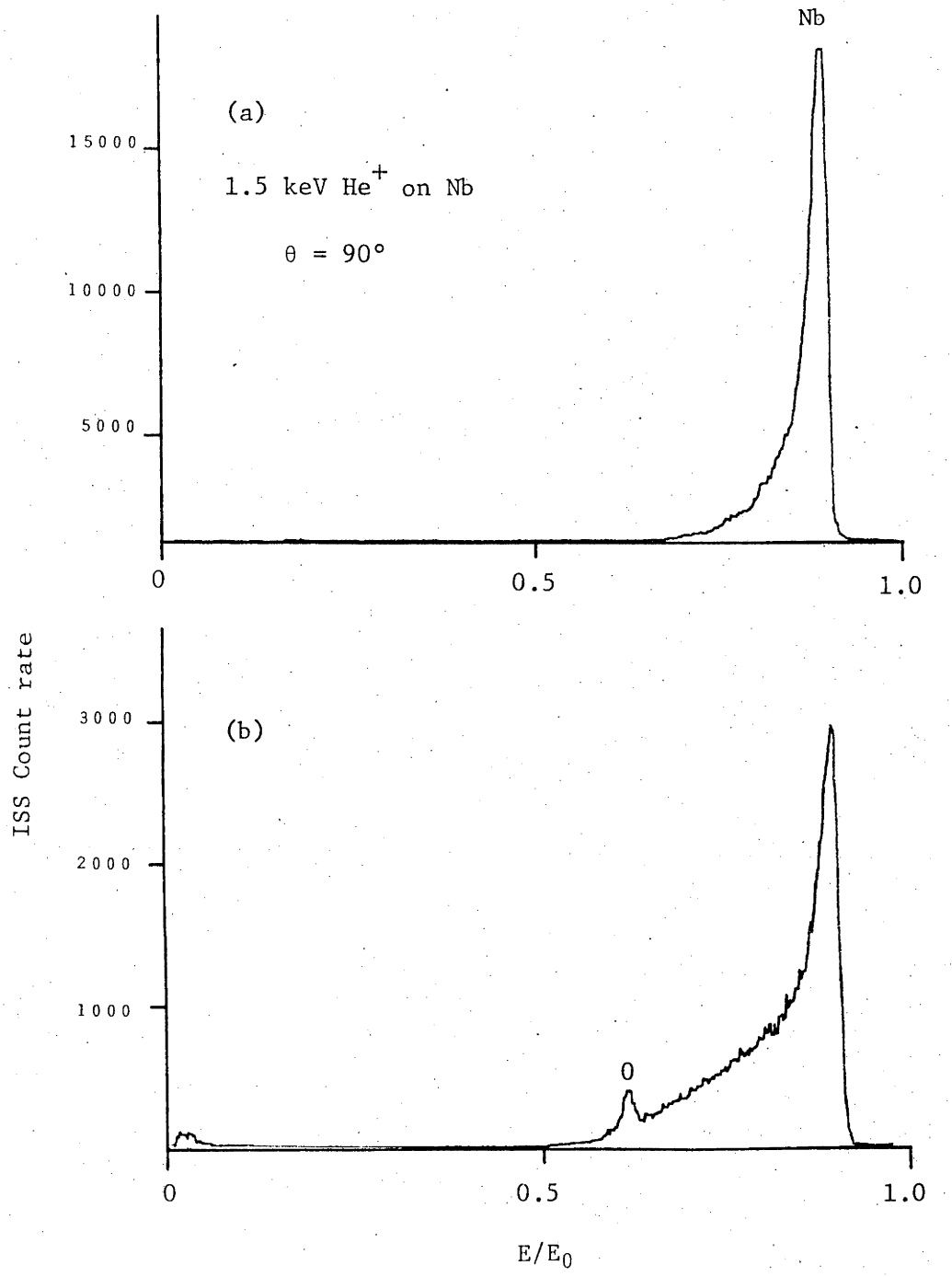

Figure 6.3 The ISS spectra obtained by 1.5 keV He^+ bombardment at 90° scattering angle for the conditions at which the photon spectra were obtained; (a) the UHV conditions with 4 keV Ar^+ bombardment and (b) the conditions for 4 keV Ar^+ bombardment with CO contamination.

leads to greater continuum emission than does O_2 contamination, and that the shapes of the broad band continua in each case show some differences. Comparison of the spectra shown in Figure 6.2 with those obtained previously for conditions insufficient to maintain surface cleanliness [3], would suggest that oxygen and carbon monoxide were not the only surface contaminants in that previous study.

The origin of the broad band emissions shown in Figure 6.2(b), (c) and (d), which do not correspond to NbI emission, is not known. These features may correlate with molecular bands from Niobium oxides, however, such a correlation has not been possible due to the lack of data on these molecular emissions. Several additional broad emissions are evident with CO adsorption indicating that different molecules may contribute to the radiation. These do not appear to be excited CO molecules with wavelengths as in Tables [4].

Accurate measurements of the wavelengths and line widths of the broad emissions from Nb could not be made due to the poor resolution of the monochromator used in obtaining Figure 6.2(b), (c) and (d). This information could not be obtained from the study shown in Figure 6.2(a) as most of the broad emissions were not detected using the Jarrel-Ash monochromator with its high resolution and higher f number. Broad band emissions have been observed from Ar^+ bombarded Ta and these are discussed in section 6.1.2.

6.1.2 *Ta continuum emission*

Ta lies in the same column of the periodic table as Nb and may be expected to exhibit some of the behaviour of Nb emission. Ta continuum emission is also of interest as it has received some attention from Belykh et al. [5] and Kiyan et al. [2], where the proposal by Rausch et al. [1] that sputtered metal oxides are responsible for the continuum emission has been criticised (section 2.3). Belykh et al. reported a net decrease in the Ta continuum emission with oxygen exposure which is inconsistent with the proposal of Rausch et al.

The Ta photon emission produced by 55 keV Ar^+ bombardment was observed using the Jarrel-Ash monochromator (resolution 0.08 nm) with an experimental geometry as shown in Figure 3.2(a) for integral yield analysis (i.e. normal bombardment with 90° observation angle). The total residual vacuum was 1×10^{-9} torr and the beam current density was 200 $\mu A/cm^2$. Further target surface characterization was provided by a secondary ion mass analyser designed to collect low energy secondary ions with mass analysis up to 500 amu. To reduce possible edge effects, the targets were bombarded for several hours while mechanically moved in a grid pattern and then bombarded in the centre of this area during the experiments.

Figure 6.4(a,b) shows a spectral scan over the region 200 - 600 nm taken under UHV conditions. Several important features are to be noted. Firstly, there is a complete absence of continuum emission shown in Figure 6.4(a) using

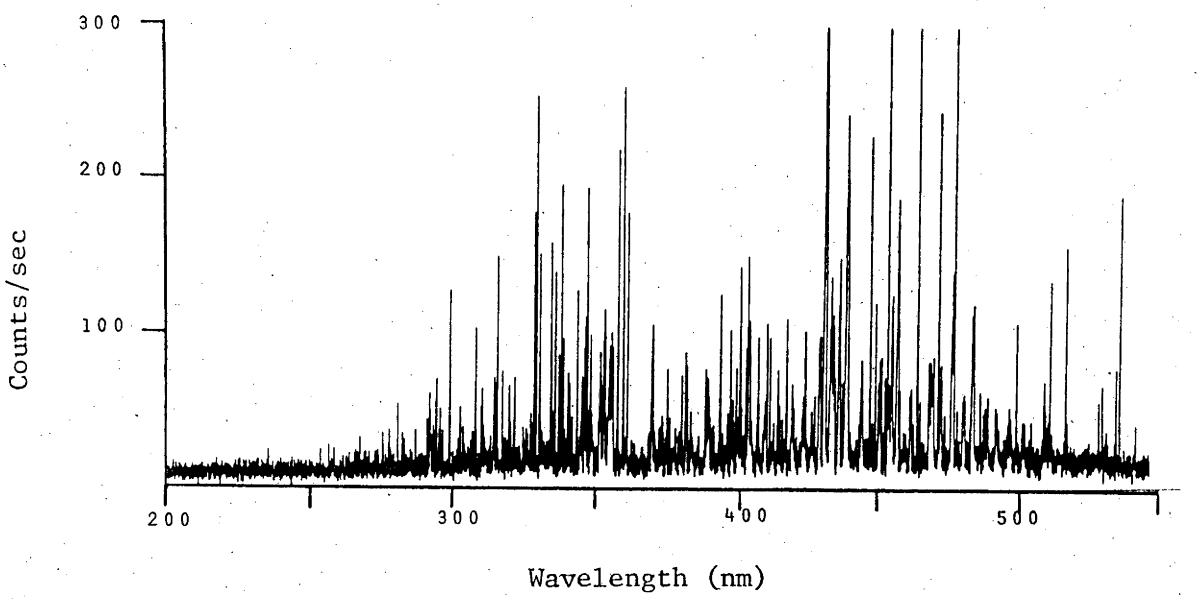

Figure 6.4(a) Ta photon spectrum from 200 - 550 nm obtained by 55 keV Ar^+ bombardment of Ta under UHV conditions. The Jarrel-Ash spectrometer was used with an instrument resolution of 0.08 nm.

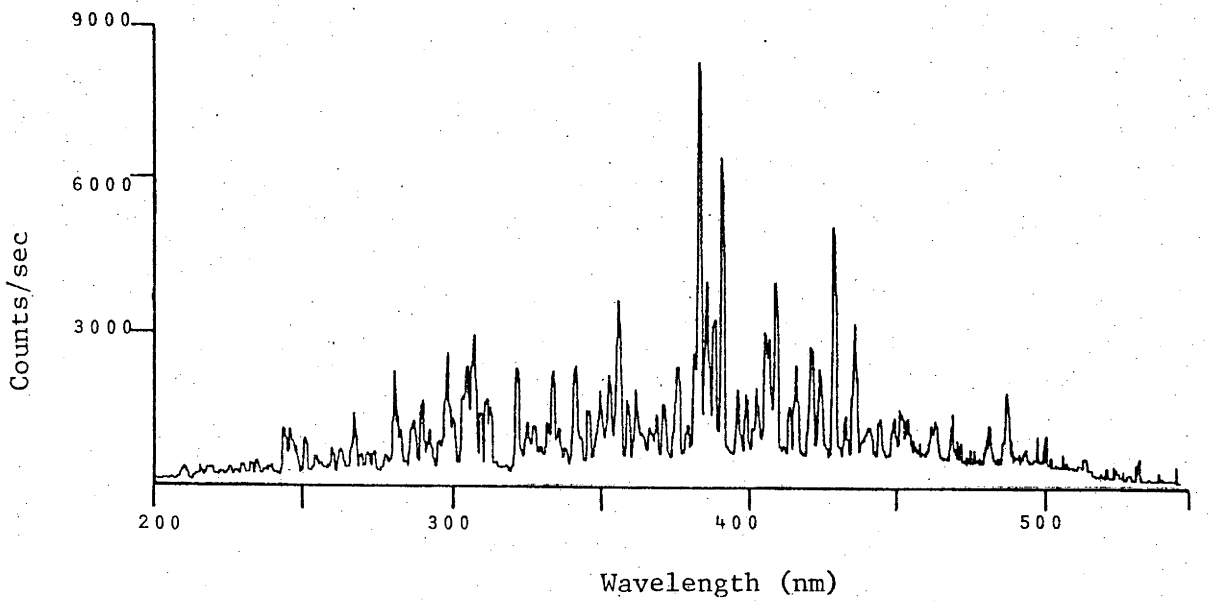

Figure 6.4(b) Ta photon spectrum obtained using the same experimental conditions as (a) but using the Bausch and Lomb spectrometer. The instrument resolution was 0.8 nm.

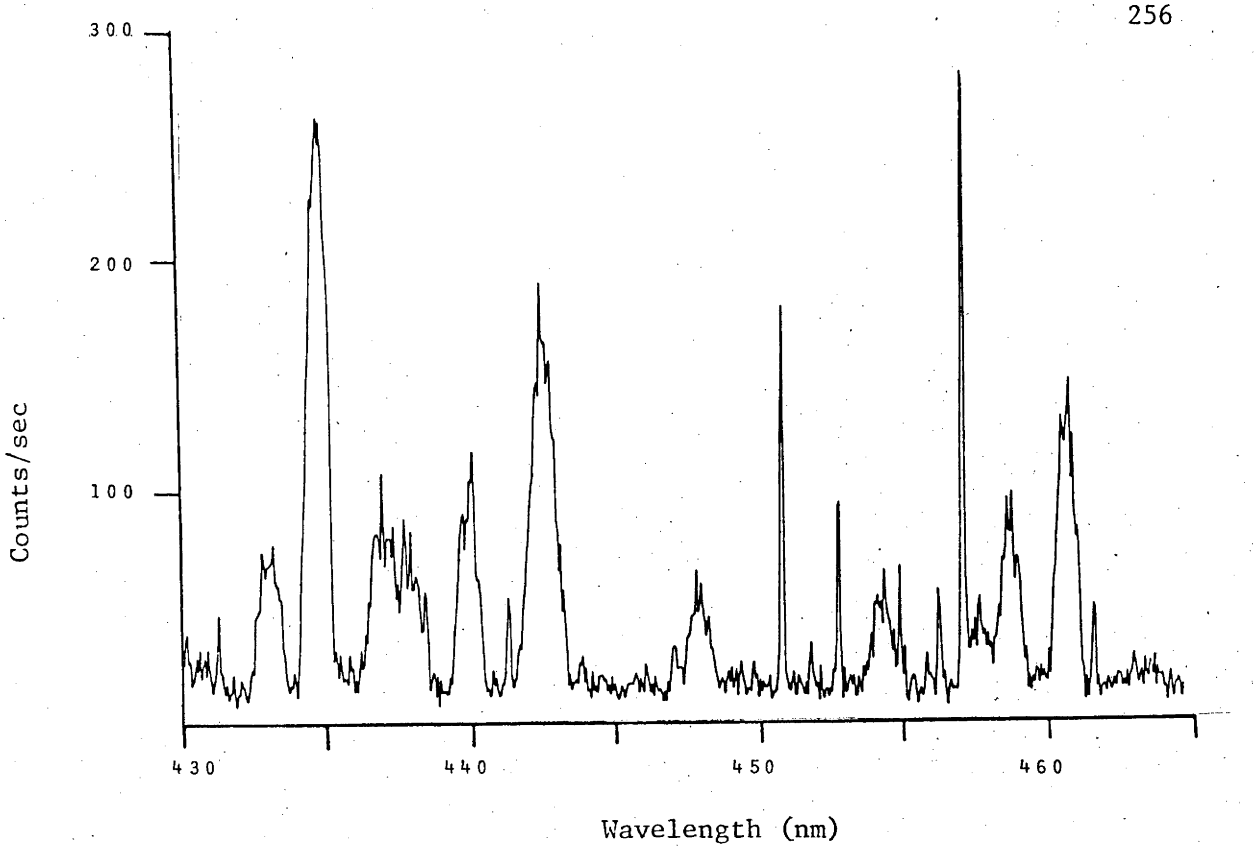

Figure 6.4(c). An expanded section of Figure 6.4(a) from 430 - 465 nm.

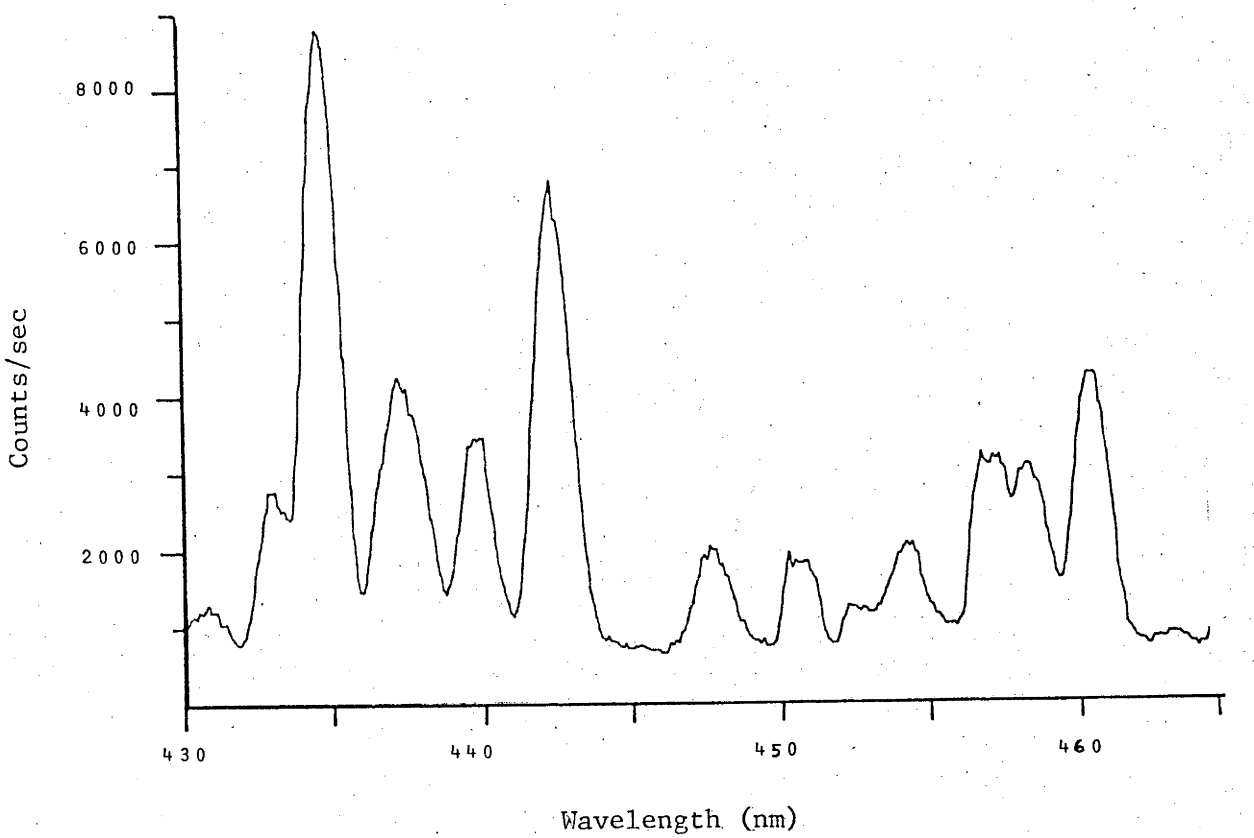

Figure 6.4(d). An expanded section of Figure 6.4(b) from 430 - 465 nm.

the better resolution monochromator, although some continuum emission is seen in Figure 6.4(b) using the poorer resolution monochromator. This underlines the influence of higher resolution monochromators discriminating against broad and weak emissions as mentioned in section 3.2. Secondly, prolific line emission from the Ta I spectrum is identifiable in the region 250-550 nm from Figure 6.4(a). Thirdly, on an expanded wavelength scale (Figure 6.4(c),(d)), many broader (0.4-1.2 nm) but discrete emissions are evident between the narrower Ta I emission lines. With poor resolution, these lines feature more prominently than the Ta I emission and dominate the spectrum of 6.4(b). High resolution (0.039 nm) analysis of the broad line at 434.8 nm did not reveal any fine structure in the emission. There are no Ta atomic emission lines which are listed in this region, eliminating the possibility that the broad lines are unresolved Ta I emission.

Wavelength identification of these features does not show correlation with listed band heads for Ta O molecular emission [6,7]. However it must be pointed out that the molecular emissions are poorly known for Ta O. Indeed, the earlier work [7] has been negated, to some extent, by further investigation [6]. Several listed TaO^+ emissions are near those found in this study but there are several examples of listed lines not being observed here and lines observed here which are not listed.

When O_2 is admitted into the vacuum system to a pressure of 1×10^{-5} torr, the spectra (shown in Figure 6.5)

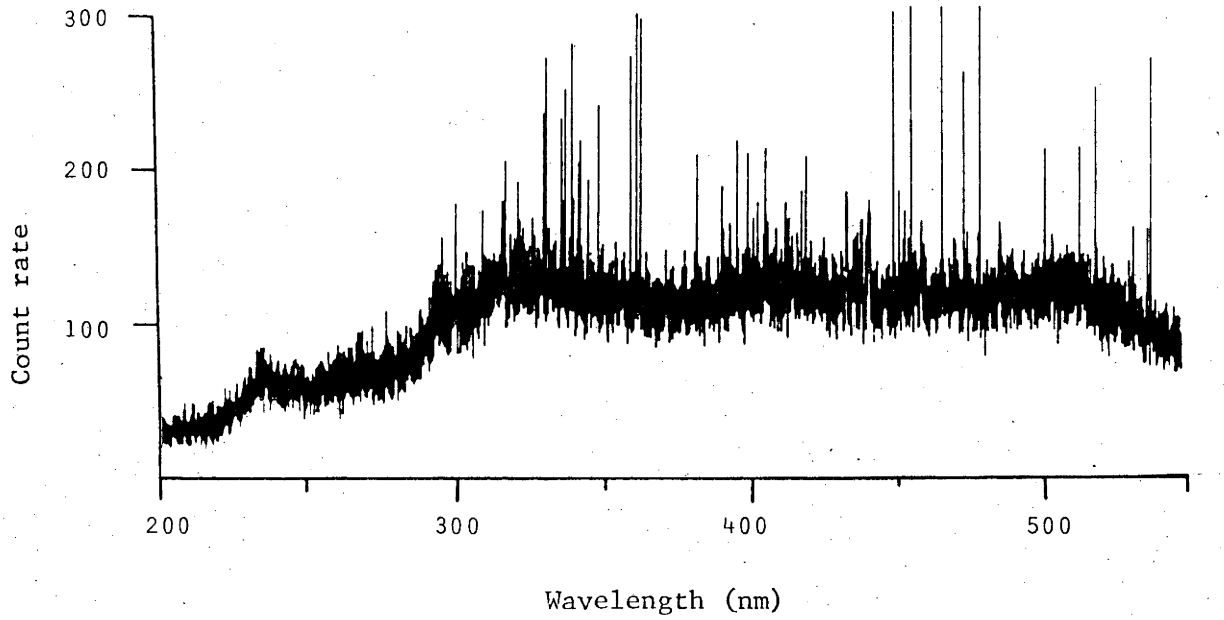

Figure 6.5(a). Ta photon spectra obtained with a background oxygen pressure of 1×10^{-5} torr during bombardment. The Jarrel-Ash monochromator was used.

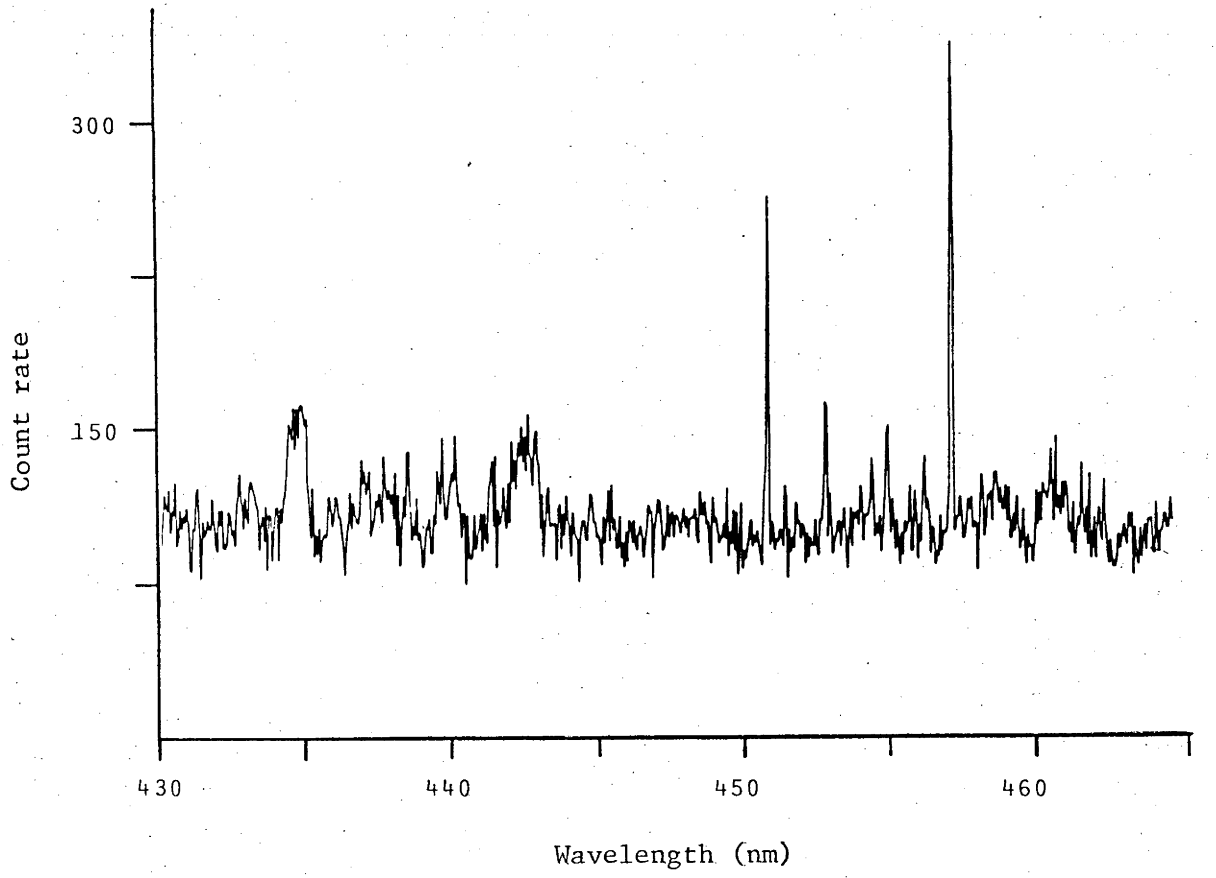

Figure 6.5(b). An expanded section of (a) above, from 430 - 465 nm.

are very similar to previously reported spectra [2,3,5,8] with a strong broad band continuum dominating the entire wavelength range scanned. The well defined continuum edge at 245 nm is very similar to that found elsewhere [8] and the continuum between 400-500 nm is similar to that found by Belykh et al. [5] and Kiyan et al. [2].

To investigate the behaviour of the broad emission at 434.8 nm with oxygen exposure, spectral scans of the region 430 nm - 455 nm were made as a function of background oxygen pressure. These are shown in Figure 6.6. It may be noted from Figure 6.6 that the continuum emission increases, as does the Ta I emission (eg. 451 nm); however, the broad emission at 434.8 nm remains at essentially the same intensity above the continuum emission level. These changes are shown more quantitatively in Figure 6.7. Also included in Figure 6.7 are data from SIMS measurements of TaO^+ emission. It can be seen that all emissions, apart from the broad line at 434.8 nm, increase with oxygen exposure. Photon emissions appear to saturate at high exposure whereas TaO^+ ion emission is still highly sensitive to further exposure. The positive dependence of the continuum emission with oxygen exposure is in direct contrast to that reported by Belykh et al. [5]. TaO^+ emission is noted to be present even under "clean" conditions and this suggests that oxygen may be diffusing from the bulk or may be from edge effects in the SIMS measurements.

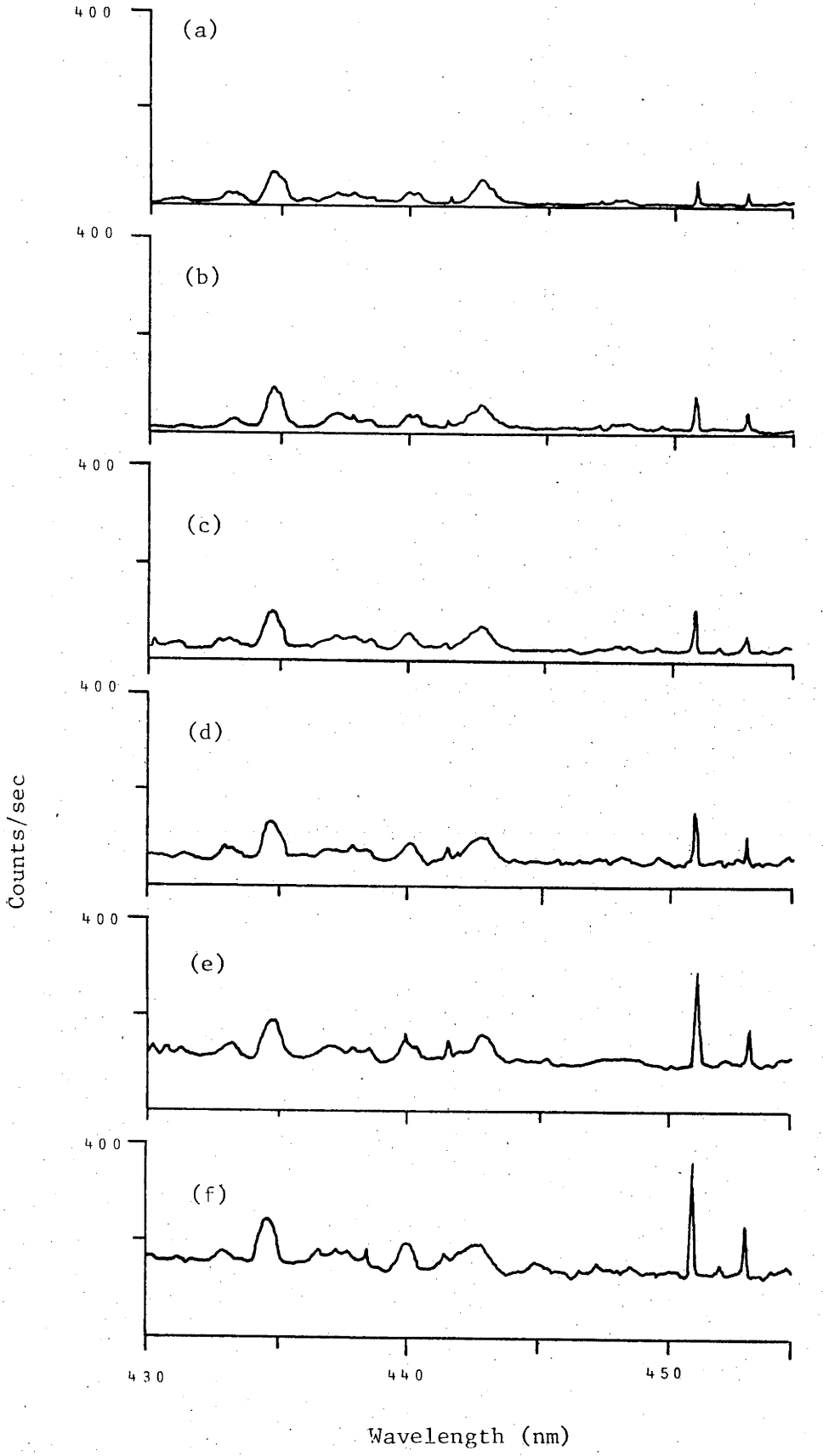

Figure 6.6 Spectral scans from 430 - 455 nm for 55 keV $Ar^{+} \rightarrow Nb$, as a function of increasing oxygen pressure in torr (a) base pressure - UHV, (b) 2×10^{-7}, (c) 8×10^{-7}, (d) 2×10^{-6}, (e) 5×10^{-6} and (f) 1×10^{-5}. The Jarrel-Ash monochromator was used.

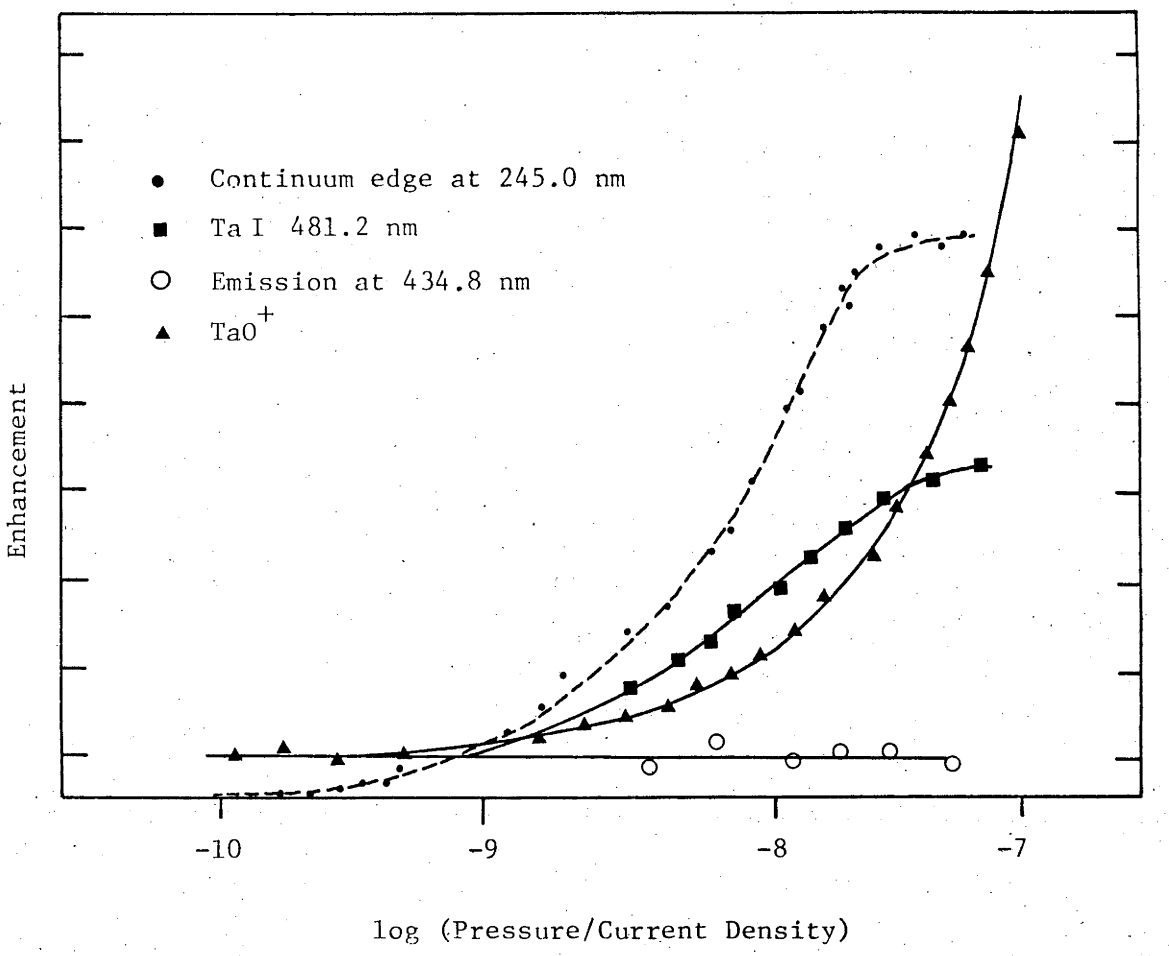

Figure 6.7 The enhancements of the ion and line emissions from Ta with oxygen exposure. The continuum emission is shown as an increased intensity, not an enhancement. (Pressure in torr and current density in $\mu A/cm^2$.)

6.1.3 *Continuum emission from Nb/V alloys*

Continuum emission at 407.0 nm has been observed from 5 keV Ar^+ bombardment of a series of Nb/V alloys. The observation geometry was again that for integral yield analysis with observation parallel to the target surface and the beam incident normal to the surface. The Jarrel-Ash monochromator (resolution 0.08 nm) was used.

The changes in the continuum emission intensity at 407.0 nm for the Nb, V, 45% Nb (#7) and 13% Nb (#5) targets with increasing background oxygen pressure are shown in Figure 6.8. The continuum enhancement curves have been normalized at the intensity peak. It may be noted from Figure 6.8 that the relative enhancement of the continuum emission decreases with increasing Nb concentration for the alloys studied. Continuum emission from the bombarded V was not observed at 407.0 nm under the cleanest conditions used here. Unlike the enhancement of the line emission from the bombarded alloys with oxygen exposure, the continuum emission intensities peak at the same incoming oxygen atom to beam ion ratio for each of the targets studied.

6.2 DISCUSSION

Atomic line spectra, broad band continuum emission and discrete broad emissions have been found during Ar^+ ion bombardment of Nb and Ta with O_2 or CO background gas contamination. Edge effects have been noted to contribute strongly to the continuum emission to the extent that they may change the shape of the continuum spectra. After

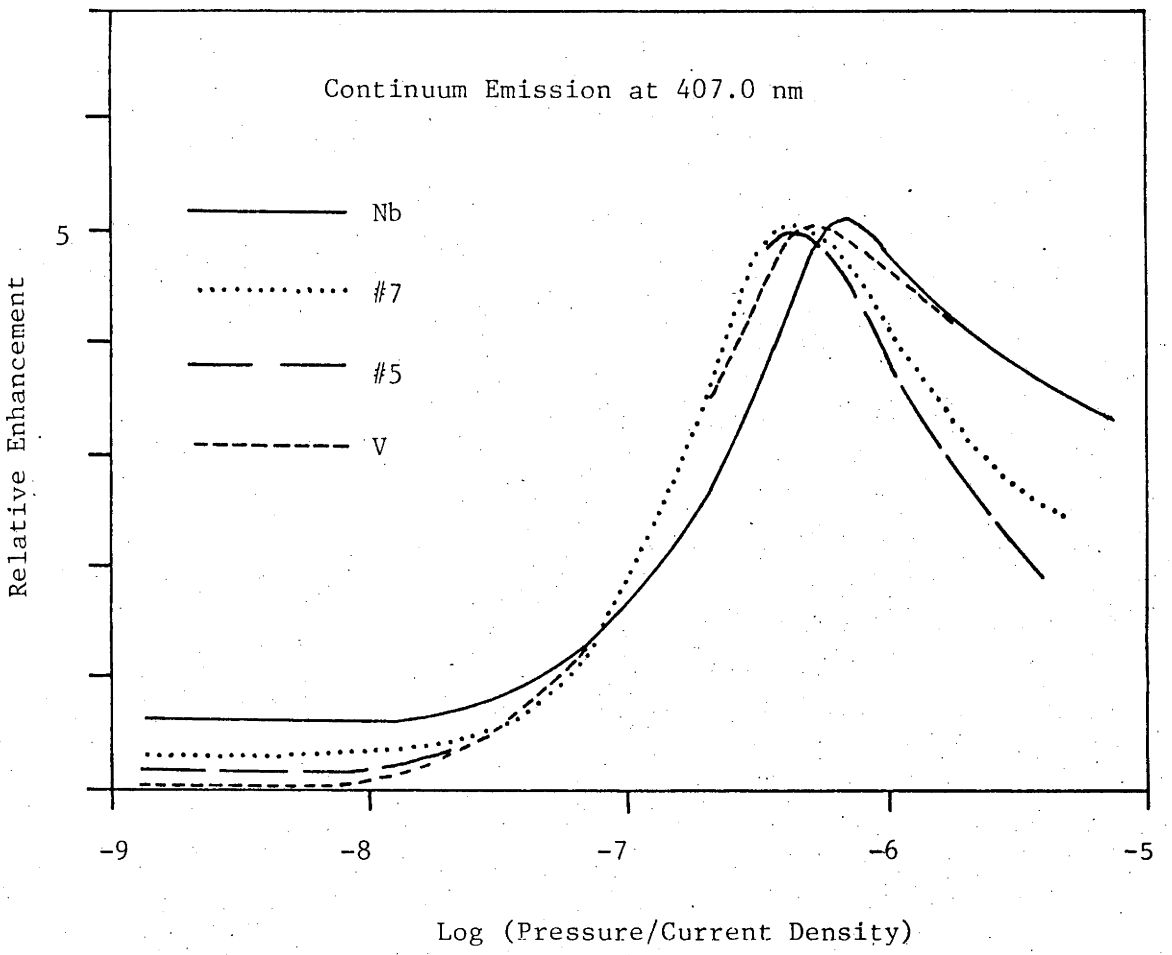

Figure 6.8 The intensity changes for the continuum emission at 407.0 nm with increasing background oxygen pressure are shown for the bombarded Nb, V #7 (45% Nb) and #5 (13% Nb) alloys. (Pressure in torr and the current density in $\mu A/cm^2$. The intensities have been normalized at the intensity peak.)

bombardment cleaning of the Nb target, the continuum spectrum was also observed to change in shape. Changes in the continuum spectra for bombarded Nb have been found to be different for O_2 and CO gas exposures. The previously reported lack of sensitivity to the surface contaminant [2] may reflect the influence of edge effects which may disguise the different emission features which should otherwise be found. Broad band continuum emission from ion bombarded Ta at 245 nm was found to increase strongly with oxygen exposure in contrast to the previously reported negative oxygen dependence [5].

The origin of this broad band continuum emission is not known. The observation of the positive dependence of the continuum emission intensity on surface contamination and that the continuum shape is influenced by the nature of the surface contaminant, indicate that the emission is most probably associated with surface contamination. This emission from Nb has been found to almost disappear when the surface oxygen component of the ISS spectrum is below the detection sensitivity of the system used here. These results support the conclusion [1] that the source of the emission may be excited molecules sputtered from the surface and these molecules may be of the form $M_nO_m^*$.

Continuum emission would then appear to be a particularly sensitive indicator for surface cleanliness when compared to the ISS system used here. Detection of the broad band emission could provide a useful surface cleanliness monitor for systems not employing an auxiliary monitor such as ISS or Auger Electron Spectroscopy.

Analytical application of the observation that the shape of the spectra induced by O_2 and CO surface contamination are slightly different would appear very limited until the source of the emission and the discrete broad emissions are known.

Although matrix effects have been noted in the Nb I and VI line emission with oxygen exposure for bombarded Nb/V alloys (Chapter 5), no matrix effects have been found for the continuum emission. The position of the enhancement peak of the continuum emission at 407.0 nm with background oxygen pressure was found to be relatively insensitive to the V or Nb concentration. This is surprising in view of the observation that the oxygen exposure required to saturate the Nb I enhancement increases with Nb concentration (Chapter 5) and that continuum emission may be associated with contamination. The position of the enhancement peak could be expected to shift to higher exposures with increasing Nb concentration of the alloy as shown by the Nb I line emission. An increase in the continuum emission observed under the cleanest conditions (lesser enhancement with oxygen exposure) is observed with increasing Nb concentration (shown in Figure 6.8). However,this may be related to the high solubility for contaminants such as O and CO in Niobium and the difficulty in removing these contaminants [9].

Broad line emission has also been observed during the bombardment of Nb and Ta. In the case of Nb, additional and changed broad line emissions are observed with CO exposure when compared to O_2 exposure (Figure 6.2), and

the failure to properly take into account the contribution of the changing continuum emission with increasing background oxygen pressure in the earlier report. The background continuum emission around the emission line was not directly monitered by Martin and Loxton. Consequently, a positive dependence of the 434.8 nm line with oxygen exposure was interpreted as in agreement with the proposed source of the emission being Ta O^+ excited molecules [10]. The poor agreement between the observed broad emissions and those listed as Ta O^+ emission lines was then attributed to the lack of reliable data on these molecular emission lines.

The possibility that the emitting species is another tantalum contaminant molecule, with the contaminant diffusing from the bulk, or a molecule of the form Ta_n^* cannot be ruled out. Sputtered molecules of the form M_n^+ have been observed by SIMS analysis but have not, to date, been identified through photon emission studies. However, the M_n^+ emission has a negative dependence on oxygen exposure [11] which would not support the proposal that the broad lines may originate from Ta_n^* molecules.

6.3 CONCLUSIONS

An investigation of the continuum emission resulting from Ar^+ bombardment of Nb and Ta and the changes induced in the emission by surface contamination with O_2 and CO, has found no behaviour contrary to the proposal by Rausch et al. [1] that continuum emission is related to surface contamination. Nb, Ta and V show a positive dependence of

the continuum emission with oxygen exposure. The extent of the continuum emission is particularly sensitive to surface contamination when compared to the ISS system used here. In the case of bombarded Nb, the continuum spectrum has been found to depend upon the nature of the surface contaminant (O_2 or CO). No matrix effects were found for this emission for the bombardment of Nb, V and Nb/V alloys.

The emission of discrete broad emission lines (0.4 - 1.2 nm wide) has been observed during the bombardment of Nb and Ta. In the case of Nb, several of these broad lines were found to change with the nature of the surface contaminant. The origin of these lines is not known. In the case of bombarded Ta, discrete broad emissions have been found which are independent of surface oxygen contamination. Again the nature of the emitting species is not known, although TaO^* molecules may be ruled out and Ta_n^* molecules appear an unlikely source.

REFERENCES

[1] E.O. Raush, A.I. Bazhin and E.W. Thomas, J. Chem. Phys. 65 (1976) 4447

[2] T.S. Kiyan, V.V. Gritsyna and Ya.M. Fogel , Sov. Phys. JETP 47 (1978) 730

[3] C.W. White and N.H. Tolk, J. Nucl. Materials 63 (1976) 506

[4] R.W.B. Pearse and A.G. Gaydon, The Identification of Molecular Spectra (Chapman and Hall, London, 1963)

[5] S.F. Belykh, V.I. Veksler, R.N. Evtukhov and Kh.A. Usmanov, Interaction of Atomic Particles with a Solid, pt.2, Khar'kov (1976) (in Russian) p.198

[6] D. Premaswarup, Indian J. Phys. 29 (1955) 109

[7] D. Premaswarup and R.F. Barrow, Nature, London 180 (1957) 602

[8] C,W, White, N.H. Tolk, J. Kraus and W.F. Van der Weg, Nucl. Instr. Methods 132 (1976) 419

[9] M. Grundner and J. Halbritter, J. Appl. Phys. 51 (1980) 397

[10] P.J. Martin and C.M. Loxton, Radiation Effects Letters 50 (1980) 161

[11] R.F. Garrett and R.J. MacDonald, presented at: Vth Intern. Conference on Ion Beam Analysis, Sydney (1981)

CHAPTER SEVEN

CONCLUSIONS

Particular care has been taken throughout this thesis to fully define the experimental parameters used and an attempt has been made to investigate the influence of these parameters. The surface cleanliness conditions and the chemical nature of any contaminant have been shown to influence the observations. Edge effects associated with surface contamination are also shown to have some effect. The incidence angle of the beam to the target surface strongly influences the average kinetic energy of the excited particles. Other experimental parameters such as the observation geometry and apparatus and the incidence energy are also noted to effect the results. The results reported here are then characteristic of the experimental parameters used for this study and need not be the same as those found in previous studies. Discrepancies observed between previous studies where the experimental parameters may not have been the same, or their influence not understood, have confused the understanding of the excitation and de-excitation processes.

In order to gain some insight into these processes, a thorough study has been made of the atomic line emission from Ti. The distribution of excited states, intensity changes with oxygen exposure and the kinetic energies of excited atoms and their change with oxygen exposure have

been examined in detail for a variety of Ti compounds and surfaces. An attempt to interpret the observations using the simple band structure model has been unsuccessful. The resonance ionisation process in particular is not expected to influence the excited atoms.

A physically more reasonable model for de-excitation of sputtered atoms using the assumption of an LTE source has been discussed. Derived reduced intensity plots, associated with the distribution of excited states, are considerably different to plots derived assuming excitation and de-excitation in an LTE plasma for Ti I. The distribution of excited states for Ti I is shown to be Boltzmann-like and no changes in the distribution attributable to resonance ionisation processes are shown. These distributions are not significantly influenced by the chemical state of the surface from which the Ti atom was sputtered. The lack of uniqueness for the fit to a Boltzmann distribution does not allow the assumption of "LTE like" excitation and consequently, these plots reveal little information on the excitation process.

The intensities of the Ti I lines show an increase, followed by a peak region and subsequent decrease, with increasing oxygen exposure. The intensity peak enhancements for normal incidence bombardment are of the order of 3 - 4 for these lines and are expected to be associated with a change in the excitation probability. The subsequent decrease appears to be related to the falling sputtering yield at high oxygen exposure.

Kinetic energy parameters, $E_{\|}$, $\bar{E}_{\perp}$ and E^*, derived through line profile measurement and decay curve measurements using the beam foil model and the Dzioba et al. model respectively, have been compared for the Ti I system. The $\bar{E}_{\perp}$ values, previously used as evidence for the influence of the resonance ionisation process on Ti I atoms with excitation energy above the metal Fermi level, are shown not to be physically reasonable when compared to the line profile measurements. The $E_{\|}$ and E^* values have similar magnitudes and behaviour with the chemical state of the bombarded target and the excitation energy of the level. Both parameters decrease with surface oxygen contamination and increase with increasing excitation energy of the atom. These similarities add credence to the model of Dzioba et al. where a threshold form for the excitation function was assumed. Application of the model of Dzioba et al. to determine E^* values has been shown to depend upon the ability to adequately resolve the intensity decay curve.

Other bombarded elements have also shown a similar excitation energy dependence for the kinetic energy parameters and have furthermore shown an increase with the ionisation state of the sputtered atom. These parameters change non-monotonically for different atom species with similar masses and excitation energies (e.g. Ti, Cr and Ni levels have similar $E_{\|}$ values but are different to Zn I levels). The $E_{\|}$ values are of the order of several eV to hundreds of eV for normal incidence bombardment. Comparison with E^* values shows the importance of ensuring that the latter are physically reasonable when

high values of the order of keV are derived. In the case of normal incidence bombardment, the $E_{||}$ values are not unreasonable for the proposal that the excited atoms are sputtered when the collision cascade intersects the surface.

The average kinetic energies of excited atoms has been shown to increase dramatically with increasing angle of incidence. This increase is expected to be related to the greater contribution of the binary collision sputtering component to the total sputtered excited atom yield. These results illustrate that caution must be used when comparing the excitation processes and observations for different angles of incidence.

The proposal that excitation may occur through quasimolecule formation and that different excitations may be observed when the collision cascade intersects the surface for a binary alloy, has been investigated for the Nb/V alloys under UHV conditions. No evidence was found for matrix effects on the Nb I and V I emissions due to different excitation producing collisions. The changing band structure of the different alloys was also found not to influence the Nb I and V I emission. This suggests that excitation is not influenced by the surface potential as the sputtered atom leaves the surface.

Intensity increases for neutral atom line emission with oxygen exposure have been observed for all of the elements studied here. These changes with oxygen exposure for normal incidence bombardment exhibit three classes of behaviour: (i) large enhancements and no saturation of

the line emissions, (ii) moderate enhancements (< 10) with intensity peaking and subsequent decrease but no continuum emission and (iii) moderate enhancements with intensity peaking and subsequent decrease and also continuum emission.

The kinetic energy parameters do not all follow the behaviour of the Ti I emission with oxygen exposure. Emission lines from some elements have been found to exhibit an increased line width with oxygen exposure (notably Aℓ), while other line widths are relatively unchanged by oxygen exposure (Si) for normal incidence bombardment. Ni I is found to exhibit both types of behaviour, depending upon the excitation level. The behaviour of the intensities and line widths with oxygen exposure vary with different excitation levels.

The different types of behaviour of the line profiles with oxygen exposure do not correlate with the classes described above for the intensity changes. The ionised atom emission line widths usually follow the behaviour of the neutral atom emission line widths although the intensity changes may not.

The previously reported observation of a particularly wide Si I emission line from bombarded Si, but a narrow line from bombarded SiO_2, could not be repeated here. The changes in the line widths with oxygen exposure were found to change slightly with incidence angle. The two observations of an increased intensity *and* unchanged (or increased) line width for the same emission line provides the clearest evidence against the band structure model used previously to interpret the Si/SiO_2 results.

Matrix effects have been found from bombarded Nb/V alloys under oxygen exposure conditions. The line intensity changes with oxygen exposure from the bombarded alloys indicate that all the Nb , V and O atoms influence the excitation process. The simple quasimolecule formation model for excitation is difficult to relate to the observations unless the O atom influences the Nb - V collisions. Alternatively, the observations may be interpreted assuming that the Nb (or V) concentration of the alloy determines the oxygen coverage and that the intensity increases are linear with coverage. Little information on the excitation processes may then be interpreted.

Application using the line emission intensities and an emission standard for photon analysis of metal alloys has been discussed. Quantitative analysis under UHV conditions has been possible for the Nb/V system with atomic concentrations determined to about 5% accuracy. The matrix effects observed with oxygen exposure exclude quantitative analysis for the Nb/V system although the influence of the oxygen exposure may be compensated for by measuring exposure curves from each alloy.

Continuum emission has been found to be strongly influenced by edge effects. This emission is very sensitive to surface contamination and, to a limited extent, to the nature of the contaminant. The observations have been consistent with the proposal by Rausch et al. that the continuum emission is associated with surface contamination. No matrix effects were found for the continuum

emission from the bombarded Nb/V alloys. The nature of the emitting species could not be identified.

Broad line emissions were observed from bombarded Nb and Ta. Some of the broad lines from Nb were found to change with the nature of the surface contaminant and the surface cleanliness. These broad emissions are possibly associated with Nb-contaminant molecules. The broad emission lines from Ta such as that at 434.8 nm, were independent of oxygen exposure and were present under the cleanest conditions. The emitting species could not be identified.

Previous experiments have failed to look intensively at the basics of the photon emission processes. In those that have, the conditions for study were often poor and ill defined. A detailed study of one system has been made here and has shown that current models for excitation and de-excitation processes do not survive rigorous testing under UHV conditions. The excitation process is not known. Under oxygen exposure conditions, quasimolecule formation and excitation through curve crossings cannot be ruled out as an excitation process. The excitation process is not expected to be very different to that for UHV conditions as the distribution of excited states has been shown to be similar. This study does form a basis for further investigation into the excitation processes.

There is a need for more attention to be paid to the experimental conditions and parameters in future experiments. Emission function measurements are expected to be very important, particularly when considering

the high E^* values derived using the model of Dzioba et al. and the assumption of a step function form for the excitation probability. These measurements should be made as a function of incidence angle, excitation energy and ionisation state of the excited atom and for different surface conditions. Further experiments involving photon emission together with secondary ion, scattered ion, secondary electron and X-ray emission are also expected to be of interest.

F.E. Smith, the brilliant barrister who was later to become the first Earl of Birkenhead and to hold many high offices, including that of Lord Chancellor, was conducting an extremely complicated case before a rather slow-witted judge. Towards the end of the proceedings the judge intimated that he found the complexity of the case too much for him, whereupon Smith proceeded, with the consent of the other side, to give, in an amazingly short space of time, a masterly summary of the evidence and the points at issue. But the judge seemed as much in the dark as ever and remarked querulously:

"I am sorry, Mr Smith, but I am none the wiser."
Smith paused, sighed deeply, and replied:
"No, my Lord. But you are better informed."

K. Edwards, "I wish I'd said that!"
(Abelard, London, 1976) p. 23.